The role of synaptic noise in cortical excitability

Greenhill, Stuart

Award date:
2008

Awarding institution:
University of Bath

THE ROLE OF SYNAPTIC NOISE IN CORTICAL EXCITABILITY

Stuart David Greenhill

A thesis submitted for the degree of Doctor of Philosophy

University of Bath
Department of Pharmacy and Pharmacology
January 2008

COPYRIGHT

Signed: _____ Date: _____

Word Count: 41,584

Table of Contents

Table of Figures

Chapter 4

Chapter 5

Chapter 6

Chapter 7

Acknowledgements

This thesis would not have been possible without the constant support and advice of my supervisor, Dr Roland Jones. His endless supply of ideas, constant encouragement and intolerance of excessive punctuation have been much appreciated, and have made the last three years both engaging and enjoyable. Secondly, I would like to thank the past and present members of the Jones Lab, Sophie Chamberlain, Jian Yang and Göher Ayman for their companionship and patience throughout some "interesting" times.

The staff and students of the Department have made my stay in Bath one of the best periods of my life, and I thank them (especially the "Magnificent" Flying Boots football team) for all the happy times we have shared. Finally, I would like to thank my family, especially my parents, whose love and support have given me the opportunity to be here in the first place, and the determination to succeed.

Abstract

The entorhinal cortex (EC) is a vital structure in the mammalian brain, implicated in the processes of learning and memory, and a possible site for the generation of seizures in temporal lobe epilepsy. Neurones in the EC are constantly bombarded with inhibitory and excitatory neurotransmitter. This background activity is thought to exert significant control on the excitability and function of neurones in cortical networks, with changes in the levels and proportion of background inhibition (I_{Bg}) and excitation (E_{Bg}) driving rhythmic oscillations in membrane potential, and even underlying the generation of epileptic seizures.

In this thesis I used a novel approach to quantify levels of background activity in the EC, and relate these levels to cellular excitability. The VmD (membrane voltage distribution) method (Rudolph *et al.*, *J Neurophysiol* **91**, 2884-96) allows the estimation of I_{Bg} and E_{Bg}, and their respective standard deviations, from intracellular recordings in principal neurones. I have applied the VmD method to pyramidal neurones in the rat medial EC in an *in vitro* slice preparation. My experiments have provided validation of the VmD method in the mEC by initially using a range of well-characterised pharmacological tools (e.g. NBQX, 2-AP5) to obtain predictable and repeatable measures of I_{Bg} and E_{Bg} and the effects of receptor or uptake blockade on these values.

The VmD method was also used to investigate lamina-specific differences in background activity and sensitivity to epileptogenesis in the mEC. Using the VmD method and the $GABA_A$ antagonist bicuculline I was able to show that there are appreciable lamina-specific differences between the ratio of inhibition to excitation and sensitivity to $GABA_A$ blockade.

Additionally, I used the method to characterise two different types of slow wave oscillatory activity (seen in highly active cortical networks) in layer III of the mEC, and to investigate the mode of action of several anticonvulsant drugs.

List of Abbreviations

R-AP5 – [R]-2-amino-5-phosphonopentanoic acid

4-AP – 4-aminopyridine

ACSF – Artificial cerebro-spinal fluid

AMPAr – α-amino-3-hydroxy-5-methyl-4-isoxazolepropionic acid receptor

ANOVA – Analysis of variance

AP – Action potential

ATP – Adenosine Triphosphate

BMO – Brief Membrane Oscillations

CA – *Cornu Ammonis*

CGP-55845A – (2S)-3-[[(1S)-1-(3,4-dichlorophenyl)ethyl]amino-2-hydroxypropyl] (phenylmethyl)-phosphinic acid

CNS – Central Nervous System

DC – Direct Current

DG – Dentate Gyrus

EAAT1-5 – Excitatory Amino Acid Transporter 1-5

E_{Bg} – Background Excitatory conductance

EC – Entorhinal Cortex

ECoG - Electrocorticogram

EEG – Electroencephalogram

EPSC – Excitatory Post-synaptic Current

EPSP – Excitatory Post-synaptic Potential

GABA – γ-amino-butyric acid

$GABA_Ar$ – γ-amino-butyric acid type A receptor

$GABA_Br$ – γ-amino-butyric acid type B receptor

GAD – Glutamic Acid Decarboxylase

GAT-1 – GABA Transporter 1

GYKI-53655 – 1-(4-aminophenyl)-3-methylcarbamoyl-4-methyl-3,4-dihydro-7,8-methylenedioxy-5H-2,3-benzodiazepine

I:E Ratio – Ratio of inhibitory conductance to excitatory conductance

I_{Bg} – Background Inhibitory conductance

I_{CaT} – Low-threshold Calcium Current

IEI – Inter-event interval

I_{ext1}- – External current 1

I_{ext2}- – External current 2

I_h – Hyperpolarisation-activated current

I_{KA} – A-type potassium current

I_{Kd} – Voltage-dependent potassium current

I_{Na} – Voltage-dependent sodium current

IPSC – Inhibitory Post-synaptic Current

IPSP – Inhibitory Post-synaptic Potential

$[K^+]_O$ – Extracellular potassium concentration

KAr – Kainate Receptor

K_{ATP} – ATP-sensitive potassium current

LD – *Lamina Dessicans*

lEC – Lateral Entorhinal Cortex

mEC – Medial Entorhinal Cortex

$[Mg^{2+}]_O$ – Extracellular magnestium concentration

MgATP – Magnesium Adenosine Triphosphate

MRI – Magnetic Resonance Imaging

NBQX – 6- nitro-7-sulphamoylbenzo[f]quinoxalone-2,3-dione disodium

NMDA – N-methyl-D-aspartate

NMDAr – N-methyl-D-aspartate receptor

NR1 – N-methyl-D-aspartate receptor 1

NR2 – N-methyl-D-aspartate receptor 2

OU – Ornstein-Uhlenbeck

PDC – L-trans-pyrrolidine-2,4-dicarboxylic acid

QMS – Quiescent membrane state

QX-314 – N-(2,6-dimethylphenyl carbamoylmethyl)triethylammonium bromide

sEPSC – Spontaneous Excitatory Post-synaptic Current

SD – Standard Deviation

sIPSC – Spontaneous Inhibitory Post-synaptic Current

SWO – Slow Wave Oscillations

TLE – Temporal Lobe Epilepsy

TMA – Trimethylamine

UBP-302 – (S)-1-(2-amino-2-carboxyethyl)-3-(2-carboxybenzyl)pyrimidine 2,4-dione

VG – Voltage-gated

VGC – Voltage-gated Channel

VGCC – Voltage-gated Calcium Channel

VGSC – Voltage-gated Sodium Channel

VmD – Membrane Voltage Distribution

ZD-7288 – (4-(*N*-ethyl-*N*-phenylamino)-1,2-dimethyl-6-(methylamino) pyridinium chloride)

CHAPTER 1

GENERAL INTRODUCTION

Introduction

Work in this laboratory has been focussed on the functional synaptic organisation of the entorhinal cortex (EC). In particular, in recent years, it has been examining how spontaneous release of excitatory (glutamate) and inhibitory (GABA) transmitters is controlled, and how this spontaneous release helps to determine overall network activity.

The aim of this thesis has been to investigate the link between cortical network activity and cellular excitability in the medial EC of the rat. This has been approached using a recently developed method, based on membrane voltage fluctuations (the "VmD Method", Rudolph *et al*., 2004) that enables us to obtain, using simple intracellular recordings, an estimation of global background excitatory and inhibitory conductance in principal neurones, at the same time, in the same cell. As it is based on intracellular recordings, the VmD method also allows measurements of cellular excitability to be made in the recorded cells, thus enabling concurrent observation of how changes in the degree and proportion of background excitation and inhibition affect the ability of principal cells to fire action potentials. This in turn provides information on the relationship between the inhibitory and excitatory systems within the EC.

The Entorhinal Cortex

The EC is a structure forming part of the limbic system, located within the rhinal sulcus in the rostral ventromedial surface of each temporal lobe (Fig 1.1). The EC can be roughly divided in to two triangular sections, as outlined in Witter *et al.* (1989). These sections, the medial entorhinal cortex (mEC) and lateral entorhinal cortex (lEC), are distinct in their connections to and from the hippocampal *cornu ammonis*, dentate gyrus and neocortex. The intricate connections between the EC and the hippocampus

have been studied since Cajal first noted them. It has long been proposed that both the EC and hippocampus are associated with memory processes (Zola-Morgan and Squire, 1993; Eichenbaum *et al.*, 1994). The rat EC is often used to model human diseases, as it has functional and anatomical similarities, especially with primates (Insausti *et al*., 1997).

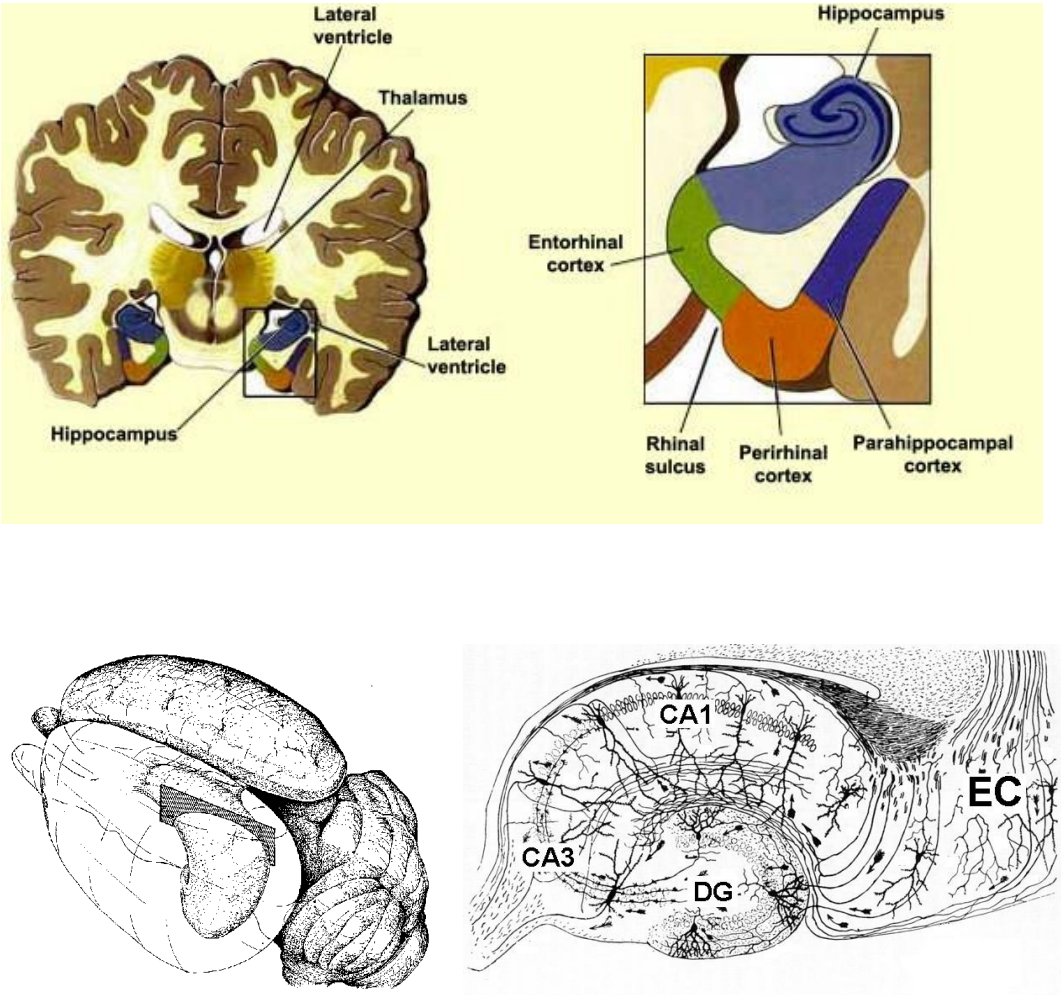

Figure 1.1: Location of the EC in the human (top) and rat brain (bottom left). Top left illustration is coronal section of human brain, taken through the front of the temporal lobes. the EC is visible in green next to the hippocampus. In the slice of rat brain (bottom right) the CA1 and CA3 areas of the hippocampus, the dentate gyrus (DG) and EC are all visible. Human illustration courtesy of McGill University. Rat illustration adapted from Cajal (1911).

The EC has been implicated in a number of diseases, such as schizophrenia, Alzheimer's disease and Parkinson's disease (Kovari *et al.,* 2003; Prasad *et al.,* 2004;

Pennanen *et al.,* 2004). However, the disease most commonly associated with dysfunction of the EC is temporal lobe epilepsy (TLE), which is thought to be the cause of seizures in around 40% of adult epilepsy (McNamara, 1992; Schwarcz *et al.,* 2000; Jones and Woodhall 2005).

Despite considerable focus on the hippocampus as the cause of TLE (Bradford, 1995; McCormick and Contreras, 2001), there is increasing evidence from surgical studies that the EC is heavily involved in seizure generation and propagation. There have been many reports of seizure activity arising independently, or even preferentially, in the EC (Rutecki *et al.,* 1989; Spencer and Spencer, 1994; Alarcon *et al*., 1997; Assaf and Ebersole, 1997; Asaf *et al*., 2003; Bartolomei *et al*., 2004, 2005).

Studies performed during operations on patients undergoing temporal lobe resection to treat intractable TLE highlighted a similarity between spikes evoked in the hippocampus by EC stimulation, and spontaneous activity in the hippocampus observed between seizures (Rutecki *et al*., 1989). These studies also showed that spontaneous activity recorded within the EC clearly preceded many similar discharges recorded within the hippocampus. Wennberg *et al.* (2002) suggested that seizures arising within the hippocampus generally fail to propagate beyond their site of onset, and have little or no clinical manifestation. However, seizures with focal onset in the amygdala or the parahippocampal cortex (see Fig. 1.1) displayed clear clinical symptoms and showed definite signs of propagation. When parahippocampal cortex-based seizures (including the EC) were considered alone, the correlation between these seizures and clinical manifestations/propagation was 100%.

In human epilepsy, as many as 30% of patients are refractive to current drug therapy, but the reasons for this lack of response are currently unknown (Sander, 1993; Kwan and Brodie, 2000). Surgical intervention to control drug-resistant TLE involves a partial temporal lobectomy removing both the hippocampus and the EC. The success

rate of this surgery appears to correlate with the amount of parahippocampus and EC removed during temporal lobe resection (Siegel *et al.*, 1990; Fried, 1993; Sperling *et al.,* 1996). Goldring *et al.*, (1992, 1993) have suggested that the removal of the EC is essential for surgical control of refractory TLE. One of the symptoms of TLE is hippocampal atrophy, as seen in MRI studies with epileptic patients. However, a large number of MRI studies have shown that the EC is significantly reduced in volume in TLE patients. Supporting the above intraoperative studies, atrophy of the EC has been observed in TLE without accompanying loss of hippocampal volume. In epilepsies arising outside of the temporal lobe, or in generalised epilepsies of unknown aetiologies, no entorhinal atrophy is evident (Bernasconi *et al.*, 1999, 2001, 2003; Jutila *et al*., 2001; Bonilha *et al*., 2003).

After acute seizure activity had been induced *in vitro* in rat brain slices, recorded seizure activity (and increased glucose consumption associated with a rise in neuronal activity) appears in the EC before spreading to other parts of the limbic system, again suggesting the EC as a source of seizure activity (Ben-Ari *et al*., 1981; Collins *et al.,* 1983; Stringer, 1994). Furthermore, *in vivo* studies in rats with chronically induced epilepsy have demonstrated events such as high frequency events and oscillations in the EC, with a high degree of similarity to events recorded in human TLE patients (e.g. Bragin *et al*., 2002, 2004). Additionally, electrophysiological studies have suggested that seizures in acutely-evoked TLE are generated by the EC, propagating from the deep to the superficial EC and on to the hippocampus (Jones and Lambert 1990a, b; Nagao *et al.,* 1996).

Anatomy and Physiology of the EC

Much of the anatomical study of the EC has focussed on its connections to and from the hippocampus (Fig. 1.2), and the rich interconnection between layers within the EC itself. As stated above, the EC can be divided into medial and lateral sub-sections. The

lateral sections project to the caudal levels of the dentate gyrus (DG), whilst the mEC projects towards more caudal sections of the DG. There is a direct relationship between the position of cells and their projection, as more medial cells in the EC project further towards the caudal end of the DG (Witter *et al.,* 1989).

The EC itself can be further divided into six layers, from layer I (the most superficial) to layer VI (the innermost layer), although the exact divisions vary between investigators. There have been many efforts made to further divide the EC, with the number of proposed subfields ranging from as little as two, to as many as 23. This thesis will employ the divisions noted in Witter *et al.* (1989). Two of the layers (I and IV) are sometimes termed "plexiform layers", and contain very few neuronal soma. Layer I contains mostly fibres, whilst layer IV, the *lamina dessicans*, has an extremely low density of neurones and is not found at the more rostral areas of the EC. There is some debate as to whether layer IV is a subdivision of layer V, or a structure in its own right. It has been postulated that the EC represents an evolutionary transition between the three-layered hippocampus and the clear six layers of the mammalian neocortex (Insausti *et al.*, 1997).

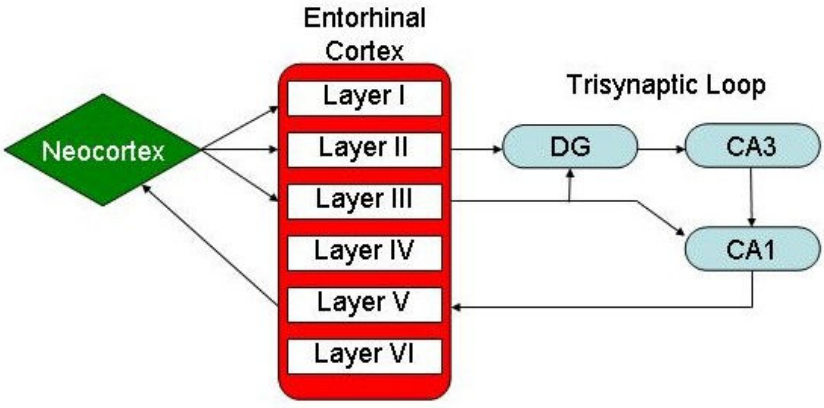

Figure 1.2: Extrinsic connectivity of the mEC. The superficial layers receive much of the input from the neocortex, with layers II and III projecting towards the hippocampus, forming the "trisynaptic loop". Layer V is densely innervated by the hippocampus, and projects to the neocortex and back to the superficial EC, leading to high levels of recurrent connections.

Laminar Structure and Internal Connectivity of the EC

Even from early anatomical studies (for example, those of Cajal, 1911 or Lorente de No, 1933) it is clear that there is an extensive network of interconnections between cells in different layers of the EC, and a number of differences in the density and morphology of neurones between these layers. As staining and imaging techniques improve, more and more is being discovered about the relationship between neurones in different layers of the EC; this information can be further supported by complex electrophysiological studies investigating the functional relationship of the layers, and their susceptibility to diseases such as epilepsy.

Layer I of the EC is only very sparsely populated with neurones, containing mostly fibres. There are small populations of both horizontal and multipolar cells, projecting and ramifying locally in a limited manner (Germroth *et al*., 1989). Layer II also contains some horizontal cells. However, the majority of neurones in layer II are spiny stellate cells, with a greater proportion in the mEC than the lEC (Alonso and Klink, 1993; Jones, 1994; Klink and Alonso, 1997). These spiny stellate cells, with many diverse and far-reaching projections, form the main output from the EC. Layer II stellate cells form the major part of the perforant pathway to the hippocampus. A single layer II cell has been shown to project axonal branches towards the entire transverse dentate gyrus (suprapyramidal and infrapyramidal blades, and the DG crest), the CA2-3 fields of the hippocampus, and the subiculum (Tamamaki and Nojyo, 1993). Their dendritic trees branch extensively throughout the three outermost layers of the EC. Given the large amount of information passing from the neocortex to the hippocampus through these layers, it is evident that layer II stellate cells provide the pivotal link between these two structures. There is limited evidence to suggest that layer II stellate cells also project to layers V and VI of the EC (Ino *et al.,* 2000; Buckmaster *et al.*, 2004).

Activity in layer II is tightly regulated by a wealth of inhibitory connections. *In vitro* electrophysiological studies have shown that layer II neurones are kept mostly quiescent and prevented from firing action potentials due to the overwhelming level of inhibitory postsynaptic potentials (IPSPs) from GABAergic interneurones (Jones, 1993, 1994; Heinemann *et al.*, 2000). These interneurones form a complex web of connections comprising of feed-forward and feed-back inhibitory links to principal cells in both layer II and layer III. The most potent inhibitory interneurones in the cortex are considered to be basket cells and chandelier cells, and these are both most abundant within layers II and III (Hendry *et al.*, 1989; DeFelipe, 1999). Horizontal inhibitory cells in layer II possess dendritic and axonal structures that are largely confined to the layer, in contrast with the principal neurones (Germroth *et al.*, 1989; Jones and Buhl, 1993).

The principal excitatory cells of layer III are pyramidal cells (Fig. 1.3). The primary function of excitatory cells in layer III is thought to differ from that of layer II principal cells. Instead of forwarding information from the cortex to the hippocampus (as layer II cells do largely through the perforant pathway), a proportion of pyramidal cells in layer III have been proposed to act as "controller cells" for pyramidal neurones in the CA1 hippocampal area. Layer III principal cells exist in two groups, those that project towards the hippocampus, and those that project within the EC. The former group forms a closed-loop system with the hippocampal CA1 cells, controlling the exit of information from the hippocampal trisynaptic pathway, whereas the latter, internally projecting cells extend their axons throughout layer III. Both groups of layer III pyramidal cells have rich dendritic trees within layers I and II (Gloveli *et al.,* 1997; Buckmaster *et al.*, 2004). This extensive interconnection between principal cells, the proposed controller role for the externally-projecting pyramidal cells, and the large amount of inhibitory control exerted within layer III would all suggest that the pyramidal cells in this layer perform a crucial information-processing function,

presumably integrating and processing cortical signals via layers I and II of the EC, then controlling the passage of this information to the hippocampus.

Layer IV, the *lamina dessicans* (LD), contains a sparse number of pyramidal cells in its deeper sections, and is rich in myelinated fibres. In the rostral sections of the EC, layer IV is not readily apparent. Cajal (1911) described the LD as a distinct layer, whereas Lorente de No (1933) described the majority of the layer as a subset of layer III, with his layer IV referring to the small group of pyramidal neurones contained within the deeper *lamina dessicans*. Whatever terminology is applied, it is clear that the majority of layer IV consists of fibres from cells in other layers traversing the LD (Amaral *et al.*, 1987).

The majority of principal cells in layers V and VI are pyramidal cells, however there are also a number of bipolar and multipolar cells (Gloveli *et al.*, 2001). The pyramidal cells in these layers possess prominent apical dendrites, extending towards the superficial layers of the EC. The axons of these cells extend into the white matter, and also towards the more superficial layers of the EC. The somata of these deep pyramidal cells are significantly smaller than those of the pyramidals in layers II and III (Buckmaster *et al.,* 2004).

Inhibition in the deeper layers of the EC is less pronounced than the tight control exerted by interneurones in the superficial layers. Excitatory postsynaptic potentials (EPSPs) dominate IPSP activity in the deep pyramidal neurones. Inhibitory responses in layer V are very weak, and in some cases they are not apparent at all (e.g. Jones and Heinemann, 1988). Woodhall *et al.* (2004) showed that there was a four-fold higher basal frequency of spontaneous IPSC activity, and a greater intensity and frequency of IPSC bursts, in layer II compared to layer V. The proportion of activity dependent inhibitory events was found to be much greater in layer V than in layer II, i.e. the inhibitory system in the superficial layers is more constitutively active than the

interneurones of the deep layers. The superficial layers of the EC are said to be more "epilepsy resistant" than the deeper layers, this is possibly explained by the increased inhibition in the superficial layers, reducing the chances of excitatory synchronisation and subsequent epileptogenesis (Jones and Lambert 1990a; Jones 1993; Woodhall *et al.*, 2004). The direct link of inhibitory activity levels and susceptibility to epileptogenesis has, however, been challenged by studies linking GABAergic inhibition with the promotion of synchronous activity (Cobb *et al.*, 1995). There is evidence to suggest that the difference in basal inhibitory activity between EC layers is due, at least in part, to lamina-specific differences in presynaptic $GABA_B$ autoreceptor activity. Bailey *et al.* (2004) found that feedback control (reduction) of GABA release by metabotropic autoreceptors occurs tonically in layer V, but *not* in layer II. This would go some way to explain the lamina-specific differences in inhibitory activity.

Transmission and Activity in the EC

Our laboratory has long been focussed on the properties of transmission in the mEC, largely due to its involvement in TLE. Several studies have been undertaken detailing the lamina-specific differences in spontaneous and evoked transmission in the mEC, providing valuable insight into the physiology and pathophysiology of this area.

Lamina-specific Differences in Activity-dependent Transmission

Early work highlighted the properties of neurones in the deeper layers. In layer V, it was shown that low-frequency stimulation of afferent pathways leads to a dominance of excitatory synaptic activity, particularly NMDA receptor-mediated responses. In contrast, inhibitory activity in layer V was weak (Jones, 1987; Jones and Heinemann, 1988). The relative dominance of excitatory activity in deeper layers has also been replicated by Funahashi and Stewart (1998) in the pre- and parasubiculum. Excitatory

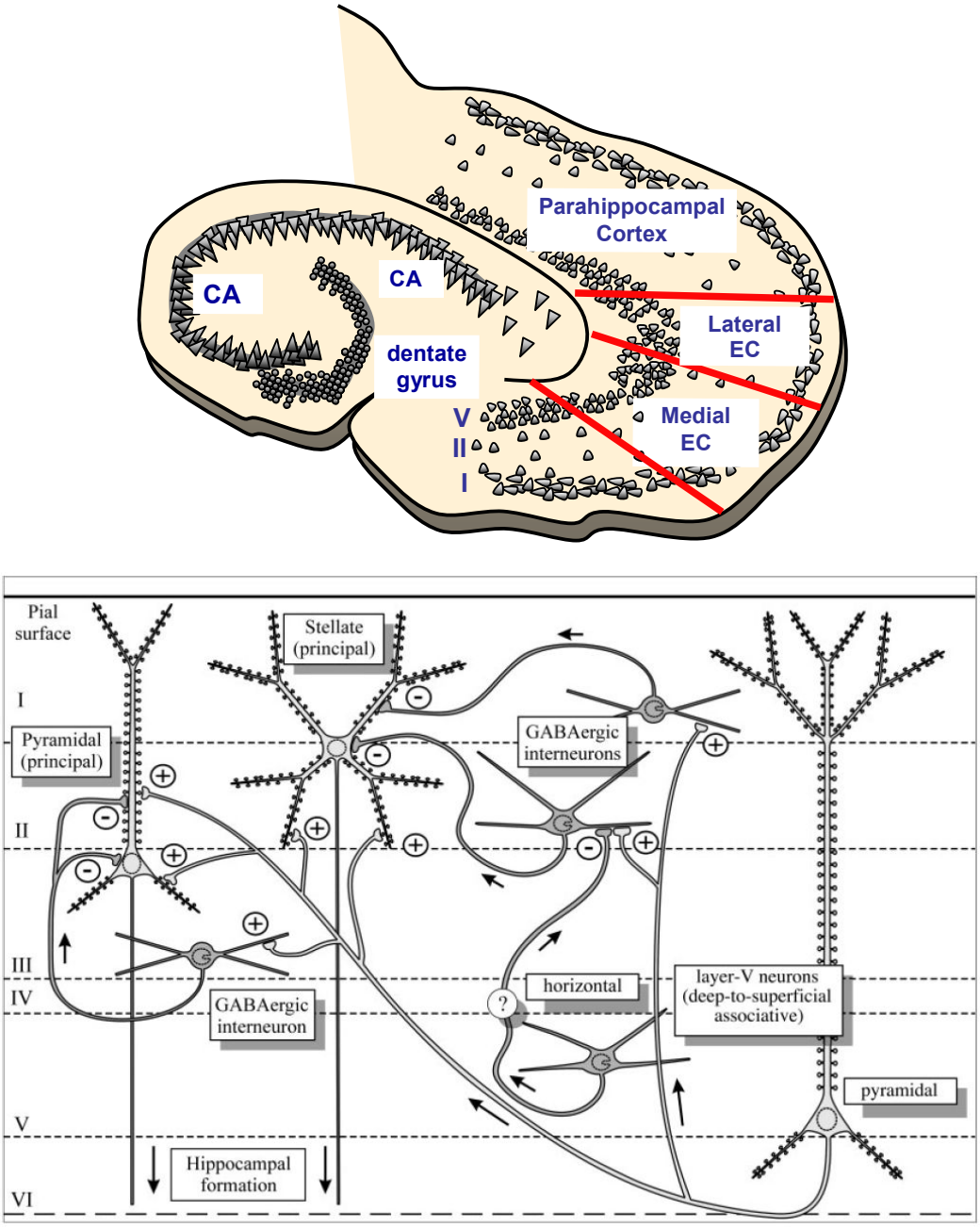

Figure 1.3: Laminar structure and intrinsic connectivity of the mEC. Top: Location of the mEC in the slice preparation used within the experiments in this thesis. Bottom: The principal cells (pyramidal in layers III and V, stellate in layer II) are well connected both to each other and to external structures such as the hippocampus and neocortex. There is a great deal of inhibitory control exerted upon the principal cells by the GABAergic interneurones, especially in the superficial layers. Diagram from van Haeften et al., 2003.

activity in layer V is subject to powerful frequency-dependent facilitation, and has been shown to cause repetitive firing and, in extreme cases, the generation of

synchronised population discharges (Jones, 1993, 1994; Cunningham *et al*., 2000). This facilitation would appear to be dependent upon the activity of NMDAr. Intracellular recordings show that layer V cells undergo a slightly larger degree of AMPAr-mediated facilitation than layer II cells, but the difference is not significant. However, NMDAr-mediated facilitation is clearly and significantly greater in layer V than in layer II (Jones and Woodhall, 2005).

Activity in layer II, contrastingly, is dominated by inhibition. Whereas low-frequency stimulation in layer V produced a greater proportion of excitatory activity, similar studies in layer II indicated that the majority of responses to this stimulation were $GABA_A$ mediated inhibitory events (Jones, 1994; Glovelli *et al*., 1997; Heinemann *et al*., 2000). However, this inhibitory dominance is highly dynamic. With increasing stimulation frequency, inhibitory interneurones in layer II become increasingly labile, to the point that activity in layer II shifts towards increased excitation at stimulation frequencies above 1 Hz (Jones, 1993, 1994, 1995; Glovelli *et al*., 1997). This frequency dependent depression of inhibitory activity is, however, even more pronounced in layer V, further emphasising the dominance of excitation in the deeper layers (Jones and Woodhall, 2005).

Lamina-specific Differences in Spontaneous Transmission

A presynaptic membrane does not have to be depolarised by an action potential in order to release neurotransmitter. Spontaneous release of single quanta is a feature thought to be common to all synapses, and enabled the formulation of the quantal theory of neurotransmission in the first place (Del Castillo and Katz, 1954; Sara *et al.*, 2005). During *in vitro* intracellular recording, principal neurones in the superficial layers of the mEC remain quiescent and do not fire action potentials constitutively, presumably due to the large amount of inhibitory innervation in layers II and III, as discussed above. However, this does not mean that there is no excitatory release on to

these cells, and patch clamp studies have shown a constant generation of EPSCs in these cells, due to the release of glutamate from surrounding neurones. It should be noted that this activity continues to some extent even in the presence of the voltage-gated sodium channel blocker tetrodotoxin (TTX), the remaining activity being termed as miniature excitatory post-synaptic currents (mEPSC) (Cunningham *et al.*, 2000).

These miniature and spontaneous events also exert a great deal of control over the target cell. A single excitatory quantum can cause the generation of an action potential in small postsynaptic neurones, whilst single inhibitory quanta may delay, or even suppress, postsynaptic firing (Lu and Trussell, 2000; Carter and Regehr, 2002). It has recently been shown that activity-independent miniature events are mediated by the release of neurotransmitter from a distinct population of presynaptic vesicles, i.e. a separate pool from vesicles releasing neurotransmitter in response to action potentials (Sara *et al.*, 2005).

Our laboratory has carried out a range of studies investigating this spontaneous activity in the EC, using whole-cell voltage clamp to monitor spontaneous EPSCs and IPSCs. Neurones throughout the EC are constantly bombarded with both glutamate and GABA, released spontaneously from surrounding pre-synaptic boutons (Berretta and Jones, 1996a; Bailey *et al*., 2004; Woodhall *et al*., 2004; Jones and Woodhall, 2005).

Excitation

Spontaneous excitatory activity, mediated by glutamate release, has been shown in both layer II and layer V to be largely independent of action potential activity, as the addition of TTX caused only a 15-20% reduction in sEPSC frequency (Berretta and Jones, 1996a). Comparing the baseline levels of spontaneous activity between deep

and superficial layers, average frequency of sEPSC activity is slightly, but significantly, higher in layer V than in layer II. Additionally, the amplitude of sEPSCs in layer V is significantly greater (Berretta and Jones, 1996a; Jones and Woodhall, 2005). The reasons for this difference could be that excitatory terminals in layer V are more proximally located than in layer II, with evidence to suggest that layer II EPSCs are subject to a greater degree of dendritic filtering. Furthermore, recurrent excitatory connections in layer V of the mEC are very common, whilst being practically non-existent in superficial layers (Dhillon and Jones, 2000).

As well as frequency and amplitude differences, there would appear to be significant differences between the receptors mediating sEPSC activity in deep and superficial EC layers. Studies in Mg^{2+}-free artificial cerebro-spinal fluid (ACSF) indicate expression of functional NMDAr in both layer II and layer V of the mEC. However, R-AP5 sensitive events were considerably more frequent in layer V, and a significant R-AP5 sensitive component exists within layer V sEPSCs recorded in normal ACSF, something not seen in layer II. This could suggest a greater expression of NMDAr in layer V. Alternatively, the expressed NMDAr could be more available to spontaneously released glutamate in deeper layers, perhaps due to differences in the site of expression (Berretta and Jones, 1996a; Jones and Woodhall, 2005).

Inhibition

As mentioned above, spontaneous inhibition of neurones in the mEC arises from the constant release of GABA, activating $GABA_A$ receptors in the post-synapse. A secondary component, a standing inhibitory current mediated through tonic $GABA_A$r activation, has been proposed and located in areas such as the cerebellum and somatosensory cortex (Brickley *et al*., 1996; Salin and Prince, 1996). However, our laboratory has not been able to demonstrate such a component in any part of the mEC (Woodhall *et al*., 2004; Jones and Woodhall, 2005) in rats aged 6-9 weeks, an age

where tonic GABA conductance would be expected to be prominent (Hall and Usowicz, 1997).

sIPSCs in the mEC possess broadly the same pharmacological characteristics, regardless of layer. However, there are significant differences in spontaneous release of GABA when layers II and V are compared. sIPSCs have a baseline frequency of approximately 12 Hz in layer II, compared with 2.5 Hz in layer V. Additionally, layer II neurones exhibited frequent and sustained bursts of sIPSC activity. These bursts were also evident in layer V, but were less frequent and contained fewer events (Woodhall *et al*., 2004).

In contrast to the largely activity-independent EPSCs found in both deep and superficial layers, there are stark differences between the proportion of activity-dependent GABA release in layer V and layer II of the mEC. Addition of TTX caused a reduction of 1-2 Hz in both layers. However, the baseline frequency of IPSCs in layer II was approximately 10-fold greater than layer V. Therefore, layer II inhibitory activity is largely (≈ 90%) activity-independent, whereas the proportion of miniature and AP-dependent IPSCs in layer V is about 1:1 (Jones and Woodhall, 2005).

Background Activity and Cellular Excitability

As discussed in the previous section, there is a constant release of both excitatory and inhibitory neurotransmitter onto cells throughout the cortex. This constant, background release differs between layers, and can have effects on the properties of principal cells within these layers. Furthermore, there is significant evidence to suggest that this background activity, a form of synaptic “noise”, contributes to the enhancement of signal detection (Stacey and Durand, 2000, 2001) and integration (Destexhe and Pare, 1999; Ho and Destexhe, 2000), and modulates gain to affect the input-output characteristics of cells (Hausser and Clark, 1997; Stevens and Zador,

1998; Chance *et al*., 2002; Fellous *et al*., 2003; Wolfart *et al.*, 2005), e.g. gain modulation (Shu *et al*., 2003a) their resting properties (Pare *et al*., 1998a, b), their firing (Harsch and Robinson, 2000) and oscillatory behaviour (Dorval and White, 2005) through the phenomenon of stochastic resonance (Rudolph *et al*., 2004).

By way of illustration (see Fig. 1.4), we can imagine a weak signal as a sine wave that peaks just below the detection threshold (e.g. the firing threshold of a neurone). With a "clean" signal, the peaks of the wave will never breach the detection threshold, and the signal will never be acknowledged by the target neurone. However, if we introduce noise to the signal, at certain points additive noise will coincide with the peak of the wave, pushing the signal above threshold and enabling its detection.

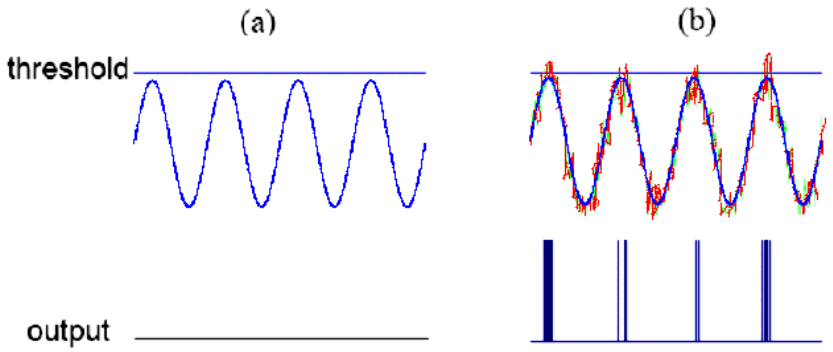

Figure 1.4: Random noise aids detection of subthreshold signals. A: A clean subthreshold signal never breaches the detection threshold, resulting in no output from the receiving cell. B: Addition of random noise, for example the constant background release of neurotransmitter, will eventually result in a peak subthreshold signal coinciding with additive noise, leading to a breach of the detection threshold and output from the target cell.

It is clear that the combination of action potential-dependent and -independent release, *in vivo* at least, provides a possible method to aid signal detection through stochastic resonance, where sub-threshold synaptic events are pushed above threshold due to the presence of background activity. Thus, the relative level of inhibitory and excitatory

background activity is a reflection of network activity and is instrumental in determining the excitability of any given neurone.

Changes in the level of background release are thought to be the cause of a range of network phenomena. There has been a great deal of recent research into the phenomenon of stochastic resonance in the modulation of neuronal and network properties, ranging from *in vitro* and *in vivo* electrophysiological approaches to *in silico* simulations of large neuronal networks (Hausser and Clark, 1997; Pare *et al.,* 1998a, b; Stacey and Durand, 2000, 2001; Rudolph *et al.*, 2004). This range of approaches has allowed the problem to be approached from both sides, the computational studies lead to modelling methods that can subsequently be used to extract more information from electrophysiological data, as will be discussed later.

In an intact brain *in vivo*, the level of background activity is so intense that it causes cortical neurones to attain a "high-conductance" state, in which the observed neurone is subject to such high levels of bombardment from surrounding cells that the membrane potential shows high-amplitude fluctuations and can be almost constantly depolarised (V_m around -65mV) when compared to quiescent cells in the absence of synaptic noise (Destexhe *et al.*, 2003; Rudolph and Destexhe, 2004). These high-conductance states are thought by some to be the cause of spontaneous sub-threshold depolarisations, "up-states", which are most prominently observed *in vivo* during slow-wave sleep and under certain types of anaesthesia. However, some contention exists as to how much background activity is necessary to cause these spontaneous depolarisations.

During intracellular recordings of principal neurones *in vivo*, and under certain conditions *in vitro*, the membrane potential of the observed neurone can be seen to suddenly undergo a sustained depolarisation, lasting several seconds and having an amplitude of as much as 20mV. These "up-states" would appear to be driven by

synchronised volleys of synaptic activity (Cowan and Wilson, 1994; Peterson *et al.*, 2003), leading to two distinct periods, one where neurones are subject to "normal" background activity, and another whereby increases in activity cause up- or high-conductance states. Steriade *et al.* (1993) first proposed the distinction of up-states as slow oscillations separate from other observed cortical rhythms found in sleep or under anaesthesia. These up-states were found exclusively in pyramidal cells with large dendritic arbours, in layers III-VI of several cortical areas (association, motor and visual). It has been proposed by Cossart *et al.* (2003) that such up-states represent "circuit attractors", an emergent network phenomenon that enables simple processing units (e.g. neurones) to function as highly complex computational units (Hopfield, 1982). This circuit attraction property may form the basis of memory retention or computational function in neuronal networks.

Waters and Helmchen (2004) show that up-states can be tracked throughout different parts of cortical neurones through matching with electrocorticogram (ECoG) recordings. By carefully matching patch-clamp recordings from somata, dendritic tufts and apical trunks with the time-course of up-states recorded with ECoG, it was concluded that up-state activity promotes action-potential back-propagation throughout the dendritic structure, with up-states occurring simultaneously across the entire neurone (instead of starting at one point and propagating outwards). Thus, up-state activity increases the back-propagation of action potentials and subsequently increases AP-mediated calcium influx in the distal apical dendritic tree; this increases the level of association between deep and superficial neurones *in vivo*, and serves as a feedback signal to enhance the accuracy of time-dependent signalling in active dendrites.

Background Release and the Generation of Up-States

The mechanistic causes of up-states are subject to some debate. It is entirely possible that the fluctuations investigated by various groups actually represent different manifestations of similar phenomena, however this does not explain the direct contradiction of certain theories on this matter. Destexhe *et al.* (2003) propose that up-states are high-conductance states triggered by intense cortical activity, and are representative of neuronal function in the awake state. This assertion was based on intracellular electrophysiology performed in awake behaving animals (e.g. Matsumura *et al.*, 1988; Baranyi *et al.*, 1993; Steriade *et al.*, 2001), where the recorded neurones were observed to have low input resistance (5 to 40 MΩ) and a depolarised, fluctuating membrane potential (-60 mV, σ_V 2-6 mV). These *in vivo* studies found consistent results regardless of the cortical area recorded.

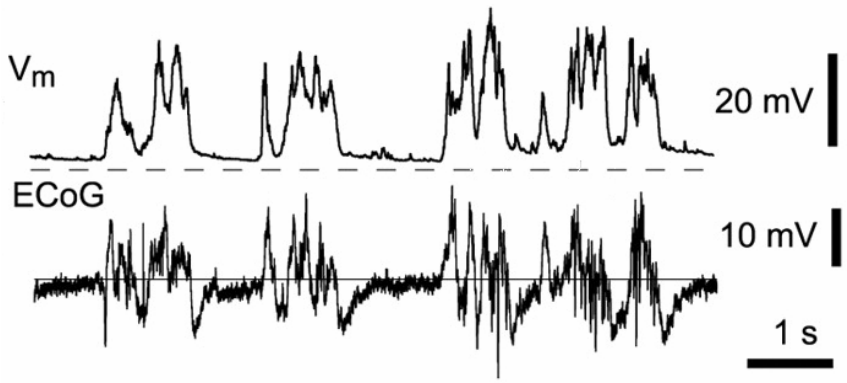

Figure 1.5: Up-state activity in the barrel cortex. The top trace is a whole-cell recording of up-states in the barrel cortex of an anaesthetised rat. The bottom trace is electrocorticogram activity, indicating a cortex-wide increase in activity during an up-state. Dashed line (top) indicates -80 mV, solid line (bottom) indicates 0 mV. Adapted from Waters and Helmchen, 2004

Waters and Helmchen (2006) contend this notion of large amounts of synaptic activity being necessary for the generation of up-states. Using a combination of patch-clamp and computational methods, they have proposed that background activity is less prominent than previously thought, and that relatively sparse amounts of excitatory activity are necessary to instigate an up-state. They also forward the notion that Destexhe's "high-conductance states" are, in fact, very small changes in the level of conductance (between 2-10 nS), with input resistance being increased by anomalous rectification. They account for differences in resistance and conductance measured by other groups to be a function of the level of action potential firing ongoing within the recorded neurones. This method of input resistance comparison has previously been rejected, however, by Destexhe *et al.* (2003), citing inconsistencies in the recording method and electrode properties between laboratories (and individual experiments) as being too variable to provide a reliable method of comparison. Furthermore, any comparison of resistance between *in vitro* studies, anaesthetised *in vivo* studies and awake behaving studies is confounded by the differences in cortical state between each approach – in the awake behaving animals, for example, the resistance changes markedly depending on what type of behaviour is being exhibited.

Differences seen between *in vitro* and *in vivo* cellular characteristics were elucidated by recordings in the presence of TTX (Pare *et al.*, 1998b). Under local perfusion of TTX *in vivo,* the recorded neurones displayed attributes closely resembling those of neurones found in acute slices. From this it was concluded that differences in activity between *in vitro* and *in vivo* recordings is due to activity-dependent neurotransmitter release *in vivo*, as opposed to any sort of cellular damage caused by the recording process, or differences between electrodes used *in vitro* and *in vivo*. Up-states can be reproduced *in vitro* by increasing overall background activity through careful adjustment of the perfused ACSF. Reducing the concentration of magnesium and increasing the concentration of potassium compared to "normal" levels simulates

increased activity across the slice by increasing NMDAr activity and lengthening action potential duration.

Using a reduced (1.25 vs 2.0 mM) Mg^{2+} concentration in the ACSF, Cunningham *et al.* (2006) were able to show that slow-wave oscillations or up-states in the EC are at least partly dependent upon the activity of GluR5-containing kainate receptors. Blockade of either NMDA or AMPA-type ionotropic glutamate receptors failed to abolish up-state generation (although the characteristics of the up-states were altered in the presence of the AMPA receptor antagonist SYM-2206). However, when the GluR5-specific antagonist, UBP-302, was added, up-state activity was abolished, both at the single-cell and network levels. Cunningham *et al.* (2006) proposed that slow-wave oscillations were highly dependent upon Glu-R5 KAr, but also partly governed by metabolic activity, based on oscillations are a function of ATP-modulated potassium channels. K_{ATP} blockade with tolbutamide led to prolonged "up" phases, and increasing K_{ATP} activity with diazoxide led to longer "down" periods. Blockade of K_{ATP} channels by MgATP slowed the transition between up- and down-state. The increased activity seen during up-states may cause rapid depletion of intracellular ATP, leading to K_{ATP} opening and the termination of the up-state.

Conductance Estimates from Membrane Fluctuations

The challenge of measuring background synaptic activity during high-conductance states has led to a range of approaches, as discussed previously. The most promising avenue would appear to be the combination of computational simulations with more traditional electrophysiology. This thesis uses a method developed by Alain Destexhe's group to quantify background levels of excitation and inhibition, at the same time, in the same cell, based on membrane voltage fluctuations recorded intracellularly from principal neurones.

The whole-cell voltage clamp approach used previously in our laboratory does not lend itself well to relating the level of background activity to cellular excitability. Generally, experimental recording conditions are established to record either excitatory or inhibitory currents in isolation. The somatic recording location means that more distally located currents may not be detectable. Most importantly, the inclusion of blockers of voltage-gated ion channels in the patch pipette solution, to improve space clamp etc., largely precludes meaningful estimates of cellular excitability. Sharp-electrode intracellular recording allows for the latter, but does not provide high enough electrical resolution for direct observation of small amplitude background synaptic events.

In 2004 Destexhe's group described a method of estimating global background synaptic conductances from measurement of fluctuations in membrane potential (termed VmD) derived from sharp electrode intracellular recordings (Rudolph *et al.,* 2004). The analytic expression of mean and standard deviation of membrane potential distribution permits simultaneous estimation of the global background excitation mediated by glutamate acting at AMPA receptors (E_{Bg}) and background inhibition (I_{Bg}, due to GABA acting via $GABA_A$ receptors). Importantly, the use of intracellular recording allows us to simultaneously obtain measurements of cellular excitability and, thus, to relate excitability to relative levels and changes in E_{Bg} and I_{Bg}.
The Destexhe group's approach to modelling background conductance from single-neurone recordings is based on two fundamental starting points, both having roots in stochastic calculus and the description of the time evolution of random processes.

The **Fokker-Planck equation** (see Eq. 6) is used to describe the time evolution of probability density functions for the velocity and position of a particle subjected to a Wiener process (Brownian motion). The equation can be used outside the confines of equations of motion in order to model processes with a relatively small number of important variables, with other factors varying in such a random and rapid manner

that they can be considered to be noise, very much like the membrane potential of a neurone in an active network. Consider that the spontaneous release of neurotransmitter onto a given cell can be described as a Poisson process (i.e. one that is random, orderly and without memory). Under intense periods of synaptic activity (high conductance states), the release of transmitter has an average frequency of 1 Hz for excitatory synapses and 5 Hz for inhibitory synapses (Destexhe and Pare, 1999). This barrage of synaptic activity causes the membrane potential to undergo a continuous random walk, and this potential distribution can be said to be a time-homogeneous Markov process (i.e. its future state does not depend upon its past state) that obeys the Fokker-Planck equation as an **Ornstein-Uhlenbeck** process.

The Ornstein-Uhlenbeck (OU) process (Uhlenbeck and Ornstein, 1930) is a stochastic process that can be used for describing low-pass filtered Gaussian white noise, which was originally forwarded in the 1930s as a model of Brownian motion:

$$dW(t) = mdV(t) + \beta V(t)dt \qquad \text{(Eq. 1)}$$

In this form (Eq 1.) the equation serves as an approximation of the one-dimensional Brownian motion of a particle in a liquid, where *W(t)* is a Wiener process (essentially white noise), *V(t)* is the particle's velocity, *m* its mass and $\beta V(t)$ is representative of a friction proportional to the velocity. The OU process is easily adapted to express a range of other situations such as harmonic motion or membrane voltage under synaptic bombardment simply by changing the meaning of the constants.

Rudolph and Destexhe (2003) use the OU process to describe the time-dependent probability density functions of several components of their neuronal models. By adapting the OU equation to predict the probable distribution of membrane voltage for a given set of conductances and cellular parameters, and then setting up a simultaneous equation using two levels of injected current to work the model backwards and predict conductances from membrane voltage distribution, they were

able to arrive at the VmD method, used in this thesis for all background conductance estimates.

The initial step (Destexhe *et al.*, 2001) was to describe the passive membrane properties of cortical neurones by the following equation (Eq 2):

$$C_m \frac{dV(t)}{dt} = -g_L(V(t) - E_L) - \frac{1}{a} I_{syn}(t) \qquad \text{(Eq. 2)}$$

Here $V(t)$ is membrane potential, C_m represents specific membrane capacitance (e.g. Gentet *et al.*, 2000), a is membrane area, g_L is leak conductance and E_L is leak reversal (this latter variable can be obtained through recordings of neurones in completely quiescent states). I_{syn} represents current mediated by receptors subject to synaptic bombardment. This passive membrane equation (Eq. 2) was incorporated (Eq. 3) into a point conductance model (Destexhe *et al.*, 2001; Rudolph *et al.*, 2004) which introduces a constant stimulating external current, I_{ext}.

$$C_m \frac{dV(t)}{dt} = g_L[E_L - V(t)] - \frac{1}{a} I_{syn}(t) + \frac{1}{a} I_{ext} \qquad \text{(Eq. 3)}$$

We now have two sources of current onto our passive membrane – the external stimulation I_{ext} and the synaptic noise, described by the total synaptic current $I_{syn}(t)$, which is split further into two independent components; excitatory conductance (with reversal potential) and inhibitory current (again with its own reversal potential). This current breakdown can be described by the following equation:

$$I_{syn}(t) = g_e(t)[V(t) - E_e] + g_i(t)[V(t) - E_i] \qquad \text{(Eq. 4)}$$

Here g_e and E_e are excitatory conductance and reversal, respectively, and g_i and E_i are inhibitory conductance and reversal. We see clearly from this equation that $I_{syn}(t)$ is merely the function of two distinct conductances over time, based on the *present* state of the membrane voltage ($V(t)$) and nothing else. The above-mentioned OU equation

can be used to describe the time-evolution of the excitatory and inhibitory conductances as a one-variable stochastic process:

$$\frac{dg_{\{e,i\}}(t)}{dt} = -\frac{1}{\tau_{\{e,i\}}}[g_{\{e,i\}}(t) - g_{\{e,i\}0}] + \sqrt{\frac{2\sigma^2_{\{e,i\}}}{\tau_{\{e,i\}}}}\chi_{\{e,i\}}(t) \qquad \text{(Eq. 5)}$$

In Equation 5, the concept of average conductances, describing the estimated mean level of excitatory (g_{e0}) and inhibitory (g_{i0}) activity mediated by AMPA and $GABA_A$ receptors, respectively, is introduced. Also taken into account are the time constants ($\tau_{\{e,i\}}$) of the receptors involved in mediating these currents. To make a workable model, these are taken to be AMPA and $GABA_A$ receptors, which are the main excitatory and inhibitory populations in cortical neurones. The random nature of synaptic activity is simulated by a white-noise process ($\chi_{\{e,i\}}$) described with zero mean and standard deviation σ_e and σ_i for excitatory and inhibitory noise respectively.

The point-conductance model described in Equations 3-5 was tested analytically and numerically against two more complex models (a single-compartment model and a detailed biophysical model) by Rudolph *et al.* (2004), using a NEURON simulation environment (Hines and Carnevale, 1997). It was concluded that the point-conductance model provided an estimation of synaptic conductance to a degree of accuracy comparable to the other, more detailed models, whilst being simpler (and faster) to simulate and more readily manipulated. Rudolph *et al.* found that the time course of the probability density function $\rho(V,t)$ of the membrane voltage (V_m) attaining voltage V at time t could be described by solving the Fokker-Planck equation for the point conductance model detailed above (as described in detail in Rudolph *et al.*, 2004). It was also observed that the voltage distribution for a neurone in an active network at physiological voltages (between around -70 and -50 mV) is only very weakly asymmetric, and could therefore be approximated to a Gaussian distribution. This allowed a simplified version of the Fokker-Planck equation for the point-conductance model to be derived, hence:

$$\rho(V) \approx \exp\left[-\frac{(V-\overline{V})^2}{2\sigma_V^2}\right] \qquad \text{(Eq. 6)}$$

Here $\rho(V)$ is the probability of voltage V, with $\overline{V}$ representing the average voltage and σ_V the standard deviation of the voltage distribution. This approximation can be further refined by replacing the exponential function in the Fokker-Plank with a Taylor expansion (a representative of a function calculated from single-point values of its derivatives) based on the maximum $\overline{V}$ of the probability $\rho(V)$. The Gaussian distribution of the voltage can then be based around the following equations:

(Eq. 7)

$$\overline{V} = \frac{S_1}{S_0} = \frac{E_L(2aC_m g_L) + E_e(2aC_m g_{e0}) + E_i(2aC_m g_{i0}) + E_e(\sigma_e^2\widetilde{\tau}_e) + E_i(\sigma_i^2\widetilde{\tau}_i) + 2aC_m I_{ext}}{(2aC_m g_L) + (2aC_m g_{e0}) + (2aC_m g_{i0}) + (\sigma_e^2\widetilde{\tau}_e) + (\sigma_i^2\widetilde{\tau}_i)}$$

This expression of the average voltage yields the Gaussian distribution:

(Eq. 8)

$$\rho(V) = \frac{1}{\sqrt{2\pi\sigma_V^2}}\exp\left[-\frac{(V-\overline{V})^2}{2\sigma_V^2}\right]$$

The variance is given by:

$$\sigma_V^2 = \frac{S_0^2(\sigma_e^2\widetilde{\tau}_e E_e^2 + \sigma_i^2\widetilde{\tau}_i E_i^2) - 2S_0S_1(\sigma_e^2\widetilde{\tau}_e E_e + \sigma_i^2\widetilde{\tau}_i E_i) + S_1^2(\sigma_e^2\widetilde{\tau}_e + \sigma_i^2\widetilde{\tau}_i)}{S_0^3}$$

(Eq. 9)

Here S_0 and S_1 are defined in the average voltage equation (Eq. 7). Using two levels of injected external current, two simultaneous equations are formed, which allows the model to be *inverted*, meaning that the values for synaptic conductance can be deduced from the voltage distribution over time. In practice, this involves taking the average and standard deviation of membrane voltage at two levels of injected current, and entering them into the following equation:

$$g_{\{e,i\}O} = \frac{(I_{ext1} - I_{ext2})[\sigma_{V_2}^2 (E_{\{i,e\}} - \overline{V}_1)^2 - \sigma_{V_1}^2 (E_{\{i,e\}} - \overline{V}_2)^2]}{[(E_e - \overline{V}_1)(E_i - \overline{V}_2) + (E_e - \overline{V}_2)(E_i - \overline{V}_1)](E_{\{e,i\}} - E_{\{i,e\}})(\overline{V}_1 - \overline{V}_2)^2}$$

$$- \frac{(I_{ext1} - I_{ext2})(E_{\{i,e\}} - \overline{V}_2) + [I_{ext2} - g_L a(E_{\{i,e\}} - E_L)](\overline{V}_1 - \overline{V}_2)}{(E_{\{e,i\}} - E_{\{i,e\}})(\overline{V}_1 - \overline{V}_2)}$$

(Eq. 10)

This (Eq. 10) is the equation central to the VmD method. It gives estimates of average background synaptic conductance, split into excitatory (g_{e0}, referred to in this thesis as E_{Bg}) and inhibitory (g_{i0}, referred to as I_{Bg}) components, based on the reversal potentials of AMPA and $GABA_A$ receptors and the passive membrane parameters such as leak conductance and input resistance. The estimates are based on working out the conductances from the membrane probability density outlined by the Fokker-Plank and Ornstein-Uhlenbeck functions used to construct the point conductance model, by finding the best-fitting parameters for a voltage distribution that is already there, rather than predicting the probable voltage generated by certain conductance parameters, the model is working *backwards* to glean information from real neurones.

The second part of the VmD equation (Eq. 11) calculates the variance (and hence standard deviation, SD) of the background synaptic conductances. This may provide important information concerning the level of synchronous activity in inhibitory and excitatory neurone populations. It has been suggested that an increase in SD in E_{Bg}, for example, would reflect increased synchronisation among principal neurones. As a result of coordinated firing, there would be time-locked release of glutamate from multiple terminals resulting in larger "peaks" of voltage changes. E_{Bg} and I_{Bg} variances are described by the following equation:

$$\sigma^2_{\{e,i\}} = \frac{2aC_m(I_{ext1} - I_{ext2})[\sigma^2_{V1}(E_{\{i,e\}} - \overline{V}_2)^2 - \sigma^2_{V2}(E_{\{i,e\}} - \overline{V}_1)^2]}{\widetilde{\tau}_{\{e,i\}}[(E_e - \overline{V}_1)(E_i - \overline{V}_2) + (E_e - \overline{V}_2)(E_i - \overline{V}_1)](E_{\{e,i\}} - E_{\{i,e\}})(\overline{V}_1 - \overline{V}_2)^2} \quad \text{(Eq. 11)}$$

This estimation of variance requires special treatment of the time constants of the modelled receptors ($\widetilde{\tau}_{\{e,i\}}$). These are referred to as "effective noise time constants", and their purpose is to improve the accuracy of the variance estimation by correcting for synaptic noise filtering effects. The time constants are defined as:

$$\widetilde{\tau}_{\{e,i\}} = \frac{2\tau_{\{e,i\}}\tau_0}{\tau_{\{e,i\}}} + \tau_0 \quad \text{where} \quad \tau_0 = \frac{aC_m}{ag_L + g_{e0} + g_{i0}} \qquad \text{(Eq. 12)}$$

Hence the time constants used in the variance estimation take into account the global background conductance estimates made in the first part of the VmD method.

The validity of the VmD method was tested by Rudolph *et al.* (2004) using a variety of methods. Firstly, two different computational models were run concurrently with VmD approximations. The VmD voltage distributions strongly agreed with those obtained through both a point conductance model and a more detailed, multi-synaptic model where noise was simulated by stochastic release from around 4000 synapses. A more demanding computational test of the method was performed by comparison with a highly detailed biophysical model, in which randomly firing synapses were distributed randomly across the soma and dendrites of the modelled "recorded" neurone. Once again, VmD-derived estimates of voltage distribution were in agreement with those obtained using the detailed model, however there was some slight discrepancy at the extreme ends of the distributions. Encouragingly, it was shown using this model that dendritic filtration of synaptic input, and active dendrites driven by voltage-sensitive currents (e.g. I_{Na}, I_{KA}, I_h) cause only minor deviations in the distributions of membrane potential and background conductance predicted by the VmD equations, that do not significantly affect the accuracy of the obtained estimates.

The final test of the reliability of the VmD method was performed using a dynamic clamp approach *in vitro*. Up-state firing cells were recorded and levels of I_{Bg} and E_{Bg} during up-state activity were estimated using the VmD method (Fig. 1.6). Stochastically fluctuating current, within the parameters estimated by the VmD equation, was then injected back into the same neurone. Upon current injection, an "artificial" up-state, closely resembling those fired spontaneously by the cell, was observed. Thus, VmD estimates are able to re-create the input to a principal neurone during an up-state, suggesting that the acquired estimates are an accurate portrayal of the synaptic activity around the observed neurone.

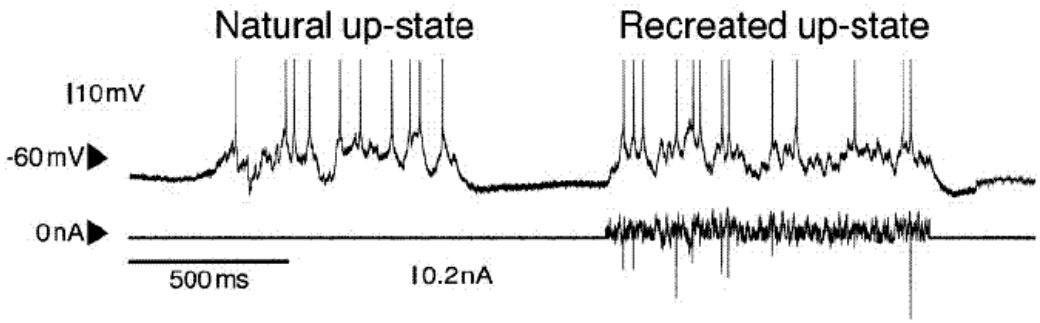

Figure 1.6: Artificial up-state activity. Using the conductance parameters gained from the VmD method, Rudolph et al. (2004) *were able to mimic up-state activity by injection of current during dynamic clamp recordings.*

In summary, it is clear that the EC is a vital brain structure, both in the normal function of the mammalian brain, and in its role in TLE. Equally clear is that background activity can exert a large amount of control over neurones throughout the cortex, leading to increased synchronisation and the appearance of high-conductance states, or up-states. Using the VmD method, I aim to link the levels of background conductance estimated with the above equations to levels of cellular excitability within the EC, and observe how one or both of these properties changes in the presence of a range of pharmacological tools.

Specific aims of this thesis:

- To test and verify the VmD method in principal cells in layers II, III and V of the mEC
- To characterise the changes in global conductance estimates mediated by a range of pharmacological tools, and link these changes to levels of cellular excitability
- To investigate the differences, if any, between conductance levels in different layers of the EC, especially with regards to seizure generation
- To observe the effects on background activity, and hence gain possible insight into the mode of action, of a range of poorly understood drugs, i.e. anticonvulsants

CHAPTER 2

METHODS

Introduction

All the experiments in this thesis were conducted in combined EC-hippocampal slices prepared from rat brain. The electrophysiological approach involved conventional, sharp-electrode intracellular recordings of membrane potential, made "blind" in slices maintained in an interface chamber. The majority of recordings were made from pyramidal neurones in layer III of the mEC. However, in one study (Chapter 5) comparison was made with stellate/pyramidal neurones of layer II and pyramidal cells in layer V.

Slice Preparation

Slices were prepared as originally outlined in Jones and Heinemann (1988). Three to four-week old male Wistar rats (50-70 g) were used in all experiments. Rats were either anaesthetised (ketamine 120 mg/kg and xylazine 80 mg/kg i.m.) and decapitated, or killed by cervical dislocation and decapitated. The entire brain was rapidly removed and placed in normal artificial cerebrospinal fluid (ACSF, see table 2.1) at ≈ 4°C. The cerebellum was removed, and the cerebrum dissected into two hemispheres by cutting the corpus callosum along the central sulcus. Sections of each cerebral hemisphere were removed by making a transverse incision several millimetres from the dorsal surface of the cerebrum, parallel to the base of the brain. This incision allows for a flat surface for mounting the brain during slicing.

The dissected cerebral hemispheres were attached by their cut dorsal surfaces to a Teflon slicing plinth using cyanoacrylate adhesive, and quickly rinsed using more ice-cold ACSF. The plinth and mounted brain were then transferred to the chamber of a Vibroslice (Campden Instruments, Loughborough, UK) filled with cold ACSF, continually gassed with 95% O_2 / 5% CO_2. Also included in the slicing solution was uric acid (300 μM), N-acetyl-cysteine (250 mM), indomethacin (45 μM) and

ketamine (200 μM). Empirical evidence from our laboratory shows that the COX inhibitor indomethacin greatly improves the quality of the obtained brain slices, with more viable cells, whilst the neuroprotective effects of anti-oxidants such as uric acid and N-acetyl-cysteine are well documented (Sekhon *et al.*, 2003; Jayalakshmi *et al.*, 2005). An improvement in slice viability is also gained through the use of ketamine, and this is likely to result from a reduction of excitotoxicity, mediated through a blockade of NMDA receptors (Church *et al.*, 1988; Fujikawa, 1995). These manipulations have been used in this laboratory for a number of years, and produce slices of high quality, with no evidence for any irreversible abnormal effects.

	Normal ACSF	**Recording ACSF**	**Up-state ACSF**
NaCl	126	126	126
KCl	3	3.75	3.75
$MgSO_4$	2	1.5	1.25
$NaHCO_3$	19	19	19
NaH_2PO_4	1.4	1.4	1.4
Glucose	10	10	10
$CaCl_2$	2	2	2

Table 2.1: Composition of artificial cerebrospinal fluid (mM)

Slices were cut with vibration set to 75% of the maximum speed of the vibroslice, moving from posterior to anterior at an ultra-slow pace (2-3 mm per minute). Once the hippocampal formation was clearly observed, along with the beginnings of the rhinal sulcus, slices were cut at 350-400 μM and transferred to a holding chamber (BSC-PC, Harvard Instruments, USA) for recovery. Slices containing the EC and hippocampus were dissected from the horizontal sections, with appearance shown in Fig. 1.3. Slices were cut and retained until the rhinal fissure was no longer apparent in the tissue block. This led to slices containing all hippocampal areas (e.g. CA1-3, dentate gyrus), subiculum, lateral and medial EC and part of the remainder of the parahippocampal cortex. mEC layers were identified based on their distance from the

A

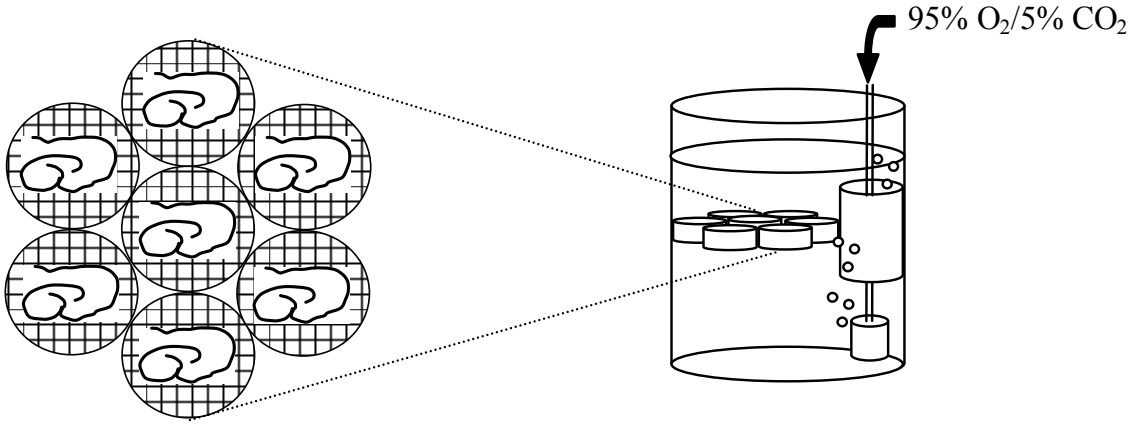

B

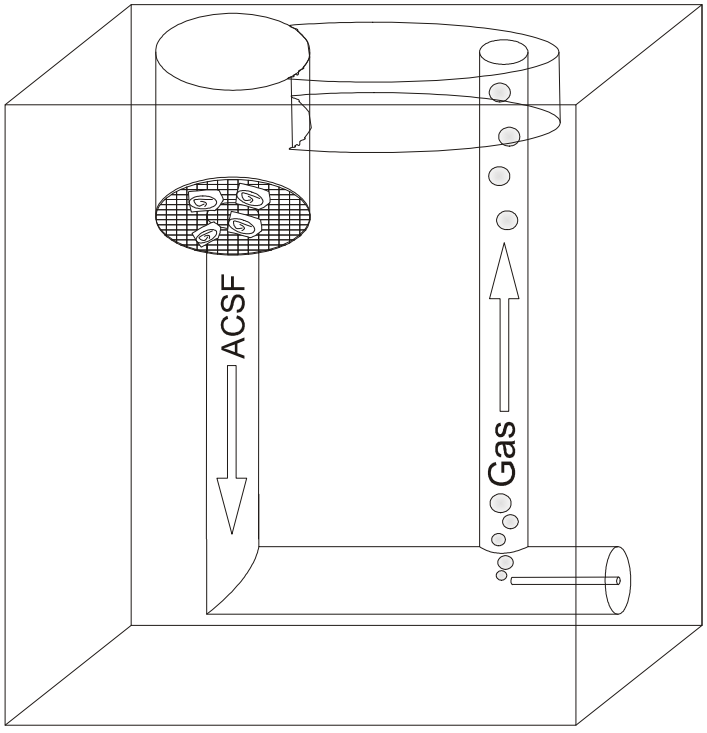

Figure 2.1: Design of brain slice holding chambers. A: Original in-house chamber constructed from syringes. B: Harvard BSC-PC made from machined Perspex. After cutting, slices are immediately transferred to the holding chamber, where they sit on a nylon mesh, fully submerged in ACSF. Carbogen gas (95% O_2 5% CO_2) is bubbled through the chamber, causing the ACSF to circulate, and ensuring that the slices are well oxygenated. Slices in these chambers can stay viable for 6-8 hours after slicing.

pia and the position of the *lamina dessicans*, if apparent. In all experiments in this thesis, no attempt was made to distinguish results obtained from ventral slices as opposed to those from more dorsal levels.

The slices were allowed to recover at room temperature for at least one hour before recording. The holding chamber for the slices was filled with normal ACSF, along with N-acetyl-cysteine (250 mM) and uric acid (300 μM). The chamber was gassed constantly with 95% O_2 / 5% CO_2 and was of a design that allowed gassed ACSF to freely circulate around the chamber, maintaining optimum conditions for slice preservation. Slices sat on a nylon net at the bottom of the main holding chamber, and were completely submerged. Two different holding chambers were used over the course of this project. Originally, I used a chamber constructed in-house from the barrels of plastic syringes and a 250 ml Pyrex beaker (Fig. 2.1A). More recently a commercially available holding chamber was substituted for this (Harvard BSC-PC; Fig. 2.1B), and subjective evidence suggests that this has provided a further increase in slice quality.

Intracellular Recording

After the recovery period, individual slices were transferred to the recording chamber for experimentation. The custom made chamber was of a standard interface design, with a heated water compartment below the recording area that maintained a constant temperature of 32°C in the recording chamber. The water in the heated compartment was maintained at around 35°C by means of a thermistor controlled power supply, in order to achieve a temperature of 32°C in the recording compartment. Carbogen gas (95% O_2 / 5% CO_2) was constantly bubbled through the distilled water in the bottom of the chamber to maintain a high degree of humidity above the slices and prevent desiccation. Vents in the side of the recording chamber allowed the humidified gas access to the slices.

Recording ACSF (or up-state ACSF) gassed with carbogen was perfused through the recording chamber using a peristaltic pump (Gilson Minipuls 3) at a rate of 1.0 to 1.5 ml/min. The ACSF was preheated to 28-30°C to prevent gas bubbles forming in the perfusion line and recording chamber. It was gassed with carbogen and had a pH of 7.3 at the recording temperature. The perfusion lines entered the heated water chamber before being directed in to the recording chamber. Slices were placed on a nylon mesh with the pial surface of the EC facing away from the ACSF flow. Levels of ACSF in the recording chamber were altered using a nylon wick positioned downstream of the slice. The wick directed the ACSF to a drain hole at the bottom of the chamber, where fluid was removed by gravity to a waste bucket. Drug solutions were introduced by switching the perfused ACSF to a drug-containing ACSF using a three-way tap. Slices were allowed to equilibrate in the chamber for 15-20 minutes before recordings were attempted, to allow for anti-oxidant washout and recovery.

Borosilicate glass pipettes (Clark/Warner Omega Dot, 1.2 mm outer diameter, 0.69 mm internal diameter with internal filament) were pulled using a Flaming-Brown horizontal puller (Sutter Instruments P-87). Pipettes were filled with 3 M potassium acetate at least one hour before recording, and allowed to rest before use. Pipettes ideally had a resistance of 75-120 MΩ. This pre-fill method allows more stable recordings to be made as minute air bubbles are eliminated from the tip of the electrode during the resting period.

Intracellular membrane potential recordings were obtained using an Axoprobe 1A (Axon Instruments, USA) in bridge mode with a 0.1X headstage. Recordings were made using a blind approach. The tip of the pipette was placed on the surface of the slice under visual control, using a binocular microscope (Leica Wild-M8). At this stage stray pipette and junction potentials were offset to zero using the voltage offset control of the amplifier. Hyperpolarising current pulses (50 ms) were injected at 1 Hz via the recording electrode using the step-command input of the amplifier and driven

by a Master-8 pulse generator (AMPI, Israel). The voltage deflection induced by the pulse was then adjusted to zero using the bridge balance control of the amplifier. At the same time any capacitance transients associated with the onset and offset of the pulses were minimised using the capacitance compensation control.

The pipette was advanced slowly through the target area of the slice at a low speed using a Leitz manual micromanipulator, and the brief negative current pulses were continued. When an increase in resistance at the pipette tip occurred, signified by an increase in the voltage deflection during the current pulses, the Buzz control of the Axoprobe was briefly activated to attempt penetration of the potential cell at the pipette tip. During the buzz an oscillating voltage is applied to the pipette via the head stage capacitor, and the duration, frequency and amplitude of the voltage are set by amplifier controls. The mechanism by which this oscillation aids electrode penetration remains unknown, but it is highly effective.

If a successful penetration was made, then constant hyperpolarising current was also injected in to the cell (0.1 – 1.0 nA) via a manual DC current command before starting recordings. This current injection stabilises the neurone at a negative potential and helps recovery from penetration. It is gradually removed as the membrane potential of the neurone stabilises towards a normal resting state. Any neurone that fired action potentials spontaneously when all manual current was removed was discarded from analysis. Neurones accepted for experimentation had stable resting potentials of > -65 mV and action potentials that overshot zero by at least 10 mV. Data were stored on a Microsoft Windows based PC and acquired using a Digidata 1200B analogue to digital converter and Axoscope software (both Axon Instruments, USA). Recordings were digitised at 5 kHz and filtered at 2 kHz.

Patch Clamp Recording

To further support the data obtained from the intracellular recordings, voltage clamp recordings of both inhibitory and excitatory spontaneous post-synaptic currents (sIPSC/sEPSC) were made from pyramidal neurones in layer III of the mEC. These spontaneous events are caused by the constant background release of both glutamate and GABA from synapses onto the recorded cell. Patch-clamp recordings of spontaneous events offer a more direct measurement of background excitation and inhibition, although these cannot be recorded at the same time, in the same cell.

Individual slices were transferred (after recovery period) to a submersion chamber (Warner Instruments, Platform P1 with an RC-22C bath) perfused with normal gassed ACSF maintained at 31°C ± 1°C by an inline heater (Warner Instruments, SH-27B with TC-324 controller), and allowed to re-equilibrate for 20 minutes. Slices were visualised using a Zeiss Axioskop upright microscope and a differential phase-contrast infra-red CCD system (Sony XC-77CE) with a CE-4 contrast enhancer (BRSL, Newbury, UK) to further improve visualisation of the slices.

Borosilicate patch pipettes (Harvard PG120T-10, 1.2 mm OD, 0.93 mm ID) were pulled to a resistance of 1-4 MΩ using a Flaming-Brown type horizontal puller (Sutter Instruments P-87) and filled with either IPSC or EPSC patch solution, as described in Table 2.2. Before recording, the osmolality of the solution was measured using an Advanced Instruments M3300 Micro-osmometer. Solutions were diluted until the measured osmolality was 285 mOsmol/kg. pH was adjusted to 7.3 using CsOH. The patch solutions both contained the sodium channel blocker QX-314 to improve space clamp, and each solution was tailored to eliminate any unwanted activity i.e. the EPSC solution minimised IPSC activity and vice versa. These are the two primary reasons why our patch clamp method is not suitable for the simultaneous

measurement of inhibition and excitation, coupled with cellular excitability measurements, which the VmD method allows in intracellular recording.

Pyramidal cells were visually selected from layer III of the mEC. No attempt was made to unequivocally identify the cells as pyramidal by dye injection, however all recorded cells possessed a clear pyramidal morphology. The micropipette was introduced to the cell membrane and a gigaseal was obtained through mouth suction. An Axon Instruments Axopatch 200B was used in voltage clamp mode (all cells were clamped at -60 mV) to record excitatory or inhibitory post-synaptic current events, dependant on the patch solution used. Access resistance was monitored at regular intervals, and if this changed by more than 10% during the course of the recording, the cell was rejected. Reversal potentials for both solutions were 0 mV.

	EPSC Solution	**IPSC Solution**
CsCl	0	100
HEPES	40	40
QX-314	1	1
EGTA	0.6	0.6
$MgCl_2$	0	5
NaCl	2	0
TEA-Cl	5	10
Phosphocreatinine	10	10
D-Gluconate	100	0
Mg-Gluconate	5	0
ATP-Na	4	4
GTP-Na	0.3	0.3

Table 2.2: Composition of patch solutions (mM)

Recordings were stored using an Axon Instruments Digidata 1200B analogue to digital converter and saved directly to the hard disc of a Windows PC using Axoscope software (Molecular Devices, USA). Recordings were digitised at 20 kHz, and filtered at 2 kHz. Analysis of spontaneous EPSCs and IPSCs was performed off-line using MiniAnalysis software (Synaptosoft, USA). Spontaneous events were detected using

a threshold-crossing algorithm, and their inter-event interval (IEI), amplitude and 50% decay time were determined. Event detection threshold was adjusted for each neurone, to obtain the smallest events discernable from the baseline noise of the recording, and maintained at the same level throughout the analysis of that neurone. 200 consecutive events were analysed from both control and drug conditions of each neurone.

These patch recordings were also used to obtain decay-time data for use with the SD estimation equation used in the VmD method. 95% decay times of both IPSCs and EPSCs were analysed using Mini-Analysis software (Synaptosoft, USA) and used to calculate the effective time-constants applied to the VmD method, as outlined in Chapter 1. These were chosen after consultation with Alain Destexhe.

Reversal Potential Measurements

In order to use the previously discussed VmD method (see Chapter 1), several parameters characterising the recorded cells were needed. Reversal potentials for AMPA and $GABA_A$ receptors, as well as leak conductance reversal, were required for each population of cells to be studied. Ideally, all these parameters should be determined for each neurone individually, but this is clearly impractical. Thus, a series of experiments was performed to obtain average reversal potentials for each layer of the mEC, which were then used in all later VmD estimations.

Reversal potentials for AMPAr and $GABA_A$r were obtained using evoked synaptic responses in the presence of a number of antagonists, at a range of membrane voltages. AMPAr mediated EPSP reversals were obtained in the presence of the $GABA_A$ antagonist bicuculline (10 μM), the $GABA_B$ antagonist CGP-55845A (5 μM), the NMDA antagonist 2-AP5 (30 μM) and the GluR5-specific kainate antagonist UBP-302 (20 μM). A bipolar stimulating electrode was placed on the surface of the slice in layer V of the lateral EC. Synaptic responses were evoked using monopolar, square-

wave pulses (0.1 ms duration, 5-30 V) delivered via the stimulating electrode at 0.05 Hz using an isolated stimulator (AMPI Iso-flex, Israel) driven by pulses from the Master-8. The amplitude of the evoked AMPAr mediated EPSPs was set at about 85% of maximal, and they were recorder over a range of membrane voltages set by manual DC injection through the recording electrode. The first responses were measured at around -100 mV, and membrane voltage was then decreased in 5 mV steps until the recording became unstable (usually at around -40 mV), due to the failure of the pipette to pass current. Bridge balance was monitored throughout and adjusted as necessary. Five EPSPs were evoked at each voltage level, and these were averaged, graphed and extrapolated to determine the reversal potential.

For $GABA_A$r reversal potentials, the same procedure was carried out. The blocking cocktail consisted of CGP-55845A (5 μM), 2-AP5 (30 μM), UBP-302 (20 μM) and the AMPAr receptor antagonist NBQX (10 μM).

Leak reversal potential is essentially the resting membrane potential of the cell when all synaptic activity is abolished. Ions flowing around the site of impalement, through voltage-dependent channels and by active transport all contribute to the resting potential of the cell, even without EPSPs and IPSPs mediated by synaptic activity. Using TTX in this instance is not appropriate, due to the constant background release of neurotransmitter from synapses surrounding the cell. Even when action potential activity is abolished, miniature EPSC/IPSC activity is still observed due to release of neurotransmitter from a distinct pool of vesicles at the pre-synaptic membrane (Sara *et al*., 2005). Instead, the AMPAr and $GABA_A$r reversal potential blocker cocktails were combined, to ensure that all major receptors were blocked. 10 minute recordings of membrane potential were then made after a resting period of 20 minutes from first impalement.

The VmD Method

Using the mean data collected for AMPAr, $GABA_Ar$ and leak reversal potentials, and employing the intracellular recording method detailed above, the VmD method (Rudolph *et al.*, 2004) was used to gain estimates of background excitatory (E_{Bg}) and inhibitory (I_{Bg}) conductance levels in principal cells of the mEC. When a stable intracellular impalement was obtained, resting membrane potential was recorded for a period of 10-15 minutes. At intervals thereafter, neurones were depolarised (for 10-15 seconds) to two sub-threshold levels by injection of known positive currents (I_{ext1} and I_{ext2}) via the recording electrode (Fig. 2.2B). The values of the currents differed from neurone to neurone, but were maintained the same throughout any individual experiment. I_{ext2} was chosen to elicit a depolarisation to within 1-2 mV of action potential threshold and I_{ext1} was adjusted to depolarise the neurone to about halfway between I_{ext2} and resting membrane potential.

Membrane potential fluctuations at these two levels were fitted to Gaussian distributions and the mean and standard deviation of the membrane potential determined (Fig. 2.2C). Leak conductance in each neurone was calculated from the ohmic response produced by a small (0.1-0.3 nA, 100 ms) hyperpolarising current, injected at resting membrane potential. This leak value was not found to differ significantly at the depolarising currents, as long as the amplifier bridge was properly balanced.

These parameters, together with the mean reversal potentials derived from preliminary experiments, allowed us to apply the VmD equation (Fig. 2.2D; Eq. 10 and 11 in Chapter 1) to quantify background inhibitory and excitatory conductances resulting from global network input onto individual neurones.

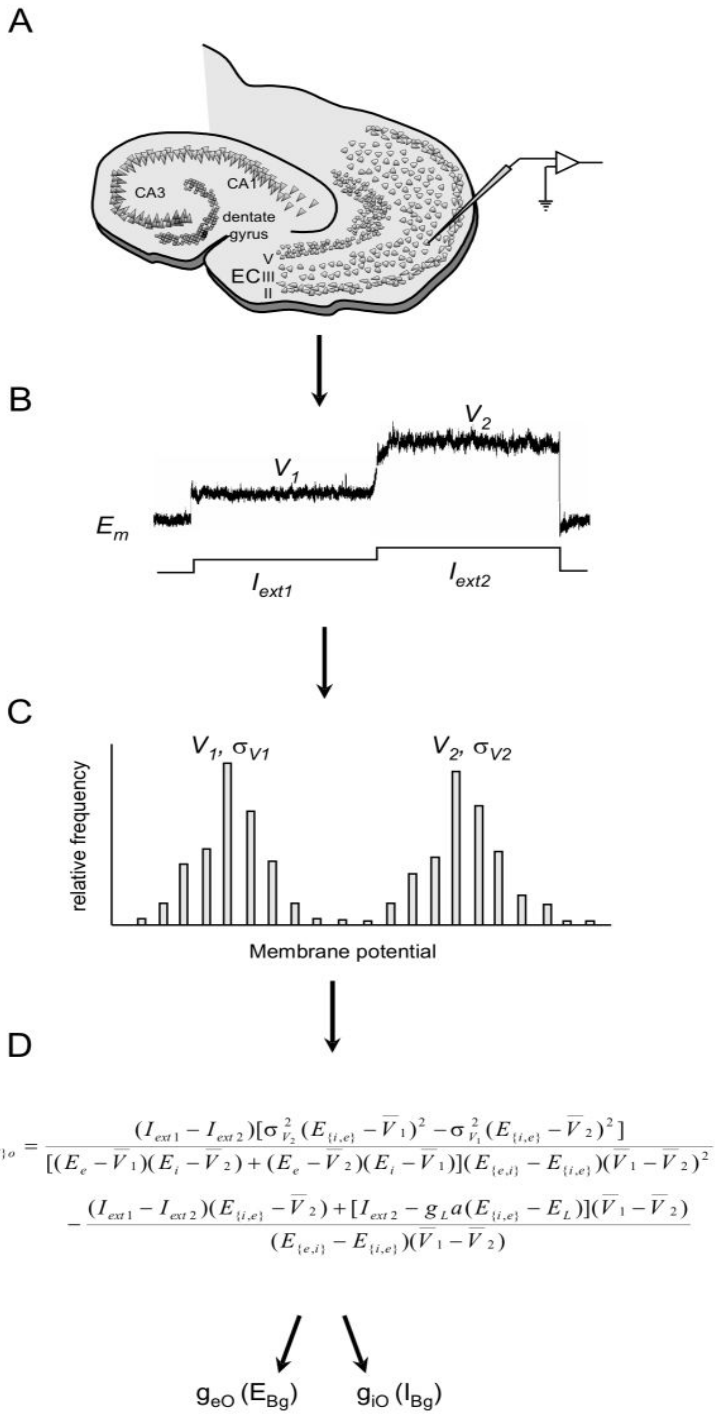

Figure 2.2: The VmD Method. A: Intracellular recordings were made from pyramidal neurones in slices of rat EC. B: At intervals, the membrane potential was depolarised by injection of two known external currents I_{ext1} and I_{ext2}. C: Membrane potential fluctuations at each current level were fitted to Gaussian distributions and the mean and standard deviation determined. D: These values, together with previously determined reversal potentials for AMPAr (E_e) and $GABA_A$ (E_I) and the leak conductance (g_La) obtained during each recording, were used to calculate I_{Bg} and E_{Bg} using the VmD method outlined by Rudolph et al. (2004).

Example Calculation

What follows is a step-by-step calculation of the conductance and standard deviation values for one VmD run from a single neurone. This was a layer III pyramidal cell recorded under control conditions (i.e. normal ACSF and no added drug). Resting membrane potential was -75.6 mV.

External Current 1 (I_{Ext1})	0.15 nA
External Current 2 (I_{Ext2})	0.33 nA
Excitatory Reversal (E_E)	6.6 mV
Inhibitory Reversal (E_I)	-66.7 mV
Average Voltage 1 (V_1)	-68.7 mV
Average Voltage 2 (V_2)	-60.3 mV
Standard Deviation 1 (σ_1)	0.6 mV
Standard Deviation 2 (σ_2)	1.22 mV
Membrane Area (a)	34636 μm^2
Specific Membrane Capacitance (C_m)	1 $\mu F/cm^2$
Excitatory Decay Time (τ_e)	13.65 ms
Inhibitory Decay Time (τ_i)	29.05 ms
Cellular Leak Conductance (ag_L)	20 nS

The equation must be calculated in a specific order. First, the conductances must be determined (Eq. 10, Chapter 1), as they need to be inserted in to the equation that determines the standard deviation.

$$g_{\{e,i\}O} = \frac{(I_{ext1} - I_{ext2})[\sigma_{V_2}^2 (E_{\{i,e\}} - \overline{V}_1)^2 - \sigma_{V_1}^2 (E_{\{i,e\}} - \overline{V}_2)^2]}{[(E_e - \overline{V}_1)(E_i - \overline{V}_2) + (E_e - \overline{V}_2)(E_i - \overline{V}_1)](E_{\{e,i\}} - E_{\{i,e\}})(\overline{V}_1 - \overline{V}_2)^2}$$

$$- \frac{(I_{ext1} - I_{ext2})(E_{\{i,e\}} - \overline{V}_2) + [I_{ext2} - g_L a(E_{\{i,e\}} - E_L)](\overline{V}_1 - \overline{V}_2)}{(E_{\{e,i\}} - E_{\{i,e\}})(\overline{V}_1 - \overline{V}_2)}$$

Excitatory and inhibitory conductances are calculated separately from each other. To achieve the value for excitatory conductance, we substitute the correct parameters into the VmD equation, thus:

$$g_{\{e\}o} = \frac{(0.15nA - 0.33nA)[0.6mV^2(-66.7mV - -68.7mV)^2 - 1.22mV^2(-66.7mV - -60.3mV)^2]}{[(6.6mV - -68.7mV)(-66.7mV - -60.3mV) + (6.6mV - -60.3mV)(-66.7mV - -68.7mV)](6.6mV - -66.7mV)(-68.7mV - -60.3mV)^2}$$

$$- \frac{(0.15nA - 0.33nA)(-66.7mV - -60.3mV) + [0.33nA - 20nS(-66.7mV - -79.0mV)](-68.7mV - -60.3mV)}{(6.6mV - -66.7mV)(-68.7mV - 60.3)}$$

This simplifies to:

$$g_{e0} = \frac{1.58E^{-21}}{-1.80151E^{-9}} - \frac{4.46E^{-13}}{-6.16E^{-14}}$$

Which gives an excitatory conductance value (g_{eo}, referred to in this thesis as E_{Bg}) of 0.724 nS. Recalculating this equation for g_{io} (referred to in this thesis as I_{Bg}) gives an inhibitory conductance value of 3.45 nS, with and I:E ratio of 4.8.

The next stage is to calculate the standard deviation of the conductance components (Eq. 11, Chapter 1), which may provide some insight into the level of synchronisation within the network (Rudolph *et al*., 2004).

$$\sigma^2_{\{e,i\}} = \frac{2aC_m(I_{ext1} - I_{ext2})[\sigma^2_{V1}(E_{\{i,e\}} - \overline{V}_2)^2 - \sigma^2_{V2}(E_{\{i,e\}} - \overline{V}_1)^2]}{\widetilde{\tau}_{\{e,i\}}[(E_e - \overline{V}_1)(E_i - \overline{V}_2) + (E_e - \overline{V}_2)(E_i - \overline{V}_1)](E_{\{e,i\}} - E_{\{i,e\}})(\overline{V}_1 - \overline{V}_2)^2}$$

Additionally, the effective noise time constant must be calculated, using the following:

$$\widetilde{\tau}_{\{e,i\}} = \frac{2\tau_{\{e,i\}}\tau_0}{\tau_{\{e,i\}}} + \tau_0 \quad \text{where} \quad \tau_0 = \frac{aC_m}{ag_L + g_{e0} + g_{i0}}$$

Substituting the necessary values into these equations, we get:

$$\sigma^2_e = \frac{-6.23E^{-20} \times 8.79E^{-12}}{4.29E^{-2} \times (-1.80151E^{-9})}$$

Taking the square root of this gives us a standard deviation of 84 pS for g_{eo}, with a value of 0.12 nS for g_{io}.

Excitability Measurements

Since the intracellular recordings were performed blind, it was imperative to properly characterise their electrophysiological properties in order to identify which cells were being recorded and ensure that pyramidal cells only were studied. Identification of interneurones, pyramidal and spiny stellate cells could all be achieved through a comparison of their resting potential, action potential characteristics and response to injected current (e.g. Heinemann *et al.*, 2000). In the majority of recordings (layer III), pyramidal cells were selected that exhibited no constitutive firing and maintained a resting membrane potential of between -65 and -80 mV.

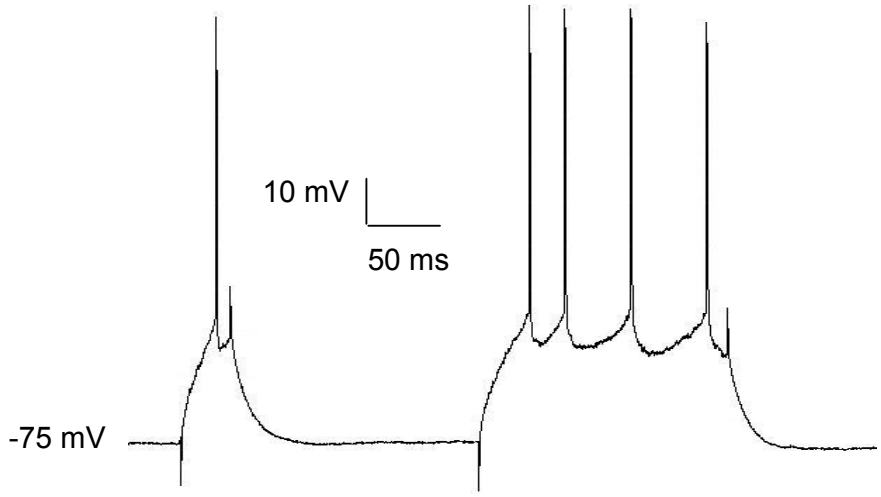

Figure 2.3: Response of layer III pyramidal cell to depolarising current. Left – a single action potential evoked by a 50ms depolarising current pulse. Right – a train of spikes generated by a supra-threshold 250 ms depolarising pulse.

The current pulses used to characterise the recorded cell-type were also used to gauge cellular excitability. Between periods of VmD measurements, the step-command input of the amplifier, driven by pulses from the Master-8, was used to inject depolarising pulses (0.1-1.0 nA) via the recording electrode. These pulses were of two types: short (50 ms) pulses with amplitude incrementally increased so that one action potential was evoked at the peak of the depolarisation, and longer (250 ms) suprathreshold

pulses, eliciting a train of action potentials. The short pulses allowed firing threshold (from rest) to be determined, and the longer pulses provided a measure of firing frequency. These parameters allowed cellular excitability to be quantified. These measurements were carried out throughout the recording, in order to constantly monitor cellular excitability and ensure that the recorded cell was healthy and viable.

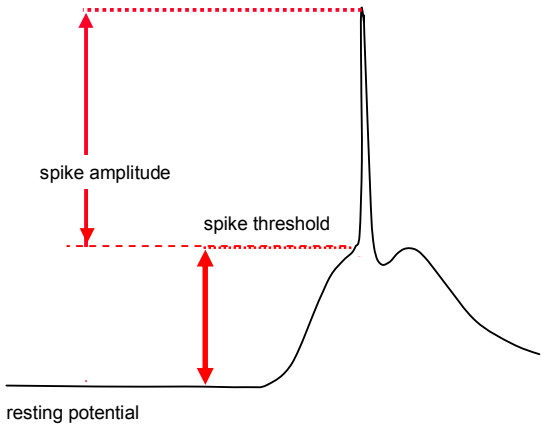

Figure 2.4: Measurement of cellular excitability from single evoked action potential. Higher spike threshold would indicate a lower probability of action potential formation, suggesting that the recorded cell is less excitable. Spike amplitude is measured to investigate the actions of the observed drugs on voltage-gated sodium channel activity, and ensure that cells remain viable throughout recording.

Results and Statistics

All values are expressed as mean ± standard error. Unless otherwise noted, all statistics are paired Student's t-tests with a threshold of P=0.05. Where one-way ANOVA have been used to compare multiple groups, Bonferroni post-hoc tests were performed on all groups where P<0.05. Statistical analysis and membrane frequency distributions were calculated using GraphPad Prism 4 software. VmD method calculations were performed using Microsoft Excel 2003.

List of Drugs Used

Unless otherwise stated, all drugs were dissolved in de-ionised water.

R-AP5 ([R]-2-amino-5-phosphonopentanoic acid; NMDA receptor antagonist; Tocris)

4-AP (4-aminopyridine; potassium channel blocker; Tocris, dissolved in 50% dimethylsulphoxide)

Bicuculline methiodide ([R-(R*,S*)]-5-(6,8-dihydro-8-oxofuro[3,4-e]-1,3-benzodioxol-6-yl)-5,6,7,8-tetra-hydro-6,6-dimethyl-1,3-dioxolo[4,5-g]isoquinolinium iodide; $GABA_A$ antagonist; Tocris)

Carbenoxolone (3β-hydroxy-11-oxoolean-12-en-30-oic acid 3-hemisuccinate; gap junction blocker; Sigma-Aldrich, UK)

CGP-55845A ((2S)-3-[[(1S)-1-(3,4-dichlorophenyl)ethyl]amino-2-hydroxypropyl](phenylmethyl)-phosphinic acid; $GABA_B$ antagonist; Tocris)

Ethosuximide (2-Ethyl-2-methylsuccinamide; anticonvulsant; Sigma-Aldrich, dissolved in 20% ethanol)

Felbamate (2-Phenyl-1,3-propanediol dicarbamate; anticonvulsant; Sigma-Aldrich)

Gabapentin (1-(aminomethyl)cyclohexaneacetic acid; anticonvulsant; Tocris)

GYKI-53655 (1-(4-aminophenyl)-3-methylcarbamoyl-4-methyl-3,4-dihydro-7,8-methylenedioxy-5H-2,3-benzodiazepine; AMPA receptor antagonist, gift from Dr Dick Evans, Bristol University)

Lamotrigine (6-(2,3-dichlorophenyl)-1,2,4-triazine-3,5-diamine; anticonvulsant; Tocris)

NBQX (6-nitro-7-sulfamoylbenzo[f]quinoxlone-2,3-dione disodium; AMPA/Kainate receptor antagonist; Tocris, UK)

PDC (L-trans-pyrrolidine-2,4-dicarboxylic acid; excitatory amino acid transporter blocker; Tocris)

Phenytoin (5,5-diphenylhydantoin; anticonvulsant; Sigma-Aldrich)

QX-314 bromide (N-(2,6-dimethylphenylcarbamoylmethyl)triethylammonium bromide; Na-channel blocker; Tocris)

Sodium Valproate (Anticonvulsant; Sigma-Aldrich)

Tiagabine ((3S)-1-[4,4-bis(3-methylthiophen-2-yl)but-3-enyl] piperidine-3-carboxylic acid; GABA uptake blocker/anticonvulsant; gift from Dr John Lambert, Aarhus University, Denmark)

TMA (Trimethylamine; Gap junction opener; Sigma-Aldrich)

TTX (Tetrodotoxin; Na-channel blocker; Alomone Labs, Israel)

UBP-302 ((S)-1-(2-amino-2-carboxyethyl)-3-(2-carboxybenzyl)pyrimidine-2,4-dione; selective GluR5 antagonist; gift from Dr David Jane, Bristol University)

CHAPTER 3

EVALUATION OF THE VmD METHOD IN THE EC

Introduction

In order to be confident in the abilities of the VmD method, its limitations and its ability to measure predictable effects of known pharmacological tools on global background conductance needed to be investigated. In this Chapter, I will outline the methods used to construct and limit the VmD method, and observe the effect of common drugs on background conductance (and hence network activity) in layer III of the mEC.

The global background conductances estimated by the VmD method represent the activity of the network in which the observed neurone is embedded. Drugs that change the activity of the network as a whole will therefore have a marked effect on the estimated conductances. The relative changes between I_{Bg} and E_{Bg} therefore provide insight in to the relationship between the two major neurone populations of the network, the principal, excitatory glutamatergic cells and inhibitory GABAergic interneurones.

Spontaneous transmitter release at central synapses has two components, that driven by sodium-dependent action potentials (APs) invading the presynaptic terminal, and an AP-independent component which reflects quantal release. AP-dependent release is often multi-quantal, and depends on calcium entry through voltage-gated calcium channels. In contrast, AP-independent ("miniature") neurotransmitter release reflects stochastic release of transmitter quanta from individual vesicles, and can occur at basal calcium levels when APs are blocked. As noted in Chapter 1, the majority of spontaneous GABA and glutamate release in both layer V and layer II neurones of the EC consists of miniature events (Berretta and Jones, 1996a; Woodhall *et al*., 2004; Jones and Woodhall, 2005). Unpublished whole-cell voltage clamp recordings in our laboratory show that sIPSC frequency in layer III neurones is reduced by around 50-60% by addition of the voltage-gated sodium channel blocker TTX, whereas the toxin

only elicits a fall of around 20% in sEPSCs (Chamberlain and Jones, unpublished observations).

Activity-independent release can be isolated by blocking action potentials with TTX. I used this approach in the current experiments to determine what proportion of I_{Bg} and E_{Bg} were attributable to activity-dependent/independent release.

In the second series of experiments in this Chapter I attempted to induce a generalised increase in network activity by increasing the extracellular concentration of K^+ (to 7.5 mM from 3.75 mM control). This shifts the reversal potential of voltage-gated (and other) potassium channels to a less negative value (e.g. Charpak *et al*., 1990), causing a general depolarisation and slowing the repolarisation of neurones during action potentials. It is likely that this would result in increased spontaneous firing of neurones coupled with increased GABA and glutamate release. Thus, this approach should, to some extent, mimic a more *in vivo*-like situation, where spontaneous activity is considerably higher (Jones and Woodhall, 2005).

The voltage-gated potassium channel blocker 4-aminopyridine (4-AP) has been shown to increase the amplitude and frequency of spontaneous postsynaptic potentials, with convulsant properties at higher concentrations (Galvan *et al.,* 1982). 4-AP blocks A-type channels (Gustafsson *et al*., 1982), which have been shown to have no bearing on VmD estimates by Rudolph *et al*., (2004). However, blockade of these channels would be expected to prolong depolarisation at inhibitory and excitatory terminals, increasing release of both glutamate and GABA. In this Chapter I have used 4-AP at two different concentrations. The overall level of conductance for both inhibitory and excitatory components would be expected to rise with each concentration. Furthermore, the $GABA_A$r blocker bicuculline and the AMPAr blocker NBQX were applied in the presence of 4-AP to investigate the changes in conductance that would be precipitated by these drugs in a high-conductance state.

Methods

All recordings were made in layer III pyramidal neurones of the rat EC, obtained from juvenile male Wistar rats (50-70g). Typically, these neurones had a resting membrane potential of -72.2 ± 0.5 mV, input resistance of 79 ± 6 MΩ and action potential amplitude (from threshold) and half-widths of 72.1 ± 1.6 mV and 0.32 ± 0.01 ms, respectively. Reversal potentials for $GABA_A$ receptors were obtained by stimulation of white or grey matter near the recording site, in the presence of the NMDAr blocker R-AP5 (30 μM), the AMPA/kainate receptor antagonist NBQX (10 μM) and the $GABA_B$ receptor antagonist CGP-55845A (5 μM). Responses to electrical stimulation were measured at a range of membrane potentials (-100 to -50 mV) and extrapolated to obtain the reversal potential at V_m=0. Similarly, AMPAr reversal potentials were calculated in the presence of R-AP5, CGP-55845A and the $GABA_A$r antagonist bicuculline (10 μM). Leak reversal potentials were measured by recording the resting membrane potential in the presence of all four of the above antagonists. All cells were allowed to rest for 5-10 minutes after impalement before recording was attempted.

The majority of cells in this Chapter were recorded with K-Ac filled pipettes. In 6 neurones, intracellular recordings using the VmD method were obtained using electrodes filled with QX-314 (5 mM) and caesium chloride (125 mM) to investigate the effects of internal voltage-gated sodium and potassium channel blockade. In these cells, VmD measurements were performed within 1-2 minutes of impalement, before the internal channel blockers dialysed into the cell. Positive current (0.2-0.5 nA) was then used at the recording electrode to aid dialysis of the channel blockers into the recorded neurone, before another VmD measurement was made at 10-15 minutes after impalement.

Whole-cell voltage clamp recordings (held at -80 mV) were made in a small series of experiments to determine decay time constants for sEPSCs and sIPSCs.

Results

Methodological Considerations

The conductance estimates provided by the VmD method are based on the Gaussian approximation of the recorded membrane voltage at the two levels of polarisation, so the range of voltages at which this approximation holds has to be considered. For this purpose, I followed Rudolph *et al*. (2004) in restricting measurements to voltage ranges between -75 mV and -50 mV. The method requires the removal of any action potential activity from recordings as the spike, and any voltage-gated ion channel activity before and after it, will substantially effect the distribution and standard deviation of the recorded membrane voltage (Rudolph *et al.,* 2004). Thus, depolarising the cell to a point where firing is constant and rapid drastically reduces the quiescent period necessary to construct the conductance model.

Thus, the depolarising current used in the present studies was adjusted so that the higher current level held the neurone slightly below its firing threshold. This allows the membrane to be at its most excitable whilst reducing the amount of action potentials that must be removed.

The estimates of E_{Bg} and I_{Bg} require knowledge of the reversal potentials for AMPA and $GABA_A$ receptors, and the leak conductance and reversal. The leak conductance can be measured simply by injecting a hyperpolarising current pulse through the recording electrode, and using Ohm's law to calculate resistance, so specific measurement of this property is not needed. It was obtained before each run of the current injection protocol used in the VmD method. However, it is impractical to measure reversal potentials on a cell-by-cell basis. The necessary use of antagonists to obtain measurements of reversal potentials necessarily blocks receptors that mediate

E_{Bg} and I_{Bg}. Thus, the reversal potentials were characterised separately and individually in neurones other than those used for VmD measurements.

Decay times, necessary to construct the "effective time constant" of the VmD method, were obtained from whole-cell patch clamp recordings made from layer III mEC pyramidal cells. Voltage clamp recordings were made as described in Chapter 2. EPSCs and IPSCs were recorded from quiescent neurones and the 95% decay time was used instead of the time constant (as recommended by Alain Destexhe, personal communication) to obtain the values necessary for the VmD equation (see Chapter 1, Eq. 11 and 12). Care was taken to ensure that both slow and fast conductances were included in the decay time.

Determination of Reversal Potentials

Reversal potentials for AMPAr-mediated EPSPs were obtained from 6 pyramidal neurones in layer III. Membrane voltage was manually clamped in 5 mV increments from -95 to -65 mV, and three EPSPs evoked at each voltage level for each cell. It was found that, at potentials less negative than -65 mV, problems were encountered with ability to pass current and membrane potential became too unstable to obtain reliable evoked measurements. Voltage offset after recording was carefully noted to ensure that the observed membrane potentials were as accurate as possible. Fig. 3.1A shows the averaged IV plots for the 6 neurones. Extrapolation of the plot gave an average reversal potential for AMPA receptors in layer III of 6.8 mV.

Reversal potentials for $GABA_A$ receptor-mediated IPSPs were obtained in a similar fashion. 6 cells were recorded at membrane voltage steps of 5mV, from -95 to -70mV. The average relationship for the peak amplitude of IPSPs plotted against V_M is shown in Fig. 3.1B. The reversal potential for these receptors was found by linear regression to be -66.7 mV.

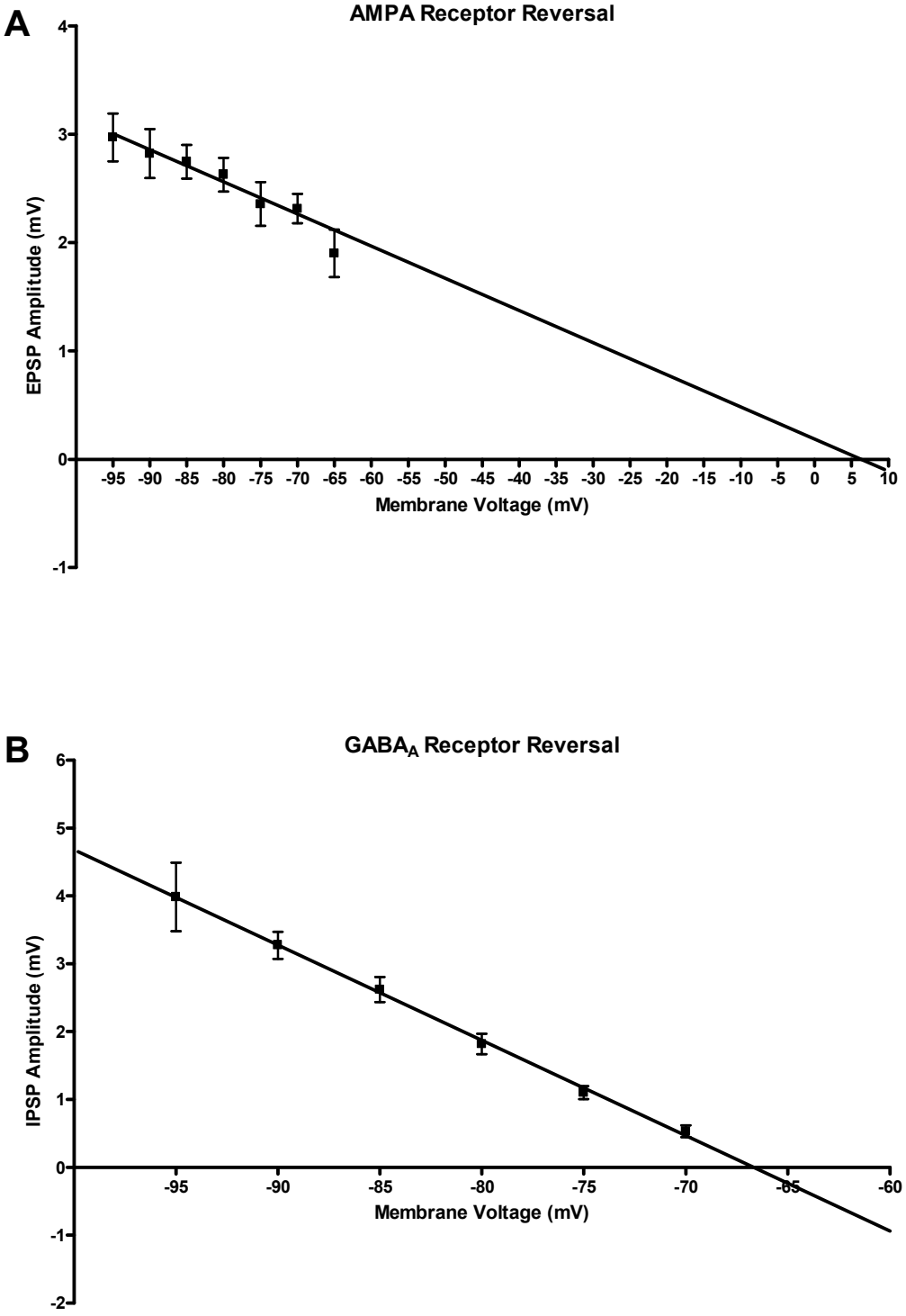

Figure 3.1: Reversal potentials for (A) AMPA and (B) $GABA_A$ receptor mediated synaptic responses in layer III. Evoked responses at a range of membrane were averaged and plotted, using linear regression, from 6 pyramidal neurones in layer III of the mEC to find the reversal potentials of AMPA and $GABA_A$ receptors. AMPAr reversal was 6.8 mV, whilst $GABA_A$r reversal was -66.7 mV.

Layer III Decay Times

Whole-cell patch clamp recordings were made from a total of 12 pyramidal cells in layer III of the mEC. The average 95% decay time for sEPSCs in 6 neurones was 13.7 ± 1.0 ms. The average 95% decay time of sIPSCs in 6 neurones was 29.1 ± 2.7 ms.

Baseline Values for E_{Bg} and I_{Bg} in Layer III

Currently, the VmD method is applicable to $GABA_A$ and AMPA receptor-mediated conductances (Rudolph *et al*., 2004), and does not take into account $GABA_B$ or NMDA receptor mediated activity. However, it is unlikely that spontaneous activation of $GABA_B$ receptors occurs in EC neurones (Woodhall *et al*., 2004), and although spontaneous currents mediated by postsynaptic NMDAr do occur in slices, such events are very infrequent (Berretta and Jones, 1996a). Thus, the vast majority of the background synaptic noise in EC neurones is mediated via AMPA and $GABA_A$ receptors.

Baseline values for E_{Bg} and I_{Bg} have been averaged in a population of 61 layer III neurones (Fig. 3.2). Mean E_{Bg} in these neurones was 2.5 ± 0.3 nS and I_{Bg} was 10.2 ± 1.6 nS, giving a ratio of approximately 4:1 in favour of inhibition. There was considerable variability in the two conductances from neurone to neurone. There are a number of practical reasons why this may be so, including the day to day variation in quality of slices, whether slices were selected from more dorsal or ventral regions, variations in preservation of intrinsic connectivity etc. It seems unlikely that the variations are due to sampling of different neuronal types. We studied regular spiking neurones in layer III, and these have an homogenous pyramidal cell morphology and electrophysiological characteristics (e.g. Dickson *et al*., 1997; Tahvildari and Alonso, 2005). Typically (n=6), these neurones had a resting potential of -72.2 ± 0.5 mV,

input resistance of 79 ± 6 MΩ and action potential amplitude (from threshold of 21.2 ± 2.3) and half-widths of 72.1 ± 1.6 mV and 0.32 ± 0.01 ms, respectively.

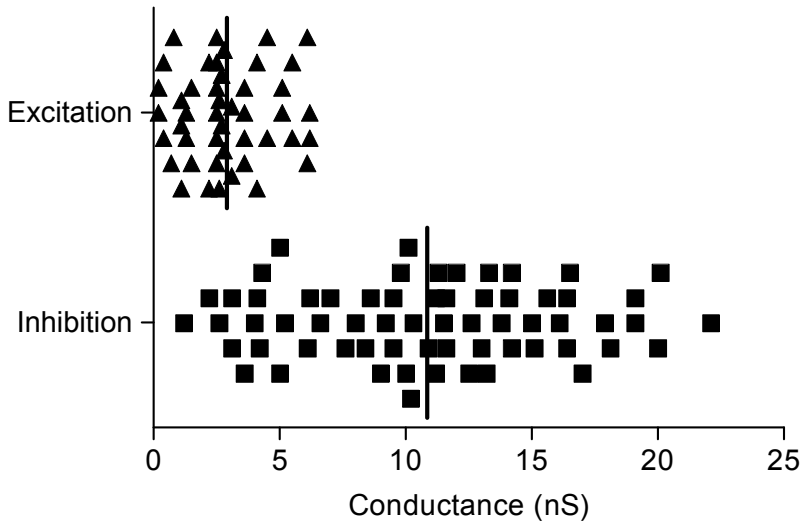

Figure 3.2: Distribution of conductance values for layer III pyramidal cells. Scatter plot shows values for E_{Bg} (top) and I_{Bg} (bottom) taken from 61 neurones in layer III of the mEC.

Despite the neurone to neurone variation I_{Bg} was consistently greater than E_{Bg}. The ratio of inhibitory to excitatory conductances (I:E) was clearly in favour of inhibition (4.08:1), and this is similar to the situation estimated from naturally occurring up-states of activity recorded in ferret occipital cortex *in vitro* (Rudolph *et al*., 2004), and cat neocortex *in vivo* (Rudolph *et al*., 2007). In other experiments in this laboratory we have been studying sEPSCs and sIPSCs using whole-cell patch clamp recording in layer III neurones. Whilst it is difficult to directly relate global conductances to spontaneous currents, it is pertinent that in a sample of 7 neurones sIPSCs had a mean frequency and amplitude of 12.4 ± 2.9 Hz and 37.4 ± 3.2 pA, whilst in a further 7 neurones the corresponding values for sEPSCs were 6.6 ± 1.2 Hz and 11.5 ± 0.9 pA. Together with the considerably longer decay times for sIPSCs noted above, it is clear that total charge transfer associated with spontaneous inhibitory events would be

considerably greater than that of spontaneous excitation (Chamberlain and Jones, unpublished observations).

High Potassium ACSF

Increasing extracellular potassium depolarised the resting membrane potential by 2.9 ± 0.7 mV. When extracellular potassium was elevated from 3.75 mM to 7.5 mM (n=7), both E_{Bg} and I_{Bg} were increased (Fig. 3.3). E_{Bg} increased from a control level of 2.4 ± 0.5 nS to 4.4 ± 1.3 nS. This increase was significant to P=0.04. I_{Bg}, however, increased substantially more, from 7.1 ± 1.6 nS to 34.0 ± 12.7 nS (significant at P=0.03). These changes caused a shift in the I:E ratio in favour of inhibition, from 3.1 ± 0.2 to 8.6 ± 2.6.

When the standard deviation (SD) of the conductances was calculated, raising the extracellular potassium had practically no effect on E_{Bg} SD: the control value was 5.0 ± 1.9 pS and in high-K^+ it was 5.1 ± 1.6 pS (P>0.05). I_{Bg} SD, similarly, showed no change (0.12 ± 0.04 nS to 0.13 ± 0.05 nS, P>0.05).

The change in I:E ratio was accompanied by changes in cellular excitability. Spike firing threshold showed a marked reduction (20.0 ± 0.6 mV to 13.0 ± 0.3 mV, P<0.001). However, surprisingly, the number of spikes generated during a 250ms depolarising pulse was unchanged (4.3 ± 0.3 vs 4.3 ± 0.9, P>0.05). The overall amplitude of action potentials evoked during a 50 ms depolarising pulse was reduced from 93.1 ± 0.7 mV to 85.0 ± 1.6 mV. This change was found to be significant at P<0.001.

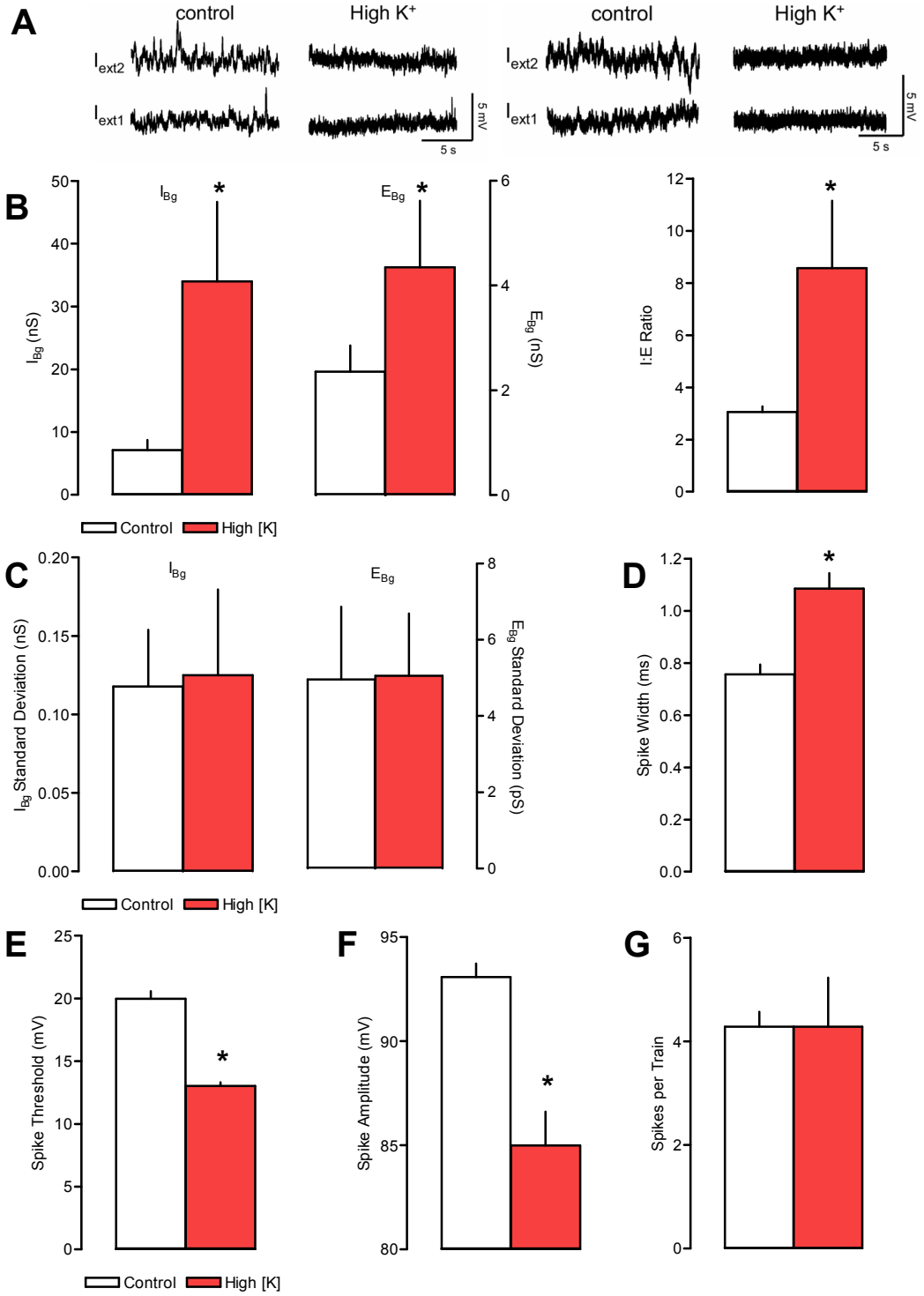

Figure 3.3: Effect of increasing $[K^+]_o$ on background activity and neuronal excitability. A: Examples of membrane potential recordings made in two layer III neurones at two levels of injected current in control and high-K^+ ACSF. B: The bars show the mean (± sem) values for background conductances, measured using the VmD approach, pooled from 7 neurones. Note the difference in scales for I_{Bg} (left) and E_{Bg} (right). This applies to all subsequent similar figures. The right hand panel shows the I:E ratio. C: Mean SD of I_{Bg} and E_{Bg} in the same neurones as in (A).

(Fig. 3.3 Cont) Note scale for E_{Bg} SD is in pS, not nS in this and subsequent figures. D: Mean action potential width measured at half height in the same neurones. E: Threshold for spike firing measured as mV from rest. F: Spike amplitude as measured from threshold G: Number of spikes generated by a 250 ms supermaximal depolarising pulse. Asterisks indicate P>0.05 by paired t-test in this and all subsequent figures.

4-Aminopyridine

4-aminopyridine was applied to 6 neurones at two concentrations (20 μM and 40 μM). Subsequently the AMPA/kainate receptor antagonist NBQX (10 μM) was added, followed by the $GABA_A$ receptor antagonist bicuculline (20 μM).

Addition of 20 μM 4-AP caused an upward trend in both I_{Bg} and E_{Bg}, with I_{Bg} going from 6.3 ± 1.1 nS to 24.6 ± 9.6 nS (Fig. 3.4). E_{Bg} increased from 1.7 ± 0.3 nS to 4.2 ± 0.8 nS. Neither change was significant by ANOVA. However, increasing the concentration of 4-AP to 40 μM caused E_{Bg} to become significantly different from control values (P=0.01) at 4.6 ± 0.7 nS. 40μM 4-AP caused a slight decrease in mean I_{Bg} (19.1 ± 4.4 nS) compared to 20 μM, however the smaller error values led to a significant difference from control (P=0.03). The I:E ratio was essentially unchanged throughout, at 3.9 ± 0.5 for control conditions, 5.2 ± 1.2 in the presence of 20 μM 4-AP, and 4.2 ± 0.9 when 4-AP was increased to 40 μM (Fig. 3.4A).

The SD of I_{Bg} and E_{Bg} was steadily decreased by the rising 4-AP concentration (Fig. 3.4B). Control values for the SD of I_{Bg} and E_{Bg} were 0.35 ± 0.20 nS and 6.5 ± 3.3 pS respectively. In the presence of 20 μM 4-AP, these decreased to 0.13 ± 0.09 nS for I_{Bg} SD and 3.2 ± 1.8 nS for E_{Bg} SD. When the 4-AP concentration was increased to 40 μM, I_{Bg} SD decreased further to 0.022 ± 0.008 nS, whilst E_{Bg} SD decreased to 1.8 ± 0.2 pS. None of these changes were found to be significant by ANOVA.

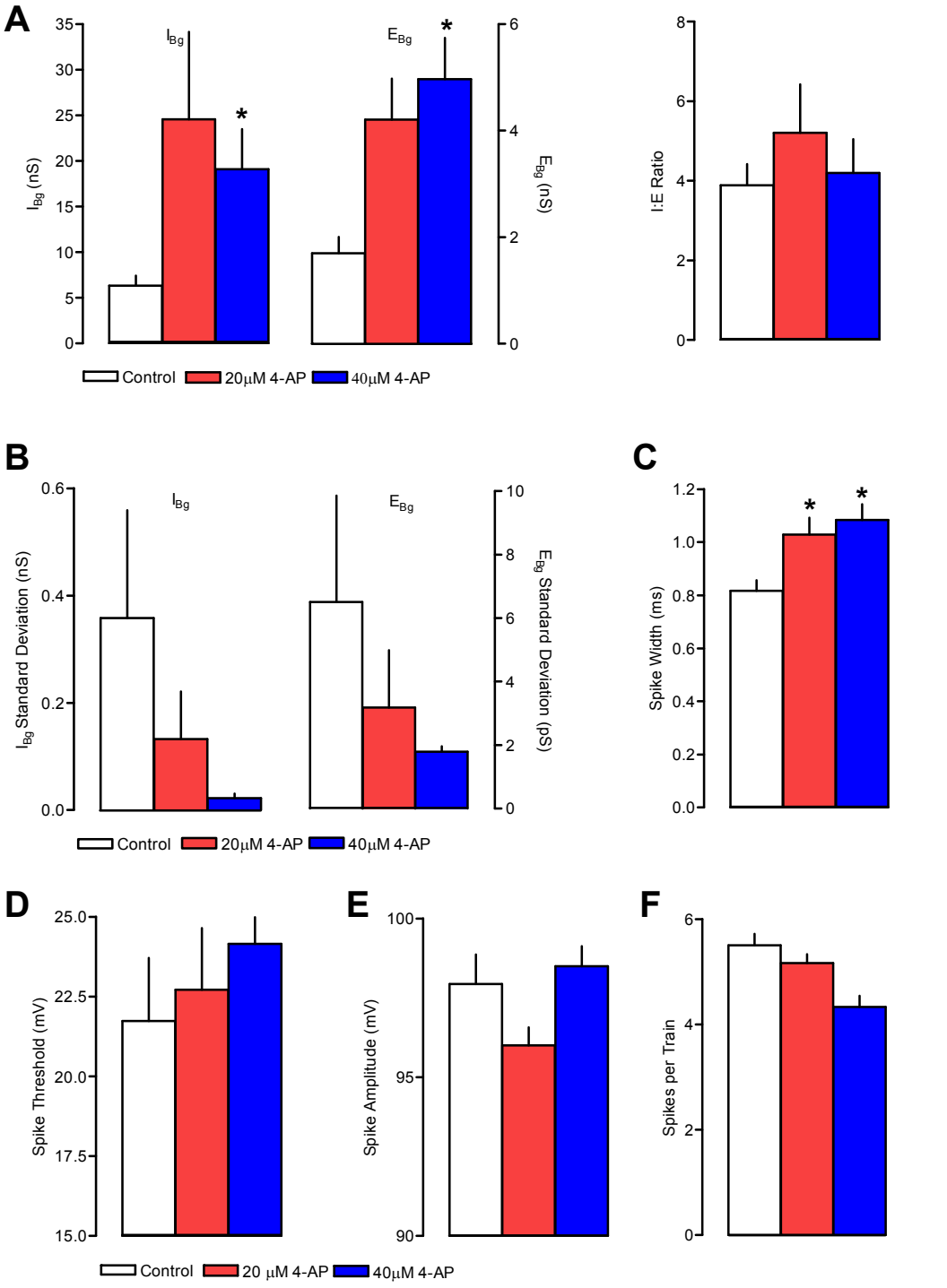

Figure 3.4: Effect of 4-AP on background activity and cellular excitability. Details as for Fig. 3.3 A: 4-AP significantly increases both I_{Bg} and E_{Bg} at a concentration of 40 μM, but does not change the I:E ratio or significantly affect the SDs (B), despite causing a noticeable downward trend in I_{Bg} SD. The increased conductance would appear to be mediated by enhanced transmitter release due to prolonged action potentials (C) which would prolong depolarisation at presynaptic terminals. However, due to the lack of change in I:E ratio, cellular excitability is not affected (D-F).

In the presence of 4-AP there appeared to be slight reduction in cellular excitability, most likely because of the increase in inhibition. From a control level of 21.7 ± 2.0 mV, spike firing threshold was essentially unchanged at 22.7 ± 1.9 mV in the presence of 20 µM 4-AP, and only slightly higher at 24.2 ± 0.8 mV with 40 µM 4-AP (P>0.05). The mean number of spikes generated by a 250 ms depolarising pulse was 5.5 ± 0.2 in control conditions, 5.2 ± 0.2 with 20 µM 4-AP and 4.3 ± 0.2 with 40 µM 4-AP. The latter change was found to be significant with ANOVA (P<0.001). The overall amplitude of evoked action potentials was unaffected (see Figs 3.4 C-E).

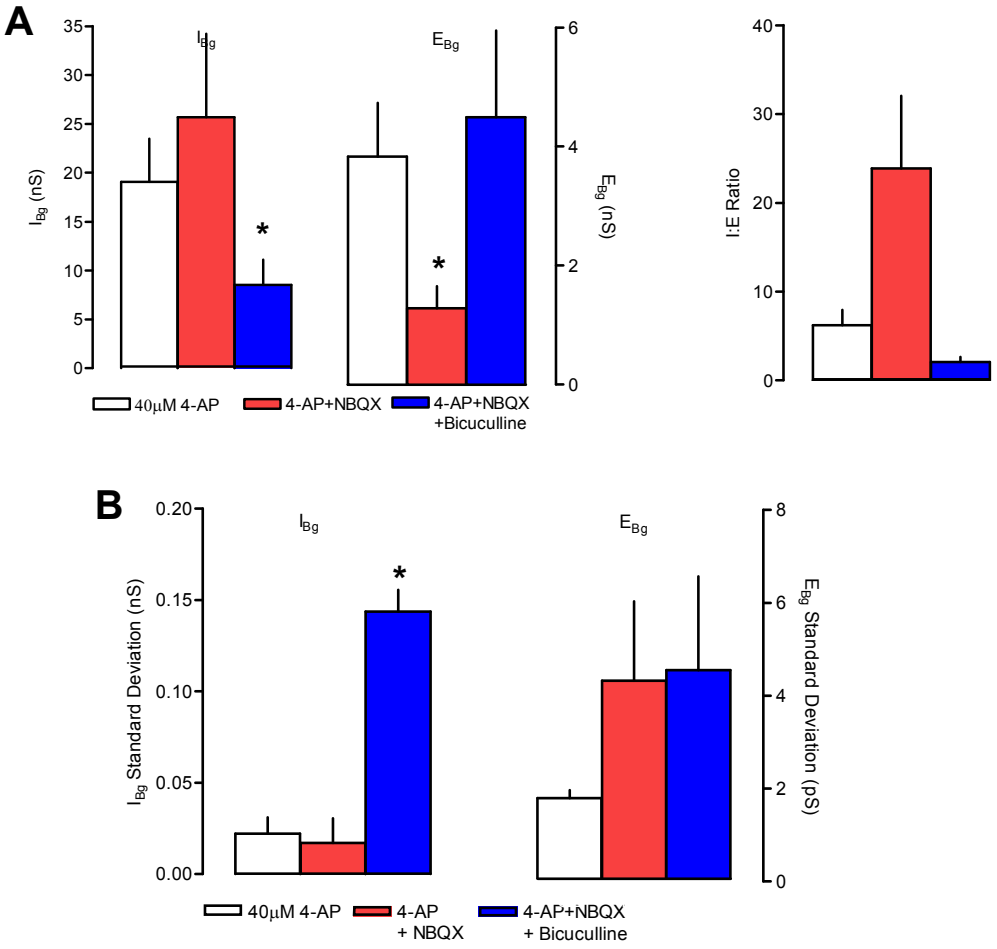

Figure 3.5: Effects of NBQX and bicuculline on background activity on 4-AP treated neurones. Details as for Fig. 3.3. A: NBQX in the presence of 4-AP causes a significant drop in E_{Bg}, but has no effect on I_{Bg}. Subsequent addition of bicuculline caused a reduction in I_{Bg}, increased E_{Bg} back to previous levels, and (B) significantly increased the SD of I_{Bg}. The I:E ratio is shifted in favour of inhibition by NBQX and excitation by bicuculline. Asterisk indicates P<0.05 by one-way ANOVA.

Further experiments used specific antagonists to determine whether the increase in I_{Bg} and E_{Bg} with 4-AP were mediated by increased activation of $GABA_A$ and AMPA receptors. Addition of the AMPAr antagonist NBQX (10 μM) during 4-AP caused a marked decrease in E_{Bg} and an increase in inhibitory conductance (Fig. 3.5A). The I:E ratio increased to 23.9 ± 8.2 compared with 4.2 ± 0.9 in 40 μM 4-AP. The SD of I_{Bg} was decreased to 0.017 ± 0.013 nS, and E_{Bg} SD was increased to 4.0 ± 1.7 pS compared to 4-AP alone (see above and Fig. 3.5B).

The subsequent and sequential addition of the $GABA_A$ antagonist bicuculline (20 μM) to these neurones caused a pronounced reduction in I_{Bg} (to 8.5 ± 5.2 nS). However, surprisingly, E_{Bg} was actually increased compared to the value obtained under NBQX (to 4.5 ± 1.5 nS). Thus, with bicuculline plus NBQX, E_{Bg} was almost the same as with 4-AP alone. I:E ratio was reduced to 2.1 ± 0.6, and SD values were 0.14 ± 0.012 nS for I_{Bg} and 5.0 ± 2.0 pS for E_{Bg}. The change in E_{Bg} elicited by NBQX was found to be significant (P=0.04), and the change in I_{Bg} mediated by bicuculline was significant at P=0.03. Of the SD measurements, only the change in I_{Bg} SD caused by bicuculline was significant (P<0.001). No ratio changes were significant by ANOVA.

Tetrodotoxin

TTX (1 μM) was added to 6 neurones, with the further addition of NBQX (10 μM) and bicuculline (10 μM) in 3 each of these neurones. A separate group (n=5) was recorded in high potassium (7.5 mM) ACSF in the presence of TTX. No measures of cellular excitability could be made as abolition of action potentials by TTX precludes estimates of spike threshold etc.

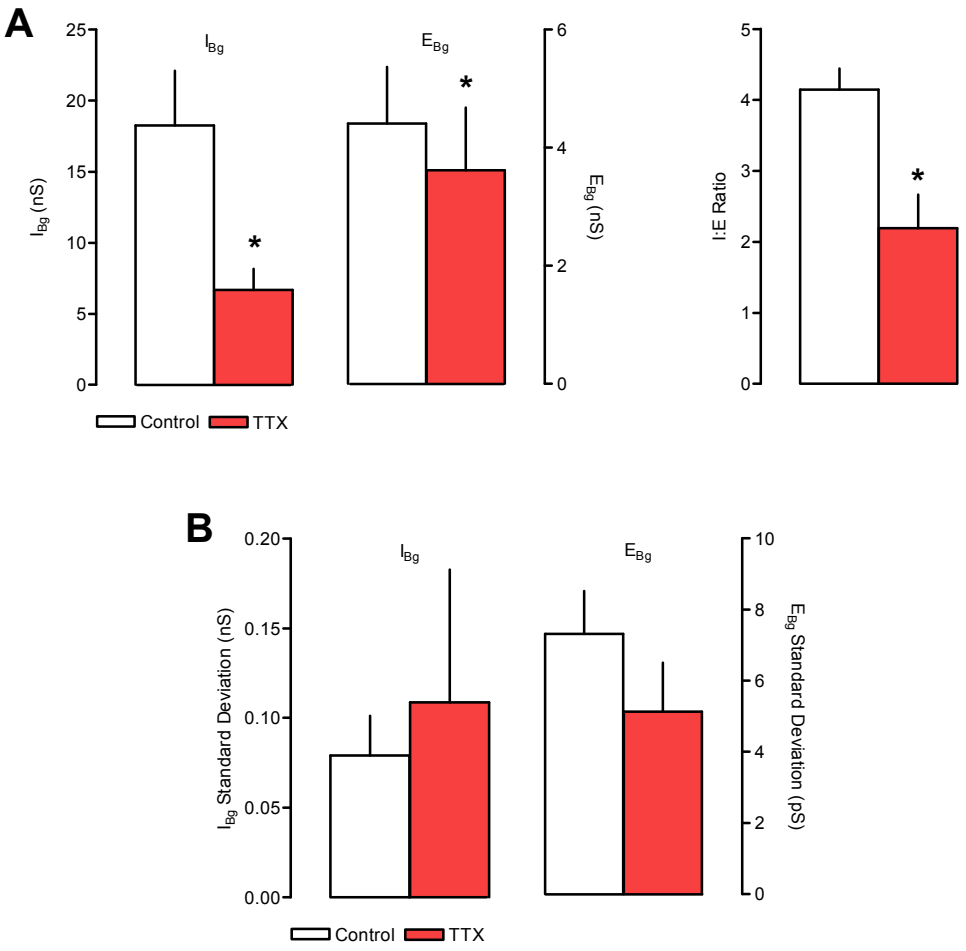

Figure 3.6: Effect of TTX (1 μM) on conductance estimates and conductance SDs in layer III pyramidal neurones. Details are as for Fig. 3.3. A: Blockade of VGSC with TTX precipitates a far larger change in I_{Bg} than in E_{Bg}, suggesting that inhibitory transmission in layer III is more dependant upon action-potential activity than excitatory transmission is. Thus, the I:E ratio shifts towards excitation when VGSC are blocked. B: The SD of I_{Bg} and E_{Bg} is unaffected by TTX. This is surprising as the SDs are thought to be a measure of synchrony, which would logically be mediated largely by action potentials.

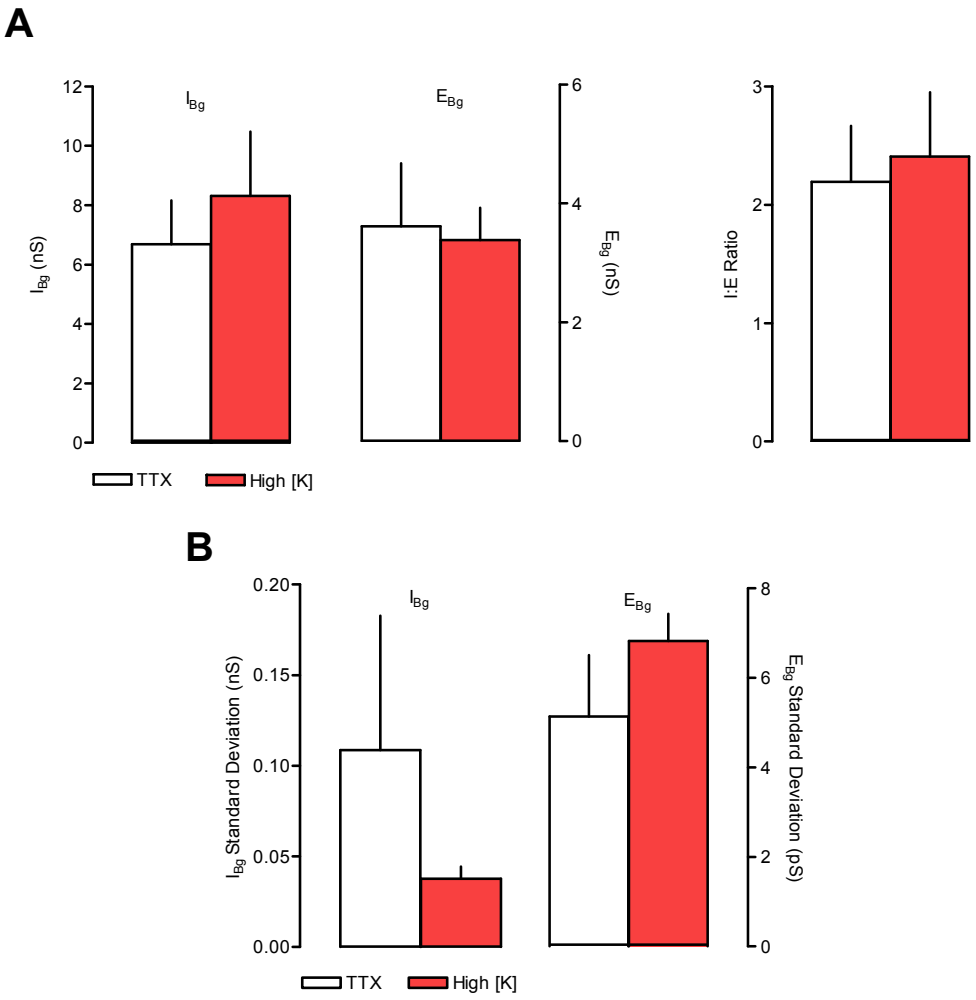

Figure 3.7: Effect of increased extracellular K^+ in neurones pre-treated with TTX. A: High-K^+ with TTX did not have a significant effect on conductance estimates. B: Similarly, the SDs of both I_{Bg} and E_{Bg} were not significantly changed, although the SD of I_{Bg} shos a trend towards reduction.

The addition of TTX caused a reduction in both E_{Bg} and I_{Bg}. However, the reduction in I_{Bg} (18.3 ± 3.8 nS to 6.7 ± 1.5 nS) was much larger than the reduction in E_{Bg} (4.4 ± 1.0 nS to 3.6 ± 1.1 nS). Both changes were found to be significant using paired t-test (P<0.01 for both, Fig. 3.6A). TTX did not cause a significant change in either I_{Bg} or E_{Bg} SD (Fig. 3.6B).

The effect of potassium-induced depolarisation during VGSC blockade was investigated by increasing extracellular potassium to 7.5 mM in the presence of TTX. Transition to high potassium ACSF only slightly increased I_{Bg} from 6.7 ± 1.5 nS to

8.3 ± 2.2 nS. E_{Bg}, however, was essentially unaffected by high potassium (3.6 ± 1.1 nS vs 3.4 ± 0.5 nS). The I:E ratio was also unaffected (2.2 ± 0.5 vs 2.4 ± 0.5). None of these changes were found to be statistically significant (Fig. 3.7A). The SD of I_{Bg} and E_{Bg} was unaffected by high K^+ with TTX (Fig. 3.7B).

Internal Voltage-gated Channel Blockade

In their description of the VmD method, Rudolph *et al*. (2004) tested the effects of including active conductances, including voltage-dependent Na^+ and K^+ currents for spike generation, I_M for spike-frequency adaptation, a transient A-type K^+ current (I_{KA}), a low-threshold Ca^{2+} current (I_{CaT}) and a hyperpolarisation-activated current (I_h) in soma and dendrites. Although greater variability and small deviation of estimated background conductances was seen in this model, overall the inclusion of these conductances had little effect. I have attempted to partially replicate this situation in my experiments by effectively *deleting* voltage-gated Na^+ and K^+ conductances by inclusion of Cs^+ and QX-314 in the recording electrode in 5 neurones.

In two of these neurones, despite no obvious differences in voltage traces, the VmD method was unable to calculate conductance values, with the neurones producing membrane voltage distributions that led to impossible conductance estimates (i.e. negative numbers). The remaining three neurones showed very little difference in background synaptic activity estimated immediately after penetration and after 15 minutes internal dialysis with Cs^+ and QX-314. I_{Bg} was 10.1 ± 2.0 nS in control conditions and 12.2 ± 2.7 nS after 15 minutes recording. Likewise, E_{Bg} was 3.2 ± 0.5 nS before and 3.6 ± 0.3 nS after VGC block (Fig. 3.8A). This meant that the I:E ratio was largely unchanged. None of the changes was statistically significant. In addition, the SD of both I_{Bg} and E_{Bg} although slightly reduced by VGC blockade, was not significantly altered (Fig. 3.8B).

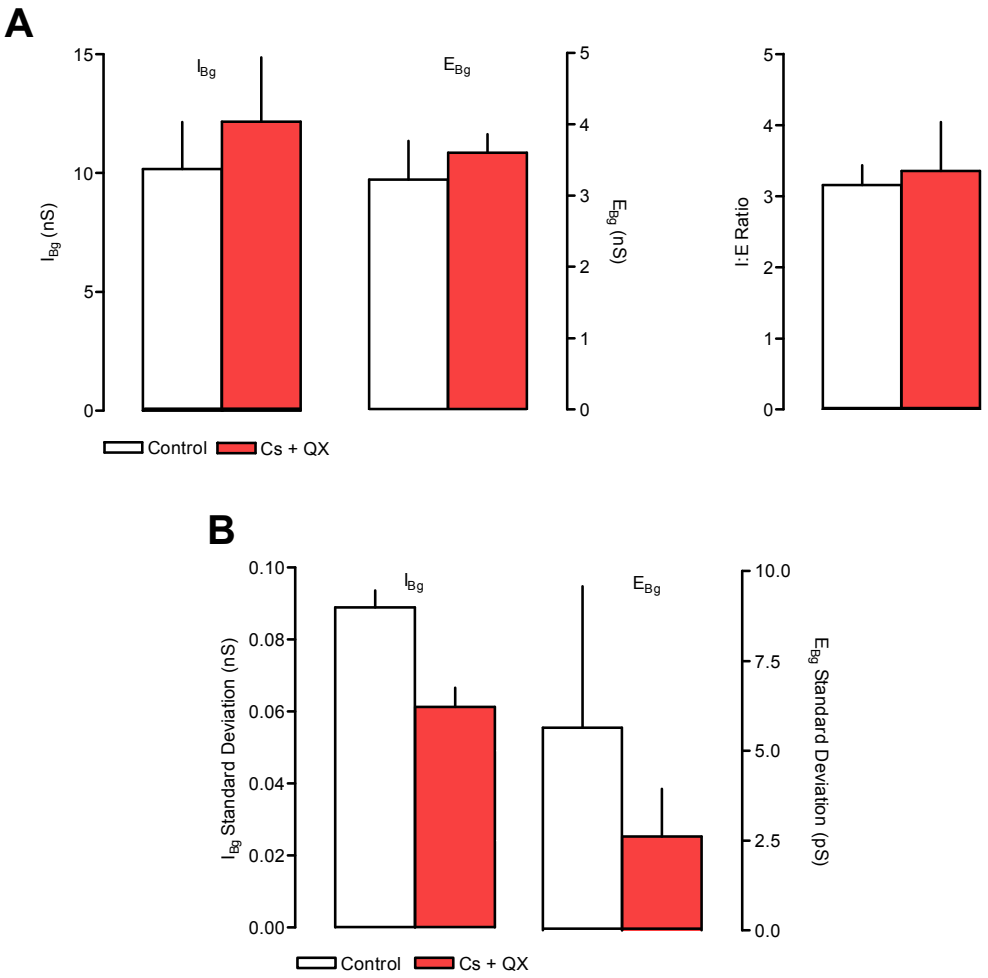

Figure 3.8: Effect of blockade of transient Na^+ and K^+ currents on background conductance estimates. A: Cs^+ and QX-314 have little or no effect on VmD measurements of background conductance in these cells. B: The SDs of I_{Bg} and E_{Bg} are also not significantly affected. This agrees with the findings of the Destexhe group (Rudolph et al., 2004).

Discussion

Sub-threshold background synaptic activity or "synaptic noise" is increasingly seen as a functional way of controlling excitability and gain in cortical neurones, and hence of the processing capabilities of cortical networks. Conversely, the characteristics of the background activity in individual elements provide information concerning the dynamic state of the network. Recording excitability of network elements and simultaneously quantifying the level of background activity presents considerable

technical problems, and most studies have employed a dynamic clamp approach to model *in vivo*-like synaptic noise and determine its effects on gain and excitability. The VmD method devised by Rudolph *et al*. (2004) potentially allows us to quantify excitatory and inhibitory synaptic noise at the same time as monitoring excitability. In the experiments in this Chapter I have provided initial evidence that this method is a valid and useful approach for the investigation of network activity even under the quiescent conditions present in acute brain slices. The results show that it is clearly possible to realistically obtain a simultaneous quantification of the naturally arising, global, background synaptic inhibition and excitation in entorhinal neurones in resting conditions.

Baseline estimations of I_{Bg} and E_{Bg} in layer III neurones clearly indicate a substantially higher level of background inhibition compared to excitation. Destexhe's group have reported a dominance of inhibition compared to excitation during spontaneous up-states recorded from ferret visual cortex slices *in vitro* (Rudolph *et al*., 2004), and in cat parietal neurones under ketamine/xylazine anaesthesia *in vivo*, using the VmD method (Rudolph *et al*., 2005). A similar ratio in favour of inhibition was recorded in the same animals during EEG-activated states following electrical stimulation in the porcine reticular formation. More recently, the same group have demonstrated dominant inhibition during natural sleep/waking states in non-anaesthetised cats (Rudolph *et al*., 2007). Other studies using different approaches have previously suggested dominant inhibitory conductances in cat visual cortical neurones under anaesthesia *in vivo* (Borg-Graham *et al*., 1998). However, others have provided evidence to suggest that excitatory and inhibitory conductances are approximately equal during spontaneous up-states in ferret cortex *in vitro* or *in vivo* (Shu *et al*., 2003b; Haider *et al*., 2006). In contrast, the VmD method applied to neurones in the anaesthetised (urethane) rat somatosensory cortex suggests that spontaneous up-states are associated with a rise in excitatory conductance with a concurrent fall in inhibition (Zou *et al*., 2005). My data add to these observations by

showing that under quiescent resting conditions in layer III of the EC *in vitro*, background synaptic noise mediated by GABA strongly dominates over excitation. This agrees with whole-cell patch clamp experiments done in this laboratory, which have shown that under the same conditions, sIPSCs are larger, longer and more frequent than sEPSCs.

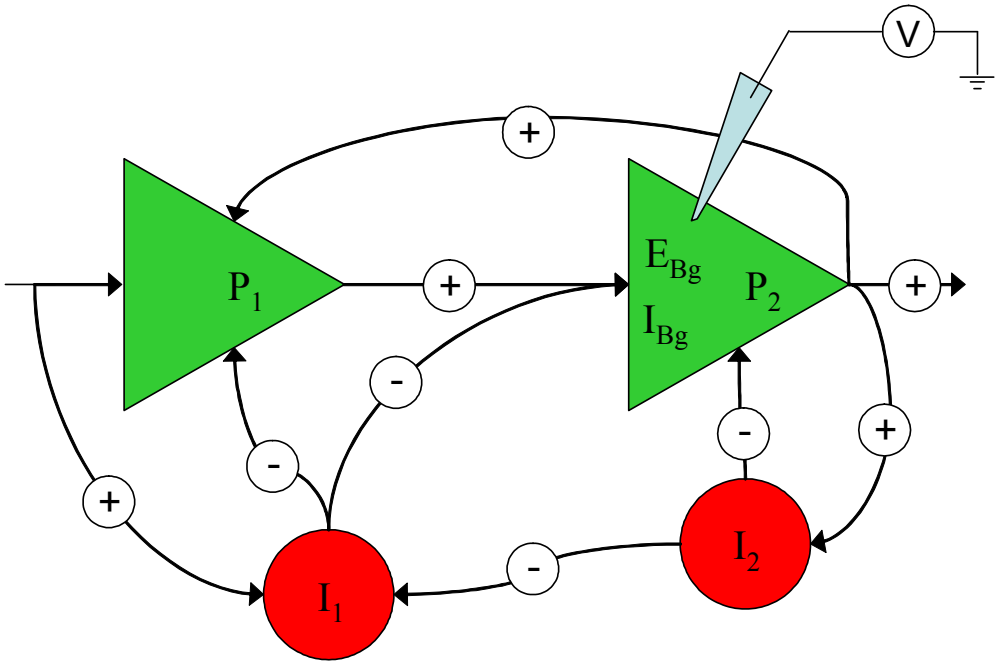

Figure 3.9: Schematic diagram of network connectivity in the mEC. The principal, pyramidal cells (P_1 and P_2) are connected both to each other and to a rich network of inhibitory interneurones (e.g. I_1 and I_2). An increase in excitatory activity will bring about a rise in inhibitory firing, due to the action of glutamate at the inhibitory cells. Thus, any change in one system's activity would be expected to affect the other, due to the level of feedback present between the two systems. Both 4-AP and high K^+ increases activity of all connections, TTX abolishes all action potential activity between cells. Under 4-AP, NBQX will reduce the activity of AMPA receptors at the post-synapse of both principal cells and, to a lesser extent, interneurones. Bicuculline will antagonise $GABA_A$ receptors at the pre- and postsynapse of both types of cells.

It is important to remember that E_{Bg} and I_{Bg} are not static background conductances, but are each the sum of dynamically varying inputs, the activity of which result from stochastic release of transmitters, and events driven by network interactions. Fig. 3.9

shows a highly simplified schematic representation how inhibitory and excitatory neurones may interact in the mEC. The principal cells (in green) modify, and are modified by, the inhibitory interneurones (in red). Thus, when the global background conductances are recorded in the central pyramidal neurone it is clear that changes in excitation will have inevitably consequent effects on inhibitory transmission, and vice versa. The activity of the interneurones is driven by the excitatory drive provided by the principal pyramidal cells, so increases or decreases in this drive would be expected to strongly affect the inhibitory component. Likewise the change in inhibition will in turn affect the level of activity in the principal neurones. So how does this network arrangement contribute to the changes in E_{Bg} and I_{Bg} observed in my experiments?

In the first series of experiments, I attempted to more closely mimic the *in vivo* situation by provoking a generalised elevation of synaptic activity across the whole network by increasing extracellular K^+. This resulted in an approximate doubling of E_{Bg}, but a much more dramatic five-fold rise in I_{Bg}. However, when these experiments were repeated in TTX, high K^+ had little effect on either background conductance. This suggests that the predominant effect of high K^+ alone was to promote action potential driven release, rather than activity-independent miniature release. Increased activity-dependent release most likely arises because cells will be depolarized closer to threshold and will fire more action potentials when K^+ is raised. The increase in E_{Bg} can be explained by increased glutamate release from excitatory afferents from other principal neurones in the slice, possibly compounded by recurrent excitatory connections between them. The increase in I_{Bg} will be dependent on increased GABA release from multiple interneurones onto the recorded principal neurone.

The greater effect on I_{Bg} compared to E_{Bg} may reflect the fact that interneurones are generally polarised less negatively than principal neurones (see Jones and Buhl, 1993; Jones, 1994) and will already be closer to firing threshold. Indeed, as noted above,

TTX alone reduces I_{Bg} to a greater extent than E_{Bg}, showing that the interneurones are likely to display a greater level of spontaneous firing than the principal neurones under baseline conditions.

Considering the network circuit (Fig. 3.9), there are a number of other points to note. Increased firing in principal neurones should also increase the excitatory drive onto the interneurones, thereby enhancing the elevation of GABA release occurring as a result of increased interneurone firing. However, as I_{Bg} rises this should actually temper the rise in E_{Bg} to some extent. Conversely, as the interneurones themselves are subject to inhibition from other interneurones, the elevation of I_{Bg} in the principal cell should be partly mitigated by increased inhibition in the interneurones.

Despite the increases in I_{Bg} and E_{Bg}, there was no change in the SD of either. This suggests that there is little added synchronisation between interneurones or pyramidal neurones when network excitability is generally increased. What is clear is that the I:E ratio is further increased in favour of inhibition when overall activity across the network is elevated. Thus, during relative quiescence in the slice, the network is inhibition-dominated. When activity is raised towards more in vivo-like levels, this dominance becomes even more marked. This mirrors the situation in the cortex of awake cats *in vivo* (Rudolph et al, 2007), experiments from which suggested that in the inhibition-dominant network action potentials were evoked in response to a drop in inhibition rather than an increase in excitation.

What implications does this have for excitability of the principal neurones in our experiments? Spike threshold was significantly reduced, which can be explained partly by the depolarizing effects of the high K^+ medium. The increase in E_{Bg} could also contribute to this although it might be expected that this would be ameliorated by the concurrent increase in I_{Bg}. Surprisingly, there was no change in the number of spikes evoked by a supra-threshold depolarizing pulse. It is possible that the increased

K^+ enabled easier generation of action potentials, but that this was counteracted by the relative increase in I_{Bg}, which then acted to reduce sustained firing. However, since changing extracellular K^+ itself clearly alters intrinsic membrane excitability, it is difficult in this instance to draw any firm conclusions about the relationship between I_{Bg}, E_{Bg} and cellular excitability.

In later experiments I studied the relative contributions of action potential driven glutamate and GABA release and that occurring by stochastic, activity-independent processes (i.e. miniature events) to global background synaptic activity. The former was eliminated by blockade of VGSC with TTX. Under these conditions both I_{Bg} and E_{Bg} decreased significantly. If we examine the schematic network in Fig. 3.9 the effects of TTX are easily explained. Action potentials in all connections will be blocked and therefore, glutamate and GABA release onto the recorded neurone will both fall. The reduction in GABA release will be the result of direct loss of spontaneous activity in the interneurones as well as the loss of excitatory drive onto them, which would normally help to promote spontaneous activity.

E_{Bg} was slightly decreased (by around 20%) but I_{Bg} was reduced sharply, to around 35% of control. This clearly indicates that activity-dependent GABA release driven by spontaneous firing in interneurones contributes much more to global inhibition, compared to the respective contribution of activity-dependent glutamate release to overall excitation. This is in line with whole-cell voltage clamp recordings in our laboratory, which show that sIPSC frequency in layer III neurones is reduced by around 50-60% by TTX whereas the toxin only elicits a fall of around 20% in sEPSCs (Chamberlain and Jones, unpublished observations).

There was little change in the SD of either I_{Bg} or E_{Bg} in the presence of TTX. If one accepts that the SD is a reflection of the degree of synchrony in the network (see Introduction) then this suggests that synchrony may be minimal under baseline

conditions, so there is no real change when spontaneous firing in both principal and interneurones is abolished.

What is abundantly clear is that any manipulation that alters even one element of the network will have consequent dynamic effects on virtually all elements of the network. This stresses the importance of being able to monitor the global effects of inhibition and excitation in the principal neurones. Changes in these global conductances can tell us not only how a substance influences excitability of the output neurones, but provides information on how it may alter interactions within the network. This provides an enormous advantage when it comes to examining and predicting how therapeutic substances may change CNS activity. Any substance administered systemically and which penetrates the blood brain barrier will have access to all elements of the network. Therefore, knowing how the substance alters I_{Bg} and E_{Bg} will provide us with information about where in the network it may act and how it then globally alters network activity. In a later chapter of this thesis I have studied the actions of one group of CNS active drugs, anticonvulsants, in this way.

As discussed in the introduction, 4-AP blocks A-type K-channels (I_{KA}). Rudolph *et al*. (2004) have shown that several voltage-dependent currents (I_{Na}, I_{Kd}, I_H, I_{CaT}, and I_{KA}) do not significantly distort conductance estimates obtained with the VmD method. Thus, blockade of I_{KA} with 4-AP will not directly change I_{Bg} or E_{Bg} estimations, in the sense that the VmD equation alone is not changed by the actions of these channels. However, E_{Bg} and I_{Bg} values can be affected by activity changes elsewhere in the network. It has been shown that blockade of A-type channels leads to an increase in presynaptic Ca^{2+} influx without changing postsynaptic Ca^{2+} influx. The presynaptic fibre volley was also increased with 4-AP (Jones and Heinemann, 1987). This suggests that there will be greater release of neurotransmitter from presynaptic terminals, leading to increases in both E_{Bg} and I_{Bg}, as was observed in this Chapter. Using whole-cell studies, Tan and Llano (1999) showed that 4-AP increases the

frequency of spontaneous IPSCs in cerebellar basket cells, and work from our own laboratory has shown that spontaneous glutamate release is mediated through dendrotoxin insensitive channels that are likely to be type-A (Cunningham and Jones, 2001).

Adding 10 μM NBQX to neurones already exposed to 4-AP produced an expected reduction in E_{Bg}, without having much effect on I_{Bg}. However, when bicuculline was subsequently added, E_{Bg} was restored to previous levels. This suggests that the activity of the inhibitory interneurones is having a marked effect on the level of excitatory transmission, i.e. when the inhibition is reduced, the excitation increases (see Fig 3.9).

Blockade of voltage gated Na^+ and K^+ channels by internal perfusion with Cs^+ and QX-314 had little effect on estimations of either I_{Bg} or E_{Bg} in a small population of neurones. The lack of change in E_{Bg} or I_{Bg} in these neurones supports the assertion (Rudolph *et al*., 2004) that active dendritic channels should have little effect on overall background synaptic conductances. There was a tendency for the SD of both conductances to decrease, which would be in line with the observation that the SD of both conductances was increased in the model when active channels were introduced (Rudolph *et al*., 2004). I cannot rule out the possibility that dendritic Ca^{2+} channels may strongly influence I_{Bg} or E_{Bg}, as I have not tested this possibility. However, it is interesting that one of the anticonvulsants I have tested, ethosuximide (see Chapter 7), is a blocker of transient Ca^{2+} channels (the Ca^{2+} conductance included by Rudolph *et al*., 2004) had little overall effect on E_{Bg} or I_{Bg}.

In conclusion, the VmD method offers insight in to the relationship between glutamatergic and GABAergic transmission in these slices, which can be carefully investigated with the application of various drugs. It would seem that the SD estimates, at least in this Chapter, do not offer a great deal of information with regards

to the synchrony of the neuronal populations. This may be a function of the vastly reduced preparation used here, compared to an intact brain. However, the conductance estimates offer a robust and predictable method for the study of network activity. In the next Chapter, I will continue to investigate the function of the mEC by using the VmD method with a range of well characterised pharmacological tools.

CHAPTER 4

PHARMACOLOGICAL CHARACTERISATION OF BACKGROUND SYNAPTIC CONDUCTANCES

Introduction

In the previous chapter I described experiments designed to validate the VmD approach in EC slices, and to determine the effects of raising or lowering network activity. In this chapter I will focus on the effects of modifying synaptic activity, by blockade of receptors pre- and postsynaptically and on the effects of blockade of neurotransmitter uptake (both glutamate and GABA).

Currently, the VmD method estimates conductances arising as a result of activation of two receptor populations, the glutamate and GABA ionotropic receptors, AMPAr and $GABA_Ar$, respectively, and does not take into account $GABA_B$ or NMDA receptor mediated activity. However, it is unlikely that spontaneous activation of $GABA_B$ receptors occurs in EC neurones (Woodhall *et al*., 2004), and although spontaneous currents mediated by postsynaptic NMDA receptors do occur in slices, such events are very infrequent (Beretta and Jones, 1996a). Thus, the vast majority of background synaptic noise in EC neurones is mediated via AMPA and $GABA_A$ receptors. Hence, the first set of experiments determined how blockade of either population of receptors would alter I_{Bg} and E_{Bg}. It is clear that the excitatory and inhibitory neurone populations do not exist in isolation, as shown by the experiments with TTX and high K^+ in the previous chapter. For example, blockade of glutamatergic activity would be expected to alter the activity of GABAergic interneurones, since the inhibitory neurones rely on excitatory input to drive their firing. Likewise, inhibitory neurones control the activity of principal cells, so reducing inhibition may well alter E_{Bg} as well as I_{Bg}.

Despite the fact that VmD does not take into account and conductance mediated by NMDA receptors in the principal cells, it is interesting to consider how alteration of NMDAr activity may affect E_{Eg} and I_{Bg} for a number of reasons. Interneurones in many regions are driven by a strong NMDAr mediated excitation (Monyer *et al*.,

1994; Glitsch and Marty, 1999; Maccaferri and Dingledine, 2002), and this is also the case in the EC (Jones and Buhl, 1993). In addition, glutamate release in the EC is facilitated by presynaptic NMDA autoreceptors (Berretta and Jones, 1996b; Woodhall *et al*., 2001; Yang *et al*., 2006). Presynaptic NMDAr have also been shown to increase GABA release in layer II of the EC (Woodhall *et al*., 2001). Thus, although they may not contribute directly to E_{Bg}, NMDAr are potentially important in controlling the background excitation and inhibition driven by network activity.

Much less is known about the role of kainate receptors (KAr) in cortical synaptic transmission. KAr consist of a tetrameric combination of subunits from two related families (GluR5-R7 and KA-1 and 2). It is thought that KA-2 requires combination with GluR5-R7 subunits to achieve surface expression, however GluR5, 6 and 7 receptors can form homomeric receptors by themselves (Gallyas *et al*., 2003; Alt *et al*., 2004). KAr have been implicated in fast synaptic transmission and presynaptic modulation of transmitter release in hippocampus and cortex (Collingridge *et al*., 1983; Clarke *et al*., 1997; Vignes *et al*., 1998). Recent work from our own laboratory has implicated KAr in glutamatergic and GABAergic transmission in layer III of the mEC. In summary, this work has shown that glutamate release can be facilitated by presynaptic GluR5 receptors, whereas another subtype may mediate weak postsynaptic excitation of principal neurones. GluR5 receptors make a substantial contribution to glutamate drive onto interneurones and may also directly facilitate GABA release onto principal cells (Chamberlain and Jones, unpublished observations). Thus, it is of interest to determine how alteration of KAr may alter network driven I_{Bg} and E_{Bg}. Pharmacologically, there are very few subunit specific kainate antagonists available for study. However, a GluR5-selective antagonist (UBP-302) is available, and has been used in the experiments in this chapter.

Reuptake is the major means of inactivation for glutamate and GABA at central synapses. Glutamate re-uptake is mediated by a family of excitatory amino acid

transporters (EAAT1-5), which facilitate the inward transportation of glutamate molecules, coupled to the inward movement of multiple sodium ions and a proton, along with the outward movement of a potassium ion (Seal and Amara, 1999). The actions of the EAAT family can be antagonised by the non-specific EAAT antagonist L-*trans*-pyrrolidine-2,4,-dicarboxylate (PDC). Similarly, GABA is removed from the synapse into neurones or glia by a sodium-dependent transporter (GAT-1) that can be blocked by the actions of tiagabine (Suzdak and Jansen, 1995).

Methods

Pyramidal cells were recorded in layer III of the mEC, in EC-hippocampal slices prepared from juvenile male Wistar rats (40-70g), as outlined in Chapter 2. VmD recordings using sharp electrodes comprise the majority of the data in this chapter. Whole cell patch clamp studies were also performed in layer III pyramidal cells to determine the effects of the glutamate transport blocker PDC, and the GABA transport blocker tiagabine on sEPSCs and sIPSCs.

Results

Effects of Blocking AMPAr

NBQX (10 μM) was tested in a total of 11 neurones. In the presence of NBQX, E_{Bg} fell, as predicted, from a control level of 2.9 ± 0.7 nS to 1.2 ± 0.5 nS (P=0.02). This was accompanied by a non-significant decrease in I_{Bg} (Fig. 4.1A, P>0.05). Overall, this resulted in a shift in the I:E ratio further in favour of inhibition, from 6.2 ± 1.0 to 13.1 ± 1.8 (P=0.02).

The SD of the background conductances before and after NBQX exhibited a clear downward trend. NBQX caused a reduction in the SD values of both E_{Bg} and I_{Bg}, as

outlined in Fig. 4.1B. I_{Bg} SD was subject to around a 3-fold drop, whilst E_{Bg} SD was reduced almost four-fold, however, surprisingly, neither was significant.

NBQX also caused a decrease in cellular excitability. The number of spikes generated by a 250 ms train showed a downward trend from 6.2 ± 0.9 to 4.2 ± 1.1 (Fig. 4.1E). Spike amplitude was unchanged (Fig. 4.1D). However, spike threshold was significantly increased (P=0.01, Fig. 4.1C) to around 5 mV more positive to rest compared to control.

NBQX is not specific for AMPA receptors. At higher concentrations it can also block KAr. So, in three further neurones, a specific AMPAr antagonist, GYKI-53655, was tested at a concentration of 25 μM. Control values for E_{Bg} and I_{Bg} in this sample were much lower than those seen in experiments with NBQX. However, the effect of GYKI-53655 was very similar.

In the presence of GYKI-53655, I_{Bg} was reduced from 5.4 ± 0.5 nS to 2.0 ± 0.7 nS. E_{Bg} was also reduced, from 1.4 ± 0.1 nS to 0.4 ± 0.1 nS. Both these changes were found to be significant (P_I=0.02 and P_E=0.01, Fig. 4.2A). The I:E ratio was not significantly altered, in contrast to the effects of NBQX where it increased substantially in favour of inhibition. Given the low number of experiments using GYKI-53655 and the marked difference in control values for I_{Bg} compared to NBQX, it would be premature to place any great significance on this result. It is also true that GYKI-53655 had less of an effect on the SD of I_{Bg} and E_{Bg} than NBQX, although again the control values, especially for inhibitory SD, were lower in this group. I_{Bg} SD was largely unchanged, although E_{Bg} SD was reduced by around 40% (Fig. 4.2B)

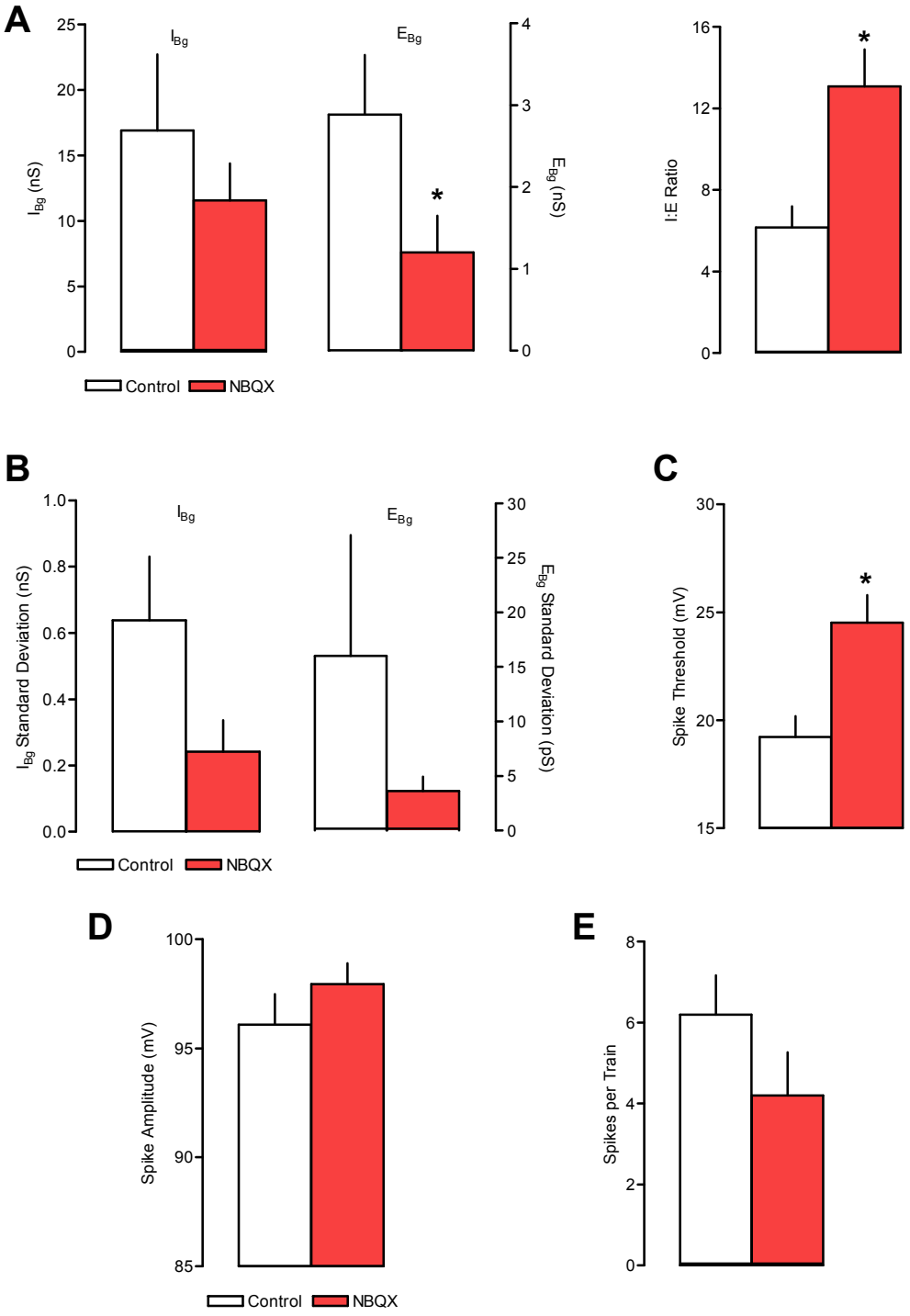

Figure 4.1: Effect of AMPAr blockade on background activity and cellular excitability estimates. NBQX (10 µM, n=11) was applied during intracellular recording from layer III principal cells. A: A small decrease in I_{Bg}, likely due to decreased drive onto interneurones, was accompanied by a significant drop in E_{Bg}. The I:E ratio shifted in favour of inhibition. B: SD estimates showed a downward trend but were not significantly altered. C: Only spike threshold was significantly changed, with no change in amplitude (D) and a small decrease in spikes/train (E).

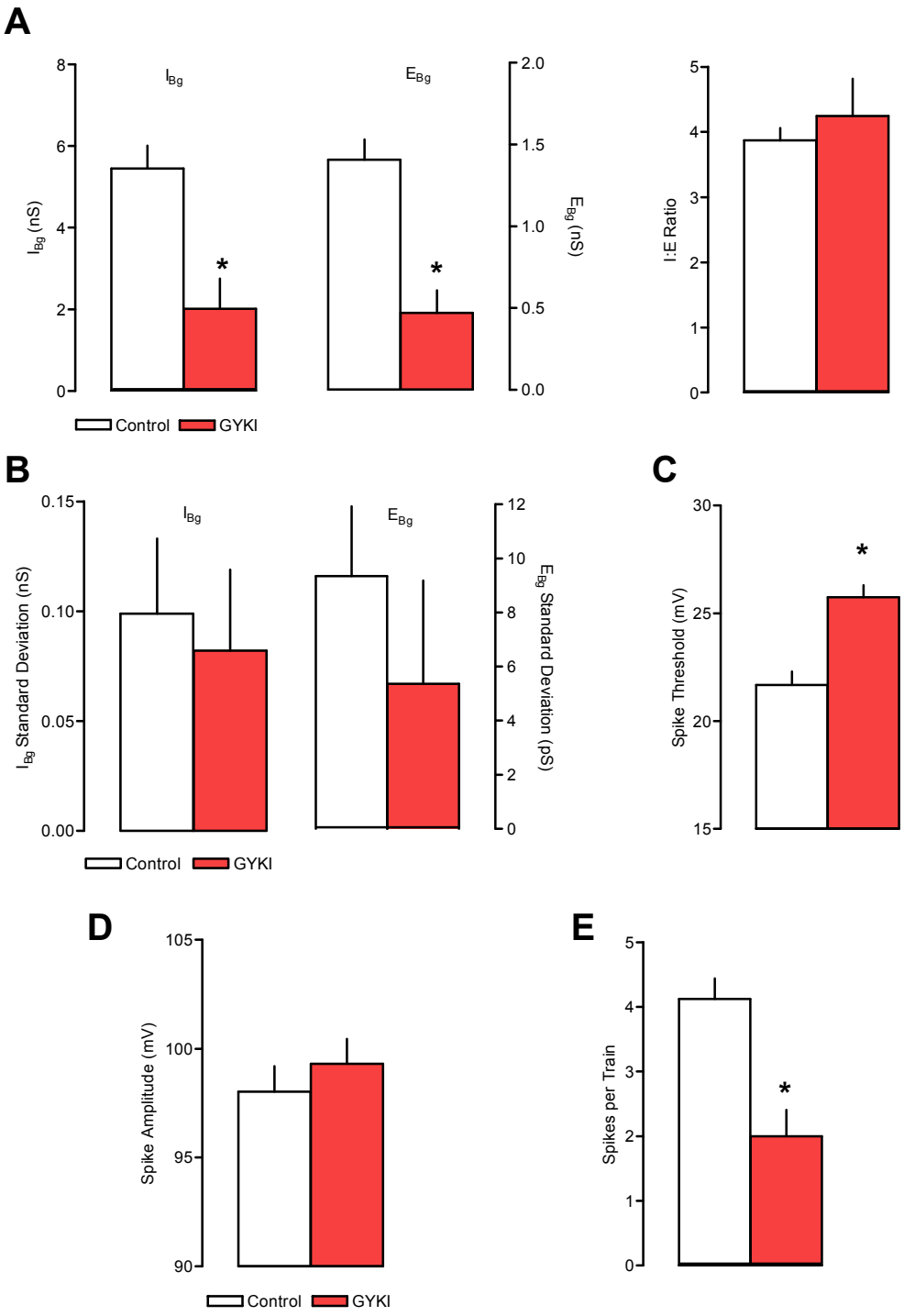

Figure 4.2: Effects of specific AMPAr blockade on conductance estimates and cellular excitability. A: Similar to NBQX, both I_{Bg} and E_{Bg} are reduced by GYKI-53655, with a small shift in I:E ratio in favour of inhibition. B: SDs are not affected, suggesting that any change seen with NBQX is mediated by KAr. C: Spike threshold is significantly increased, with no change in amplitude (D) and a significant reduction in the number of spikes generated by a 250 ms pulse (E). This suggests reduced cellular excitability with GYKI-53655.

As with NBQX, cellular excitability was reduced by GYKI-53655. Spike threshold increased from a control value of 21.6 ± 0.6 mV to 25.7 ± 0.5 mV (P=0.002, Fig. 4.2C). At the same time, spikes evoked during the depolarising pulse fell by around 50% (P=0.006, Fig. 4.2E), without accompanying change in action potential amplitude (Fig. 4.2D). Thus, it is clear that blocking AMPA receptors drastically reduces E_{Bg}, but that I_{Bg} is also concurrently reduced meaning that overall, background inhibition comes to predominate further. This change is reflected by indications of decreased cellular excitability.

Blockade of NMDA Receptors

As noted previously, the VmD method does not account for NMDA receptors in estimation of E_{Bg}, so it might be expected that NMDA receptor blockade would have little effect. The competitive NMDAr antagonist R-AP5 was used at a concentration of 30 μM on a total of 7 neurones. Overall, NMDAr blockade had relatively weak effects on the global background inhibitory and excitatory conductances (Fig. 4.3A). I_{Bg} was not significantly affected, from 15.0 ± 5.6 nS to 10.1 ± 3.0 nS in the presence of R-AP5 (P>0.05). At the same time, E_{Bg} was little altered, from a control level of 3.2 ± 0.9 nS to 2.8 ± 0.5 nS (P>0.05). The end result was little change in the I:E ratio (Fig 4.3A, P>0.05).

It was possible to split the neurones in this group into two subgroups, based on the control levels of background conductances. In four neurones (Fig. 4.4), values of E_{Bg} and I_{Bg} were very similar to those recorded in the general population as a whole. R-AP5 had little or no effect on conductance values in these neurones. However, the other three cells showed much higher levels of baseline inhibition and excitation. In these cells addition of 30 μM R-AP5 caused a reduction in I_{Bg}, from 32.1 ± 11.9 nS to 9.8 ± 3.7 nS. Concurrently, E_{Bg} was reduced from 5.4 ± 1.8 to 1.7 ± 0.6 nS.

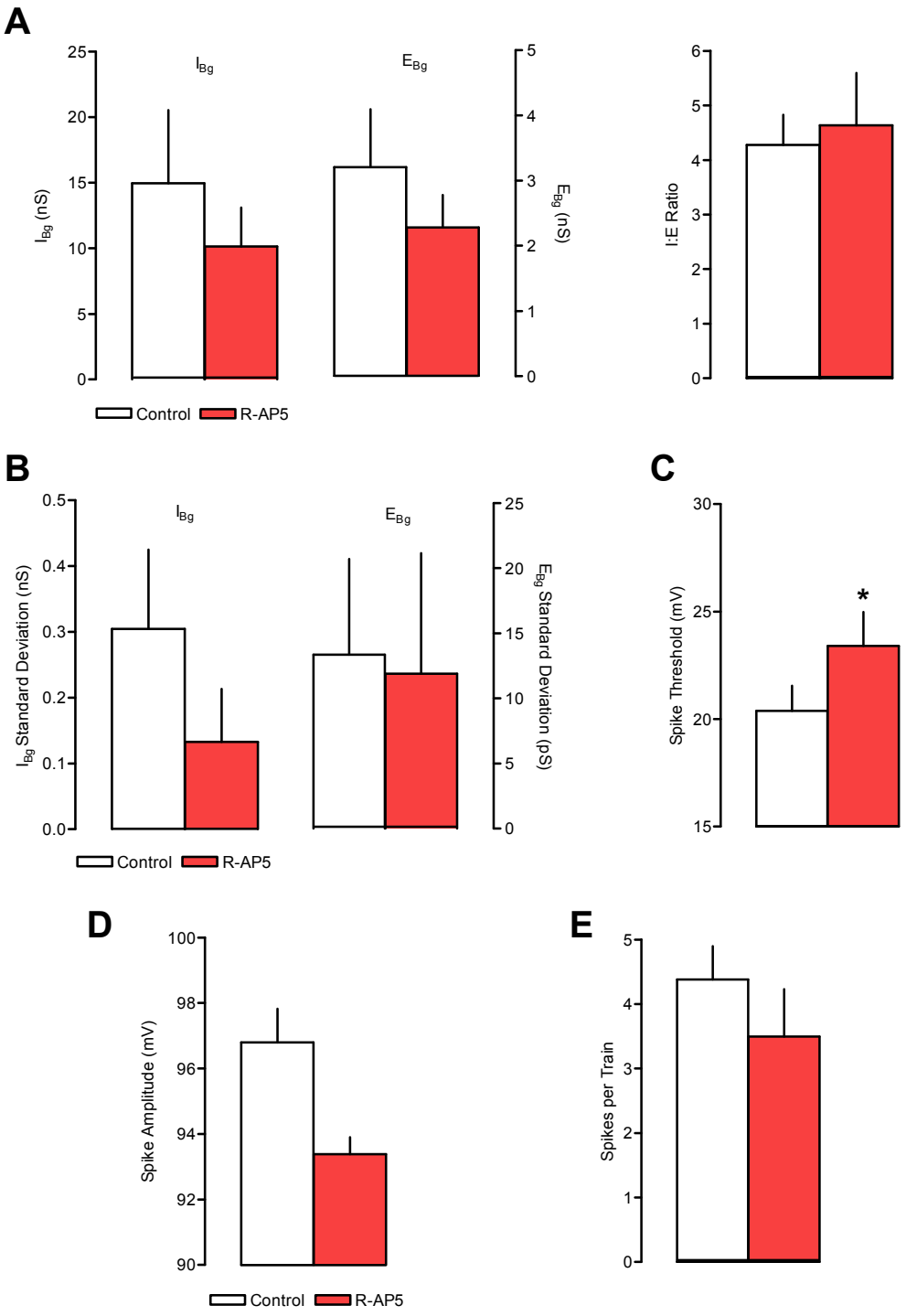

Figure 4.3: NMDAr blockade has little effect on conductance estimates. A: Slight downward trends are seen in both I_{Bg} and E_{Bg} in the presence of R-AP5 (30 μM) though these are not significant. I:E ratio is unchanged. B: The SD of I_{Bg} is slightly reduced, but neither SD is significantly altered by NMDAr blockade. C: Spike threshold is slightly, but significantly, increased by R-AP5. D: Neither spike amplitude or (E) spikes per 250 ms pulse are significantly altered during NMDAr block.

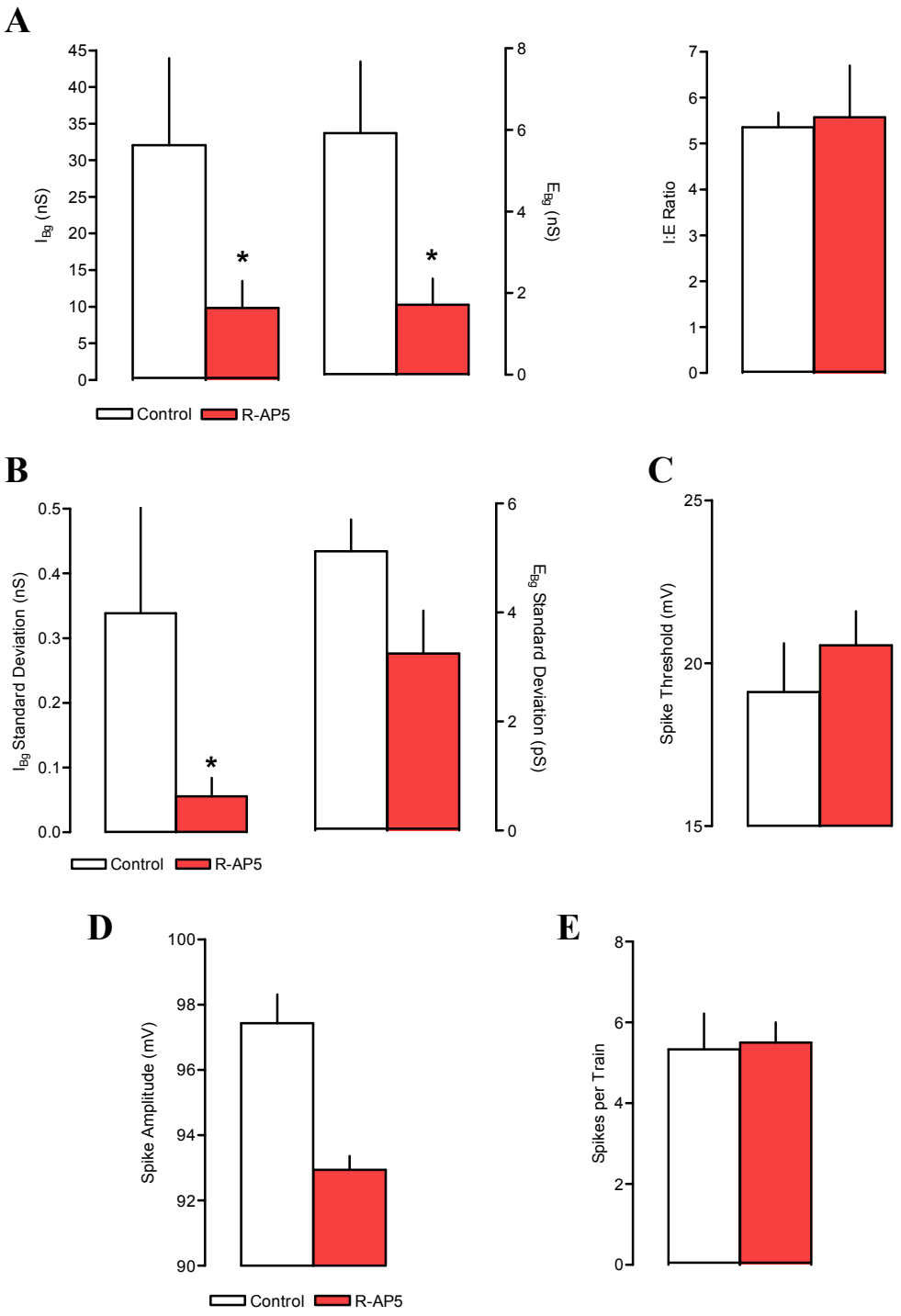

Figure 4.4: Effect of NMDAr blockade on high-activity networks. In a subgroup of the R-AP5 treated cells, those showing higher levels of baseline activity were significantly affected by addition of 30 µM R-AP5. A: Both inhibitory and excitatory conductance was reduced. B: There was no change in I:E ratio. C: Only the SD of I_{Bg} was significantly altered. C-E: No change in cellular excitability was observed.

The I:E ratio was unchanged (control = 5.4 ± 0.3, drug = 5.6 ± 1.1). Thus, these results may suggest that NMDA receptors may help to maintain a high level of baseline network activity in some slices. The reasons why this may be so are discussed below.

In the total population of 7 neurones, NMDAr blockade decreased the SD of I_{Bg} without affecting that of E_{Bg} (Fig. 4.3B). If the SDs are accepted as a measure of population synchrony, this may indicate that inhibitory interneurones rely on NMDA receptor mediated drive for synchronisation, whereas principal neurones may not.

The weak overall effects of R-AP5 on I_{Bg}, E_{Bg} and I:E ratio were reflected by cellular excitability changes that were marginal. Spike firing threshold rose from 20.4 ± 1.2 mV to 23.4 ± 1.6 mV (P=0.01). However, the number of spikes generated by a 250 ms train was not significantly affected. Spike amplitude was also unaffected (Fig. 4.3 C-E).

Blockade of GluR5 Kainate Receptors

A contribution of KAr to background excitability is not directly accounted for in VmD measurements, as mentioned earlier. However, in studies in layer III neurones, a role for the GluR5 subtype in controlling both glutamate and GABA release has been demonstrated in this lab (Chamberlain and Jones, unpublished observations), so it was of interest to study effects on E_{Bg} and I_{Bg}.

The GluR5-specific antagonist UBP-302 was tested at a concentration of 20 μM in 6 pyramidal neurones. Control values were 10.8 ± 3.4 nS for I_{Bg}, 2.7 ± 1.0 for E_{Bg}, with a mean I:E ratio of 4.6 ± 0.4.

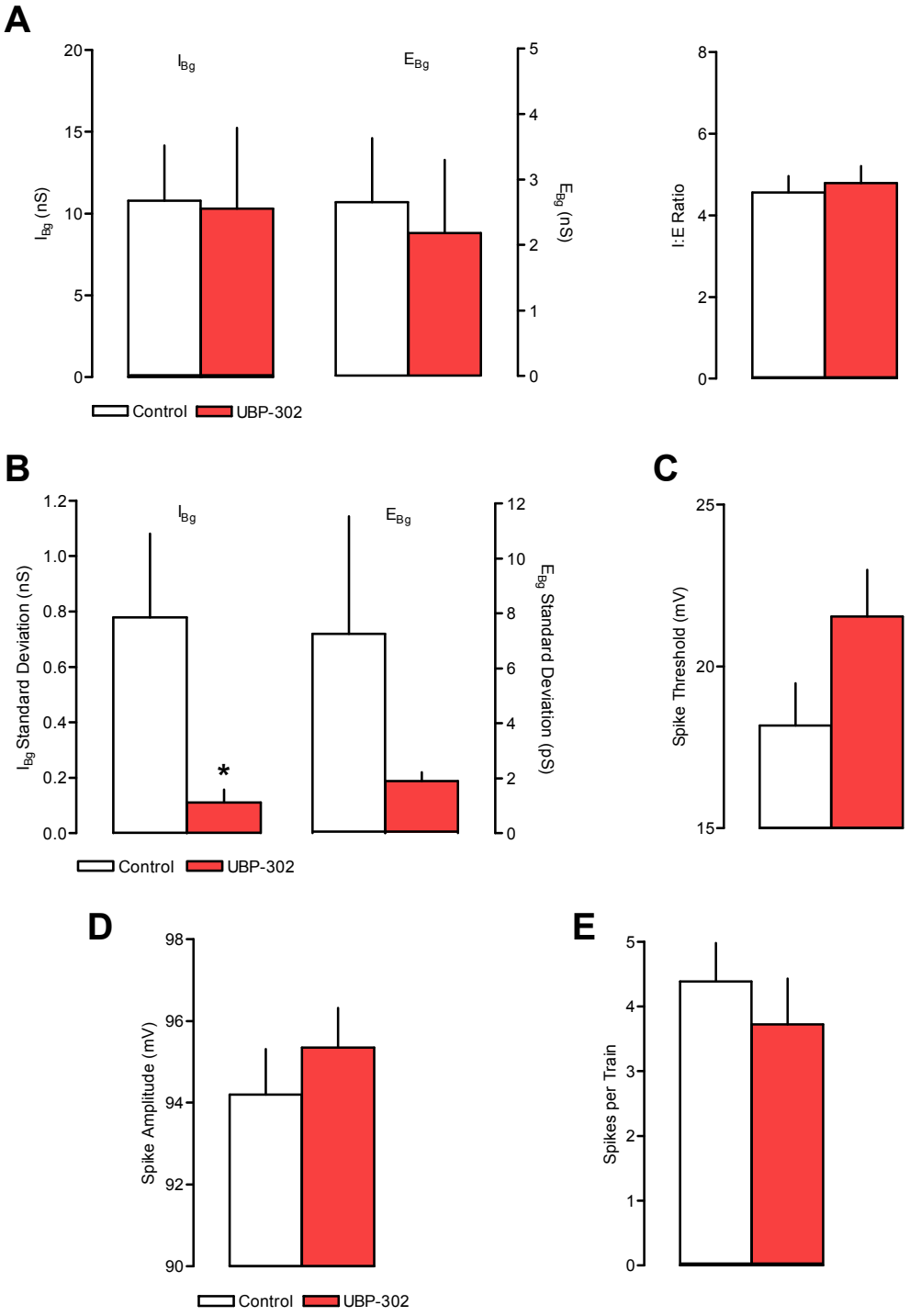

Figure 4.5: Blockade of Glu-R5-containing KAr with UBP-302 (20 µM). Whilst there is little effect on I_{Bg}, E_{Bg} or I:E ratio (A), and no appreciable change in cellular excitability (C-E), the obvious reduction in conductance SD may indicate that these receptors have a role to play in synchrony either within or between neurone populations. This notion is supported by studies observing slow-wave activity in the cortex (e.g. Cunningham et al., 2006).

The antagonist had little effect on any of these conductance values. I_{Bg} and I_{Bg} were both unchanged leading to no change in the I:E ratio. This is illustrated by Fig. 4.5A.

However, the addition of UBP-302 did have noticeable effects on the SD of both I_{Bg} and E_{Bg}. I_{Bg} SD was reduced from 0.78 ± 0.30 nS to 0.11 ± 0.04 nS (P=0.04). E_{Bg} SD was not significantly reduced, although there was a clear trend towards this (see Fig. 4.5B). The reduction in SDs may suggest that kainate receptors play a role in synchronisation of principal and interneurone populations in layer III.

Cellular excitability was largely unaffected in the presence of UBP-302. However, spike firing threshold was slightly increased, and the number of spikes evoked in a train fell by around 10% (Fig. 4.5 C and E). Action potential amplitude was not affected (Fig. 4.5D). These results would suggest that, whilst it has little effect on overall synaptic activity or cellular excitability, blockade of GluR5-containing kainate receptors may alter network synchronisation.

Blockade of Glutamate Uptake

Having determined the effects of blockade of pre- and postsynaptic ionotropic glutamate receptors on background synaptic activity, it was interesting to see what the effect of increasing activation of these receptors would have. To that end, I attempted to increase the ambient levels of glutamate by blocking its re-uptake. The restricted glutamate analogue PDC was used to study the effect of EAAT blockade using both VmD and whole cell patch clamp methods.

VmD

The VmD method was applied to 6 pyramidal neurones. Again, it should be noted that the control values for both background conductances were rather lower than usual, in

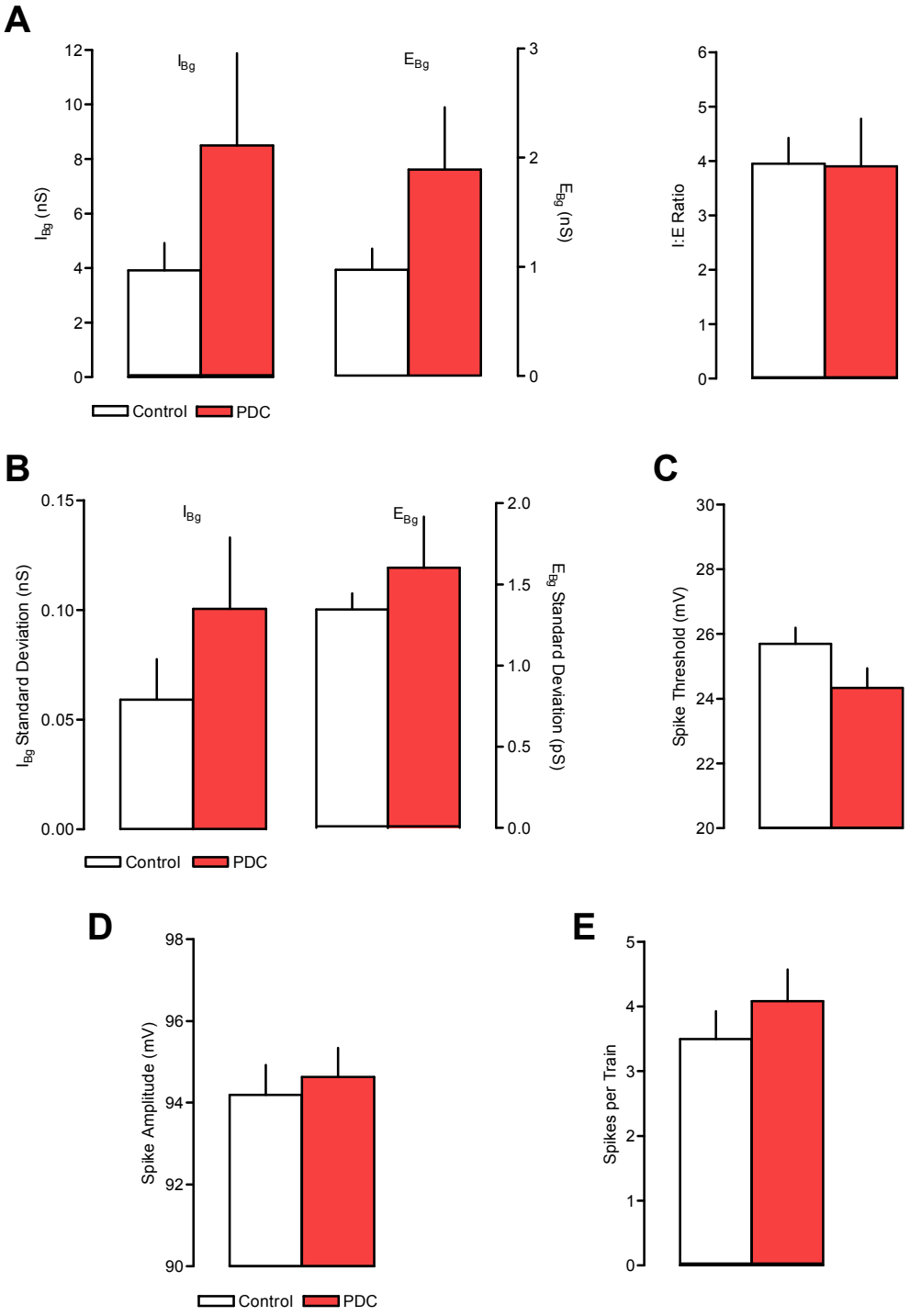

Figure 4.6: Effect of glutamate uptake blockade with PDC (50 µM). I_{Bg} and E_{Bg} are increased by uniform amounts, although neither is changed significantly, leading to little change in I:E ratio (A). Similarly, I_{Bg} and E_{Bg} SD are both slightly increased (B). The lack of change in I:E ratio leads to no change in cellular excitability (C-E) in the presence of PDC.

this sample of neurones. Perfusion with PDC (50 μM) caused little overall change in the I:E ratio, as a result of a uniform rise in both I_{Bg} and E_{Bg}.

I_{Bg} was increased from 3.9 ± 1.0 nS to 8.5 ± 3.4 nS (P>0.05). Similarly, E_{Bg} increased by nearly two-fold, from 1.0 ± 0.2 nS to 1.9 ± 0.5 nS (P>0.05). At the same time, the SD of I_{Bg} and E_{Bg} did not change significantly, although both were increased (Fig. 4.6B). SD of I_{Bg} increased by 69%, whilst SD of E_{Bg} increased by 23%.

Despite the rise in E_{Bg}, PDC had little effect on cellular excitability measurements. Spike firing threshold, spikes generated during a 250 ms depolarising pulse and action potential amplitude were not significantly changed (Fig. 4.6 C-E).

Whole Cell Patch Clamp

Since the E_{Bg} and I_{Bg} depend on global integration of spontaneous transmitter release (see Introduction) it was decided to compare the effects of PDC on VmD measurements to effects on spontaneous synaptic currents in layer III neurones, as these had not been investigated previously. sIPSCs and sEPSCs were recorded in a total of 12 layer III pyramidal neurones (6 per group). In pooled data analysis, 200 consecutive events were analysed in each neurone, in the presence and absence of the drug.

The results of the patch clamp studies of sEPSCs are summarised in Fig. 4.7. It is possible to see an increase in the frequency of sEPSCs in the raw voltage clamp traces from one neurone shown in Fig. 4.7A, and by the pooled data from Fig. 4.7B. Addition of PDC (50 μM) caused a leftward shift in the cumulative probability curve

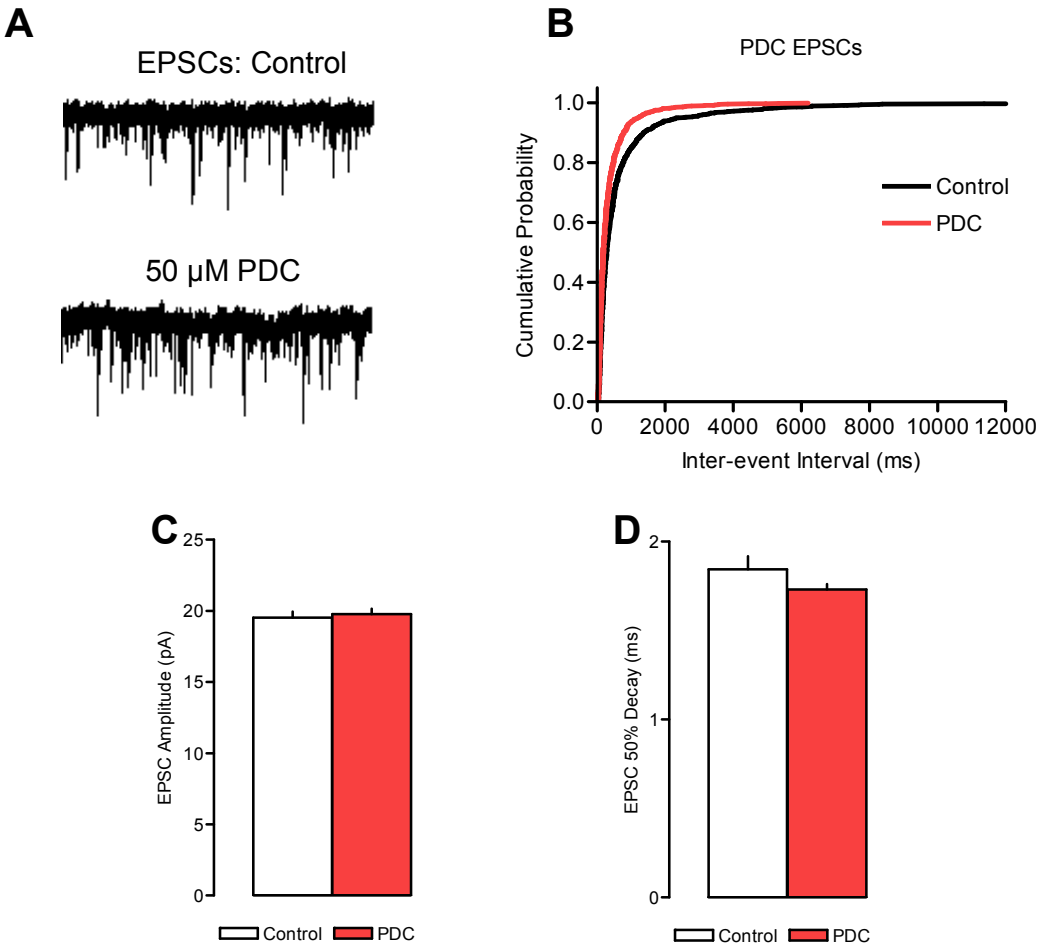

Figure 4.7: Effect of EAAT blockade on sEPSC activity in layer III pyramidal cells. A: Example traces from whole-cell recording of one layer III mEC pyramidal neurone show that between control (top) and PDC (50 µM) there is a discernable increase in frequency during PDC application. B: The inter-event interval curve shifts to the left with PDC, indicating increased sEPSC frequency during EAAT blockade. C: Mean amplitude of sEPSCs is unchanged by PDC. D: sEPSC decay time is similarly unaffected.

for IEI (Fig. 4.7B). This indicates a reduction in IEI, the corollary of which is an increase in the frequency of EPSCs. Apart from the increased frequency of sEPSCs, there was little alteration in other properties. PDC had little effect on the kinetics of the observed excitatory events. 50% decay times were measured as the increased frequency made it difficult to observe the slower component of the events. Average sEPSC amplitude was also largely unaffected by the addition of PDC (Fig. 4.7D).

Fig. 4.8 illustrates the effects of PDC on sIPSCs in layer III neurones. The voltage clamp records in 4.8A show a high frequency of events in the control situation, with

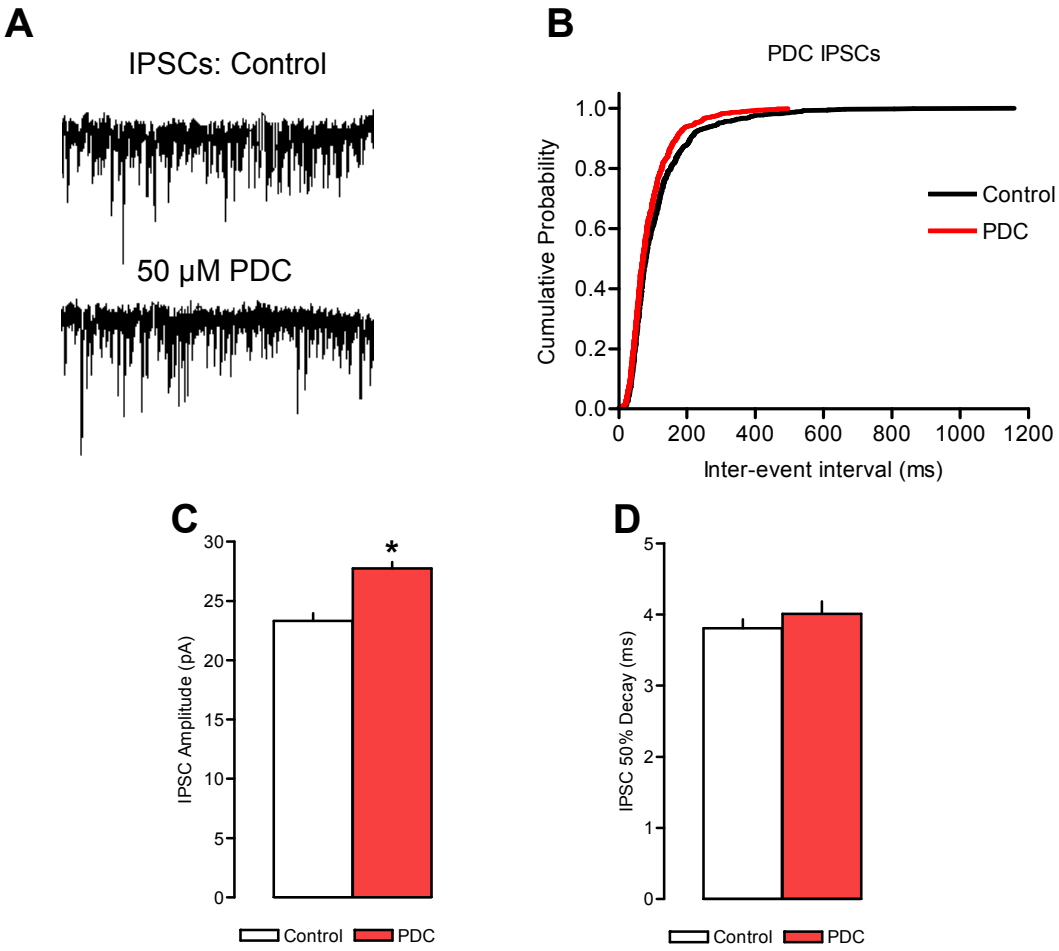

Figure 4.8: Effect of PDC on sIPSC activity in layer III. Details as for Fig. 4.7. A: Looking at the example trace shown, there is no readily noticeable difference between activity during control and PDC states. B: The IEI curve shifts slightly to the left with PDC, indicating slightly increased frequency. C: sIPSC amplitude is significantly increased, probably accounting for the majority of the increase seen with the VmD method. D: Decay time is unaffected.

no obviously discernable change in PDC. However, in pooled data the mean IEI was decreased from 110.4 ± 2.9 ms to 89.6 ± 1.9 ms by PDC. Again, this is shown by the leftward shift in the IEI curve, indicating an increase in sIPSC frequency (Fig. 4.8B).

PDC also caused a small but significant increase in the average amplitude of IPSCs in these cells (23.3 ± 0.6 pA control, 27.7 ± 0.5 pA PDC, $P<0.001$). However, neither the 50% decay time of sIPSCs nor the 10-90% rise time (1.9 ± 0.2 ms to 2.1 ± 0.3 ms) were altered (Fig. 4.8C-D).

Blockade of GABA Re-uptake

Thus, it is clear that blockade of $GABA_A$ receptors powerfully reduces I_{Bg} as would be expected, but with concurrent effects on E_{Bg}. In the next series of experiments, I investigated the effects of enhancing GABA transmission using the GABA uptake blocker, tiagabine.

In a similar study to the PDC data above, tiagabine was investigated using both VmD and whole cell voltage clamp approaches. In the VmD studies, a concentration of 4 μM tiagabine was used, as it was found that higher concentrations caused unpredictable and spontaneous depolarisations of the membrane potential. In subsequent voltage clamp studies, tiagabine was tested at both 4 and 12 μM.

VmD

VmD conductance and SD estimates were obtained from a total of 6 pyramidal neurones. Addition of tiagabine (4 μM) caused a large, six-fold rise in I_{Bg} from a control level of 8.1 ± 2.1 nS to 48.8 ± 16.8 nS ($P=0.0017$), although there was little change in SD. Surprisingly, perhaps, E_{Bg} also increased but to a much lesser degree, from 1.8 ± 0.4 nS to 3.9 ± 1.0 nS ($P>0.05$). Although E_{Bg} was more than doubled, the overall change shifted the I:E ratio very heavily in favour of inhibition, from 4.5 ± 0.2 to 12.5 ± 4.4 ($P=0.026$, Fig. 4.9A).

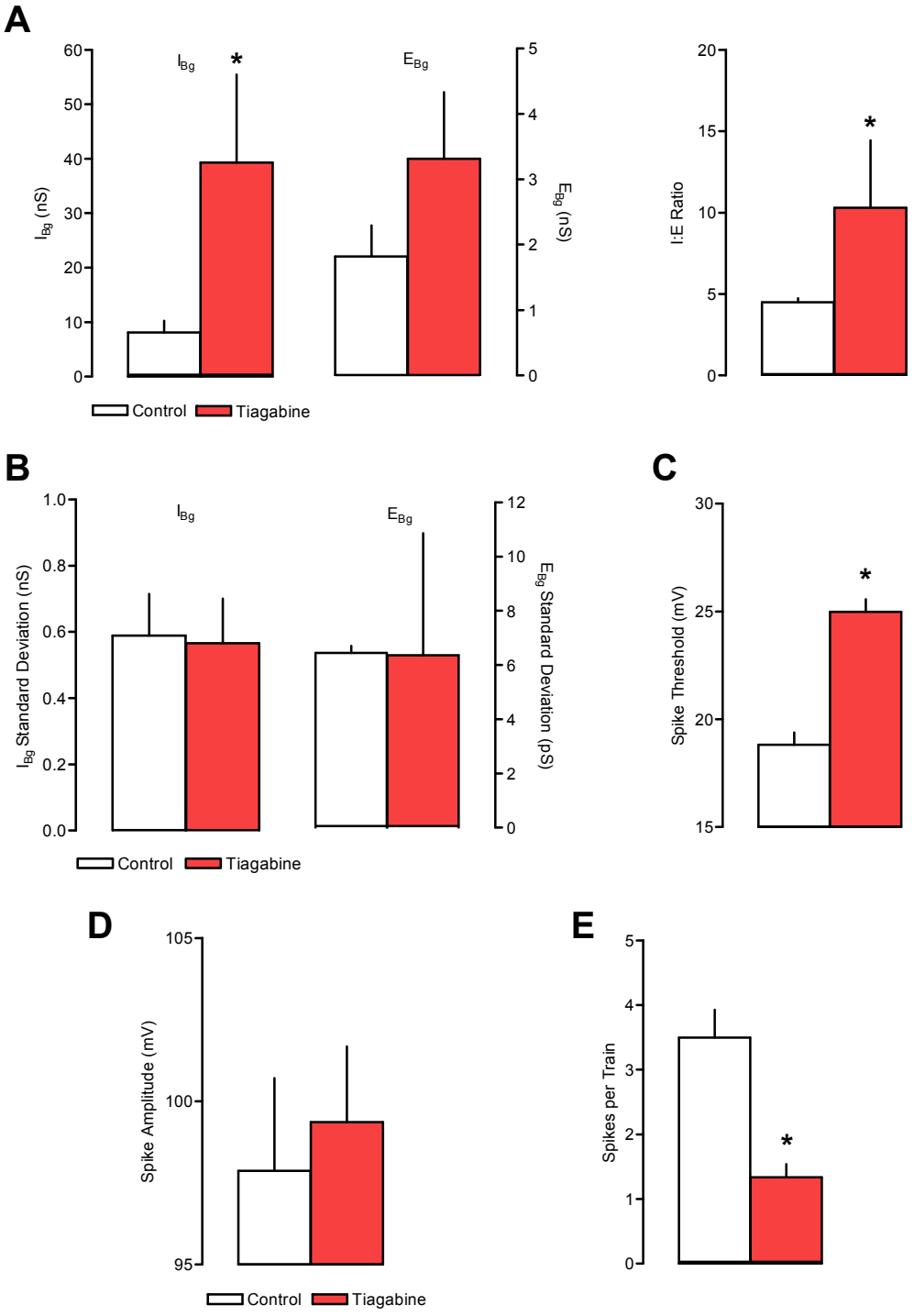

Figure 4.9: Effects of GABA uptake blockade on conductance estimates and cellular excitability. A: In all neurones, ttiagabine (4 µM) causes a persistent upward trend in E_{Bg} and a significant increase in I_{Bg}. The I:E ratio is shifted two-fold in favour of inhibition. B: SD of I_{Bg} or E_{Bg} is not significantly changed by GAT-1 blockade. C: Spike threshold is made 5 mV less negative from rest during tiagabine application. D: Spike amplitude is not changed. E: The number of spikes during a 250 ms pulse is reduced 3-fold by tiagabine.

This large shift in I:E ratio was accompanied by an appreciable effect on neuronal excitability. Tiagabine raised the action potential firing threshold from 18.8 ± 0.5 mV to 24.9 ± 0.5 mV positive to rest (P<0.001). The number of spikes generated during a 250 ms depolarisation fell substantially from 3.5 ± 0.4 to 1.3 ± 0.21 (P=0.001), but action potential amplitude was unaffected (Fig. 4.9C-E).

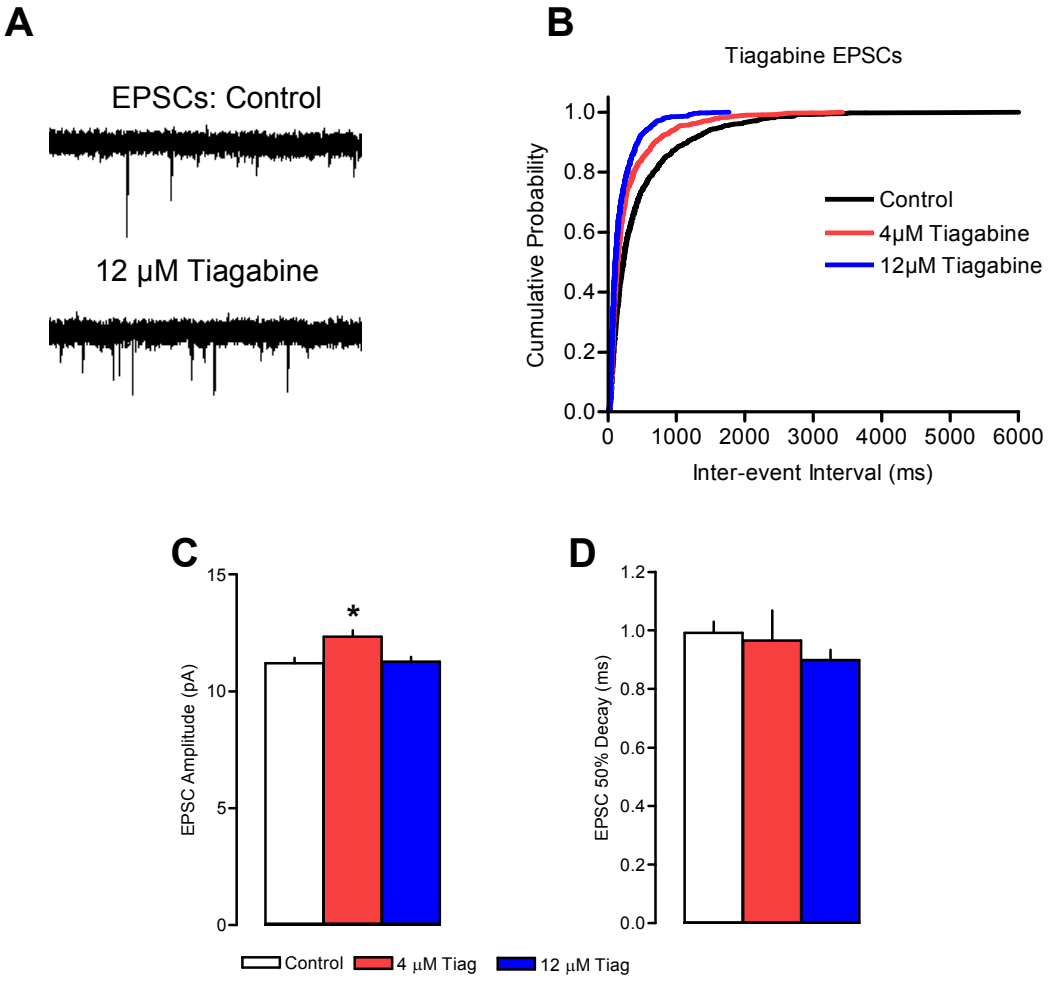

Figure 4.10: Effect of increasing tiagabine concentration on sEPSCs. A: The example traces, somewhat surprisingly, clearly show an increase in EPSC frequency with 12 µM tiagabine. B: This is supported by the IEI data, showing a concentration-dependent shift to the left with tiagabine. This is in agreement with the VmD data for this drug (Fig. 4.9). C: At 4 µM, sEPSC amplitude was significantly increased, with the subsequent reduction in 12 µM possibly due to depletion of glutamate from presynaptic stores. D: Decay time is not significantly affected, but shows a downward trend with increasing tiagabine.

Whole Cell Patch Clamp

As with PDC, whole-cell patch clamp recordings of the effects of tiagabine on spontaneous transmitter release had not previously been conducted in these neurones. To correlate effects on spontaneous release with estimate of I_{Bg} and E_{Bg} I studied the effects of tiagabine on sEPSCs and sIPSCs in a total of 12 neurones (6 for each group). As in the PDC experiments, 200 consecutive events were analysed for each of the control and drug periods in each neurone. The results are summarised in figures 4.10 and 4.11. Tiagabine had a contrasting effect on EPSCs and IPSCs, however the results were perhaps not what would be expected, especially when the VmD data above are considered.

The effect of increasing tiagabine concentration on sEPSCs is illustrated in Fig. 4.10. An increase in EPSC frequency with tiagabine can be seen in the trace from a single neurone in Fig. 4.10A, and is supported by the increasing leftward shift in the IEI curve seen in Fig. 4.10B. Additionally, EPSC amplitude was slightly, but significantly, increased from control (11.2 ± 0.2 pA) by 4 μM (12.3 ± 0.3 pA) and 12 μM tiagabine (11.3 ± 0.2 pA, $P<0.01$, ANOVA). EPSC decay time showed a downward trend in increasing concentrations of tiagabine, from 0.99 ± 0.04 ms to 0.89 ± 0.04 ms in 12 μM tiagabine ($P>0.05$).

The results obtained for IPSCs in tiagabine were surprising, especially with reference to the VmD data. As seen in Fig. 4.11A and B, increasing concentrations of tiagabine actually cause a reduction in sIPSC frequency, illustrated by a rightward shift in the IEI curve (Fig. 4.11B). However, the kinetics of the observed events may provide some explanation for the VmD results. IPSC amplitude and decay time increased steadily with tiagabine concentration (Fig. 4.11C-D). Amplitude increased from 17.8 ± 0.5 pA to 21.8 ± 1.1 pA in the presence of 12 μM tiagabine ($P=0.004$). Similarly, 50% decay times were increased from 3.65 ± 0.06 ms to 4.51 ± 0.15 ms ($P<0.001$).

These results indicate that, although frequency of IPSC activity is reduced, the longer duration and larger amplitude of the GABAergic events may account for the observed increases in background inhibitory conductance.

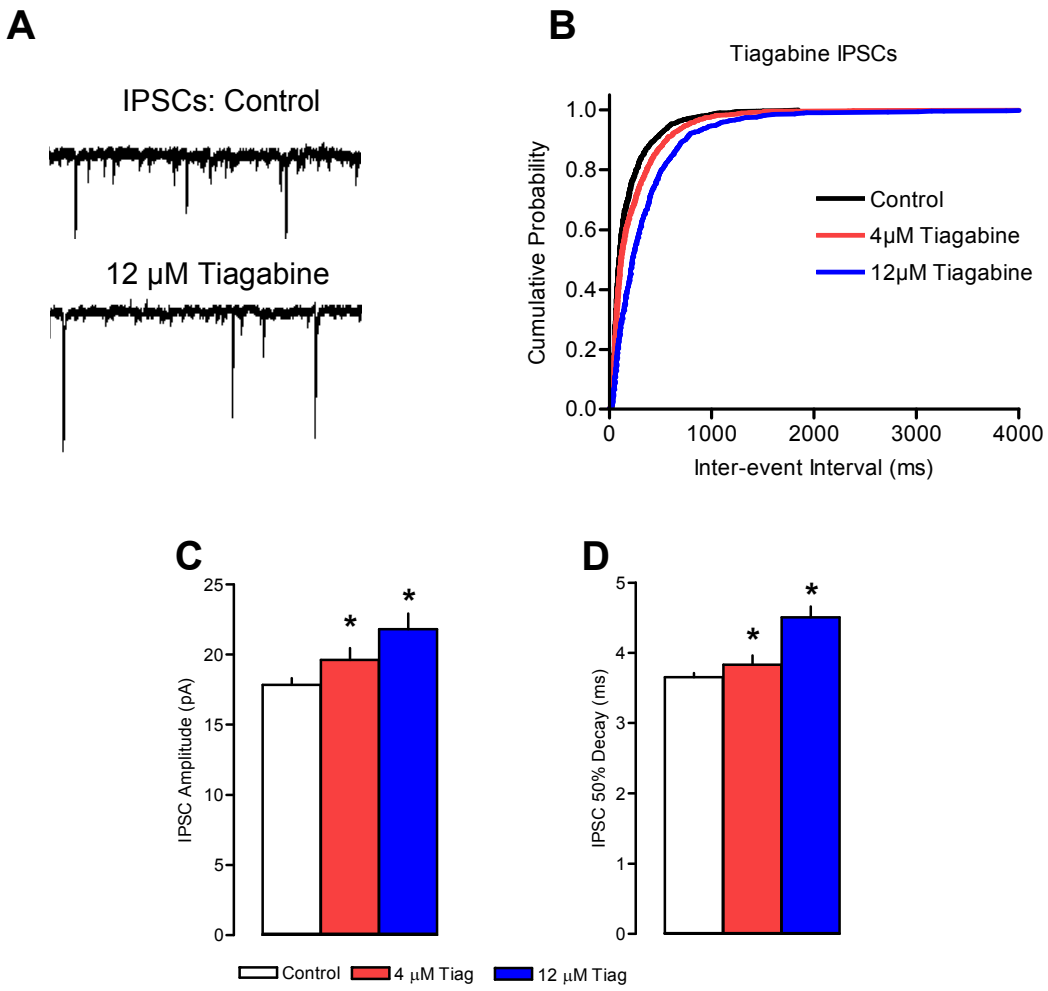

Figure 4.11: Tiagabine reduces sIPSC frequency in a concentration-dependent manner. A: In contrast to the EPSC data (Fig. 4.10), example traces show a reduction in sIPSC frequency with tiagabine. However, an increase in amplitude is clearly evident. B: The IEI curve shifts right with increasing tiagabine, supporting the trend seen in (A). C: However, any decrease in IPSC frequency may be cancelled out by the observed significant concentration-dependent increases in amplitude. D: Similarly, decay time is significantly increased with tiagabine, suggesting that, in agreement with the VmD data (Fig, 4.9), I_{Bg} may actually be increased, despite reductions in sIPSC frequency.

Blockade of $GABA_Ar$ or AMPAr During VGSC Blockade

I have previously demonstrated the effects of the VGSC blocker TTX on conductance estimates layer III pyramidal cells (Chapter 3). Subsequent to TTX application, $GABA_Ar$ or AMPAr were blocked using bicuculline (10 µM, n=3) and NBQX (10 µM, n=3) respectively. In the presence of TTX (1 µM), I_{Bg} = 6.7 ± 1.5 nS, E_{Bg} = 3.6 ± 1.1 nS and I:E ratio = 2.2 ± 0.5.

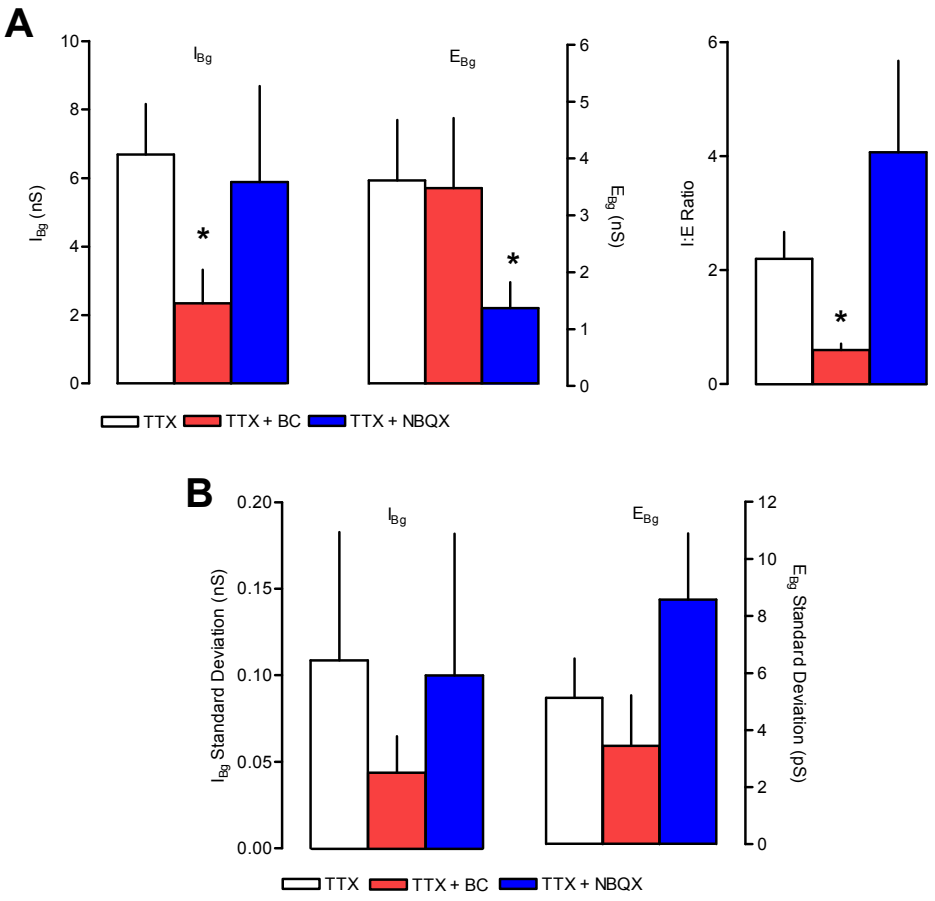

Figure 4.12: Addition of bicuculline and NBQX to TTX treated cells. Graphs show VmD estimates in cells treated with 1 µM TTX. Conductance values in TTX were I_{Bg} = 6.7 ± 1.5 nS, E_{Bg} = 3.6 ± 1.1 nS, I:E ratio = 2.2 ± 0.5. A: Addition of bicuculline (10 µM) causes a significant decrease in I_{Bg}, leaving E_{Bg} unchanged and significantly shifting the I:E ratio in favour of excitation(to 0.6 ± 0.1). Conversely, treatment with NBQX (10 µM) caused no change in I_{Bg}, but a significant decrease in E_{Bg}. The I:E ratio displayed a trend towards increased inhibition (to 4.1± 1.6) but this was not significant. B: None of the SD estimates were affected by bicuculline or NBQX. This was to be expected, as action-potential mediated network connections would be abolished by TTX.

Addition of bicuculline (10 μM) in the presence of TTX caused a significant reduction in I_{Bg} (to 2.3 ± 1.0 nS, P=0.02), but E_{Bg} was unaffected (at 3.5 ± 1.2 nS, Fig. 4.12A). The SDs of I_{Bg} and E_{Bg} were not affected.

NBQX (10 μM), in the presence of 1 μM TTX, had essentially the opposite effect to bicuculline. Compared to TTX alone, E_{Bg} was decreased at 1.4 ± 0.5 nS (P=0.02), whereas I_{Bg} was unaffected at 5.9 ± 2.8 nS. Similarly to bicuculline, neither SD was affected by NBQX addition (Fig. 4.12B)

Discussion

The experiments in this chapter were designed to investigate the control exerted on background activity, and hence cellular excitability, by a range of receptor populations. However, the VmD method is designed only to incorporate conductance mediated by postsynaptic AMPA and $GABA_A$ receptors in the recorded cell, giving values for E_{Bg} and I_{Bg}, respectively. As stated in Chapter 3, spontaneous activation of $GABA_B$ receptors is highly unlikely in EC neurones under normal circumstances (Woodhall *et al*., 2004), and spontaneous NMDAr-mediated events are very infrequent (Berretta and Jones, 1996a). Background synaptic noise in EC neurones is, therefore, overwhelmingly reliant on the activation of AMPA and $GABA_A$ receptors. We are confident, therefore, that a reliable and repeatable measure of background activity can be obtained through the current version of the VmD method.

The Destexhe group has considered, and is working on, the incorporation of multiple excitatory components to a revised version of the VmD method. However, the mathematical equations necessary to support multiple excitatory (or inhibitory) inputs in this way become exponentially more complex with increasing numbers of components. Thus, given the already highly complex nature of the VmD method and the equations used to construct and test it, it may not be practicable to include more

than AMPA and $GABA_A$ receptors at this time (Alain Destexhe, personal communication).

The VmD results obtained in the presence of both NBQX and GYKI-53665 indicate that AMPA receptors are indeed mediating the majority of excitatory transmission in these cells. E_{Bg} in both cases was significantly reduced to around 33% of control levels. This reduction could logically be attributed to the reduction in postsynaptic AMPAr activity, something that is directly measured in the VmD equation. Theoretically, it is possible that recurrent excitatory drive, as seen between cells P_2 and P_1 in Fig. 4.13, could account for some of the background activity abolished by AMPAr antagonists (Dhillon and Jones, 2000). However, in our VmD studies with TTX and NBQX, it is clear that recurrent, action potential dependent excitatory activity has very little bearing on E_{Bg} measured in these experiments.

Both NBQX and GYKI-53655 cause a clear reduction in I_{Bg}. With reference to the above-mentioned TTX experiments, the majority of inhibitory transmission in layer III of the mEC would appear to be activity-dependent. Thus, the most likely explanation for the reduction in I_{Bg} mediated by the AMPAr antagonists is a reduction in excitatory drive onto inhibitory interneurones. A further reduction in inhibitory transmission could be mediated through reduction of GABA release due to blockade of presynaptic AMPAr (and, in the case of NBQX, KAr) at inhibitory terminals (Bureau and Mulle, 1998; Rusakov *et al.,* 2005), however the co-application of TTX and NBQX in Chapter 3 showed only a slight, insignificant reduction in I_{Bg}.

NBQX causes a far larger reduction in levels of I_{Bg} and E_{Bg} SD than GYKI-53655. If we are to continue to accept that these SD measurements provide an idea of the synchronisation of neuronal populations, it must be concluded that the greater effects seen with NBQX are due to its action at KAr, the role of which will be discussed later.

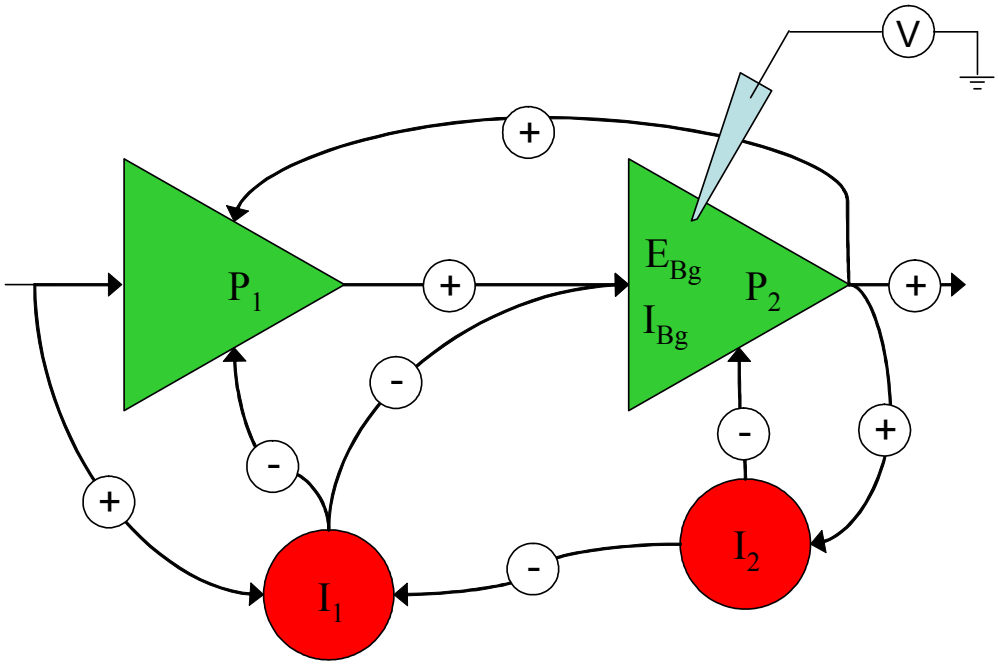

Figure 4.13: Schematic diagram of network connectivity in the mEC. Antagonism of one population of receptors, for example AMPAr, could have secondary effects across the network, not just at the postsynaptic membrane. Blockade of AMPAr could reduce recurrent excitation (P_2 -> P_1 -> P_2) or excitatory drive onto interneurones (I_1 and I_2) leading to changes in the observed conductances not mediated directly at the postsynapse. During application of uptake blockers (i.e. PDC and tiagabine) the affected neurotransmitter (glutamate and GABA, respectively) would be more available at all synapses across the network, leading to changes in the activity of both principal cells and interneurones. Coupled with the high levels of recurrent connection, uptake blockade has complex effects across the whole network.

Cellular excitability is significantly reduced by both NBQX and GYKI-53655. Considering the lack of significant change in I_{Bg} in the presence of these drugs, this suggests either that excitability is predominantly controlled by levels of E_{Bg}, or that it is dependent on the I:E ratio. The latter theory is more likely to be correct, as we will see from studies with anticonvulsants in Chapter 7.

Blockade of NMDA receptors with R-AP5 had only moderate effects on I_{Bg} and E_{Bg}. As mentioned previously, postsynaptic NMDAr at the recorded cell do not form part

of the VmD estimates. Therefore, any changes seen in conductance or SD must be mediated through network transmission changes or modulation of transmitter release by presynaptic NMDAr. Blockade of presynaptic NMDAr would directly reduce glutamate release, thus reducing E_{Bg}. These presynaptic NMDAr have been shown to be tonically active (Berretta and Jones, 1996b; Woodhall *et al*., 2001; Yang *et al*., 2006) so their blockade is likely to be the chief mediator of any reduction in E_{Bg}. Alternatively, some reduction in E_{Bg} could be due to reduced NMDAr activity in recurrent excitatory connections (Dhillon and Jones, 2000), but as discussed for AMPAr blockade this would appear to contribute little to E_{Bg} observed in these studies.

Reduction of I_{Bg} by R-AP5 could be due to a reduction in GABA release mediated by antagonism of presynaptic NMDA receptors on inhibitory terminals. However, it is not clear whether layer III inhibitory terminals contain presynaptic NMDAr. Previous studies from our laboratory have indicated the presence of NMDAr at inhibitory terminals in layer II of the mEC, but not in layer V (Woodhall *et al*., 2001). What is more likely is a reduction of the NMDAr-mediated excitatory drive onto inhibitory interneurones, which mediates much of their AP-dependent activity (Jones and Buhl, 1993; Monyer *et al*., 1994; Glitsch and Marty, 1999; Maccaferri and Dingledine, 2002). This reduction in drive may be supported by the observed reduction in I_{Bg} SD with R-AP5, which would indicate reduced synchrony of interneurone activation.

Spike firing threshold is slightly, but significantly, reduced in the presence of R-AP5. This is difficult to explain in terms of direct activity of NMDAr at the postsynaptic membrane, but may be related to the reduction in E_{Bg}. However, the I:E ratio does not change significantly. It may be that a reduction in E_{Bg} alone is enough to significantly reduce firing threshold in certain cases.

The effects of R-AP5 on the subgroup of neurones exhibiting markedly higher control levels of E_{Bg} and I_{Bg} provide some insight into the mechanism of conductance modulation by NMDAr antagonism. These cells may have higher levels of baseline conductance due to the presence of a more intact network within the slices. This would cause a circular increase in glutamate release; the higher baseline release of glutamate from excitatory synapses would trigger more facilitation of release by presynaptic NMDAr, further increasing E_{Bg}. This higher level of excitation may lead to an increase in levels of recurrent excitation between principal cells (see Fig. 4.13) leading to even greater amounts of glutamate being released from excitatory synapses. Furthermore, the network-wide elevation in glutamate release (and hence E_{Bg}) would be expected to increase drive onto inhibitory interneurones, leading to increased I_{Bg}. Thus, given the crucial role that presynaptic NMDAr play in this sequence of events, it is unsurprising that addition of R-AP5 precipitates a large reduction in both E_{Bg} and I_{Bg}. That the I:E ratio is unchanged by R-AP5 supports the notion of network driven increases in conductance, since the reduction in E_{Bg} appears to remove the excitatory drive from inhibitory cells, leading to a commensurate reduction in I_{Bg}.

The use of UBP-302 to block GluR5-containing KAr has no significant effect on background conductance or cellular excitability. Whole-cell patch clamp studies from our laboratory have indicated that KAr present on the postsynaptic membrane do not contain GluR5. Furthermore, the GluR5-containing KAr that have been shown to mediate facilitation of glutamate and GABA release are not tonically active, so in these quiescent slices the addition of a KAr antagonist would have little effect (Chamberlain and Jones, unpublished observations).

In contrast to conductance and excitability measurements, blockade of GluR5-containing KAr does have an appreciable effect on SD estimates for both I_{Bg} and E_{Bg}. This suggests that, whilst having little bearing on levels of background conductance, these KAr are responsible for maintaining some degree of neuronal synchrony.

Evidence to support this notion comes from studies involving up-state behaviour in cortical networks (Cunningham *et al*., 2006), where the use of UBP-302 abolishes sub-threshold oscillations which would appear to be reliant on a high degree of network synchrony. This oscillatory behaviour will be discussed in more detail in Chapter 6. An interesting avenue for research could possibly be the use of a specific GluR5 antagonist as an anticonvulsant. Given the minimal effects on both overall conductance and cellular excitability, coupled with the reduction in synchrony, a drug such as UBP-302 could be used to reduce the likelihood of seizure generation without disrupting normal network function, as epileptiform activity is essentially the synchronised firing of many neurones across a network.

The blockade of glutamate uptake with PDC causes an increase in both I_{Bg} and E_{Bg}. The increase in E_{Bg} could be further enhanced by activation of presynaptic NMDA receptors, and increased input from recurrent excitatory connections. However, the lack of change in E_{Bg} SD, and hence no change in the synchronicity of the excitatory neurone population, would suggest that these recurrent connections to not play a large role in the observed E_{Bg} increase. The observed increase in I_{Bg} is likely to be down to increased excitatory drive onto interneurones. Again, there may be further enhancement of interneurone activity by NMDAr-mediated facilitation of glutamate release onto inhibitory cells. Considering both conductance components together, it may be that the overall value of E_{Bg} has been underestimated in this instance, as the increase in I_{Bg} may be acting to dampen some of the excitatory activity throughout the network.

PDC does not cause a large change in the SD of E_{Bg} or I_{Bg}, and has no effect on the I:E ratio, as both conductance components rise by proportionally equal amounts. The lack of change in cellular excitability suggests that the I:E ratio does have some bearing on the degree of cellular excitability.

The use of whole-cell patch clamp studies in conjunction with the VmD method allows for further investigation of changes in synaptic activity in the presence of this drug. The increase in sEPSC frequency, without a change in decay time, was somewhat surprising. Blockade of glutamate uptake would be expected to increase the persistence of glutamate at the binding sites of postsynaptic receptors, leading to increased activation time. However, no such increase in event duration was observed. The increase in frequency may be due to activation of presynaptic NMDA receptors, leading to a more depolarised presynaptic membrane and a higher probability of glutamate release. Furthermore, there was no increase in EPSC amplitude. This may suggest that the AMPA receptor population in the recorded cells is close to saturation. The increase in frequency would result in a greater overall conductance, which fits in with the observations made using the VmD method.

Considering IPSC activity under PDC, the observed increase in frequency is most likely due to increased excitatory drive onto inhibitory interneurones, caused by the increased persistence of glutamate at the synapse. The increase in excitatory drive would necessarily increase the amount of multi-quantal, activity-dependent GABA release from inhibitory terminals, leading to the significant increase in decay time seen in this study. The increase in $GABA_A$-mediated conductance, along with the increase in excitatory drive onto interneurones, accounts for the rise in I_{Bg} and the slight rise in I_{Bg} SD seen in the VmD study.

The use of tiagabine to block the uptake of GABA yields some surprising results, in both the VmD method and patch clamp studies. As would be expected, levels of I_{Bg} estimated by VmD are significantly increased in the presence of tiagabine. This can simply be explained by the increased amount of GABA present in the synapse. However, tiagabine also causes a noticeable rise in E_{Bg}. There is mounting evidence to challenge the traditional view of GABA as a hyperpolarising, inhibitory transmitter. Presynaptic $GABA_Ar$ are thought to be depolarising due to a high concentration of

chloride ions in glutamatergic terminals causing outward movement of Cl^- (Jang *et al*., 2001). It has been shown that these receptors can facilitate glutamate release in the hippocampus (Jang *et al*., 2006; Alle and Geiger, 2007) and locus coeruleus (Koga *et al.*, 2005). Presynaptic $GABA_A$ receptors have also been shown to facilitate GABA release (Xiao *et al*., 2007). The fact that E_{Bg} was not reduced by a $GABA_A$ antagonist such as bicuculline (see Chapter 5) suggests that these receptors are not tonically active, and only affect glutamate release in the presence of large amounts of GABA.

Furthermore, blockade of GABA uptake by tiagabine or NO-771 has been shown to induce spontaneous depolarisations of neurones in seizure prone mice (Hu and Davies, 1997; Davies and Shakesby, 1999). Initial trials with high concentrations of tiagabine in our own laboratory led to spontaneous slow depolarisations in slices obtained from healthy juvenile rats. The most likely mediator for these depolarising events is the presynaptic $GABA_A$r mentioned above.

Of further interest is the effect of tiagabine on both IPSCs and EPSCs in the patch clamp studies. Tiagabine shows a concentration-dependent increase in sEPSC frequency, most probably due to the actions of the presynaptic $GABA_A$ receptors discussed above. What is more surprising is the reduction in sIPSC frequency precipitated by increasing concentrations of tiagabine. Increased amounts of GABA in the synapse may lead to the activation of presynaptic $GABA_B$ receptors. These metabotropic receptors have been shown to inhibit the release of GABA from presynaptic terminals, however their activity has been shown to be tonic in deeper layers and phasic in more superficial layers of the mEC (Bailey *et al*., 2004). The reduction in IPSC frequency is, however, accompanied by concentration-dependent increases in both amplitude and duration of inhibitory events. Thus the total charge transfer mediated by postsynaptic $GABA_A$ receptors may be increased from control levels, in agreement with the large rise in I_{Bg} seen in the VmD experiments.

CHAPTER 5

LAMINA-SPECIFIC DIFFERENCES IN BACKGROUND SYNAPTIC ACTIVITY

Introduction

As previously stated in Chapter 1, the EC is divided in to six anatomical layers, although some controversy exists as to the exact classification, e.g. the *lamina dessicans*. All the experiments to validate the viability of the VmD approach described in previous chapters have been conducted in layer III. This is largely because previous work in our laboratory (Cunningham *et al*., 2006) has shown that this area has a propensity to develop synchronised slow-wave oscillations (SWO), and later experiments (Chapter 6) have used the VmD method to characterise I:E changes leading to SWO generation. In the current Chapter I have compared I_{Bg} and E_{Bg} in two further populations of neurones, those in layer V and layer II of the mEC.

As discussed in Chapter 1, there are a number of differences in the structure and nature of inhibitory connections between layers in the mEC, which may affect the susceptibility of these layers to epileptic activity. Briefly, there would appear to be a greater degree of inhibitory control exerted over neurones in superficial layers than in deep layers. Layer II principal cells, consisting mostly of spiny stellate cells, form the major part of the output from EC to hippocampus, with projections towards the dentate gyrus, CA2-3 hippocampus and subiculum (Alonso and Klink, 1993; (Tamamaki and Nojyo, 1993; Jones, 1994; Klink and Alonso, 1997). Inhibition in layer II is mediated by basket and chandelier cells, providing tight control of principal cell activity with dendritic trees that are confined mostly within the layer (Germroth *et al.*, 1989; Jones and Buhl, 1993). Layer III principal neurones are mostly pyramidal cells, many of which act as "controller cells" for neurones in CA1 (see Chapter 1). Inhibition in layer III is again mediated by basket and chandelier cells (Hendry *et al.*, 1989; DeFelipe, 1999). Excitation in layer V is also mediated by pyramidal cells, however these cells mostly project back towards the superficial layers of the EC, see Figs. 1.2 and 1.3.

There is a significant difference in the inhibitory properties of layer V and layers II and III. Previous studies, mainly from our own laboratory, have indicated clear electrophysiological differences between the levels of inhibitory transmission in layers II and V. Principal cells in layer II are kept mostly quiescent, and prevented from firing action potentials, by the high level of inhibitory activity in this layer (Jones, 1993 and 1994; Heinemann *et al.*, 2000). In contrast, activity in layer V is dominated by excitation, with inhibitory responses sometimes not being apparent at all (Jones and Heinemann, 1988). Furthermore, inhibitory activity in superficial layers is more constitutively active, with a greater proportion of IPSCs being action potential independent than in layer V (Woodhall *et al*., 2004). These results suggest that neurones in different parts of the EC are subject to differing balances of network control.

Considering the lamina-specific differences in inhibitory control of principal cells, the superficial layers of the EC have been labelled as "epilepsy resistant", with the deeper layers being "epilepsy prone" (Jones and Lambert 1990a; Jones 1993; Woodhall *et al.*, 2004). However, in human patients and in animal models of chronic epilepsy, there is evidence for a preferential loss of neurones in layer III of the EC (Du and Schwarz, 1992; Du *et al.*, 1993, 1995). Additionally, changes in recurrent inhibition in layer II result in excessive output towards the dentate gyrus in the pilocarpine model of epilepsy in rats (Kobayashi *et al*., 2003; Kumar *et al*., 2007). Bear *et al.* (1996) found that electrically induced chronic epilepsy in rats led to a prolongation of evoked responses in superficial layers, that could be shortened by application of 2-AP5. The same group found that, again in electrically induced chronic epilepsy, deep-layer neurones in the EC of epileptic rats were hyperexcitable, partly due to an increase in NMDA-mediated excitation (Fountain *et al*., 1998). Scharfman *et al.* (1998) found that, in a rat model of chronic epilepsy induced by injection of amino-oxyacetic acid, similar prolongations of excitatory discharges to those found by Bear *et al*. above

were seen in superficial neurones in the EC. In deeper layers, ictal discharges occurred after a short delay in some neurones.

Several *in vitro* studies of acutely generated seizures have shown that, within the EC itself, seizure events are initiated in the deeper layers (V-VI) and propagate ictal discharges to both deeper and more superficial areas of the EC and beyond. This role of the deep layers in the generation of seizures lends weight to the notion that they are "seizure sensitive", compared to the more "seizure resistant" areas in the superficial layers (Jones and Lambert, 1990a, b; Jones, 1993; Avioli *et al.*, 1996; Lopantsev and Avioli, 1996; D'Arcangelo *et al.*, 2001). This picture of the lamina-specific differences in the EC has been mirrored in studies of seizure initiation in the neocortex (Hoffman and Prince, 1995; Barkai *et al*., 1995; Badea *et al*., 2001; Yang and Benardo, 2002). Furthermore, in agreement with the results of similar studies investigating acutely invoked seizures *in vivo* (e.g. Ben-Ari *et al*., 1981; Collins *et al.,* 1983; Stringer, 1994), this acute seizure activity would appear to originate in the EC and spread to adjacent areas of the limbic system (Jones and Lambert, 1990a; Iijima *et al*., 1996; Avioli *et al*., 1996; Bucheim *et al*., 2002; Weissinger *et al*., 2000; D'Arcangelo *et al*., 2001). These studies serve to support the notion of the EC as a crucial structure in TLE, and highlight the importance of understanding the lamina-specific differences in excitability and epilepsy sensitivity that may underlie the generation of seizures in animal models and, ultimately, human patients.

To investigate the differences in background activity between layers in the mEC, and any differences in susceptibility to acutely-evoked epileptiform activity, this chapter will focus on using the VmD method to obtain estimates of I_{Bg} and E_{Bg} in layers II, III and V of the mEC, and how these change over time in response to the application of the $GABA_A$ antagonist bicuculline, used in several studies to mimic epilepsy *in vitro* (e.g. Jones, 1988; Jones and Lambert, 1990a, b). The time-course of onset of epileptic activity, and changes in background conductance, in each layer should give some

indication of the susceptibility of each layer to acute seizures, with faster onset indicating increased propensity towards seizures. In order to properly characterise I_{Bg} and E_{Bg} in layers II and III, values for AMPAr and $GABA_A$r reversal must also be obtained.

Methods

All experiments were carried out on EC-hippocampal slices taken from juvenile male Wistar rats, as described in Chapter 2. In order to apply the VmD method to principal cells in layers II and V it was necessary to first determine reversal potentials for AMPAr-mediated EPSPs and $GABA_A$r-mediated IPSPs in these two populations. Reversal potentials of AMPA and $GABA_A$ receptors, leak reversal potentials, and sEPSC and sIPSC decay times, for layer II and V pyramidal cells were obtained in the same manner as those for layer III cells, as described in Chapter 3.

The VmD method was used to obtain the time-course of action of the $GABA_A$r receptor antagonist, bicuculline (10 μM). Cells were allowed to equilibrate for 5-10 minutes after impalement, after which time recording was started and control values were measured using the two-current protocol described previously. Bicuculline was then perfused over the slice for a period of up to 15 minutes, with estimates of I_{Bg} and E_{Bg} being made every two minutes. Epileptic seizure activity (as seen in Fig. 5.7) was observed in the majority of cells. A final estimate of conductances was made after seizure activity began. Accurate measurement of conductances was not possible after the establishment of regular seizure activity. With continued perfusion of bicuculline, regular and frequent seizures were observed in most slices. This makes it difficult to obtain stable periods of membrane potential necessary for accurate VmD estimations, due to both the seizure itself and the refractory period after each discharge. As such, the obtained time-courses display the run-up to the initial seizure, and the final values obtained after this event.

Results

Layer II and V Reversal Potentials

Reversal potential recordings were made from a total of 12 pyramidal neurones, 3 in each group for $GABA_Ar$ and AMPAr reversal potentials for both layer II and layer V. The results obtained do not differ greatly from the values measured in layer III pyramidal cells, as outlined in Chapter 3. The reversal potentials for AMPAr, $GABA_Ar$ and leak conductance can be compared in table 5.1. Graphs of AMPAr-mediated EPSPs and $GABA_Ar$-mediated IPSPs at a range of membrane voltages in layers II and V can be seen in figures 5.1 and 5.2 respectively.

	Reversal Potentials (mV)			**Decay Times (ms)**	
Layer	**AMPAr**	**$GABA_Ar$**	**Leak**	**EPSC**	**IPSC**
II	3.9	-66.1	-77.6		
III	6.8	-66.7	-78.1	13.7	29.1
V	6.1	-65.2	-78.8		

Table 5.1: Reversal potentials for layers II, III and V of the mEC. Average reversal values, especially for leak and $GABA_Ar$ reversal, are very similar across the layers.

Comparison of Laminar Baseline Values

The baseline values of I_{Bg}, E_{Bg} and their respective SDs give some idea of the differences in transmission and synchrony between layers in the mEC. In layer II (n=6), I_{Bg} = 12.3 ± 2.0 nS, E_{Bg} = 3.3 ± 0.4 nS and I:E ratio = 3.6 ± 0.3. Baseline SD in layer II was higher than for other populations, suggesting greater synchrony in control conditions. I_{Bg} SD was 2.1 ± 1.1 nS, and E_{Bg} SD was 46.0 ± 9.1 pS. The average number of spikes generated by a 250 ms depolarisation was 4.0 ± 0.4, and the mean baseline spike threshold was 18.8 ± 0.4 mV.

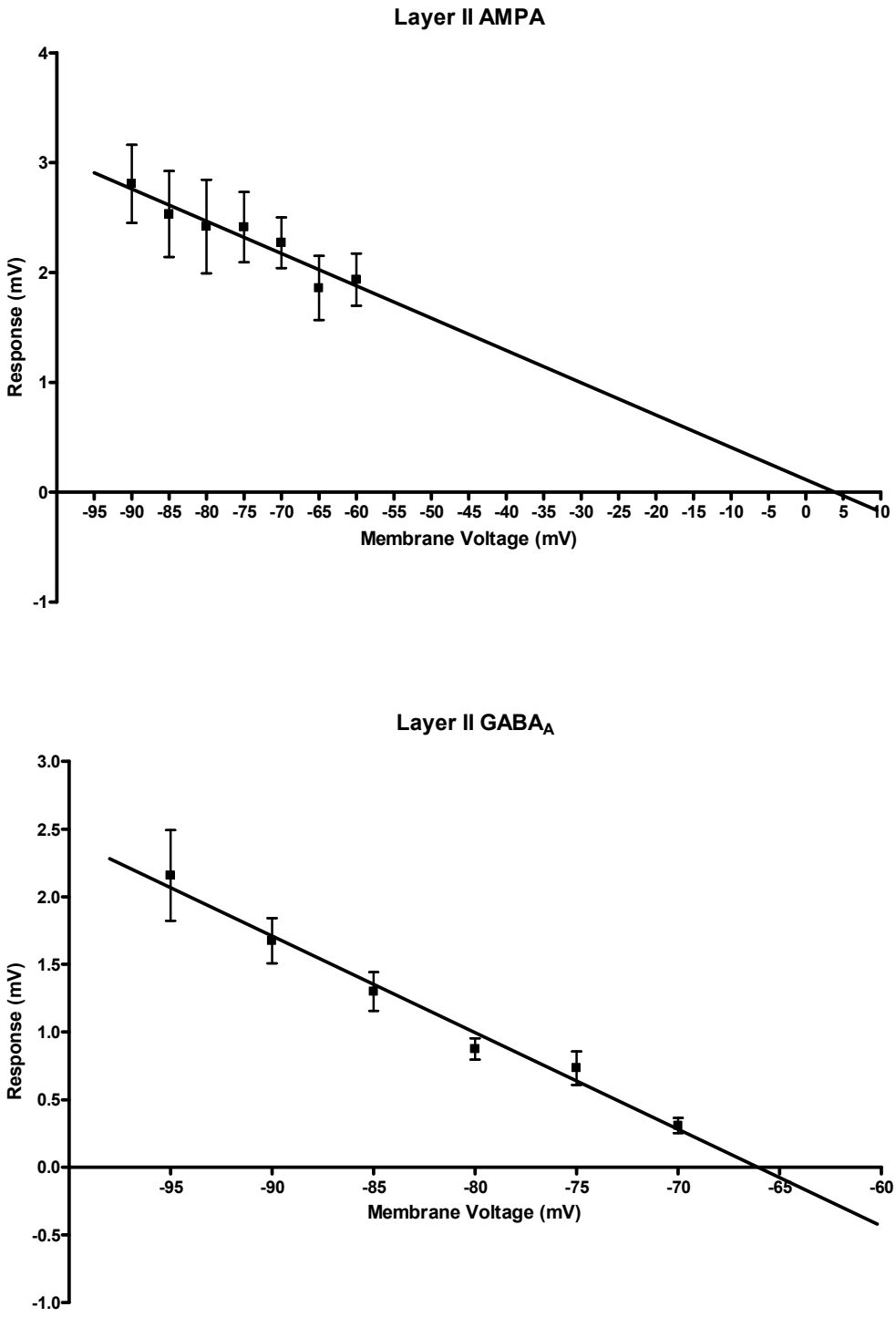

Figure 5.1: Reversal potential graphs for AMPA and $GABA_A$ receptors in layer II of the mEC. Evoked responses at a range of membrane potentials in the presence of antagonists for other ionotropic receptors were averaged and graphed, using linear regression, to find the reversal potentials of 3.91 mV for AMPA and -66.05 mV for $GABA_A$ receptors. Each graph represents pooled data from 3 neurones.

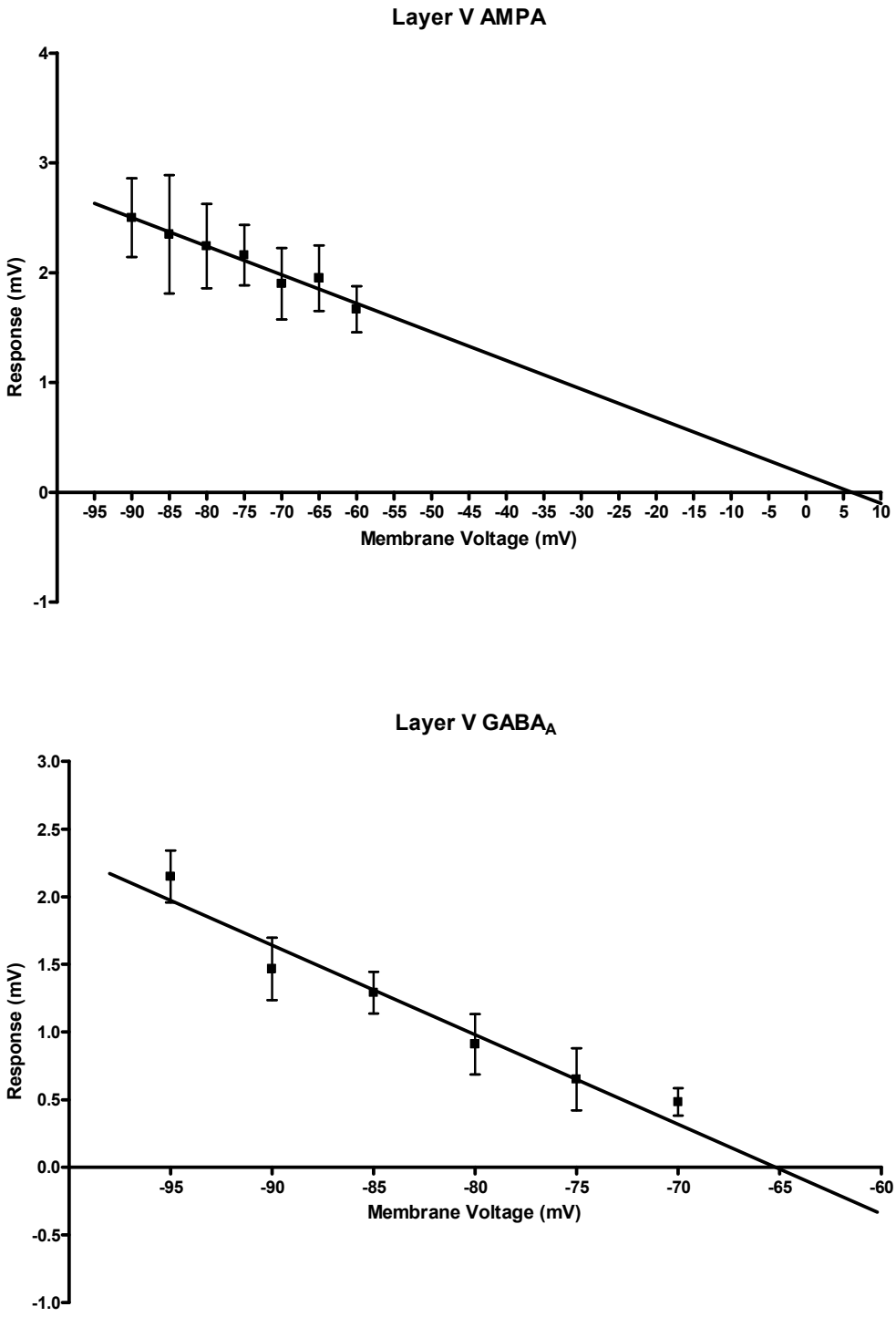

Figure 5.2: Reversal potential graphs for AMPA and $GABA_A$ receptors in layer V of the mEC. Evoked responses at a range of membrane potentials in the presence of antagonists for other ionotropic receptors were averaged and graphed, using linear regression, to find the reversal potentials of 6.10 mV for AMPA and -65.20 mV for $GABA_A$ receptors. Each graph represents pooled data from 3 neurones.

The majority of neurones recorded in this thesis were from layer III, allowing a larger group to be used for control values. In 61 cells, as previously stated (Chapter 3), baseline I_{Bg} = 10.2 ± 1.6 nS, E_{Bg} = 2.5 ± 0.3 nS and I:E = 4.1 ± 0.3. I_{Bg} SD was 0.3 ± 0.1 nS and E_{Bg} SD = 7.8 ± 1.3 pS. Cellular excitability values were 20.5 ± 0.7 mV for firing threshold, and 4.4 ± 0.3 spikes per train.

Layer V values were as follows (n=5): I_{Bg} = 6.8 ± 1.6 nS, E_{Bg} = 2.8 ± 0.6 nS and I:E ratio = 2.5 ± 0.4. SD was 0.30 ± 0.2 nS for I_{Bg} and 4.7 ± 1.6 pS for E_{Bg}. Spike firing threshold was 24.2 ± 0.5 mV and average spikes per 250 ms pulse was 2.7 ± 0.2. From these results it is clear that there is a much higher level of synchrony present in both inhibitory and excitatory populations within layer II. Layer V has the lowest baseline levels of inhibition and an I:E ratio that is more in favour of excitation than the superficial layers. This reflects previous studies by our laboratory and others, suggesting that activity in layer V is less biased towards inhibition compared to layers II and III.

Effects of Bicuculline in Layer II

Having calculated the baseline levels of I_{Bg} and E_{Bg} in the three layers, I now determined time-course of changes during application of the convulsant $GABA_A$ blocker, bicuculline.

Three neurones exhibited consistent seizure activity upon application of bicuculline (10 μM). The cells that did not display any discernable epileptiform activity were recorded for up to 25 minutes, but no events were observed. Lack of epileptiform activity did not appear to be dependant upon the level of network preservation in the slices used, as cells exhibiting and lacking epileptic activity were recorded from slices taken from the same animals, on the same day.

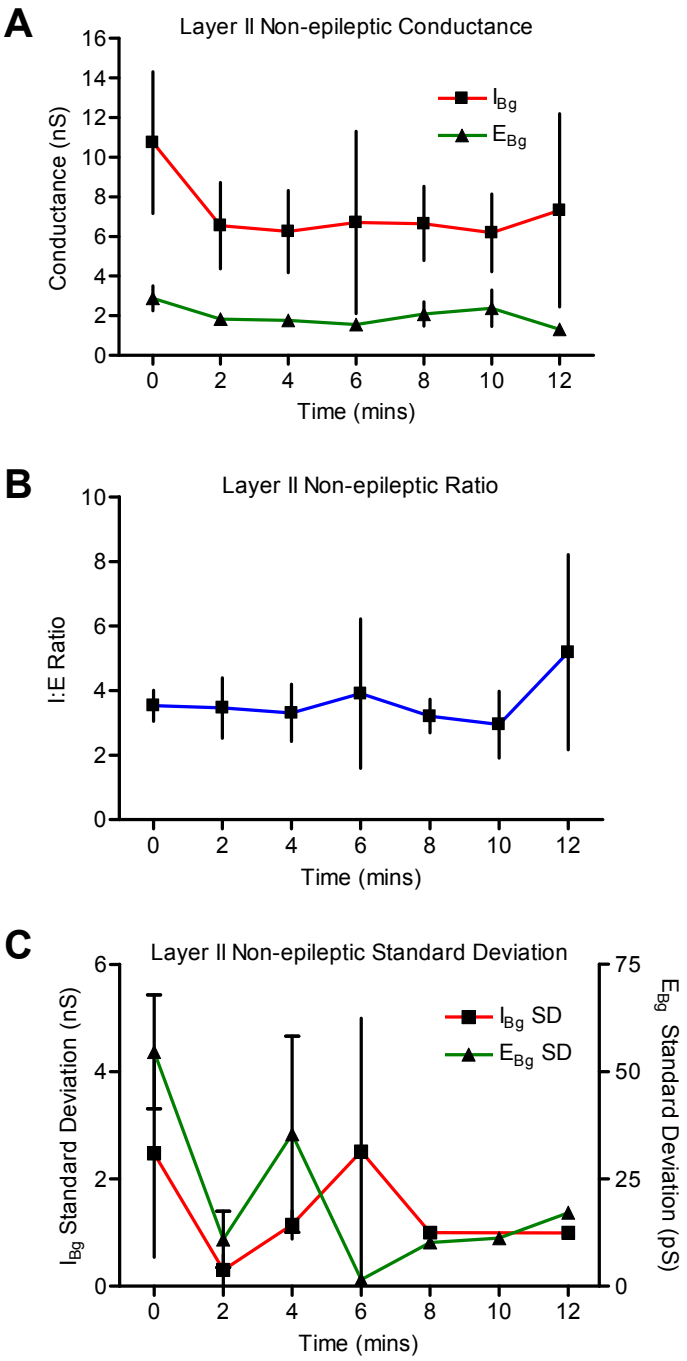

Figure 5.3: Time-course of bicuculline in layer II non-epileptic cells. A: Apart from a drop in I_{Bg} 2 minutes after bicuculline (10 µM) addition, conductance values are largely unchanged in these cells. B: The lack of significant change in E_{Bg} or I_{Bg} leads to no overall change in the I:E ratio throughout. C: SD estimates for E_{Bg} and I_{Bg} fluctuate throughout, but do not show a significant change. None of these cells exhibited any epileptiform events (n=3)

Conductance measurements were carried out over a 12 minute period in 6 pyramidal cells from mEC layer II. In three neurones where no epileptiform events were observed, there was an initial reduction in I_{Bg} from 10.7 ± 3.6 nS to 6.6 ± 2.2 nS after 2 minutes exposure to bicuculline ($P > 0.05$), after which no change was evident. E_{Bg} was generally unchanged throughout the experiment. The I:E ratio was unchanged apart from a sharp rise at the end of the experiment (Fig. 5.3A-B). In the unresponsive neurones, SD estimates for both I_{Bg} and E_{Bg} fluctuated rapidly throughout the experiment. However, there was no significant change in either component at any time point (Fig. 5.3C).

The remaining three layer II neurones exhibited epileptiform events at an average of 447.0 ± 17.6 seconds (7.5 minutes) after the start of bicuculline perfusion. E_{Bg} was unchanged throughout, staying close to its initial value of 3.7 ± 0.4 nS. In contrast, I_{Bg} exhibited a clear reduction between 2 and 4 minutes after bicuculline addition, to 46% of its initial value (Fig. 5.4A). After this initial reduction, I_{Bg} remained steady until the end of the experiment.

The change in I_{Bg} was reflected in the I:E ratio for these cells (Fig. 5.4B). From an initial value of 3.6 ± 0.3, I:E was reduced to 1.8 ± 0.2 at 4 minutes, attaining a final value of 1.5 ± 0.1 after 12 minutes in the presence of 10 μM bicuculline. Despite these clear trends, changes in conductance and I:E ratio were not significant at any time point.

The SD estimates of I_{Bg} and E_{Bg} arguably provide the most interesting data in this layer (Fig. 5.4C). Immediately after exposure to bicuculline, the SD of both conductance components is noticeably reduced. However, in the run up to the first seizures at approximately 7.5 minutes, both I_{Bg} and E_{Bg} SD are steadily increased. This suggests an increase in the level of synchronisation in both excitatory and

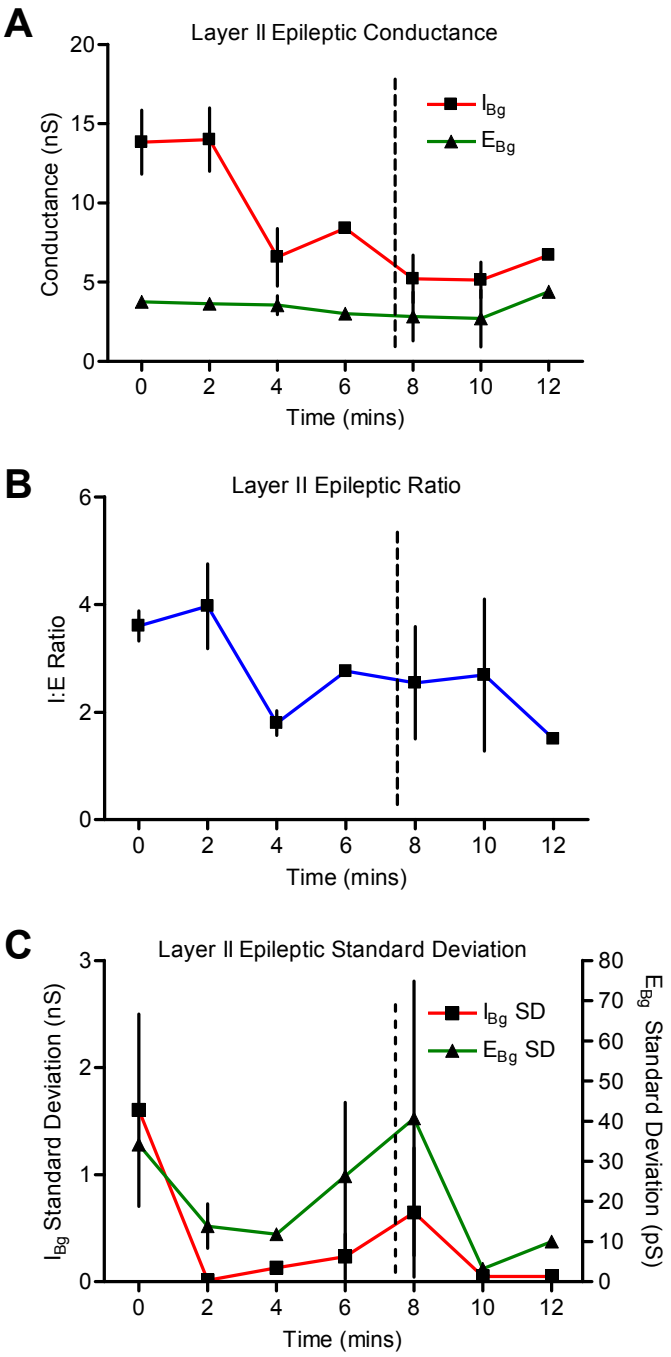

Figure 5.4: Time-course of bicuculline in layer II epileptic cells. Dotted line shows average time of first seizure. A: E_{Bg} levels are unchanged throughout. I_{Bg}, however, shows a sharp reduction after 2 minutes, from 13.8 ± 2.0 to 6.6 ± 1.8 nS. B: This rapid change in I_{Bg} is reflected in the I:E ratio. C: The SD of both I_{Bg} and E_{Bg} is reduced rapidly after bicuculline addition. However, in the period leading up to the first seizure event, both SDs show a steady increase. This suggests increased synchrony in both populations preceding an epileptiform event.

inhibitory populations before epileptiform activity. Again, however, despite a clear trend in both excitatory and inhibitory components, the changes in SD were not significant throughout. The value of *a* in these cells was 32426 μm.

Cellular excitability measurements were taken after each VmD measurement. Changes were not significant in either responsive or unresponsive neurones. In pooled data from all six layer II cells, neither spike threshold (18.8 ± 0.4 mV vs 17.0 ± 0.7 mV) nor spikes per train (4.0 ± 0.4 vs 5.7 ± 0.5) showed any change after 12 minutes of bicuculline perfusion.

Effects of Bicuculline in Layer III

In a similar manner to the study in layer II, the time-course of the effect of bicuculline was observed in 6 neurones in layer III of the mEC. All of these cells eventually exhibited epileptiform activity, in contrast with the findings in layer II.

The development of epileptiform activity in layer III was faster than that seen in layer II. Cells displayed epileptiform activity after 4-7 minutes, with a mean value of 313.5 ± 42.7 seconds (5.2 minutes). This value contrasts with the 7.5 minute mean for activity to develop in layer II cells. Control conductance levels in bicuculline-treated layer III neurones were slightly lower than the mean values generally found in this layer, with initial measurements of I_{Bg} = 7.1 ± 0.9 nS, E_{Bg} = 1.2 ± 0.3 nS, and an I:E ratio of 4.8 ± 0.4.

Layer III cells, upon exposure to bicuculline (10 μM), exhibited a steady and rapid reduction in I_{Bg}, up to and beyond the point of seizure initiation. E_{Bg} was largely unaffected, causing a shift in the I:E ratio firmly in favour of excitatory activity. This is illustrated in Fig. 5.5. I_{Bg} was decreased from 7.1 ± 0.9 nS to 1.5 ± 0.5 nS after 8

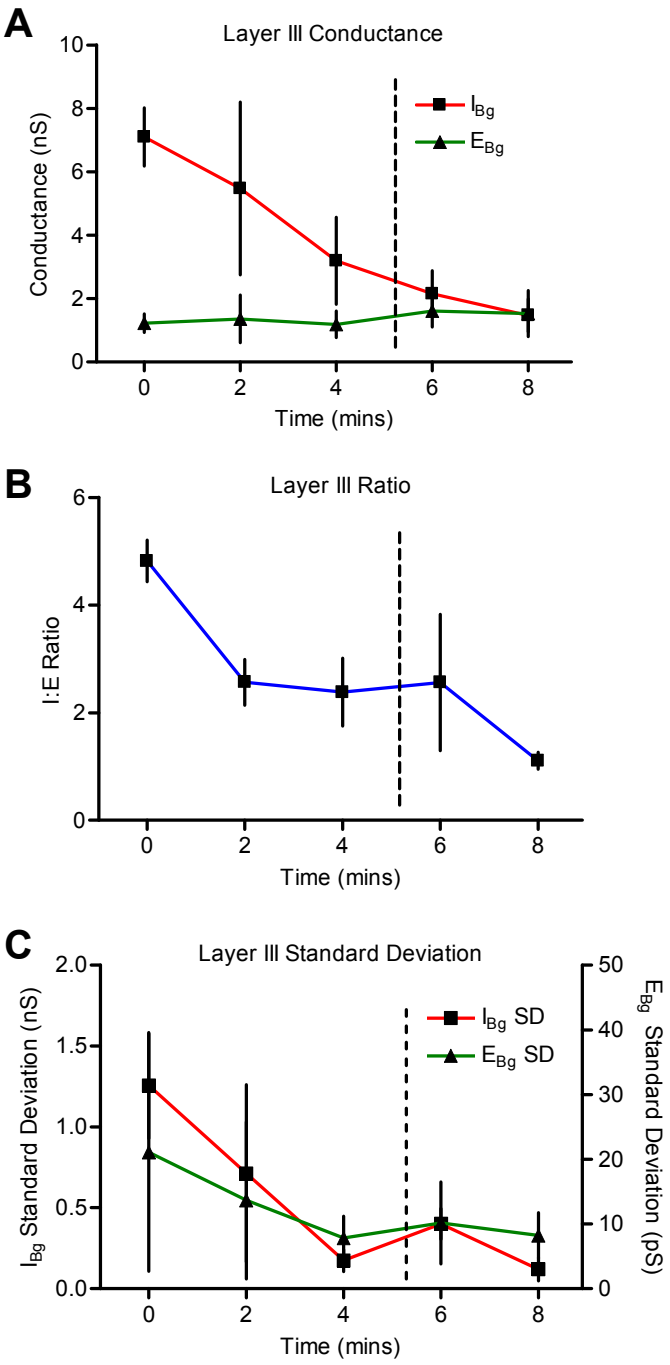

Figure 5.5: Time-course of bicuculline in layer III principal cells. As in Fig. 5.4, the dotted lines indicate the mean time of initial epileptiform activity. A: I_{Bg} shows a marked decline throughout the experiment, up to and beyond the first seizure. E_{Bg} is unchanged. B: The change in I_{Bg} is reflected in the steady movement of I:E ratio in favour of excitation. C: I_{Bg} SD initially drops to a low of 0.17 ± 0.07 nS at 4 minutes, before increasing again to 0.40 ± 0.09 nS as seizure activity begins. The SD of E_{Bg} is slightly decreased throughout.

minutes of bicuculline perfusion. E_{Bg} tended to increase slightly throughout the experiment, but was not significantly changed from the initial value (Fig. 5.5A). The I:E ratio fell to 1.1 ± 0.1 after 8 minutes, indicating almost equal amounts of I_{Bg} and E_{Bg} (Fig 5.5B).

During bicuculline perfusion, the SD of I_{Bg} was rapidly reduced from 1.3 ± 0.3 nS to a final level of 0.12 ± 0.07 nS after 8 minutes (Fig. 5.5C, a = 34636). E_{Bg} SD also decreased from 21.0 ± 18.0 pS to 8.1 ± 4.2 pS. The difference between the SD of I_{Bg} in control recording and after 8 minutes perfusion with bicuculline was significant (P=0.028), whereas the change in the SD of E_{Bg} was not (P>0.05, t-test). Similar to the findings in layer II, cellular excitability was not significantly altered by bicuculline. Firing threshold was 20.6 ± 1.1 mV in control recordings and 18.2 ± 0.9 mV after 8 minutes (P>0.05). The number of spikes generated by a 250 ms depolarising pulse was also not significantly affected (4.3 ± 0.3 to 5.5 ± 1.0 after 8 minutes).

Effects of Bicuculline in Layer V

The time-course of the effects of bicuculline (10 μM) was studied in 5 pyramidal neurones in layer V of the mEC. All of these recorded cells displayed rapid epileptiform activity within 5-8 minutes of bicuculline addition.

During application of bicuculline, I_{Bg} displayed a rapid and sustained drop from 6.8 ± 1.6 nS, being more than halved after 2 minutes and reaching 1.9 ± 0.6 nS by only 4 minutes. After this it remained largely the same, reaching 1.4 ± 0.4 nS after 8 minutes. E_{Bg} displayed little change throughout after an initial fall from 2.8 ± 0.6 nS to 1.9 ± 0.5 nS. Thereafter it tended to increase again slightly, but was still reduced, compared

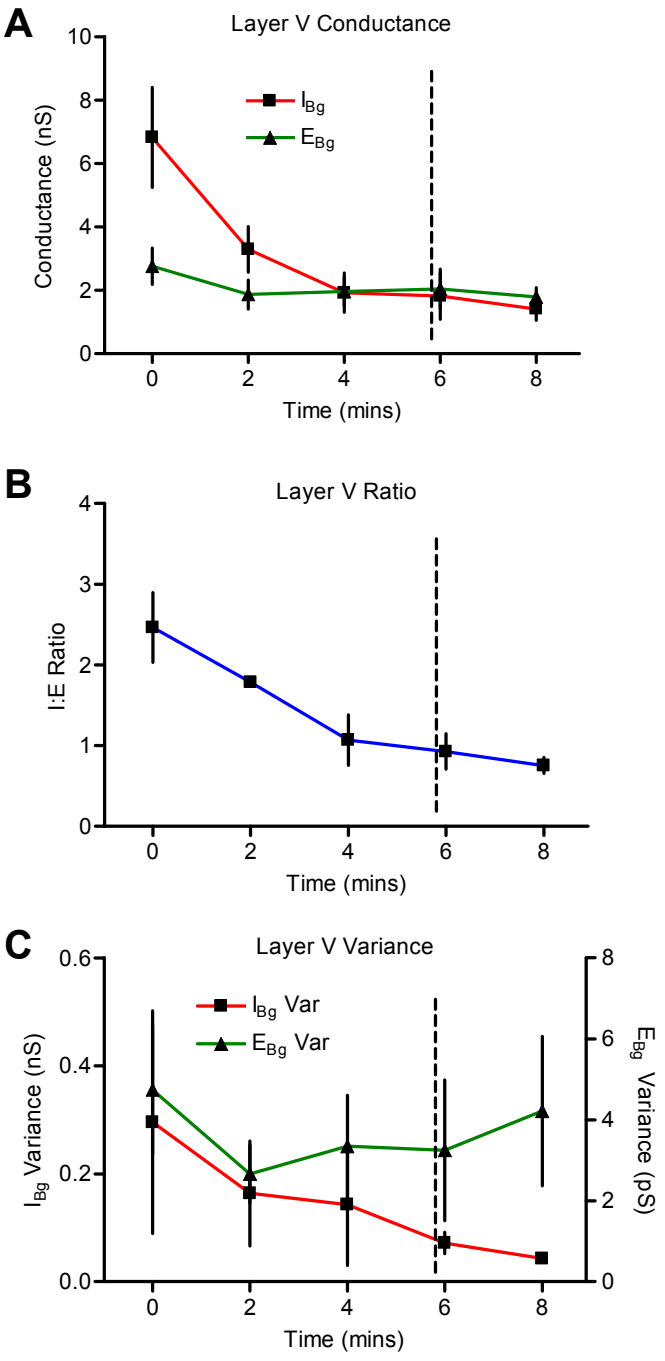

Figure 5.6: Time-course of bicuculline in layer V. Dotted line shows mean seizure point. A: I_{Bg} is quickly reduced to 1.9 ± 0.6 nS after 4 minutes, after which time the reduction is far slower. E_{Bg} undergoes a small initial reduction and then remains largely unchanged. B: I:E ratio decreases throughout, mirroring the trend seen with I_{Bg}. With an endpoint of 0.8 ± 0.1, I:E ratio in the presence of bicuculline shows dominance of E_{Bg} over I_{Bg}. C: The SD of I_{Bg} is reduced steadily throughout. E_{Bg} SD shows an initial dip at 2 minutes, and then recovers to near-control levels.

to control, at 1.8 ± 0.3 nS after 8 minutes (Fig. 5.6A). The I:E ratio was reduced from 2.5 ± 0.4 to 1.0 ± 0.3 after 4 minutes, and fell slightly further to 0.8 ± 0.1 after 8 minutes (Fig. 5.6B). This indicates that, after 8 minutes of bicuculline perfusion, E_{Bg} actually dominates I_{Bg} in these neurones. The changes in I_{Bg} and I:E ratio were both found to be significant by ANOVA (P_I=0.005 and P_R=0.002), whereas E_{Bg} was not found to have changed significantly.

The SDs of the I_{Bg} and E_{Bg} were very low in layer V, compared to values obtained for neurones in superficial layers. From a control value of 0.30 ± 0.20 nS, I_{Bg} SD fell steadily throughout, reaching 0.043 ± 0.006 nS after 8 minutes. E_{Bg} SD was very low, starting on 4.7 ± 1.6 pS. Although there was no significant change at 8 minutes (4.2 ± 1.8 ps) compared to control, it is interesting that after an initial fall (2.7 ± 0.7 pS after 2 minutes), the SD of E_{Bg} then increased again back to control levels (Fig. 5.6C). Neither change in SD was found to be statistically significant.

Bicuculline had a slight but significant effect on cellular excitability in layer V. Spike amplitude remained largely unchanged, however spike threshold was reduced steadily throughout, from 24.2 ± 0.5 mV in control recordings to 20.7 ± 0.8 mV after 8 minutes (P=0.004). The number of spikes generated by a 250 ms pulse was not significantly affected.

Laminar Comparison of Epileptiform Activity

In addition to observed differences in the time-course of seizure initiation, and changes in I_{Bg}, E_{Bg}, and their respective SDs, there was a clear difference between epileptiform events in different layers. Typical events are illustrated in Fig. 5.7.

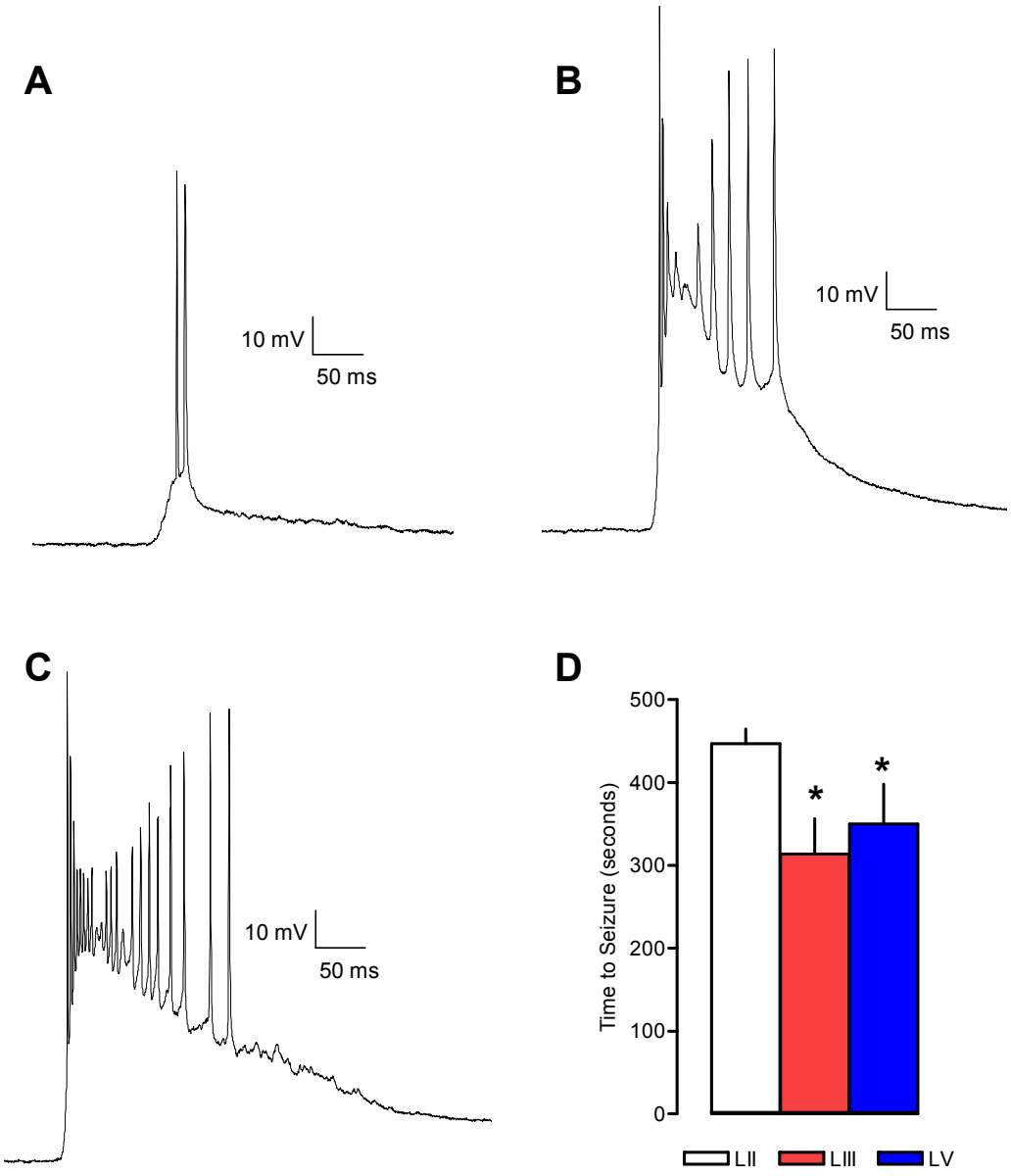

Figure 5.7: Comparison of epileptiform events in layers II, III and V of the mEC. A: Layer II events are shorter, have smaller amplitude and have shorter refractory periods than in either of the other two layers. B: Layer III events are more emphatic than layer II, with greater and more frequent spikes, longer duration and greater amplitude. C: Layer V events are the most violent of all, with very high frequency spike activity and high amplitude, taking several seconds to recover to baseline membrane potential. These differences in event length and amplitude reflect the laminar means for I:E ratio (LII = 1.5 ± 0.1, LIII = 1.1 ± 0.1, LV = 0.8 ± 0.1). D: Epileptiform activity takes significantly longer to develop in layers III and V compared to layer II. Some cells exhibited varying patterns of epileptiform activity, but these traces represent the vast majority of events in each layer.

The duration, amplitude and firing frequency of epileptiform events would appear to correlate with the I:E ratio in the presence of bicuculline in each layer. Typically, layer II neurones (I:E = 1.5 ± 0.1) display small, short epileptiform bursts. Layer III bursts are longer and larger (I:E = 1.1 ± 0.1), with layer V events the most prolonged and depolarised (I:E = 0.8 ± 0.1). Furthermore, layer II cells take significantly longer to develop signs of epileptic activity (447.0 ± 17.6 seconds) compared to layers III and V (313.5 ± 42.7 and 350.0 ± 48.0 seconds). These results would appear to support the theory that deeper layers are progressively more susceptible to epilepsy compared with layer II.

Discussion

The VmD data from different layers of the mEC provides further insight into differences in transmission and excitability between these layers. From baseline data in each layer, it is possible to obtain an idea of the normal resting conditions, i.e. the balance of inhibition and excitation, in deep and superficial layers. Ideally, simultaneous intracellular recordings, using the VmD method, from layers II, III and V in the same slice would give the most accurate picture of lamina-specific differences in I:E ratio and excitability, however this was not possible with our current experimental setup.

	Conductance (nS)			**SD (pS)**	
Layer	**I_{Bg}**	**E_{Bg}**	**I:E**	**I_{Bg}**	**E_{Bg}**
II	12.3	3.3	3.6	2120	46.0
III	10.2	2.5	4.1	302	7.8
V	6.8	2.8	2.5	296	4.7

Table 5.2: Comparison of baseline values for layers II, III and V of the mEC

Table 5.2 provides a simple means of comparing baseline conductance and SD values across layers. The two most noticeable differences are the low I_{Bg} in layer V, and the

high degree of SD (of both I_{Bg} and E_{Bg}) in layer II. E_{Bg} in layer V is not significantly less than mean E_{Bg} levels in the superficial layers, leading to an I:E ratio more in favour of inhibition in layer V.

The results obtained using the VmD method in this chapter are in agreement with a number of patch clamp and intracellular studies, which suggest that inhibitory control of layer II principal neurones is far greater than in deeper layers (Finch *et al*., 1986; Jones, 1987; Finch *et al*., 1988; Jones and Heinemann, 1988; Jones and Buhl, 1993; Jones, 1993; 1994; Heinemann *et al*., 2000). Overall I_{Bg} levels in control conditions were greatest in layer II, followed by layer III. Baseline conditions in layer V indicate that I_{Bg} levels are almost 50% less in layer V compared to layer II (6.8 nS vs 12.3 nS). E_{Bg} levels are comparable across all three layers, the corollary of which is an I:E ratio in layer V that is more in favour of excitation compared to the other two layers.

The VmD method is based on the actions of AMPAr and $GABA_A$r, and as such provides a reliable estimate of background conductance levels, as we have seen throughout this thesis. However, the reliance on only two populations of receptors leads to a risk of underestimation in certain circumstances. Whereas spontaneous excitation is almost exclusively mediated by AMPAr in superficial layers of the mEC (with presynaptic NMDAr facilitating glutamate release), there is evidence to suggest that a significant component of spontaneous excitatory transmission in layer V is mediated by postsynaptic NMDAr, again with facilitation of glutamate release by presynaptic NMDAr (Berretta and Jones, 1996a, b; Jones and Woodhall, 2005). In whole-cell patch clamp studies, sEPSC frequency and amplitude has been found to be greater in layer V than in layer II (Berretta and Jones, 1996a). This is not reflected in the VmD values for E_{Bg} in this Chapter (3.3 nS in layer II, 2.8 nS in layer V). It is likely that the VmD method is underestimating the actual amount of excitatory activity in layer V, further shifting the "real" I:E ratio in favour of excitation compared to other layers.

There is little risk of this underestimation occurring when I_{Bg} is considered. Whole-cell patch clamp studies from our own laboratory have indicated that spontaneous inhibition in both layer II and layer V is mediated postsynaptically by $GABA_Ar$, with $GABA_B$ autoreceptors regulating GABA release from inhibitory terminals (Bailey *et al*., 2004; Woodhall *et al*., 2004). The levels of spontaneous inhibition seen in deep and superficial layers in these patch clamp studies are in agreement with the VmD data in this Chapter. Woodhall *et al.* (2004) showed that sIPSCs in layer II occurred at an average of around 12.5 Hz, whereas the mean frequency in layer V was 2.5 Hz. The amplitude of sIPSCs in layer II was also slightly higher.

Levels of I_{Bg} and E_{Bg} SD may give some indication of the degree of synchronicity within inhibitory and excitatory populations, respectively. If so, the baseline data indicate that inhibitory activity in layer II is highly co-ordinated. In the study by Woodhall *et al.* (2004) mentioned above, it was found that high-frequency bursts of sIPSCs occurred on a regular and frequent basis. This is indicative of a high level of synchrony in layer II. Additionally, E_{Bg} SD in layer II suggests an unusually high level of excitatory synchrony compared to other layers. Whether this synchronisation is a function of the high level of I_{Bg}, i.e. transmission-mediated, or through a high level of recurrent connections, i.e. anatomically-mediated, is unclear. It is likely to be due to a combination of both factors.

Contrary to the conductance levels, cellular excitability measurements would indicate that layer II neurones are most excitable, with layer V neurones having the highest firing threshold and lowest firing frequency in control conditions. This is in contradiction to the expected values, as an I:E ratio in favour of inhibition, with high levels of I_{Bg}, would be expected to lead to low cellular excitability. However, the neurones recorded in different layers may be of differing cell types (e.g. pyramidal cells in layers III and V, stellate cells in layer II), each with their own cellular

morphology and passive channel properties, which may in this instance have more bearing on firing threshold/rate than overall and relative conductance levels. No attempt was made to unequivocally identify cellular morphology in these experiments. This discrepancy between I:E ratio and cellular excitability was overturned in the presence of bicuculline. Addition of bicuculline caused a slight reduction in firing threshold compared to resting potential in all three layers. However, the change in threshold was greater in layer III than in layer II, and in layer V bicuculline causes the largest reduction of all (14.5% over 8 minutes), a significant difference compared to control values (P = 0.004). Layer V may start with the highest firing threshold, but this appears to be more sensitive to $GABA_A$r blockade than in superficial layers. This may be a function of the fact that the I:E ratio with bicuculline is biased in favour of E_{Bg} in layer V (0.8 ± 0.1), something that is not seen in other layers.

The lamina-specific differences in baseline I_{Bg} and E_{Bg} are reflected in the relative speed of onset of epileptiform activity, the characteristics of the epileptiform events, and the response of each layer to the addition of bicuculline. In layer II, only half of the 6 neurones exposed to bicuculline exhibited epileptiform activity. The non-epileptic cells showed a slight reduction in I_{Bg}, but this was not significant. This is somewhat surprising, as VmD estimates of background inhibition are based directly on the actions of $GABA_A$r, of which bicuculline is a competitive antagonist. It may be that the high level of inhibitory activity in layer II causes a displacement of bicuculline from $GABA_A$r, however this theory is undermined by the fact that the layer II neurones that eventually exhibited seizure activity had higher baseline levels of I_{Bg} than those that did not. Since epileptiform activity is population driven, and takes place throughout the EC in a co-ordinated fashion, apparently driven by layer V (Jones and Lambert, 1990a, b), differences in epileptic susceptibility seen from slice to slice could be due to the effects of bicuculline elsewhere in the mEC.

In all layers, initiation of seizure behaviour is preceded by clear declines in I_{Bg}, with I:E ratio shifting in favour of inhibition. Interestingly, in layer II, the first sign of epileptic activity is preceded by clear upward trends in the SD of both I_{Bg} and E_{Bg}, suggesting increased synchronisation in both inhibitory and excitatory populations. No clear SD trend is evident in the layer II cells that do not display epileptiform events. It may be that this apparent change in levels of synchronisation underlies the generation of seizures in layer II.

The degree of severity of epileptiform activity, and the classic picture of lamina-specific differences in epileptic sensitivity, is reflected in the values of I:E ratio for each layer in the presence of bicuculline. E_{Bg} is increasingly favoured by the I:E ratio in progressively deeper layers, and this is evident in the prolonged and larger-amplitude epileptiform events in layer V compared to layer III, which in turn has larger and longer events than layer II. Paired recordings in slices have shown that epileptiform activity in layer V precedes activity in layers II, III and VI by several milliseconds (Jones and Lambert 1990a, b). This implicates layer V in the initiation and propagation of epileptic activity not just in the EC, but possibly throughout the entire mesial temporal lobe.

The results in this Chapter highlight the lamina-specific differences in I_{Bg} and E_{Bg} that appear to underlie the susceptibility of each layer to acutely-evoked seizures. Certainly, the relatively low level of I_{Bg} in layer V would support studies implicating it in seizure generation and propagation, with the high I_{Bg} level in layer II leading to greater "seizure resistance" in superficial layers (Jones and Lambert, 1990a, b; Avoli *et al*., 1996; Lopantsev and Avoli, 1996; D'Arcangelo *et al*., 2001). However, some studies using resected human tissue and animal models of chronic epilepsy have implicated layer II in seizure generation, possibly due to higher levels of synchronisation (Silva-Barrat *et al*., 1988; Louvel *et al*., 1992; Scharfman *et al*., 1998; Kohling *et al.,* 1998, 1999). Certainly, the SD of I_{Bg} and E_{Bg} in layer II suggests a

significantly higher level of network synchronisation in this area of the mEC. This purported seizure susceptibility, however, is not supported in acutely evoked epileptiform activity, with paired recordings indicating generation in layer V (Jones and Lambert 1990a, b) and the VmD data in this Chapter indicating larger, longer and more easily evoked seizures in deeper layers.

CHAPTER 6

BRIEF MEMBRANE OSCILLATIONS IN THE EC

Introduction

We have seen, in previous data chapters, that interference with individual receptor populations, or small changes in environment, can have wide-ranging effects on the activity of the entire network throughout the EC. Furthermore, the effect of a single drug can vary between layers within the mEC. Within a physiological context, small changes in the activity of neurone populations can have dramatic effects on the membrane voltage of an individual cell, manifested in brief membrane oscillations (BMO), or up-states, events that are easily recordable using intracellular electrophysiology. In this Chapter, I will investigate the phenomenon of membrane oscillations within layer III of the mEC, and use the VmD method in an attempt to quantify some of the network activity underlying these events.

As discussed previously, cortical neurones, whether in the intact brain or an acutely prepared slice, are subject to constant background synaptic bombardment. It is this "synaptic noise" that forms the basis of the membrane voltage equation used as the core of the VmD method. The constant neurotransmitter release, and subsequent postsynaptic activity, is believed to aid the detection of at- or below-threshold signals due to the additive effect of random noise on a "weak" signal, i.e. stochastic resonance. This stochastic noise is increasingly thought to be an important factor in a variety of cellular and network processes throughout the mammalian brain; regulating signal integration from a number of neurones, modulating signal gain and determining the excitability of single neurones, or populations (Ho and Destexhe 2000; Chance *et al*., 2002; Dorval and White, 2005; Wolfart *et al*., 2005). Increases in the intensity of background conductance have been implicated in the generation of BMO and up-states, as mentioned above. However, there is much debate as to the exact nature of the conductance changes necessary to mediate such events.

The advantage of using the VmD method to investigate background noise, and any subsequent consequences of changes in its level, is that it is complementary to a range of studies carried out using other means, from more traditional electrophysiology studies to the computer-based simulations that gave rise to the VmD method in the first place. Indeed, the VmD method was originally devised to study periods of increased background activity, leading to BMO (termed "high-conductance states" by the Destxhe group) and, under certain circumstances, the subthreshold oscillations in membrane potential known as "up-states" (Hausser and Clark, 1997; Pare *et al*., 1998a, b; Stacey and Durand, 2000, 2001; Destexhe *et al*., 2003; Rudolph *et al*., 2004; Rudolph and Destexhe, 2004). These can be so intense in an intact brain that neurones undergoing BMO are constantly depolarised in comparison to cells in quiescent periods. Whether periods of high background conductance are the sole cause of observed up-state activity is hotly debated, with conflicting theories from a number of high-profile groups (e.g. Destexhe *et al*., 2003; Rudolph *et al*., 2004; Rudolph and Destexhe, 2004; *c.f.* Waters and Helmchen, 2004, 2006)

The differentiation of spontaneous up-state activity caused by periods of differing background activity, as opposed to other, more regular oscillations associated with such things as sleep or memory formation, was initially made by Steriade *et al.* (1993), in pyramidal cells of certain morphology, usually cells with large dendritic arbours. Sanchez-Vives and McCormick (2000) showed that, in the visual cortex of anaesthetised cats, up-state activity is initiated in layer V and propagates vertically to layer VI and the superficial layers. There are several conflicting theories behind the generation and function of these up states. Walters and Helmchen (2004) showed using combined patch clamp and electrocorticogram studies that up-state activity is co-ordinated throughout the recorded neurones simultaneously, through an increase in action potential back-propagation mediated by an increase in the activity of dendritic sodium channels and/or a reduction in dendritic potassium channel activity, and would appear to also coincide with a marked increase in activity across the cortex.

However, Waters and Helmchen (2006) question the requirement of an increase in synaptic activity in the generation of up-state activity, citing instead small increases coupled with increases in input resistance caused by current rectification. Using short hyperpolarising current injections during whole-cell recordings of up-state activity in rat neocortical neurones *in vivo*, the membrane resistance of the recorded cells was monitored throughout. During up-state activity the resistance of the recorded neurone increased, with a small increase in conductance of 2-10 nS.

In contrast to the assertions of Waters and Helmchen, the Destexhe group (Destexhe *et al*., 2003; Rudolph *et al*., 2004; Rudolph and Destexhe, 2004; Rudolph *et al*., 2007) have maintained that up-states are generated by periods of intense and co-ordinated cortical activity. Their theory is that up-state activity is representative of the behaviour of neurones in the intact brains of awake, behaving animals, and so is the most accurate representation of a fully functional neurone. Indeed, Cossart *et al.* (2003) have proposed that up-state activity may form the basis of memory retention or computational function in neuronal networks, by functioning as "circuit attractors", a proposed method of enabling large collections of simple processing units (i.e. neurones) to perform complex computational tasks (Hopfield, 1982). Furthermore, Shu *et al*., (2003a) have demonstrated that barrages of increased excitatory and inhibitory activity enhance neuronal responsiveness and increase the accuracy of spike-timing. These co-ordinated barrages are thought to be controlled by the actions of feedback pathways. McCormick *et al*. (2003) have suggested that up- and down-states are the natural result of the extensive recurrent connections in the cortex, with inhibitory interneurones playing a crucial role (Sanchez-Vives and McCormick, 2000).

Studies in awake animals have shown that neurones in behaving subjects possess low input resistance and a depolarised membrane potential in comparison to quiescent cells seen in slices or anaesthetised animals. This would appear to support a much higher level of neurotransmitter release in these subjects (Matsumura *et al*., 1988;

Baranyi *et al.*, 1993; Steriade *et al.*, 2001). Furthermore, the technique of resistance comparison (by injection of hyperpolarising pulses and application of Ohm's law) used by Walters and Helmchen to propose their "low conductance" up-states, with little change in overall synaptic activity, has previously been questioned by the Destexhe group (Destexhe *et al.*, 2003) as too unreliable and non-transferable between studies or laboratories, due to differences in tissue preparations, electrode properties and recording conditions. Further support for the high-conductance theory of up-states comes from the use of the sodium channel blocker TTX in *in vivo* studies. Neurones recorded from intact brains in anaesthetised animals displayed, in the presence of TTX, resistance and potential characteristics similar to those found in neurones recorded from acute brain slices (i.e. a reduced preparation). These results logically support the reduced nature of slice preparations, but also rule out any differences in membrane potential or resistance characteristics that may have been caused by slice preparation, lending further weight to the notion of increased activity leading to up-states.

Cunningham *et al.* (2006) proposed an alternative explanation for up-state activity in the EC. They suggest that the major drive behind up-state activity is GluR5 containing kainate receptors, increasing activity by potentiating GABA and glutamate release through action at presynaptic terminals, but also postulate that the oscillations are a function of ATP-modulated potassium channels. Blockade of these channels with tolbutamide led to the prolongation of "up" phases, whereas enhancing the activation of K_{ATP} channels with diazoxide led to increased "down" periods. Blockade of K_{ATP} channels by MgATP slowed the transition between up- and down-state. The results suggest that increased activity during up-states leads to rapid depletion of intracellular ATP levels, which in turn causes the activation of K_{ATP} channels and the termination of the up-state.

In the studies discussed above, up-state activity is readily observed *in vivo* due to the high level of baseline activity in the intact brain. However, in reduced preparations (i.e. brain slices) it is usually necessary to increase activity levels to obtain oscillatory behaviour such as BMO and up-states. This can easily be achieved by lowering the magnesium concentration in the recording ACSF (e.g. see McCormick *et al*., 2003; Cunningham *et al*, 2006) to increase activation of pre- and postsynaptic NMDAr, increasing release of glutamate and GABA (Jones and Heinemann, 1989; Jones 1994). Here, I have used a modified ACSF in acute brain slices to induce up-state behaviour in the mEC. The VmD method has been used in an attempt to characterise differences in transmission between high-conductance states and quiescent periods. Both up-states and brief membrane oscillations (i.e. periods of obviously increased potential fluctuation that do not lead to spontaneous depolarisations) have been studied with a range of drugs.

Methods

EC-hippocampal slices were prepared from juvenile male Wistar rats (40-70g) as described in Chapter 2. To induce up-state behaviour, slices were cut in normal ACSF without additional ketamine (which was found to reduce the likelihood of up-state activity), and stored for 2 hours at room temperature in a modified ACSF after slicing. This modified solution contained higher $[K^+]_O$ (3.75 mM) and lower $[Mg^{2+}]_O$ (1.25mM) compared to normal (see Ch. 2), and was used in the majority of experiments in this Chapter, with the exception of the Mg^{2+} ramp group. The longer recovery time was found to be necessary to obtain reliable up-state behaviour. All recordings were made from pyramidal neurones in layer III of the mEC.

A separate group of 6 neurones were subjected to a magnesium ramp, to study the effects of decreasing concentration. Recording was started in ACSF with 1.5 mM

$[Mg^{2+}]_O$, which was then reduced by 0.5 mM every 5 minutes, giving a run of 1.5mM to 0.0mM $[Mg^{2+}]_O$ across the duration of the experiment, until it was nominally zero.

Results

Identification and Classification of Brief Membrane Oscillations

Up-states, where the membrane voltage spontaneously depolarises, often for several seconds, are easy to identify and differentiate from epileptiform activity by their amplitude, duration and shape, and as such can be identified by eye both during and after the recording as obvious depolarisations. However, other events were encountered that were obvious increases in the SD of the membrane potential, referred to here as brief membrane oscillations (BMO). These BMO are far harder to identify post-hoc, and identification involves assessing the entire voltage trace on a second-by-second basis and comparing membrane voltage fluctuations with the surrounding trace, looking for periods of increased variability. Once BMO states have been identified, they can be separated from quiescent membrane periods during VmD calculations. This gives two readings per cell; one for the normal, quiescent membrane state (QMS) and one for the rapid bursts that characterise the BMO.

Characterisation of Up-states

Up-state activity was successfully evoked in a total of 10 cells. Several drugs were used to characterise the receptor populations involved in the generation and maintenance of up-state activity: the NMDAr antagonist 2-AP5, the AMPAr/KAr antagonist NBQX, the GluR5-containing KAr antagonist UBP-302, the gap-junction opener trimethylamine, and the gap-junction antagonist carbenoxelone.

An illustration of up-state activity, along with an expanded, single up-state showing clearly spontaneous synaptic activity, can be seen in Fig. 6.1. Mean baseline values for up-state activity were as follows: amplitude = 6.3 ± 1.0 mV, duration = 2.2 ± 0.4 s, frequency = 0.22 ± 0.11 Hz.

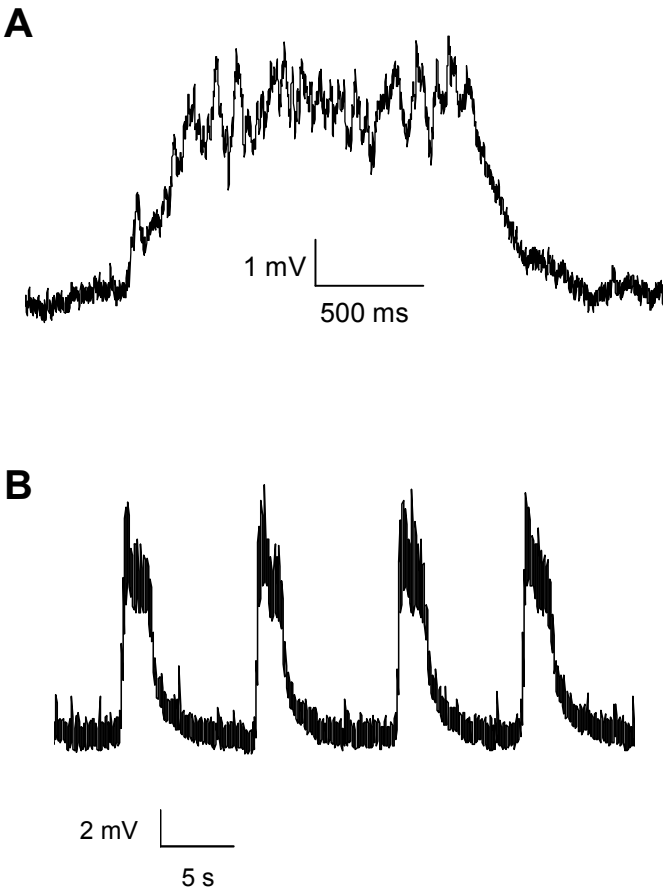

Figure 6.1: Up-states in a layer III mEC pyramidal neurone. Traces in this and subsequent figures show membrane voltage levels obtained through intracellular recording from single LIII pyramidal neurones. A: Expanded trace of a single up-state shows clear spontaneous synaptic activity on the rising edge and plateau of the event. B: Up-states exhibit rhythmic activity with a mean frequency of 0.22 ± 0.11 Hz

AMPAr

Up-states in layer III neurones consist of large amplitude depolarisations with spontaneous synaptic events superimposed (Fig. 6.1). Since most fast synaptic excitation at cortical synapses is mediated by AMPAr, it seemed logical to test for an involvement of these receptors in up-state generation so the contribution of AMPAr to

up-state activity was assessed. When a low concentration (5 μM) of the AMPAr/KAr blocker NBQX was perfused, the frequency of up-states slowed from 0.16 Hz to 0.08 Hz, without significant changes in amplitude. A representative trace is illustrated in Fig. 6.2. Upon washout, the frequency of the up-states was restored to control levels.

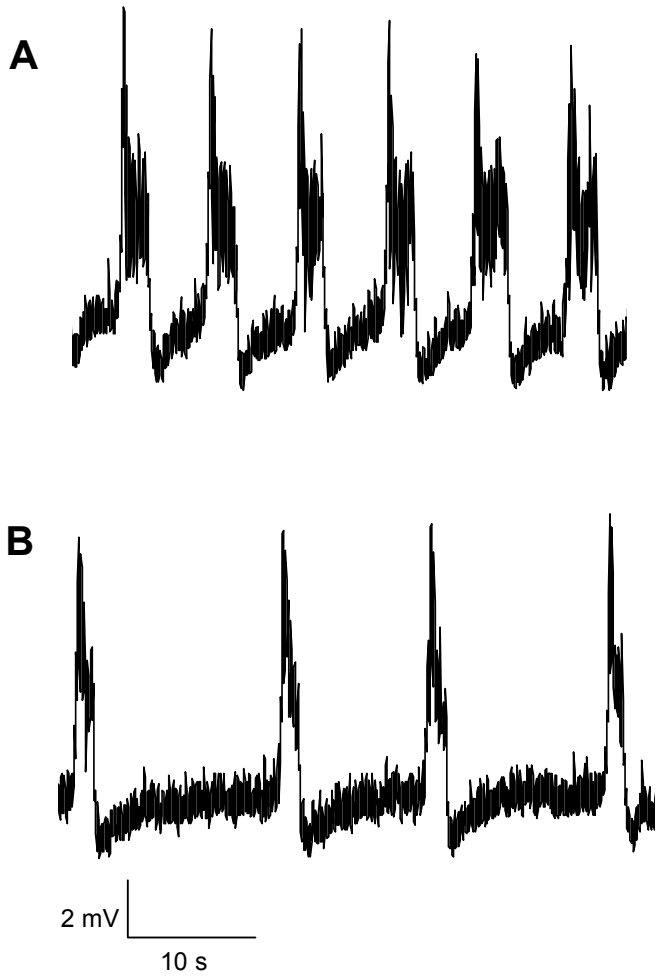

Figure 6.2: Effect of NBQX on up-states in layer III. A: In control conditions, these up-states exhibited a mean frequency of 0.16 Hz. B: Addition of NBQX (5 μM) caused a 50% reduction in frequency, without significant change to up-state amplitude.

NMDAr

NMDAr are tightly regulated by the voltage-dependent block exerted by Mg^{2+}. Removal of $[Mg^{2+}]_O$ elicits prolonged epileptiform discharges in EC neurones (Jones

and Heinemann 1988, 1989; Jones 1994), so a progressive lowering of $[Mg^{2+}]_O$ may eventually give rise to up-states involving increased activation of NMDAr. When the NMDAr antagonist 2-AP5 (30 μM) was perfused (n=3), up-state frequency was reduced within 5 minutes. In 2 out of 3 cells, 2-AP5 abolished up-states. Fig. 6.3 shows a representative trace from one neurone. Whilst the remaining cell showed reduced frequency and amplitude, the up-states were not abolished. This suggests that NMDAr have more of a role in the generation of up-states than AMPAr.

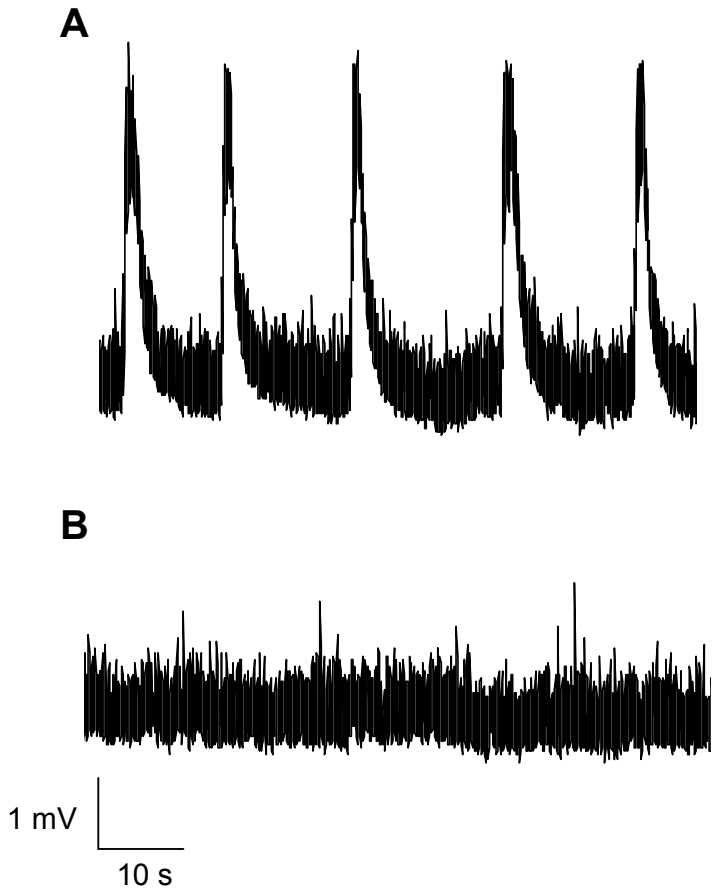

Figure 6.3: Effect of NMDAr blockade by 2-AP5 on up-state activity. A: In control conditions, up-state behaviour was frequent and regular. B: Addition of 2-AP5 first slowed, then abolished, up-state activity in 2 out of 3 cells. The other cell shows reduced frequency and amplitude but up-states were not abolished.

KAr

GluR5-containing KAr appeared to be crucial to the generation and maintenance of up-states in layer III. Application of UBP-302 (20 μM) abolished up-states in all tested cells (n=8). Upon wash-out of UBP-302, up-state activity was restored, with a similar frequency, but slightly reduced amplitude, compared with control (P>0.05). One representative recording is illustrated in Fig. 6.4. Large amplitude up-states occurred at highly regular intervals. These were interspersed with less regular and smaller amplitude events. Application of UBP-302 abolished both.

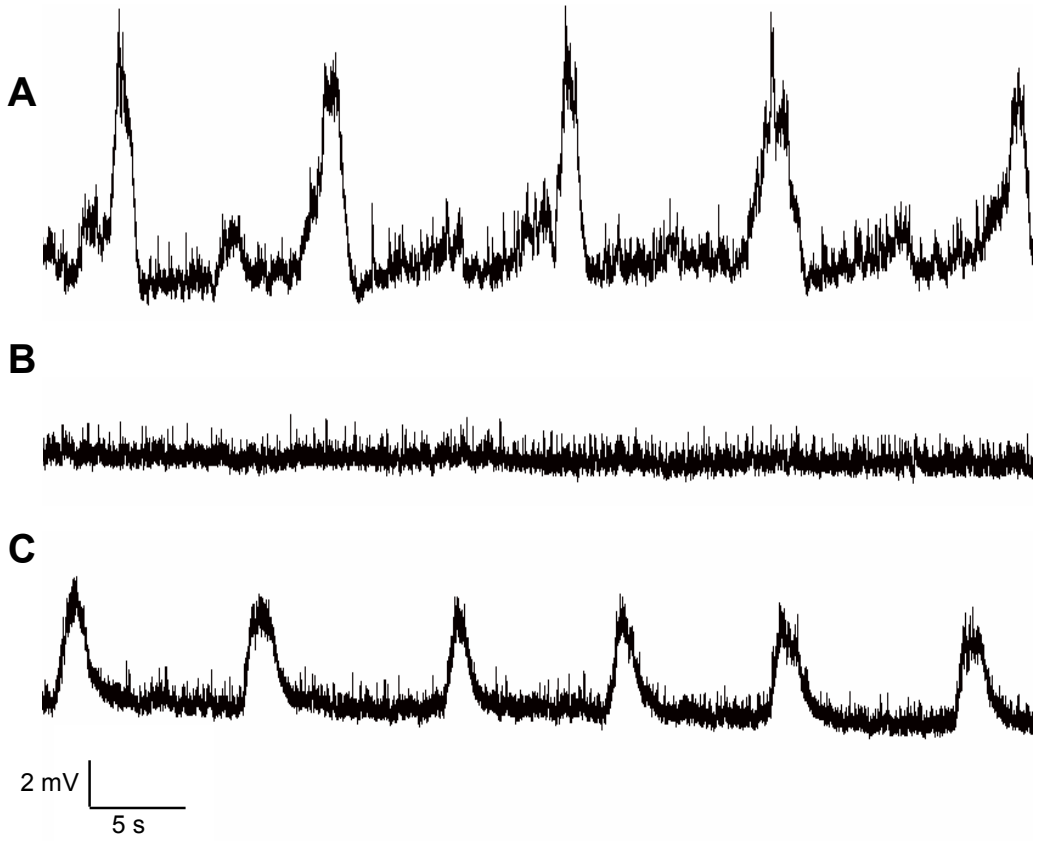

Figure 6.4: Effects of GluR5 KAr blockade on up-state activity in layer III. A: In control conditions up-states have an average frequency of 0.22 Hz. B: After addition of 20μM UBP-302, no up-state activity was observed, although baseline membrane noise remained at a similar level. C: After 10 minutes wash in drug-free ACSF, up-state activity spontaneously returned, with similar frequency but slightly reduced amplitude.

Gap Junctions

There is much evidence to suggest that electrical synapses (i.e. gap junctions) play a major role in the synchronisation of sub-threshold activity in the cerebral cortex (see Connors and Long, 2004 for review). Thus, I considered the possibility that gap junctions may be involved in synchronisation leading to up-states in the EC. Increasing gap junction activity might be expected to increase the synchronisation of sub-threshold synaptic events, leading to increased up-states. Conversely, decreasing electrical synapse activity might be predicted to reduce network-wide synchrony and activity. The role of gap-junctions in up-state activity was investigated through the use of trimethylamine (TMA) and carbenoxelone.

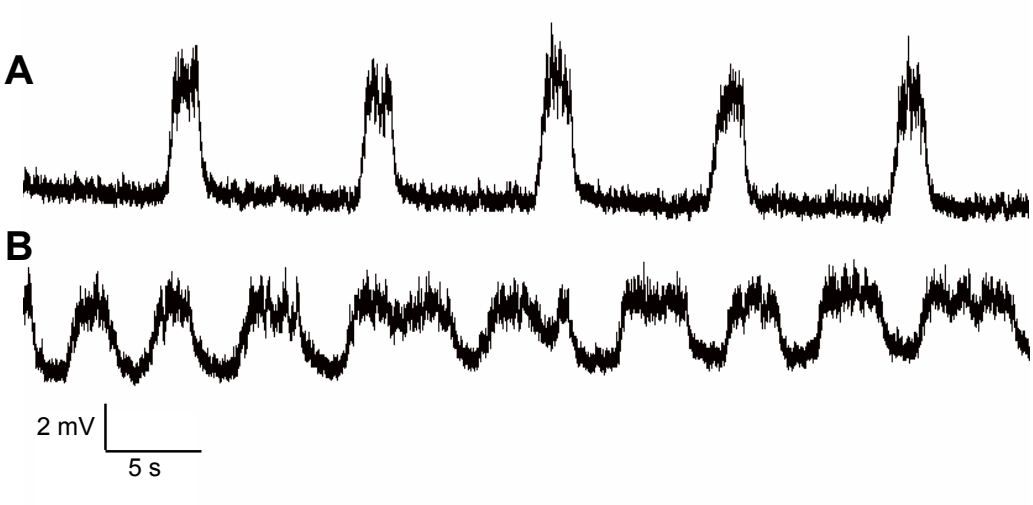

Figure 6.5: Effect of increased gap junction activity on up-state activity in layer III of the mEC. Top trace (A) shows normal up-state activity in a typical cell. After addition of 1mM TMA (B), up-state activity increases in frequency, with a slight reduction in amplitude. At peak activity, up-state generation under TMA is so frequent that the membrane spends more time in a depolarised state than in a resting state.

Addition of the gap-junction opener, TMA (1 mM), caused a dramatic increase in the frequency (0.15 ± 0.02 Hz to 0.31 ± 0.06 Hz, P=0.03) and duration of up-states, to the point where the membrane potential was essentially shifted to a prolonged up-state

with only occasional periods of normal membrane potential. A representative trace from one neurone is illustrated in Fig. 6.5. Washout of the TMA restored up-state activity to normal levels. In contrast, the gap junction blocker, carbenoxelone (200 μM), did not alter the amplitude or frequency of up-states. Thus, it appears that gap junction opening can enhance existing up-state generation, but they do not appear to be tonically involved in initiating or maintaining activity.

I_{Bg} and E_{Bg} During Progressive Depletion of $[Mg^{2+}]_O$

The up-states described above were induced by lowering $[Mg^{2+}]_O$ to 1.25 mM (compared to 1.5 mM). In addition, a common method of inducing acute epilepsy in slices is to record in a Mg^{2+}-free environment (e.g. Jones and Heinemann 1988, 1989; Jones 1994). The pharmacological experiments above have shown that up-states may be modified by AMPAr, NMDAr and GluR5 KAr. In addition, Mg^{2+}-free epileptic activity has been shown to be blocked by NMDAr antagonists and modified by AMPAr antagonists (Jones and Lambert, 1990a, b). VmD measurements (Chapter 4) in normal $[Mg^{2+}]_O$ showed that background inhibition and excitation could be modified by blocking NMDAr or GluR5 KAr, which themselves do not feature in the VmD estimates. Thus, in the present studies I examined changes in I_{Bg} and E_{Bg} during a progressive lowering of $[Mg^{2+}]_O$ from 1.5 to 0 mM (Mg-ramp).

Mg^{2+}-ramps were obtained in 6 pyramidal neurones in layer III. Initial $[Mg^{2+}]_O$ was 1.5mM, and this was lowered in steps of 0.5 mM every 10 minutes until 0 mM $[Mg^{2+}]_O$ was reached. Conductance estimates were performed every 2 minutes. Of these neurones, two cells exhibited up-states at 1.5-1.0 mM $[Mg^{2+}]_O$, and all cells exhibited acute epileptic activity during perfusion with Mg^{2+}-free ACSF. Conductance measurements were made outside periods of epileptic activity.

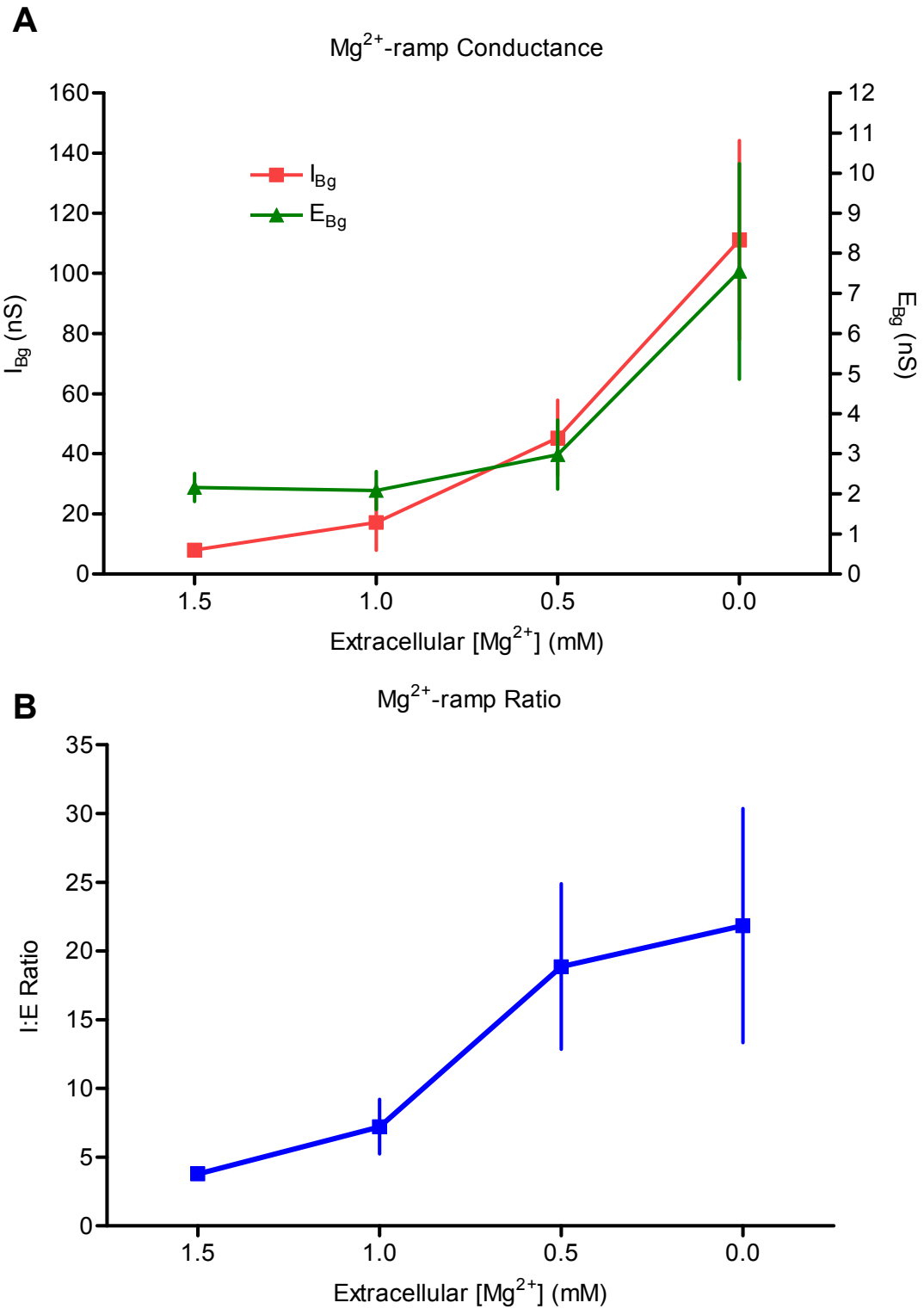

Figure 6.6: Conductance estimates in decreasing $[Mg^{2+}]_O$ in layer III mEC pyramidal neurones. Control levels are comparable to that found throughout this thesis in layer III. A: Stepwise lowering of $[Mg^{2+}]_O$ causes large rises in both E_{Bg} and I_{Bg}, however the increase in I_{Bg} is proportionally much larger. B: This leads to a final I:E ratio (at 0 mM $[Mg^{2+}]_O$) of 22:1 in favour of inhibition, compared to 4:1 in control conditions

Control values were 8.0 ± 1.3 nS for I_{Bg}, 2.2 ± 0.4 nS for E_{Bg} and I:E ratio was 3.8 ± 0.3 in 1.5 mM $[Mg^{2+}]_O$. Lowering $[Mg^{2+}]_O$ elicited a progressive rise in both E_{Bg} and I_{Bg} (Fig. 6.6A). I_{Bg} increased throughout the Mg^{2+}-ramp. However, E_{Bg} was practically unaltered at 1 mM $[Mg^{2+}]_O$, but rose thereafter. Comparing values obtained at 1.5 mM $[Mg^{2+}]_O$ with those in zero $[Mg^{2+}]_O$, E_{Bg} showed a 3.5 fold increase, reaching a final level of 7.6 ± 2.7 nS. I_{Bg} was affected to an even greater extent, undergoing nearly a 14 fold increase to reach 111.1 ± 33.1 nS in Mg^{2+}-free ACSF. This was manifest as a large change in I:E ratio, which attained a final value of 21.8 ± 8.51 in Mg-free ACSF. Changes between 1.5 and 0 mM $[Mg^{2+}]_O$ were found to be significant using ANOVA (P_I<0.001, P_E=0.016 and P_R=0.037).

Changes in the SD of I_{Bg} and E_{Bg} were also examined. I_{Bg} SD increased from an initial value of 0.12 ± 0.06 nS in 1.5 mM $[Mg^{2+}]_O$ to 0.32 ± 0.16, a 2.5 fold increase in magnesium free ACSF (Fig. 6.7A). However, the relative change in E_{Bg} SD was even greater, increasing from 1.8 ± 0.3 pS in 1.5 mM $[Mg^{2+}]_O$ to 8.1 ± 0.4 pS in Mg^{2+}-free ACSF. This represents a 4.5 fold increase over the control value. The changes in SD indicate increasing synchrony in both excitatory and inhibitory drives onto the principal cells. These are likely to be interconnected as it has been shown that interneurones can actually synchronise activity in principal cells. Thus, overall reduced $[Mg^{2+}]_O$ causes elevated synchrony in the whole network, and this could be involved in the generation of epileptic responses. Neither change, however, was found to be significant using ANOVA.

Lowering $[Mg^{2+}]_O$ had conflicting results on cellular excitability measurements. The firing threshold of action potentials was reduced steadily throughout the Mg-ramp from 22.3 ± 1.3 mV in 1.5 mM $[Mg^{2+}]_O$ to 16.2 ± 0.9 mV in zero $[Mg^{2+}]_O$, indicating increased excitability (P=0.004, t-test). However, the spikes evoked by a 250 ms depolarising pulse was not significantly affected by reducing $[Mg^{2+}]_O$ (2.8 ± 0.7 to 2.1 ± 0.5).

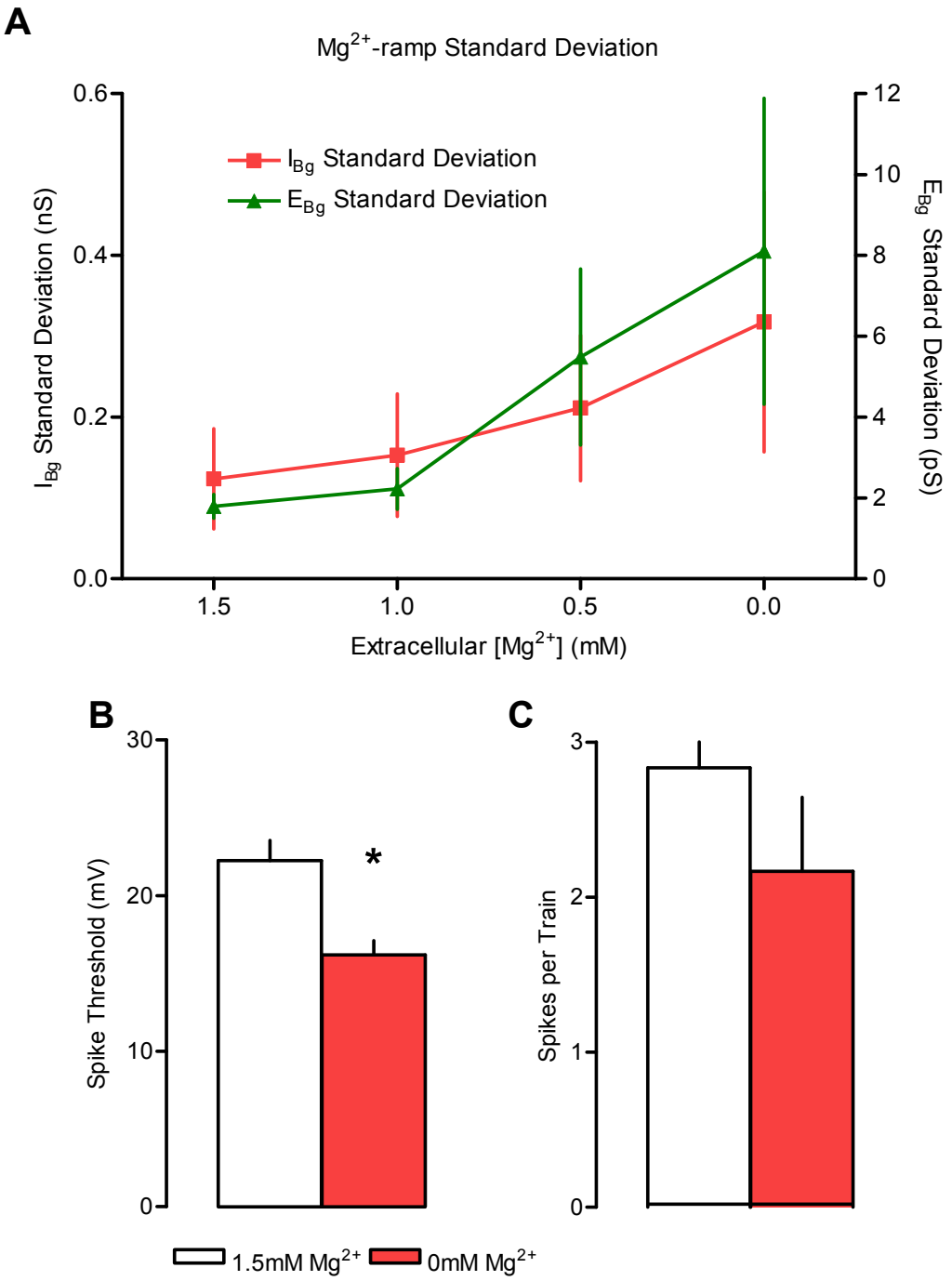

Figure 6.7: SD estimates and cellular excitability measurements in Mg^{2+}-ramp experiments. A: The change in SD estimates is the reverse of that seen in the conductance results, as the level of I_{Bg} SD increases proportionally less than the level of E_{Bg} SD. This indicates higher levels of synchrony in both populations, however in Mg^{2+}-free ACSF the excitatory cells have a proportionally higher degree of synchrony compared to the interneurones. B: Cellular excitability measurements show conflicting results, with spike threshold falling significantly. C: However, the number of spikes per train is also slightly reduced.

VmD Measurement of Up-states

In one neurone where a Mg^{2+}-ramp experiment was conducted, at approximately 1 mM $[Mg^{2+}]_O$ up-states with plateaus long enough (several hundred ms) to obtain VmD measurements were observed, allowing estimates of I_{Bg} and E_{Bg} to be made during up-states (Fig. 6.8). 6-8 up-states were analysed at each conductance level. VmD conductance values for up-state peaks were 21.5 nS for I_{Bg}, and 7.0 nS for E_{Bg}. This gave an I:E ratio of 3.1 at the plateau of up-states. I_{Bg} SD was very high: 1.93 nS. E_{Bg} SD was close to normal control values, at 6.77 pS. These data suggest that up-states are periods of high conductance, accompanied by increased synchrony in inhibitory populations. The up-state data described during this chapter was largely obtained before the VmD method was perfected, so no conductance data is available for them. Subsequent experiments were performed using slices taken from rats killed by cervical dislocation, as opposed those given ketamine and decapitated. The latter group of rats exhibited up-states in most slices, however with the cervical dislocation group, used after VmD recordings were made available, up-state activity was almost impossible to obtain.

However, cervically dislocated rats did exhibit brief membrane oscillations (BMO) in 1.25 mM $[Mg^{2+}]_O$, which were readily distinguishable from normal quiescent membrane states (QMS) as periods of increased membrane potential variability, but did not cause up-state like depolarisations. These BMO were studied using the VmD method.

Measurement of BMO

VmD analysis of BMO (n=7) revealed extremely interesting results. The fluctuations in membrane potential did not involve large increases in overall conductance, but were associated with a brief change in I:E ratio. Control conditions in these cells were

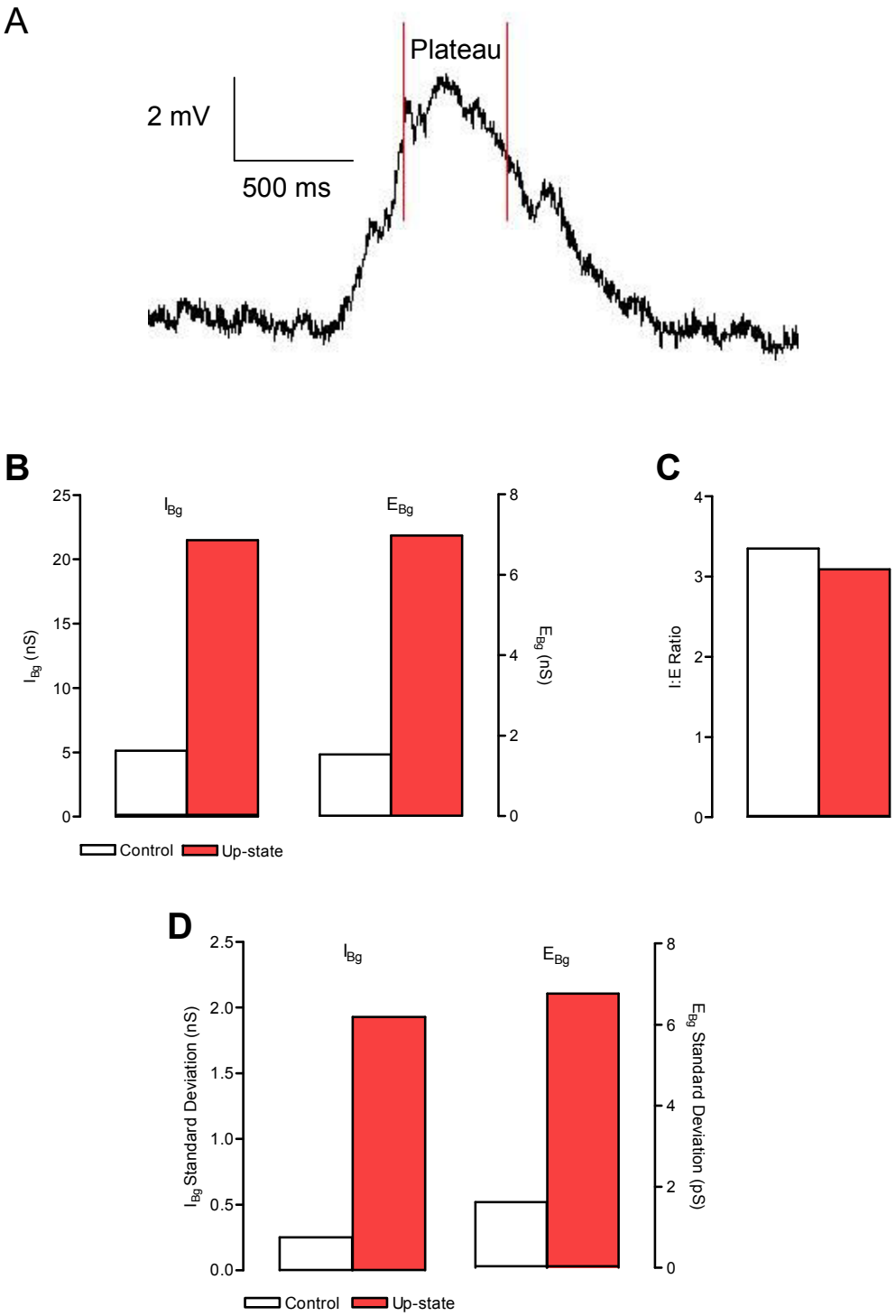

Figure 6.8: VmD measurement of up-states. A: During one Mg-ramp recording, up-states with plateaus long enough to obtain VmD measurements from were observed. The membrane voltage values between the red lines for 6-8 up-states per injected current level were pooled and treated as one set of VmD data. B: Values of I_{Bg} and E_{Bg} were both substantially increased, by proportionally equal amounts. C: This led to little change in overall I:E ratio. D: The SD of both I_{Bg} and E_{Bg} is substantially increased, suggesting a large increase in synchrony within and between inhibitory and excitatory populations.

within the normal range of observations for layer III cells in 1.25 mM $[Mg^{2+}]_O$. I_{Bg} was 4.0 ± 0.5 nS, E_{Bg} was 1.1 ± 0.2 nS, and the mean I:E ratio was 3.9 ± 0.3. During a BMO, I_{Bg} was noticeably reduced to 1.6 ± 0.5 nS. At the same time E_{Bg} was increased to 2.4 ± 0.8 nS. This gave an I:E ratio of 1.0 ± 0.2 during a BMO (Fig. 6.9). This represents a brief change in ratio of almost 4 fold in favour of excitation. The increase in E_{Bg} was reflected in the SD measurements. Control I_{Bg} SD was 0.15 ± 0.04 nS, control E_{Bg} SD was 1.4 ± 0.2 pS. During a BMO, I_{Bg} SD was little altered at 0.19 ± 0.04 nS, with the SD of E_{Bg} showing an upward trend with a nearly 6 fold increase, to 8.1 ± 5.9 pS. Because of the difficulty in obtaining BMO recordings, n-numbers are low. The high S.E.M. of the E_{Bg} SD means that it is not a significant change, although more experiments may improve the errors. If so, this would indicate that the relative synchrony of excitatory activity is greatly increased during these membrane potential fluctuations. The changes in I:E ratio and I_{Bg} was significant ($P<0.05$, paired t-test). None of the changes in SD were found to be significant.

Effects of Tiagabine on BMO

The fact that BMO appeared to involve loss of background inhibition prompted me to study the effects of tiagabine (4 μM, n=4) on their occurrence. Previous experiments showed that the GABA uptake blocker caused a substantial increase in I_{Bg}. The drug abolished BMO in all four neurones. At the same time, it increased I_{Bg} from 4.0 ± 0.8 nS to 8.5 ± 0.9 nS, and left excitatory conductance largely unchanged at 0.9 ± 0.2 nS from 1.2 ± 0.3 nS. This led to a final I:E ratio of 9.7 ± 0.8 (vs 3.6 ± 0.4 control). The large increase in I_{Bg} is likely to be responsible for the abolition of the BMO periods. Tiagabine did not significantly change the SD of either I_{Bg} or E_{Bg}.

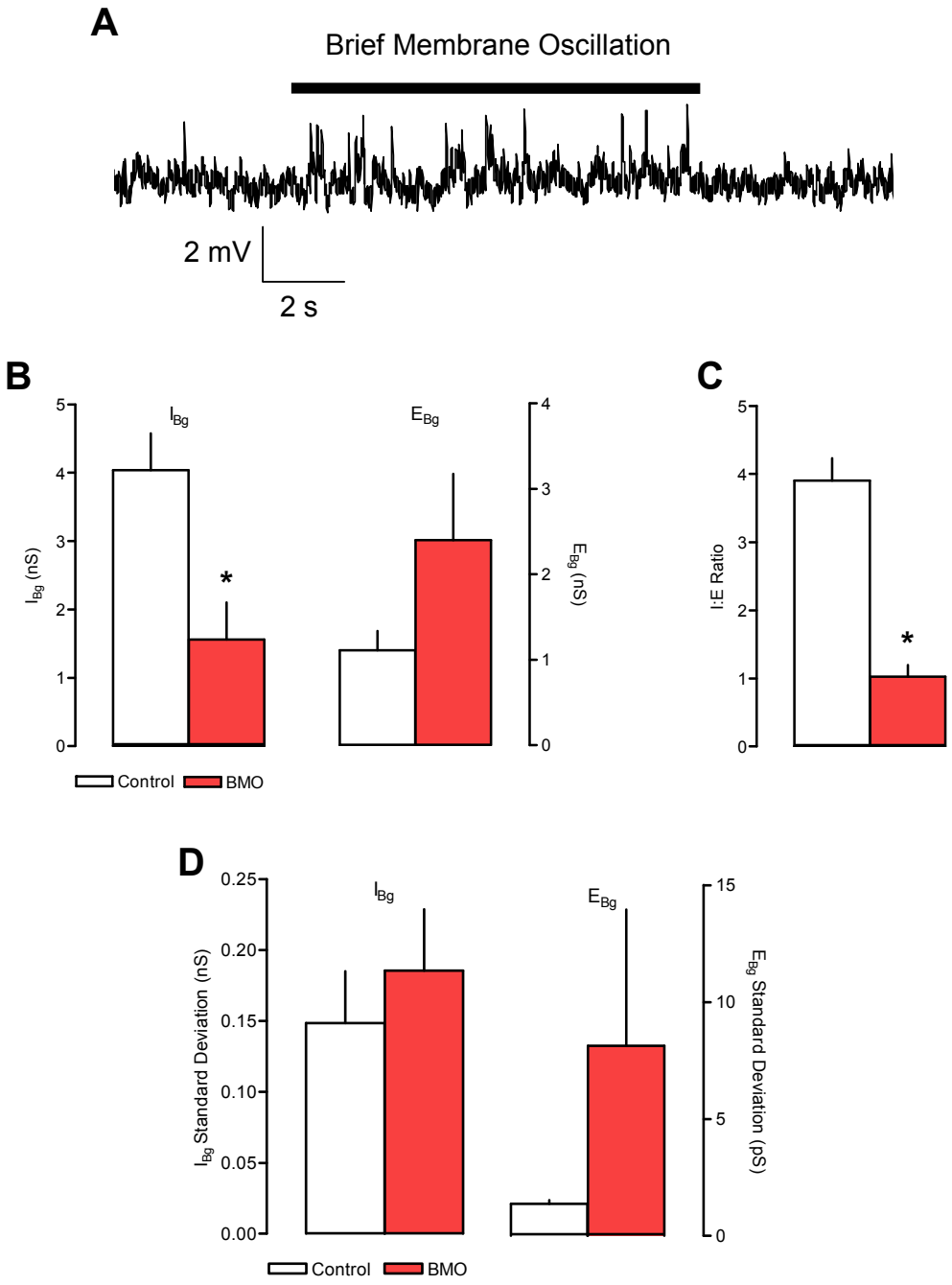

Figure 6.9: Characterisation of background conductance during brief membrane oscillations. A: Example of BMO, indicated by solid black line over trace. Increased membrane potential SD can clearly be seen. B: VmD values for control and BMO states. I_{Bg} is significantly reduced, with a smaller increase in E_{Bg}. I:E ratio is significantly shifted in favour of inhibition (3.9 vs 1.0). D: Although not significant, there is a clear trend in favour of E_{Bg} SD increase. I_{Bg} SD is not affected. Thus, BMO are associated with brief reductions in I_{Bg} and increases in the SD of E_{Bg}.

Discussion

Oscillations in cortical networks, associated with changes in background activity, are thought to play an important role in the processing of sensory information, memory formation and other highly complex computational tasks (Cossart *et al*., 2003). In this Chapter I have characterised two separate oscillatory behaviours, up-states and BMO, which would appear to have distinct profiles of background synaptic activity.

Up-states, as outlined in the introduction to this Chapter, have been the subject of some debate with regards to the level of synaptic bombardment necessary for their generation. Waters and Helmchen (2006) suggest that, due to rectification by voltage sensitive channels and associated increases in membrane resistance, only small increases in background activity are required for up-state generation. In contrast, the Destexhe group (Destexhe *et al*., 2003; Rudolph *et al*., 2004; Rudolph and Destexhe, 2004; Rudolph *et al*., 2007) maintain that up-states are a result of brief periods of significantly increased conductance, with high levels of synchronisation between and within neuronal populations.

The VmD data gathered from up-states in this Chapter is in agreement with the latter theory. Despite only one neurone being suitable for VmD analysis, the increases in I_{Bg}, E_{Bg} and their respective SDs are clearly associated with up-state events. The I:E ratio does not change between baseline and up-state periods, suggesting a proportionally equal rise in background excitation and inhibition. The wealth of recurrent connections in the mEC leads to close association between inhibitory and excitatory populations, with changes in the activity of one having an appreciable effect on the other, as seen in earlier Chapters. Thus, a rapid and pronounced increase in E_{Bg} would precipitate a similar increase in I_{Bg}. In a similar fashion to the generation of epileptiform activity in the mEC, Sanchez-Vives and McCormick (2000) found that up-state behaviour is initiated in layer V and propagates towards the superficial layers.

A valuable future study could involve simultaneous VmD measurements from layers III and V of the mEC, to investigate possible lamina-specific changes in background activity which precede, or coincide with, up-state activity.

Aside from the VmD data, the pharmacological characterisation of up-states performed in this Chapter would suggest that GluR5-containing KAr have a crucial role in the generation and maintenance of up-state activity. Whole-cell patch clamp studies from our laboratory have strongly suggested that GluR5-KAr enhance both glutamate and GABA release through action at presynaptic terminals (Chamberlain and Jones, unpublished observations). If it is accepted that the increase in background activity seen with the VmD method is the driving force behind up-state activity, it may be that activation of presynaptic KAr provides a further drive in up-state generation.

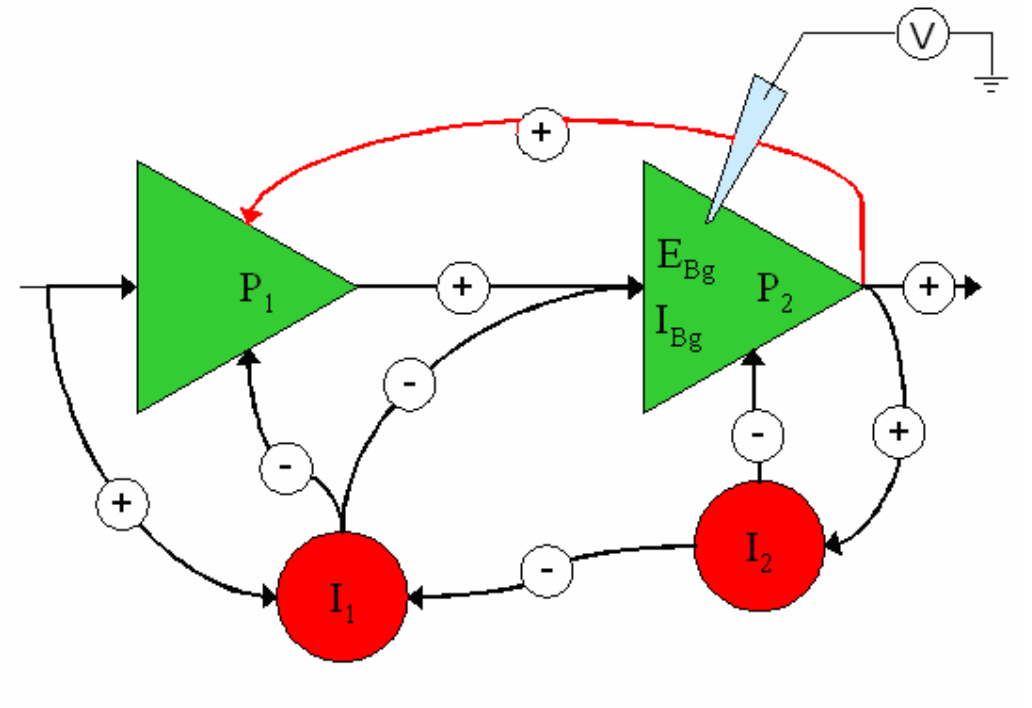

Figure 6.10: Network connections in the mEC. As before, green triangles represent principal cells, and red circles represent interneurones. The wealth of recurrent connections (red line) is thought to be an important factor in the generation of up-state behaviour. Small increases in transmitter release could be boosted through activation of GluR5-KAr and/or presynaptic NMDAr, meaning that these receptors play a pivotal role in up-state activity.

Further enhancement of transmitter release may come from presynaptic NMDAr, explaining the sensitivity of up-states to NMDAr blockade with 2-AP5. Another possibility is that up-state activity is sensitive to 2-AP5 due to the role that postsynaptic NMDAr play in excitatory transmission in layer V. As discussed above, up-states are thought to originate in deeper layers and propagate vertically (Sanchez-Vives and McCormick, 2000). Our laboratory has shown that a significant component of background excitation in layer V is mediated by postsynaptic NMDAr (Berretta and Jones, 1996a), the blockade of which may significantly reduce excitatory activity in layer V, and reduce the probability of up-state generation and propagation.

The majority of fast excitatory transmission in cortical networks is mediated by postsynaptic AMPAr. However, addition of the AMPAr/KAr antagonist NBQX did not completely abolish up-state activity in all cells. The effect of NBQX on up-states in this Chapter is not clear cut. The abolition seen in 66% of cells, and the reduction in frequency seen in the other, may be due to an overall reduction in E_{Bg} due to AMPAr blockade. However, it may be caused, at least in part, by the antagonism of pre- or postsynaptic KAr under NBQX. This could be resolved by further studies with more specific antagonists, such as GYKI-53665 (specific AMPAr antagonist) although there are few suitable specific antagonists for non-GluR5 containing KAr.

Opening gap junctions with TMA leads to an appreciable increase in the frequency and duration of up-state activity. However, reduction of gap junction activity with carbenoxelone has no effect on up-states. Thus, it would seem that whilst gap junction activity can enhance existing up-states, tonic activation of gap junctions is not involved in the normal generation of up-state activity.

The large increases in conductance seen during stepwise reduction of extracellular magnesium are not surprising. NMDAr are known to exist both presynaptically and postsynaptically at excitatory synapses in the mEC (Berretta and Jones, 1996a, b;

Jones and Woodhall, 2005; Yang *et al*., 2006). Furthermore, NMDAr are known to play a large role in the function of GABAergic interneurones (Monyer *et al*., 1994; Glitsch and Marty, 1999; Maccaferri and Dingledine, 2002; Duguid and Smart, 2004; Tzingounis and Nicoll, 2004). By reducing the extracellular concentration of magnesium, the voltage-dependent blockage of the NMDAr pore by Mg^{2+} ions is lessened, and NMDAr mediated depolarisation is more likely. This would increase the depolarisation of both the presynaptic and postsynaptic membrane, leading to increased release of both glutamate and GABA, and the greater likelihood of action potential formation. Thus, since the effects of $[Mg^{2+}]_o$ reduction take place on both sides of the synapse, and would be expected to cause a positive feedback effect on transmitter release (i.e. NMDAr activity increases glutamate release, which further increases NMDAr activity both pre- and postsynaptically) the rise in activity seen during stepwise $[Mg^{2+}]_o$ reduction is rapid and emphatic. Furthermore, given the above-mentioned link between NMDAr and interneurones, the shift in the I:E ratio towards inhibition is a predictable response to removal of voltage-dependent Mg^{2+} blockade of NMDAr.

Decreasing $[Mg^{2+}]_o$ to 1.25 mM gives rise, in some cells, to brief membrane oscillations (BMO). The VmD data from these events suggest that they are distinct from up-states, in that there is no overall increase in background conductance. Instead, a brief but significant drop in I_{Bg} leads to an I:E ratio of approximately 1:1, accompanied by an increase in the synchrony of excitatory neurones.

The function of these BMO provides an interesting avenue for investigation. They may be associated, precursor events to up-states, that would trigger spontaneous depolarisations if conditions were favourable (i.e. greater levels of transmitter release, as seen *in vivo* or with reduced $[Mg^{2+}]_o$ *in vitro*). These BMO events are strongly reminiscent of sharp wave activity seen throughout the hippocampus and EC in behaving animals (Chrobak and Buzsaki, 1994, 1996). These sharp waves are periods

of highly co-ordinated activity that are most prominent in the CA1 area of the hippocampus (Buzsaki *et al*., 1983; Buzsaki, 1986; Suzuki and Smith, 1987), but are also evident in the deeper layers of the mEC. They have been postulated as a mechanism for the transfer of memory traces from hippocampus to EC (Ylinen *et al*., 1995). Chrobak and Buzsaki (1994) claim that sharp waves are not evident in the superficial layers of the EC and associated retrohippocampal structures, instead demonstrating the prominence of a similar but unrelated theta-wave activity in these superficial layers in behaving animals. However, the BMO events observed in this Chapter are seemingly random, and do not display the highly rhythmic activity associated with theta waves, as well as having a far slower frequency.

A possible method for the investigation of these BMO is the combination of VmD recording with multi-electrode extracellular, or paired intracellular, recordings. This would allow any slice-wide waves to be tracked in real time, which would then give an estimation of the direction of propagation, and possible site of origin.

CHAPTER 7

EFFECT OF ANTICONVULSANTS ON BACKGROUND SYNAPTIC ACTIVITY

Introduction

The effective diagnosis and treatment of various types of epilepsy presents an ongoing challenge for physicians and pharmacologists alike. Epilepsy is the most common serious neurological condition in the developed world, with a prevalence of 5-10 cases per 1000 population. Of these patients, one third will die in a manner related directly to their epilepsy (Brodie *et al*., 1997). The mean duration of epilepsy is 10 years, but 20-30% of patients will experience lifelong epilepsy. Modern pharmacotherapy enables the control of many types of seizures of varying severity. However, 30% of patients are, or will become, refractory to any form of pharmacological intervention. Of those, a further 30% will be unresponsive to surgical intervention (Sander, 1993; Brodie *et al*., 1997; Kwan and Brodie, 2000). The EC has increasingly become a focus of attention for those studying mechanisms of epilepsy, and understanding where current treatment regimes fall short. The most common form of epilepsy in adults is temporal lobe epilepsy (TLE), accounting for around 40% of seizures in adults. Surgical studies have suggested that the success of anterior temporal lobectomy or selective amygdalohippocampectomy is directly correlated to the amount of EC tissue removed (Fried, 1993). The role of the EC as the "gateway" between hippocampus and neocortex implicate it in the propagation of seizures arising from hippocampal sclerosis. Indeed, the EC itself has been cited as an initiation point for seizures in TLE (Jones and Lambert, 1990a, b; Siegel *et al.*, 1990; Fried, 1993; Nagao *et al.,* 1996; Sperling *et al.,* 1996; Schwarcz *et al.,* 2000; Dupont *et al.,* 2001; Jones and Woodhall, 2005).

Frontline pharmacotherapy for epilepsy has long been based on empirical results rather than rational drug design. As a consequence, the mode-of-action of many anticonvulsant drugs is poorly understood. Several common drugs have been the subject of debate with regards to their cellular and synaptic effects. Studies in this laboratory have used whole-cell patch clamp recording to show that a number of

clinically effective drugs modify the spontaneous release of GABA and glutamate at EC synapses. In this Chapter I have used the VmD method to determine how these effects relate to global background activity and excitability.

Phenytoin

Used in the treatment of generalised tonic-clonic and complex partial seizures, phenytoin has been in use since the 1950s (Mattson *et al.,* 1985; Cunningham *et al.,* 2000). There is contention concerning its primary mode of action. Many studies have suggested that phenytoin acts via blockade of VGSC in a use- and voltage-dependent manner (e.g. McLean and MacDonald, 1983; Matsuki *et al.,* 1984; Yaari *et al.,* 1986; Tomaselli *et al.,* 1989; Ragsdale *et al.,* 1991; Rogawski and Loscher, 2004; White *et al.,* 2007), leading to a reduction of sustained repetitive action potential activity in postsynaptic neurones. However, consequence of VGSC blockade might also be altered transmitter release.

Previous studies in this laboratory (Cunningham *et al.,* 2000) used whole-cell patch clamp studies in the mEC to show that phenytoin could reduce the spontaneous release of glutamate but increased release of GABA. Both effects persisted in the presence of TTX, showing that blockade of sodium channels was not responsible for alterations in release. Phenytoin did not appear to affect postsynaptic glutamate receptors (rise time, amplitude and decay time of EPSCs were not affected) so it seems likely that it had actions on the release mechanisms at both GABA and glutamate synapses. The basis of these effects remains unknown, but they could contribute to the anticonvulsant effects of the drug.

Ethosuximide

Ethosuximide is the drug of first choice in the treatment of absence seizures. It is equally effective as valproate. The prevailing view on the clinical action of ethosuximide is that it blocks T-type calcium channels (MacDonald and Kelly, 1994). However, as with all anticonvulsants, this is unlikely to be the only factor involved in the mode of action of ethosuximide. Coulter *et al*. (1989a) first showed blockade of low-threshold calcium currents (I_{CaT}) by ethosuximide. In the same year a study in isolated neurones from the ventrobasal complex of guinea pig (Coulter *et al.,* 1989b; Kostyuk *et al*., 1992), suggested that the action of ethosuximide on I_{CaT} was voltage dependent (more pronounced at hyperpolarised potentials). Gomora and colleagues (2001) confirmed these findings in cloned human T-type calcium channels, inactive-state preferential binding by ethosuximide was observed. Other studies suggested that persistent Na^+ channels and Ca^{2+}-activated K^+-channels may be more likely targets for the action of ethosuximide (Leresche *et al*., 1998). Additionally, Löscher and Frey (1977) showed that ethosuximide was able to reverse isoniazid-mediated inhibition of GAD, suggesting that the drug may have some effects on GABA synthesis.

Gabapentin

Gabapentin was approved for use in antiepileptic polytherapy in 1994. It is a 3-substituted GABA analogue, and as such was developed on the premise that it would exert anticonvulsant effects through mimicking/enhancing GABAergic transmission. However, a large consensus suggests that gabapentin has little or no effect on various aspects of GABA transmission.

Taylor *et al*. (1998) discussed a number of proposed mechanisms of the action of gabapentin. There is little or no evidence to support direct interaction of gabapentin with either $GABA_A$ or $GABA_B$ receptors, as it does not displace GABA binding

(Taylor *et al*., 1998; Jensen *et al*., 2002). It does not alter GABA uptake into neurones (or glia), nor does it alter electrophysiological responses to GABA (Rock *et al.,* 1993; Su *et al*., 1995). Maneuf *et al.* (2003) has summarised the efforts to identify and purify a "gabapentin binding protein". This was identified as the $\alpha_2\delta_{1\text{-}2}$ subunit of the VGCC (Gee *et al*., 1996). No definitive data exist as to the location of these in the EC.

In studies from this laboratory, gabapentin (and the related drug pregabalin) was found to reduce both activity dependent and independent glutamate release in the EC. The results suggested a dual mechanism of the action of gabapentin. This was mediated partly by blockade of P/Q-type VGCCs, and partly by an unknown effect downstream of Ca^{2+} entry (Cunningham *et al*., 2004).

Felbamate

Felbamate was the first of the new generation of anticonvulsants introduced in the 1990s, having been approved for use in 1993. Its clinical use is now limited as a result of rare, but often fatal, side effects such as aplastic anaemia (Pellock and Brodie, 1997).

The anticonvulsant effects of felbamate have largely been considered to result from blockade of NMDA receptors. Kuo *et al*. (2004) demonstrated that the action of felbamate in the blockade of NMDA currents is use dependent, whilst other studies have shown that felbamate is specific for receptors composed of NR1a/NR2B subunits (Harty and Rogawski, 2000). Recent work from our laboratory has shown that felbamate, like other anticonvulsants, reduces spontaneous glutamate release at EC synapses. This effect seems to be entirely dependent on blocking the tonic facilitatory presynaptic NMDA receptor. In contrast, the reduction of glutamate release by phenytoin and gabapentin was independent of presynaptic NMDAr blockade (Yang *et al*., 2007).

Felbamate has also been shown to potentiate the action of $GABA_A$ receptors in cultured neurones, enhancing Cl^- current by acting at a site close to, but distinct from, the picrotoxin site, and separate from the barbiturate, GABA, benzodiazepine, zinc and neurosteroid sites (Rho *et al*., 1994; Kume *et al*., 1996; Rho *et al*., 1997). Further investigation showed that the action of felbamate at $GABA_Ar$ was subunit specific, and depended heavily on the right combination of α, β and γ subunits ($\alpha_1\beta_2\gamma_{2S}$, $\alpha_1\beta_3\gamma_{2S}$, $\alpha_2\beta_2\gamma_{2S}$ and $\alpha_2\beta_3\gamma_{2S}$) expressed within the $GABA_A$ receptor, with no effect or negative modulation of other subunit combinations (Simeone *et al*., 2006).

Valproate

Valproic acid has a long history as an antiepileptic, used to treat generalised and partial seizures (Löscher, 1999). Valproate is primarily considered to act as an enhancer of GABA (Löscher, 1981), by blocking breakdown through antagonism of GABA aminotransferase (Löscher, 1993) or increasing synthesis by increasing glutamic acid decarboxylase (GAD) activity (Wikinski *et al*., 1996). Some have found that valproate has a biphasic effect on GABA levels, reducing release at low concentration and enhancing release at higher concentrations (Wolf *et al*., 1988; Biggs *et al*., 1992). Valproate has also been suggested to act upon VGSC to reduce repetitive firing in cortical neurones (McLean and MacDonald, 1986; Taverna *et al.,* 1998). Additionally, some studies suggest a valproate-mediated block of postsynaptic NMDA receptors and the displacement of glutamate from AMPA receptors (Wamil and McLean, 1991; Zeise *et al.,* 1991; Gean *et al.,* 1994; Kunig *et al.,* 1998).

Work from our laboratory (Cunningham *et al.,* 2003) has shown a reduction in the frequency (but not amplitude) of both sEPSCs and sIPSCs (with a greater reduction in sEPSC frequency). Both these effects were abolished in the presence of TTX suggesting valproate reduces glutamate and GABA release by blocking presynaptic VGSC. In addition, the decay time of sIPSCs was increased by valproate, indicating

that the drug can potentiate the action of $GABA_A$ receptors in the postsynaptic membrane. This may occur through interaction with the benzodiazepine site on the receptor.

Lamotrigine

Lamotrigine has been approved for use since the mid-1990s. It has been shown to be effective in the treatment of partial seizures in patients who are refractory to other pharmacotherapies (Goa *et al.,* 1993). Lamotrigine has been suggested to act in a similar fashion phenytoin by blockade of VGSC (Miller *et al.,* 1986; Cheung *et al.,* 1992; Xie *et al.,* 1995; Dichter and Brodie, 1996) and reduction of the repetitive firing of somatic action potentials (Calabresi *et al*., 1999; Salvati *et al*., 1999). A number of studies have suggested that lamotrigine acts largely upon presynaptic sodium channels and decreases glutamate release (Leach *et al.,* 1986; Waldmeier *et al.,* 1995, 1996; Wang *et al.,* 1996a; Calabresi *et al.,* 1999). Blockade of voltage-gated calcium channels (VGCC) has also been suggested to be involved in the action of lamotrigine (Wang *et al.,* 1996a, b; Stefani *et al.,* 1997)

Again, previous work in this laboratory (Cunningham and Jones, 2000) has used whole-cell patch clamp recordings in the mEC to demonstrate that lamotrigine, like phenytoin, decreases spontaneous glutamate release and increases GABA release in both the presence and absence of TTX. Thus VGSC block is not a prerequisite for the effects of lamotrigine on release.

Methods

Slices were prepared from juvenile male Wistar rats (40-60g) as outlined in Chapter 2. Intracellular recordings were obtained from layer III pyramidal cells in the mEC. The VmD method was utilised as previously described. After a control period of recording,

perfusion was switched to ACSF containing the required anticonvulsant drug. Drug perfusion was continued for at least 20 minutes, or until the cell was lost. Concentrations of anticonvulsants were chosen to be similar to their therapeutic levels.

Results

Phenytoin

Phenytoin was applied to a total of 9 neurones at two separate concentrations (20 μM, n=6, 50 μM, n=3). At 50 μM, effects on conductance and SD values were similar to those seen in 20 μM phenytoin. However, action potential amplitude was significantly reduced, affecting cellular excitability. Thus, the remaining studies were performed in 20 μM phenytoin. Control values for the cells tested with 20 μM were: I_{Bg} 5.1 ± 0.7 nS, E_{Bg} 1.1 ± 0.2 nS, and I:E ratio was 5.1 ± 0.7.

Addition of 20 μM phenytoin caused a rise in I_{Bg} (Fig. 7.1A), to 9.3 ± 1.6 nS. E_{Bg}, however, was slightly reduced (to 0.6 ± 0.2 nS). This led to a change of ratio in favour of inhibition, to 24.6 ± 7.3. Both the change in inhibitory conductance (P=0.01), and the increase in ratio (P=0.04), were statistically significant, however E_{Bg} was not (P>0.05). 20 μM phenytoin appeared to reduce the SD for both I_{Bg} and E_{Bg} (Fig. 7.1B), but these changes were not significant (P>0.05), although a trend is evident.

At this concentration, phenytoin had clear, significant effects on cellular excitability (Fig. 7.1C-E). Firing threshold increased from 17.1 ± 1.0 mV to 24.3 ± 1.0 mV (P<0.001), and the number of spikes generated during a depolarising current step fell from 5.3 ± 0.5 to 3.5 ± 0.3 (P<0.001). However, there was no change in action potential amplitude. Additionally, during evoked spike trains, phenytoin did not significantly change the amplitude of the final action potential in each train, or the relative amplitudes of the first and last spikes.

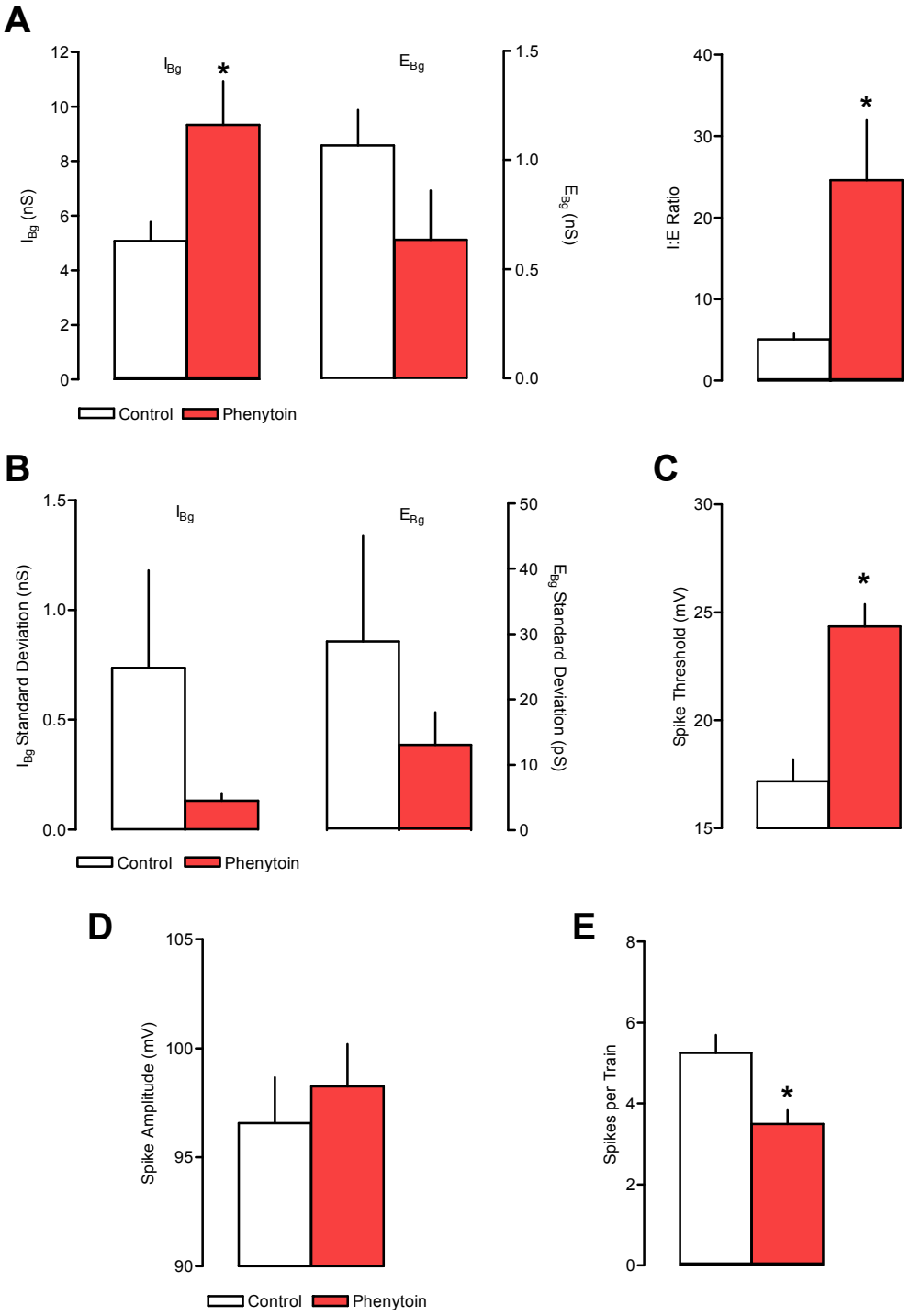

Figure 7.1: Effects of phenytoin on background activity and cellular excitability. A: Phenytoin (50 μM) causes a significant increase in I_{Bg} (5.1 ± 0.7 to 9.3 ± 1.6 nS), with no significant change in E_{Bg}. This leads to a shift in the I:E ratio in favour of inhibition. B: Despite downward trends in the SD of both I_{Bg} and E_{Bg}, no significant change was caused by lamotrigine. C: Spike threshold was significantly increased, without affecting action potential amplitude (D). Likewise, the number of spikes per 250 ms depolarisation was significantly reduced (E).

Ethosuximide

The effect of ethosuximide (250 μM) was investigated in a total of 6 neurones. The addition of ethosuximide did not dramatically alter background synaptic activity. From a control value of 5.8 ± 0.6 nS, I_{Bg} increased to 9.1 ± 3.0 nS after 15 minutes perfusion with the drug. E_{Bg} was hardly affected (1.38 ± 0.16 nS vs 1.15 ± 0.29 nS, Fig. 7.2A). Neither change was significant (P>0.05, t-test). However, overall the I:E ratio resulting from the combined changes in the conductances, from 4.3 ± 0.3 to 7.6 ± 1.3, was significant at P=0.03. Ethosuximide also had no significant effect on the SDs.

Despite the weak effect on background activity, ethosuximide did have appreciable effects on cellular excitability. Spike firing threshold was increased from 21.6 ± 0.9 mV to 26.0 ± 1.2 mV (P=0.016), and the number of spikes evoked by depolarisation was reduced from 4.8 ± 0.2 to 3.0 ± 0.5 (P=0.003), without effect on the amplitude of spikes not significantly affected (P>0.05, Fig. 7.2C-E).

Gabapentin

Gabapentin was tested in 6 neurones, at a concentration of 25 μM. In contrast to many of the other anticonvulsant drugs tested, gabapentin had little effect on I_{Bg} in these neurones. The control level of 4.5 ± 1.3 nS was initially unaltered after 15 minutes in gabapentin (4.9 ± 1.3 nS). There was a reduction in E_{Bg} (1.1 ± 0.3 to 0.5 ± 0.1 nS), but this was still not statistically significant (P=0.12). Although the individual changes were not profound, the I:E ratio nevertheless changed from 4.1 ± 0.7 to 8.6 ± 1.9 in favour of inhibition, and the change was significant (P=0.04, Fig. 7.3A). Gabapentin had no significant effect on the SDs of I_{Bg} or E_{Bg} (Fig. 7.3B).

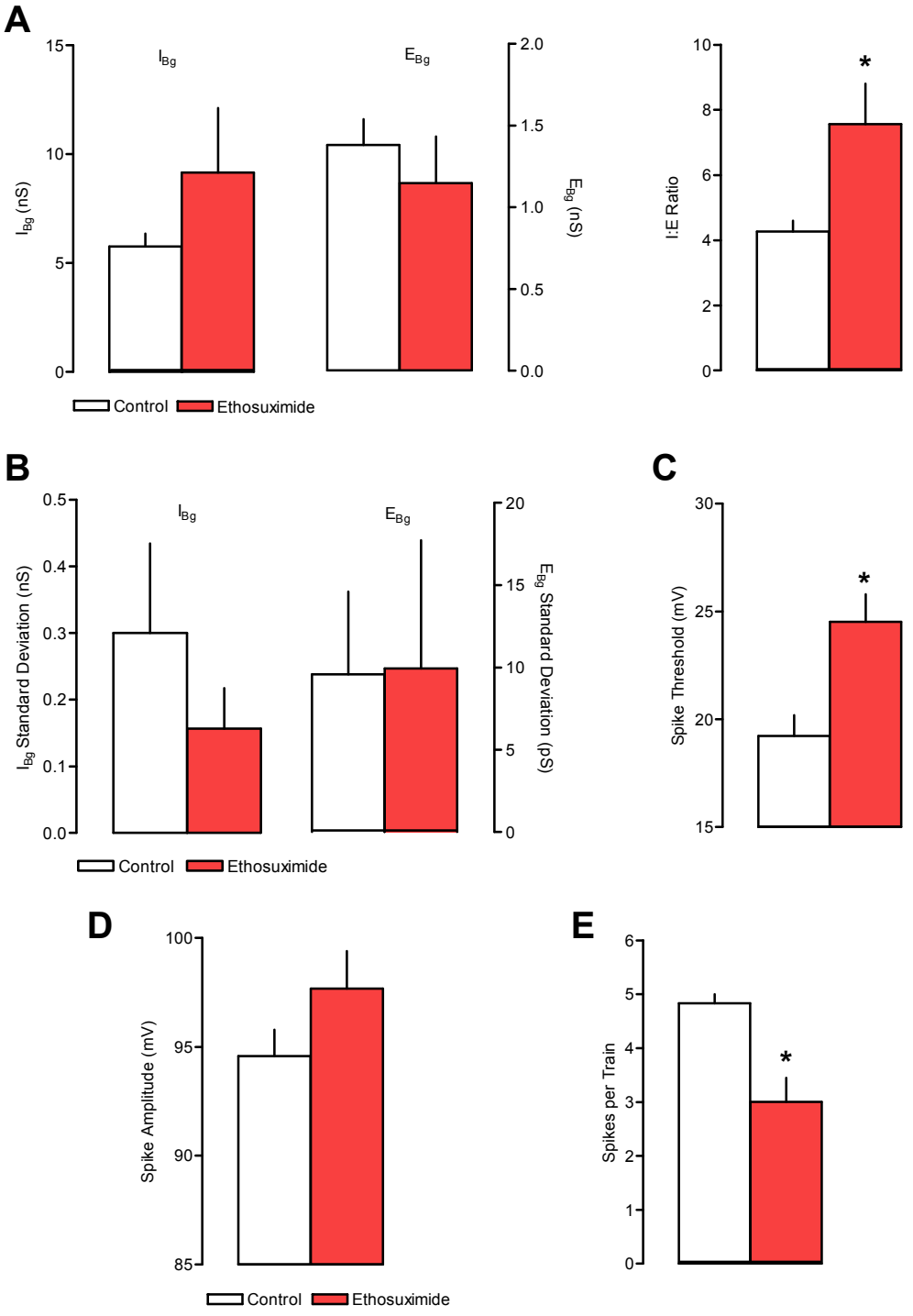

Figure 7.2: Effects of ethosuximide on background activity and cellular excitability. A: Ethosuximide (250 μM) has no significant effect on individual conductances, although I_{Bg} is slightly increased and E_{Bg} slightly decreased. These combine to cause a significant shift in I:E ratio towards inhibition. B: SDs of I_{Bg} and E_{Bg} are not affected. C-E: Cellular excitability is decreased, with spike threshold increasing and spikes/train decreasing significantly. AP amplitude is not affected.

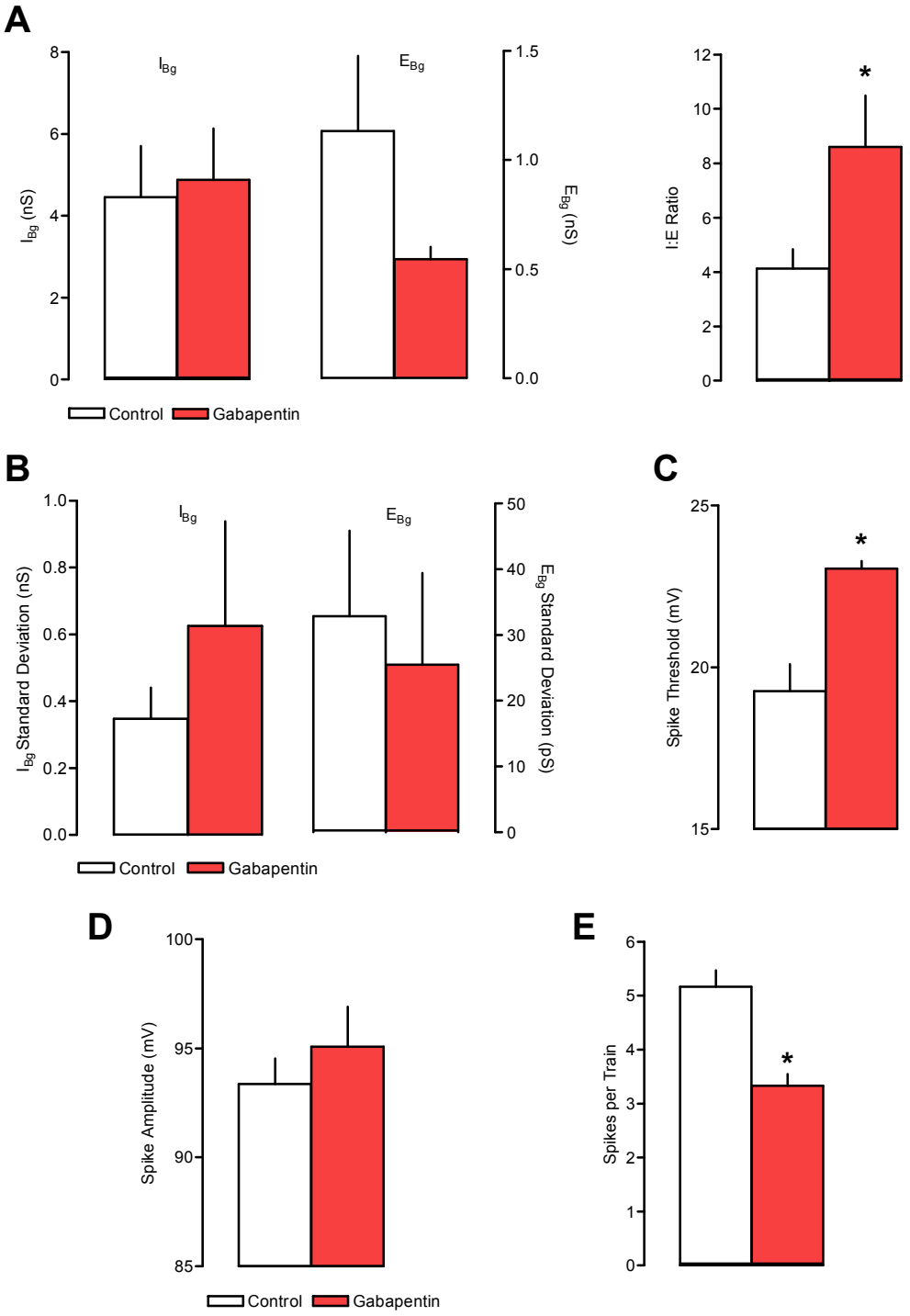

Figure 7.3: Effects of gabapentin (25 μM) on background activity and cellular excitability. A: Neither conductance component is significantly altered, however E_{Bg} shows a clear downward trend. I:E ratio shifts significantly towards inhibition (4.1 ± 0.7 to 8.6 ± 1.9). B: Conductance SDs are not affected by gabapentin. C-E: As with other anticonvulants, cellular excitability is decreased, with spike threshold increasing and spikes/train falling. AP amplitude is unchanged.

As with ethosuximide, although the changes in I_{Bg} and E_{Bg} were small, cellular excitability was significantly changed by gabapentin. Spike threshold increased from 19.3 ± 0.8 mV to 23.0 ± 0.3 mV after 15 minutes (*P*=0.002), with the number of spikes evoked by depolarisation falling from 5.2 ± 0.3 to 3.3 ± 0.2 (*P*=0.001). Overall spike amplitude was unaffected (Fig. 7.3C-E).

Felbamate

Felbamate, at a concentration of 100 μM, was tested in 6 neurones. Whilst the change was not significant, felbamate was unique amongst the drugs tested in causing a slight depression of I_{Bg}, although clearly the change was not close to significance (Fig. 7.4A). E_{Bg} also fell, from 2.3 ± 1.3 nS to 0.4 ± 0.1 nS, but again the difference was not significant (*P*=0.17). However, when the I:E ratio was considered, there was a marked change from 4.6 ± 1.0 to 15.6 ± 3.5, which proved to be significant (*P*=0.013.) Neither the SD of E_{Bg} nor I_{Bg} changed significantly in the presence of felbamate.

Again, despite the non-significant overall changes in E_{Bg} or I_{Bg}, the relative changes (i.e. the I:E ratio) proved to be a good predictor of excitability changes. Thus, spike firing threshold was raised from 20.3 ± 1.7 mV to 24.4 ± 1.0 mV (significant at *P*=0.02). Similarly, spikes generated per 250 depolarising pulse fell from 5.2 ± 0.4 to 2.5 ± 0.2 under felbamate (*P*=0.007). Once again, the overall height of evoked action potentials was largely unaffected by the addition of this anticonvulsant (Fig. 7.4C-E).

Valproate

Sodium valproate (500 μM) was perfused for 15 minutes, with a conductance estimate made every 5 minutes. Valproate induced a marked elevation in background inhibition, with I_{Bg} increasing from a control value of 10.2 ± 2.0 nS to 23.1 ± 4.4 nS

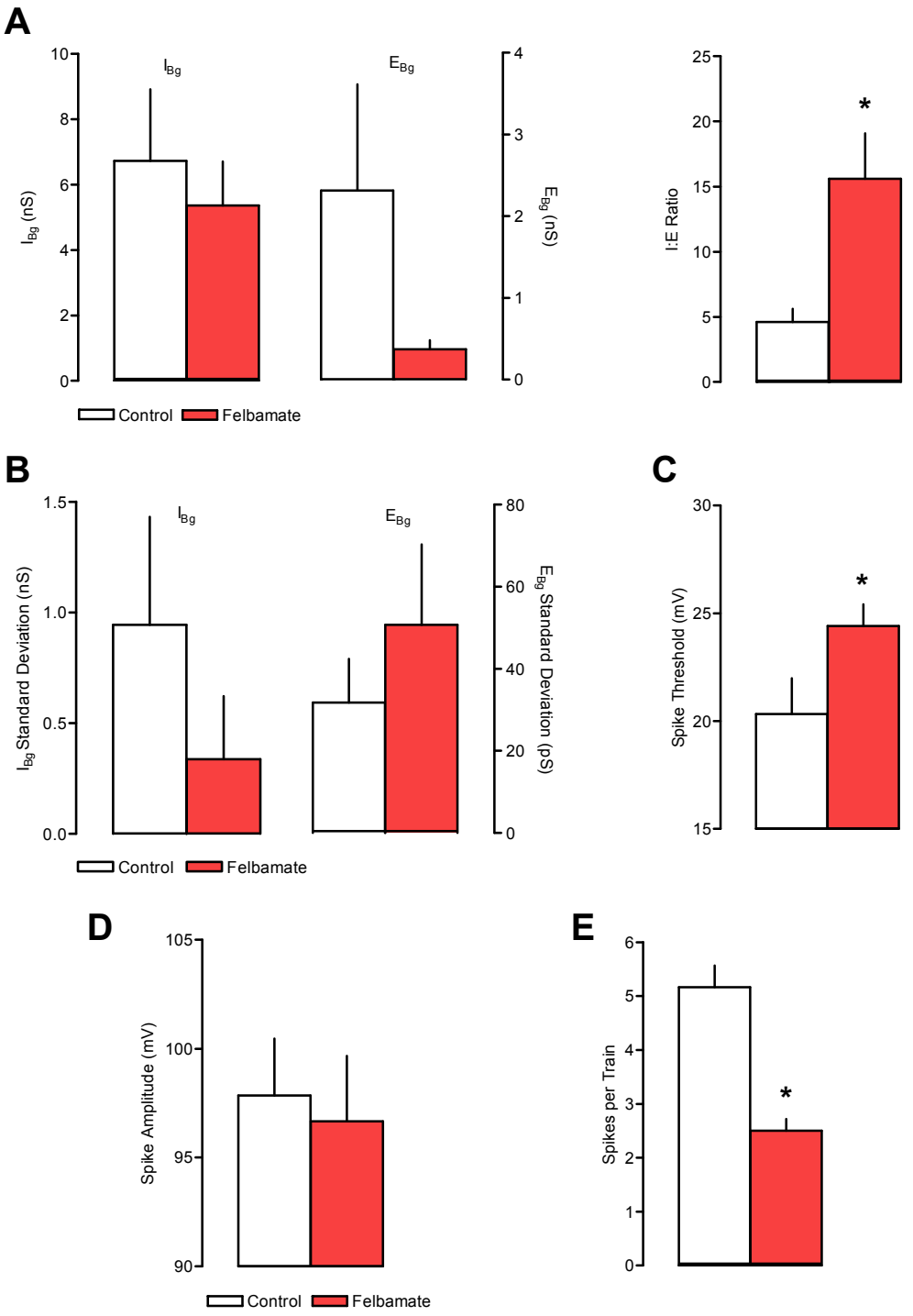

Figure 7.4: Effects of felbamate on background activity and cellular excitability. A: Felbamate (100 µM) had little effect on I_{Bg}, and did not significantly affect E_{Bg}, despite showing a noticeable reduction. Once again, small changes combined to significantly change the I:E ratio. B: SDs were not significantly altered in felbamate. C-E: Cellular excitability was reduced without changing AP amplitude, with both spike threshold and number of spikes per 250 ms depolarisation being significantly changed.

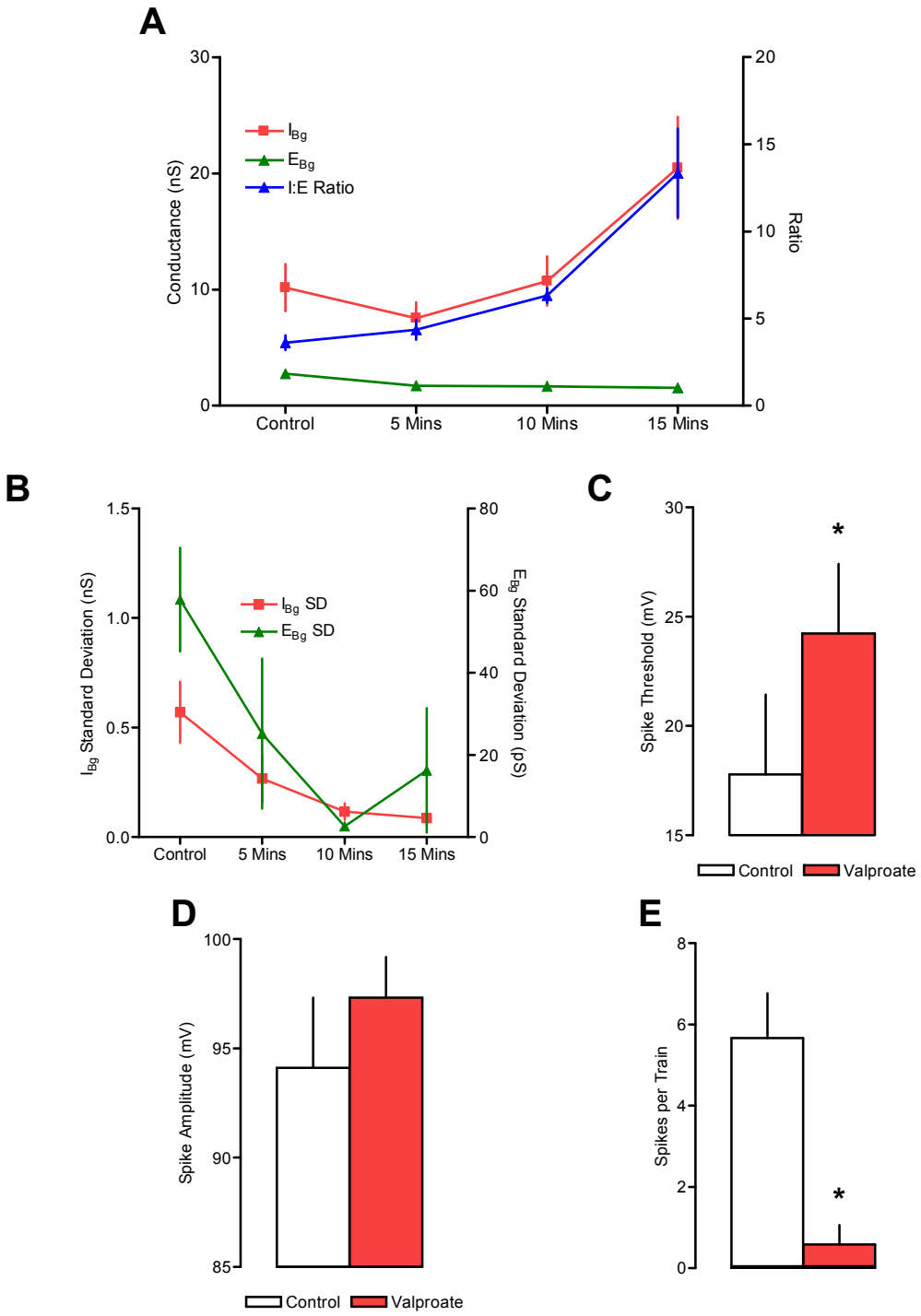

Figure 7.5: Time-course of valproate action on VmD estimates. A: Over 15 minutes, E_{Bg} is largely unaffected, being only slightly reduced by valproate (500 µM). I_{Bg} first falls, then increases significantly. This leads to a significant increase in I:E ratio. B: SD estimates show a downward trend, but are not significantly changed. C-E: Cellular excitability is significantly reduced, with action potential amplitude unaffected.

after 15 minutes. Conversely, E_{Bg} fell from an initial value of 2.8 ± 0.4 nS to 1.7 ± 0.3 nS under valproate. These changes were reflected by a change in the I:E ratio, from 3.6 ± 0.4 to 14.1 ± 3.0. The changes in I_{Bg} (P=0.028), E_{Bg} (P=0.041) and I:E ratio (P=0.01) were all significant (ANOVA).

Examination of the time-course of the valproate (Fig. 7.5A) showed an interesting effect. After 5 minutes, I_{Bg} was actually depressed, although not significantly so. Thereafter it remained close to the control value before increasing sharply after 15 minutes. In contrast, E_{Bg} decreased steadily throughout.

Valproate caused a reduction in the SD of both I_{Bg} and E_{Bg}. The SD of I_{Bg} fell from 0.6 ± 0.1 to 0.09 ± 0.03 nS after 15 minutes (significant at P=0.003), whilst that of E_{Bg} fell steadily throughout, and was significantly reduced after 10 minutes (P=0.005) before increasing slightly at 15 minutes (Fig. 7.5B).

Finally, valproate had quite marked effects on cellular excitability. The action potential threshold rose from 17.8 ± 3.6 mV to 24.2 ± 3.2 mV after 15 minutes (significant at P=0.01), whilst the number of spikes generated by the depolarising pulse fell from 5.7 ± 1.1 to 0.6 ± 0.5 (P=0.006, t-test). Valproate had no significant effect on the amplitude of evoke action potentials (Fig. 7.5D).

Lamotrigine

Lamotrigine was applied at two different concentrations to a total of 8 neurones, 6 with 20 μM, and 2 at 200 μM. Similar to results in phenytoin, 200 μM lamotrigine caused a large reduction in AP amplitude, as well as having a detrimental effect on the stability of the baseline membrane voltage. VmD estimates showed similar effects to those obtained in 20 μM. During the studies with 20 μM, VmD measurements were

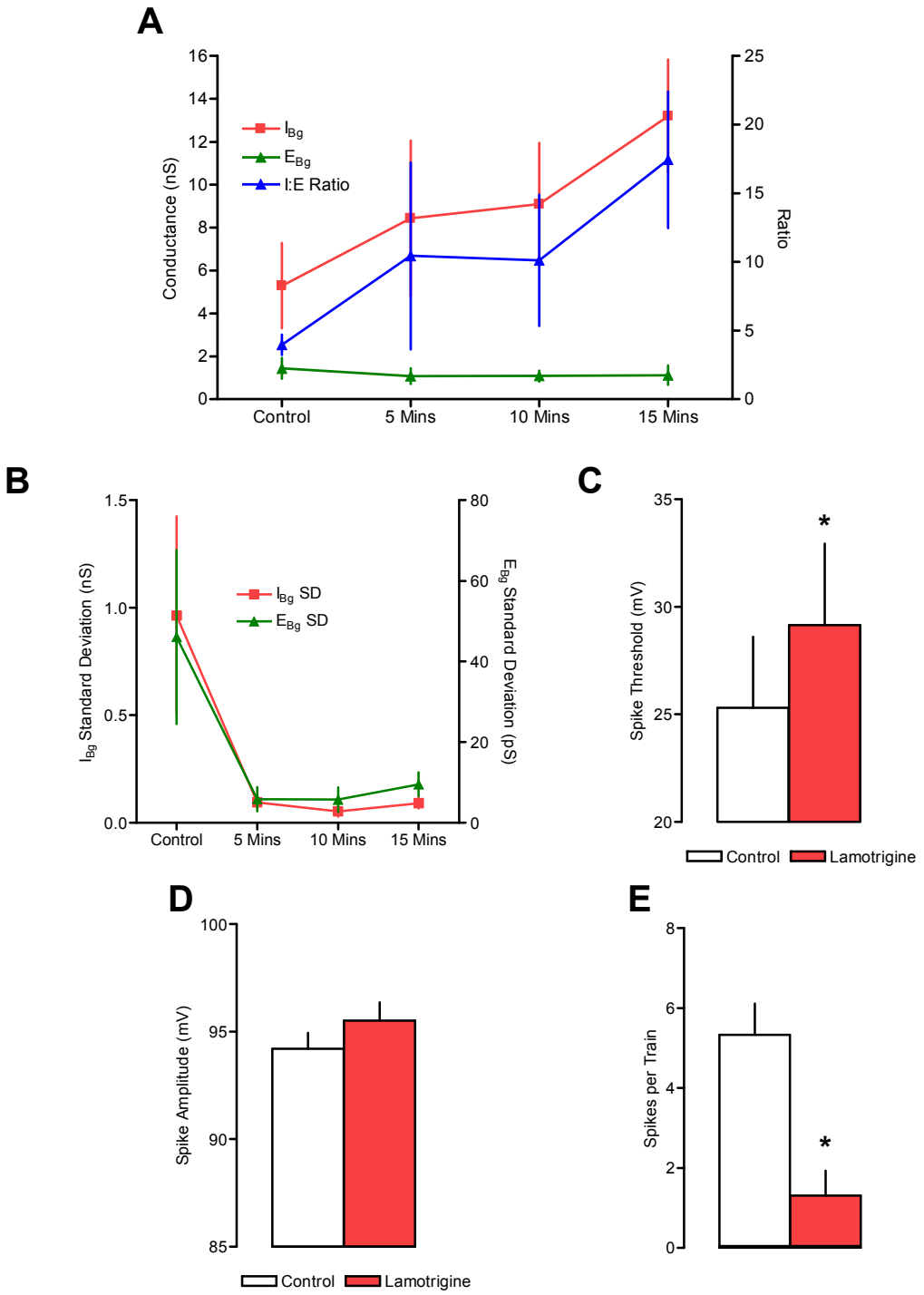

Figure 7.6: Time-course of lamotrigine action. A: E_{Bg} is not significantly altered throughout by lamotrigine (20 µM), but I_{Bg} increases throughout, shifting I:E ratio in favour of inhibition. B: Although a clear trend is evident, the SDs of I_{Bg} and E_{Bg} were not affected. C-E: As with the other anticonvulsants, cellular excitability was reduced without significant effect on action potential amplitude.

made every 5 minutes during a 15-minute perfusion period, to follow the time-course of the effect of the drug.

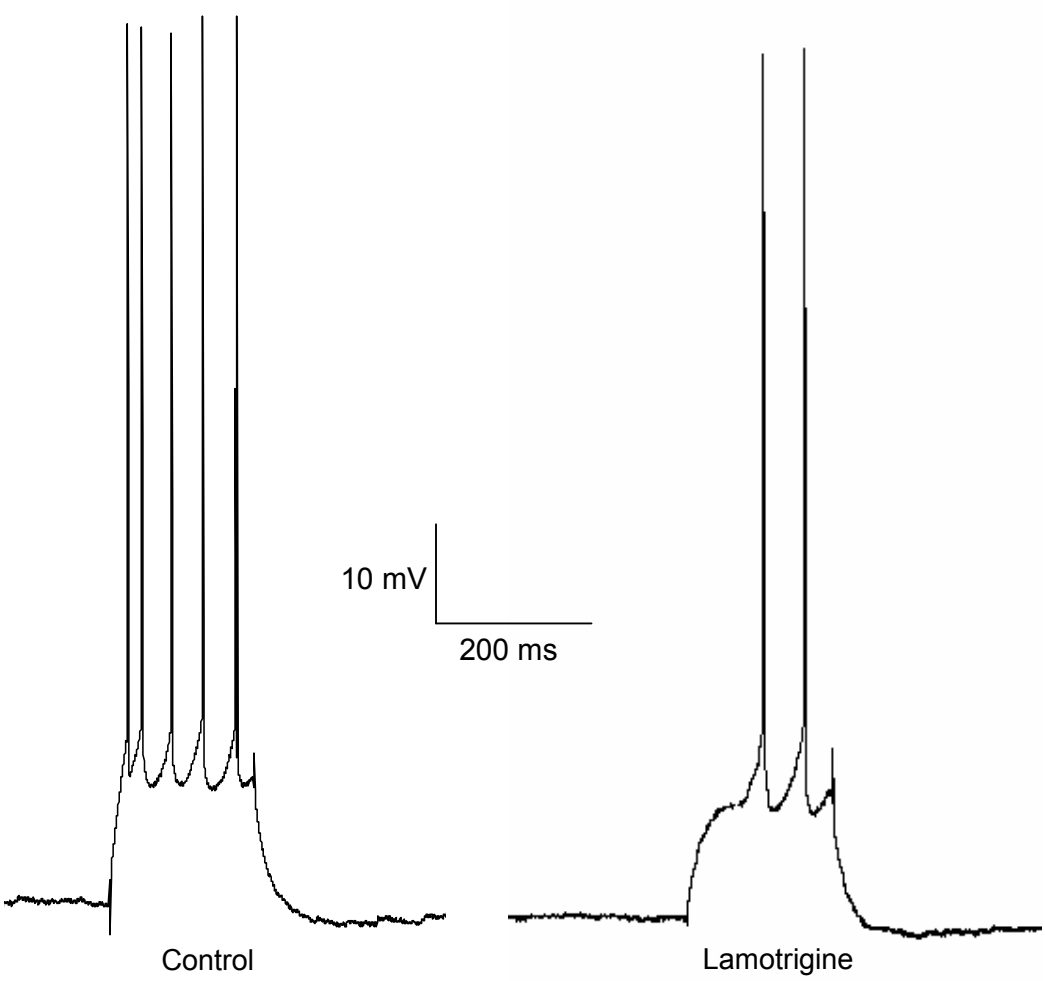

Figure 7.7: Spike train frequency, but not amplitude, is reduced by lamotrigine. Although the number of spikes in a 250 ms pulse is reduced, the amplitude of the action potentials is not affected. Likewise, no use-dependent reduction in spike amplitude is evident.

During the application of lamotrigine (20 μM), I_{Bg} increased steadily from a control value of 5.3 ± 2.0 nS to 13.2 ± 2.6 nS after 15 minutes of drug perfusion. E_{Bg} was not significantly affected (Fig 7.6A). This led to a marked change in I:E ratio. From a control value of 4.0 ± 0.7, the I:E ratio shifted to 17.5 ± 5.0 nS after 15 minutes perfusion with lamotrigine. The changes in both I_{Bg} (P=0.008) and I:E ratio (P=0.04) at 15 minutes were found to be significantly different to control (ANOVA). When SD

was measured, lamotrigine had no significant effect on the SD of either E_{Bg} or I_{Bg}, despite causing a sharp drop in both levels after only 5 minutes of perfusion (Fig. 7.6B).

Cellular excitability was markedly affected by lamotrigine. Spike threshold increased steadily throughout, from 25.3 ± 3.3 mV to 29.1 ± 3.8 mV after 15 minutes (P=0.014). Similarly, the number of spikes generated by a 250 ms depolarising step fell from 5.3 ± 0.8 to 1.3 ± 0.6 after 15 minutes (P=0.011). The amplitude of action potentials was unaffected (Fig. 7.6D), and the relative amplitudes of the first and last spikes in a train was also unchanged (Fig. 7.7)

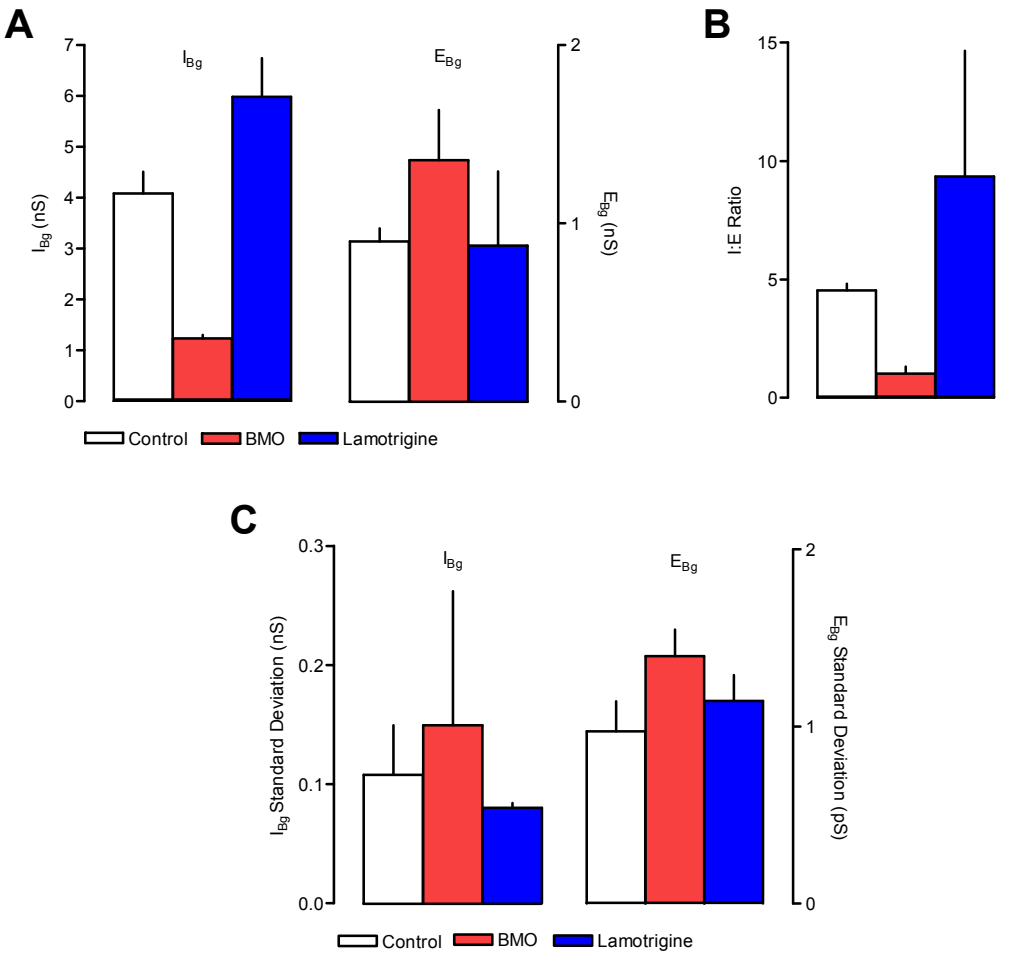

Figure 7.8: Effect of lamotrigine on BMO. A: I_{Bg} is reduced, and E_{Bg} increased, during oscillations. Lamotrigine restores control levels and shifts I:E ratio in favour of inhibition, stopping BMO activity. B: SDs are not affected.

Lamotrigine was applied to a separate group of cells exhibiting BMO activity (see Chapter 6). The addition of lamotrigine (20 μM) caused the abolition of BMO activity in all cells. Control values were: I_{Bg} = 4.1 ± 0.4 nS, E_{Bg} = 0.9 ± 0.1 nS and I:E ratio = 4.5 ± 0.3. During BMO, the level of I_{Bg} fell to 1.23 ± 0.07 nS (*P*=0.03), whilst E_{Bg} increased slightly to 1.4 ± 0.3 nS (*P*>0.05). This gave an I:E ratio of 1.0 ± 0.3 (*P*=0.001). During BMO, the SDs of I_{Bg} and E_{Bg} were not significantly changed. The addition of lamotrigine caused a sizable increase in I_{Bg} without affecting E_{Bg} compared to control levels: I_{Bg} was 6.0 ± 0.8 nS and E_{Bg} was 0.9 ± 0.4 nS (Fig. 7.8).

Discussion

The conclusion from my experiments is that anticonvulsants increase the ratio of I_{Bg} to E_{Bg}, lowering cellular excitability and reducing the probability of action potentials firing in the postsynaptic neurone. The VmD estimates of background activity (particularly I:E ratio) appear to be good indicators of cellular excitability. All of the tested anticonvulsant drugs had significantly shifted the I:E ratio in favour of inhibition after 15 minutes. Likewise, cellular excitability was significantly reduced by all 6 drugs. Even when changes in I_{Bg} and E_{Bg} individually are not significant, as with ethosuximide, the combined effect of these changes is the significant shift in I:E ratio, and subsequently a significant reduction in cellular excitability. However, it is clear from other studies, and differences in the background conductance effects seen in this Chapter, that the mechanism of action of these drugs varies considerably. It may be that, regardless of its effects at the synapse or within the cell, the overall efficacy of a drug as an anticonvulsant lies in the changes it makes to network activity as a whole.

As stated in the introduction, many studies have suggested that the anticonvulsant effects of phenytoin are mediated through use- and voltage-dependent blockade of VGSCs (McLean and MacDonald, 1983; Matsuki *et al.,* 1984; Yaari *et al.,* 1986;

Tomaselli *et al.,* 1989; Ragsdale *et al.,* 1991; Rogawski and Loscher, 2004; White *et al.,* 2007)). However, whole-cell patch clamp studies from our laboratory (Cunningham *et al.,* 2000) show that release of both glutamate and GABA is modulated by phenytoin by a mechanism that is independent of VGSC activity.

The VmD estimates in phenytoin show an increase in I_{Bg} and a decrease in E_{Bg} relative to control values, although the change in E_{Bg} is not significant. Nevertheless, I:E ratio is significantly shifted in favour of inhibition. This is in agreement with the reciprocal modulation of glutamate and GABA release by phenytoin seen by Cunningham *et al.* (2000). Additionally, at 20 μM, single AP amplitude, and spike train amplitude, are unaffected. This suggests that use- and voltage-dependent blockade of VGSCs is not a significant factor in phenytoin activity at this concentration. The basis of release modulation, and its effects on I_{Bg} and E_{Bg}, is unclear. Dendrotoxin-sensitive K^+-channels are unlikely to be involved (Cunningham and Jones, 2001), however one possibility may be direct interaction with presynaptic $GABA_B$ receptors, or their associated K^+-channels (Cunningham and Jones, unpublished observations). Certainly, as release is modulated in the presence of TTX in our previous patch clamp studies, a significant proportion of the change in background activity will be independent of network function. However, since my experiments were performed in an intact network, emergent network responses cannot be ruled out.

Ethosuximide is a good example of small, insignificant changes in I_{Bg} and E_{Bg} combining to cause a significant change in both I:E ratio and cellular excitablilty. Conductance and SD estimates were seemingly unaffected by the addition of ethosuximide. However, since I_{Bg} was slightly increased, and E_{Bg} was slightly decreased, these changes combined to lower cellular excitability.

The consensus on the mode of action of ethosuximide is as a blocker of open T-type Ca^{2+}-channels (Coulter *et al.,* 1989a, b; Gomora *et al*., 2001). Given that the VmD method is reliant upon the activity of AMPAr and $GABA_A$r for its estimates of E_{Bg} and I_{Bg} respectively, any observed effects of ethosuximide are likely to be network-mediated. The action of ethosuximide on VGCC has been suggested to be more pronounced at hyperpolarised potentials (Coulter *et al*., 1989b). In our preparation, principal cells generally display a more hyperpolarised resting potential compared to interneurones. Thus, ethosuximide may have a more marked effect at excitatory terminals than at inhibitory ones, favouring reduction in glutamate release over a reduction in GABA release. However, this does not explain the observed increase in I_{Bg} which causes most of the I:E ratio shift. One possible explanation may come from ethosuximide-mediated changes in input resistance and tonic firing rates observed by Leresche *et al.* (1998). This study showed that, at membrane potentials less negative than -60 mV, ethosuximide causes an increase in tonic firing in rat and cat thalamocortical neurones, possibly due to effects on persistent Na^+ currents and Ca^{2+}-activated K^+-channels. In Chapter 3, it was shown that I_{Bg} is more dependent upon action potential activity than E_{Bg}. It may be that the higher levels of tonic firing in interneurones are potentiated by ethosuximide, with little effect on principal cells.

Work from our laboratory, and others, has suggested that the primary action of gabapentin is the inhibition of glutamate release through direct interaction with presynaptic voltage gated calcium channels, with a possible downstream effect that reduces the frequency of miniature glutamate-mediated events in the presence of the VGSC blocker TTX (Maneuf *et al.*, 2003; Cunningham *et al.*, 2004). There is a wealth of evidence to suggest that gabapentin reduces Ca^{2+} influx through blockade both of N- and P/Q-type VGCC, but it may preferentially target P/Q-type channels (Dooley *et al*., 2002; van Hooft *et al*., 2002; Cunningham *et al*., 2004). However, some studies have failed to show any effect of gabapentin subsets of VGCCs (Schumacher *et al*., 1998; van Hooft *et al*., 2002). Gabapentin is rapidly taken into

neurones by the actions of the L-amino acid transporter, leading to an intracellular concentration 10-fold higher than that found extracellularly (Welty *et* al., 1993; Su *et al*., 1995). This suggests that much of its effects on background excitation may be mediated by inhibition of release through intracellular mechanisms.

Binding and microdialysis studies have suggested that gabapentin has little effect on GABA transmission. Gabapentin is unable to displace GABA from either $GABA_A$ or $GABA_B$ receptors (e.g. see Taylor *et al*., 1998). Timmerman *et al* (2000) found that gabapentin did not alter extracellular GABA levels in rat subsantia nigra. There is, however, evidence that gabapentin blocks presynaptic NMDAr, which would reduce the release of both glutamate and GABA (Suarez *et al*., 2005; Hara and Sata, 2007).

My results show no appreciable change in I_{Bg} with gabapentin, with a reduction in E_{Bg} that is not significant. Taken together, conductance values in gabapentin cause the I:E ratio to shift significantly in favour of inhibition, decreasing cellular excitability. Although the individual changes are not significant, the VmD results suggest that there must be some modulation of release by gabapentin. Considering the evidence provided by other studies, the shift in I:E ratio is most likely mediated by a reduction of glutamate release.

The action of felbamate is largely mediated through blockade of NMDAr (Harty and Rogawski, 2000; Kuo *et al*., 2004; Yang *et al*., 2007). Since E_{Bg} estimates are based on the actions of AMPAr, any effects seen on background excitation estimates will most likely be indirect, although some evidence exists to suggest that, at high concentrations, felbamate can reduce AMPAr-mediated excitatory events (Pugliese and Corradetti, 1996). Recent work from this laboratory has shown that felbamate reduces the frequency of sEPSCs through blockade of presynaptic NMDAr (Yang *et al*., 2007). There is evidence that felbamate may be weakly specific for NR2B-containing NMDAr (Harty and Rogawski, 2000). These have been found on

excitatory terminals (Woodhall *et al*., 2001; Yang *et al*., 2006) and on interneurones (Chen and Reiner, 1996; Szinyei *et al*., 2003), suggesting that felbamate could reduce both glutamate and GABA transmission, through inhibition of glutamate release and reduction of NMDAr activity at interneurones, a major driver of their activity (Jones and Buhl, 1993; Maccaferri and Dingledine, 2002). However, any reduction of GABA release onto principal cells could be mitigated by the benzodiazepine-like action of felbamate at $GABA_A$ receptors (Rho *et al*., 1994; Kume *et al*., 1996; Rho *et al*., 1997).

The VmD results obtained for felbamate are in agreement with data from other studies. The change in E_{Bg}, whilst not significant, was appreciably larger than that seen in I_{Bg} which, uniquely in this chapter, was slightly lower in the presence of the drug compared to control. This change in E_{Bg} led to a significant change in I:E ratio, lowering cellular excitability. The reduction in E_{Bg} is most likely due lower glutamate release caused by blockade of presynaptic NMDAr, as shown in Yang *et al* (2007).

Valproate has been suggested to act as an enhancer of GABA transmission through increased synthesis or reduced breakdown (Löscher, 1993; Wikinski *et al*., 1996). However, whole-cell patch clamp studies from this laboratory have shown that valproate, most probably through antagonism of VGSCs, reduces the release of both glutamate and GABA in the mEC (Cunningham *et al*., 2003). Additionally, valproate has been suggested as an antagonist of AMPAr and NMDAr (Wamil and McLean, 1991; Zeise *et al.,* 1991; Gean *et al.,* 1994; Kunig *et al.,* 1998).

VmD estimates in valproate show slightly reduced E_{Bg} with significantly increased I_{Bg} leading, as with all other anticonvulsants, to an inhibition-favouring I:E ratio and a reduction in cellular excitability. The reduction in E_{Bg} is likely due to the VGSC-dependent decrease in glutamate release seen in our previous whole-cell studies, with a possible contribution from AMPAr blockade and/or further reduction of glutamate release due to blockade of presynaptic NMDAr. Although sIPSCs are reduced in

frequency by valproate, their decay time is increased, with no change in amplitude (Cunningham *et al*., 2003). Thus, the overall inhibitory conductance is increased, despite the frequency reduction. Additionally, the increase in I_{Bg} may lead to further reduction of excitatory activity due to network effects.

An interesting point to note is the biphasic effect of valproate in the time-course studies. I_{Bg} initially decreases, before showing a significant increase. This pattern is supported by other studies, which suggest that GABA release is reduced by valproate at low concentrations, and enhanced at higher concentrations (Wolf *et al*., 1988; Biggs *et al*., 1992).

Lamotrigine and phenytoin have similar proposed modes of action (Cunningham and Jones, 2000), in that sEPSC frequency is decreased, whilst sIPSC frequency is increased, by a VGSC-independent mechanism. The VmD results show a very slight reduction in E_{Bg}, and a significant increase in I_{Bg}. Again, the I:E ratio shifts in favour of inhibition in lamotrigine, and cellular excitability is decreased. The lack of change in single AP amplitude, or that of spikes on the evoked trains, suggests that VGSCs are not significantly blocked by lamotrigine at this concentration. The actions of presynaptic VGSCs cannot be ruled out using the VmD method, although Cunningham and Jones (2000) suggested the observed effects of lamotrigine are largely VGSC independent.

CHAPTER 8

GENERAL DISCUSSION

This thesis has validated the VmD method as a means for estimating background activity in relation to cellular excitability in the mEC. By using a range of pharmacological tools and supporting my pharmacological data with whole-cell patch clamp recordings and physiological studies such as layer comparisons, insight into the nature of background release and how changes in I_{Bg}, E_{Bg} and I:E ratio affect the excitability of principal neurones has been gained.

Initially, it was important to properly characterise and validate the VmD method in our experimental setup. To that end, the first two data chapters focus on the use of well-established pharmacological tools to determine how changes in receptor activity, the availability of glutamate and GABA at the synapse and VGC blockade affect levels of background activity, population synchrony and cellular excitability. The VmD calculation incorporates the actions of only AMPA and $GABA_A$ receptors, but the rich reciprocal connections present within the EC, and the presence of autoreceptors that modulate release at the presynapse (e.g. NMDA, KAr) means that, within our slices, the addition of a drug is not a straightforward change of activity at the postsynaptic membrane.

Encouragingly, the results obtained with receptor antagonists such as NBQX, GYKI-53665 and bicuculline were as predicted, with most change seen in the conductance component that was directly affected (e.g. E_{Bg} for NBQX and GYKI) and consequent effects on the other component due to, for example, a reduction in excitatory drive on to interneurones. The use of drugs that have little or no direct effect on receptors at the postsynapse, but alter network activity in some way (e.g. 4-AP, PDC, tiagabine) produces more complex effects. However, the VmD data obtained concurred wel with previous work from our laboratory and others, especially when taken in conjunction with whole-cell patch clamp data, as with PDC and tiagabine. Ideally, future studies would utilise patch clamp experiments alongside all VmD experiments. A useful avenue for investigation would be simultaneous whole-cell and intracellular recording

from two different principal neurones in the same layer of the same slice, so that VmD data (and cellular excitability measurements) could be gathered side-by-side with a direct measure of EPSC or IPSC activity. This would allow the time-course of I_{Bg} and E_{Bg} changes to be directly correlated with shifts in the amplitude and frequency of post-synaptic events.

Some very interesting data came from the comparison of the VmD and patch clamp data obtained with tiagabine. Although I_{Bg} increased,the frequency of sIPSCs was reduced. However, there was a significant increase in sIPSC amplitude and duration seen in the patch clamp experiments, suggesting that the VmD estimations depend on the total charge transfer, not just the frequency, of the $GABA_A$ (and most likely AMPA) receptors. Thus, the VmD method is a true measure of integrated conductance in these cells.

Another point of note is the notion of specific GluR5 receptor antagonists as possible anticonvulsants. If I_{Bg} and E_{Bg} SD can be taken as an indication of the synchrony of the inhibitory and excitatory populations, reductions in SD could indicate a decreased propensity for seizure generation. Addition of UBP-302 does not significantly affect I_{Bg}, E_{Bg} or I:E ratio, and does not change cellular excitability. However, there is a significant reduction in the SD of I_{Bg}, and the SD of E_{Bg} exhibits a clear downward trend. Thus, it may be that UBP-302, or similar drugs, are ideal anticonvulsants, reducing synchrony without compromising other network functions.

The VmD method was further validated by the use of ion channel blockers such as Cs^+, QX-314 and 4-AP. The Destexhe group suggest that estimations of I_{Bg} and E_{Bg} are not significantly distorted by the presence of active currents in the dendrites and soma. The lack of change in conductance estimates seen after internal dialysis with Cs/QX-314 supports this assertion. The increase in conductance levels seen with 4-AP is probably not a result of blockade of A-type K-channels in the soma, but is more

likely due to prolonged depolarisation of the presynaptic terminals, resulting in increased transmitter release, due to block of K-channels in the terminals. To further test the robustness of the VmD method, other channel blockers could be investigated (e.g. I_H antagonist ZD-7288).

Our laboratory has long been focussed on lamina-specific differences in the EC, using both intracellular and whole-cell recordings to quantify significant differences in the frequency and characteristics of inhibitory, excitatory and epileptiform events. The bicuculline time-course data obtained in Chapter 5 provides two sets of data, that of the normal resting values in our cells, and the lamina-specific differences in sensitivity to bicuculline. The baseline values of conductance and SD differ noticeably between layers, especially when layers II and III are compared to layer V. Given that previous work from this lab has indicated a predominance of inhibition in layer II, and greater levels of excitation in layer V, the indication that the I:E ratio in layers II and III is approximately 1.5 times greater (i.e. more in favour of inhibition) than layer V. Additionally, in layer II the onset of epileptiform activity is delayed compared to the deeper layers, and such events are smaller and shorter than those in layer III and layer V.

The data obtained with bicuculline support previous assertions from our laboratory that layer II is “seizure resistant”, whilst layer V is “seizure sensitive”. An interesting further study would be to make simultaneous intracellular recordings from layers II, III and V in the presence and absence of bicuculline, so that the onset of epileptiform activity could be monitored in terms of synchrony and background activity across the layers. Furthermore, the generation and propagation of seizure activity could be tracked in real time around the slice. A further alternative would be to use the VmD method in one or two simultaneous intracellular recordings, combined with a multi-electrode array for field potential measurement across the whole slice. This would

trace the propagation of epileptiform activity more accurately, whilst still providing a measure of background activity in key layers (e.g. II and V).

The two different conductance profiles seen for up-states and BMO suggest that they are two discrete phenomena. The up-states seem to be periods of vastly increased conductance, with similar I:E ratios to baseline conditions. Conversely, BMO are not associated with overall increases in conductance, but show a shift in the I:E ratio in favour of excitation. It may be that these events are related, BMO may be precursor events to up-states, or "failed" up-states that have not developed properly. The use of lamotrigine to abolish BMO suggests that they can be affected in a similar manner to epileptiform activity. Further useful investigation could come from patch clamp studies of BMO activity. It may be that simultaneous patch clamp and intracellular recordings will offer more information about the network basis of these events. Multi-layer intracellular recordings would provide some information about the laminar basis of BMO generation and propagation.

The actions of the anticonvulsants examined in this thesis are thought to vary considerably, from reciprocal modulation of glutamate and GABA release to blockade of sodium or calcium VG channels. However, their overall effects on transmission and excitability are all somewhat similar. I_{Bg} is generally increased, and E_{Bg} is generally decreased. Even if these changes are not significant, they combine to cause a significant change in the I:E ratio in favour of inhibition. Furthermore, cellular excitability is reduced, to a degree which reflects the change seen in I:E ratio. Thus, it may be that the overall network effects of anticonvulsant drugs are far more important than their effects at the synapse.

In conclusion, I have validated the VmD method, a novel way to obtain estimates of background activity from intracellular recordings, in quiescent slices from rat brain. The method has proved to be a useful and powerful way of extracting information

from relatively simple electrophysiological recordings to provide insight into the functions of cortical networks, and the impact changes in low-level neurotransmitter release have on cellular excitability.

References

Alarcon G, Seoane JJG, Binnie CD, Miguel MCM, Juler J, Polkey CE, Elwes RDC, & Blasco JMO. (1997). Origin and propagation of interictal discharges in the acute electrocorticogram - Implications for pathophysiology and surgical treatment of temporal lobe epilepsy. *Brain* **12**, 2259-2282

Alle H & Geiger JRP (2007). GABAergic spill-over transmission onto hippocampal mossy fiber boutons. *J Neurosci* **27**, 942-950

Alonso A & Klink R (1993). Differential electroresponsiveness of stellate and pyramidal-like cells of the medial entorhinal cortex layer II. *J Neurophysiol* **70**, 128-143

Alt A, Weiss B, Ogden AM, Knauss JL, Oler J, Ho K, Large TH & Bleakman D (2004). Pharmacological characterization of glutamatergic agonists and antagonists at recombinant human homomeric and heteromeric kainate receptors in vitro. *Neuropharmacology* **46**, 793-806

Amaral DG, Insausti R & Cowan WM (1987). The entorhinal cortex of the monkey: cytoarchitectonic organisation. *J Comp Neurol* **264**, 326-355

Assaf BA & Ebersole JS. (1997). Continuous source imaging of scalp ictal rhythms in temporal lobe epilepsy. *Epilepsia* **38**, 1114-1123

Assaf BA, Karkar KM, Laxer KD, Garcia PA, Austin EJ, Barbaro NM & Aminoff MJ. (2003). Ictal magnetoencephalography in temporal and extratemporal lobe epilepsy. *Epilepsia* **44**, 1320-1327

Avoli M, Barbarosie M, Lucke A, Nagao T, Lopantsev V & Kohling R (1996). Synchronous GABA-mediated potentials and epileptiform discharges in the rat limbic system in vitro. *J Neurosci* **16**, 3912-3924

Badea T, Goldberg J, Mao B & Yuste R (2001). Calcium imaging of epileptiform events with single-cell resolution. *J Neurobiol* **48**, 215-227

Bailey SJ, Dhillon A, Woodhall GL & Jones RSG (2004). Lamina-specific differences in $GABA_B$ autoreceptor-mediated regulation of spontaneous GABA release in rat entorhinal cortex. *Neuropharmacology* **46**, 31-42

Baranyi A, Szente MB & Woody CD (1993). Electrophysiological characterization of different types of neurons recorded *in vivo* in the motor cortex of the cat. II. Membrane parameters, action potentials, current-induced voltage responses and electrotonic structures. *J Neurophysiol* **69**, 1865–1879

Barkai E, Friedman A, Grossman Y & Gutnick MJ (1995). Laminar pattern of synaptic inhibition during convulsive activity induced by 4-aminopyridine in neocortical slices. *J Neurophysiol* **73**, 1462-1467

Bartolomei F, Wendling F, Regis J, Gavaret M, Guye M & Chauvel P. (2004). Pre-ictal synchronicity in limbic networks of mesial temporal lobe epilepsy. *Epilepsy Res* **61**, 89-104

Bartolomei F, Khalil M, Wendling F, Sontheimer A, Regis J, Ranjeva JP, Guye M & Chauvel P. (2005). Entorhinal cortex involvement in human mesial temporal lobe epilepsy: an electrophysiologic and volumetric study. *Epilepsia* **46**, 677-687

Bear J, Fountain NB & Lothman EW (1996). Responses of the superficial entorhinal cortex in vitro in slices from naive and chronically epileptic rats. *J Neurophysiol* **76**, 2928-2940

Ben-Ari Y, Tremblay E, Riche D, Ghilini G & Naquet R. (1981). Electrographic, clinical and pathological alterations following systemic administration of kainic acid, bicuculline or pentetrazole: metabolic mapping using the deoxyglucose method with special reference to the pathology of epilepsy. *Neuroscience* **6**, 1361-1391

Bernasconi N, Andermann F, Arnold DL & Bernasconi A. (2003). Entorhinal cortex MRI assessment in temporal, extratemporal, and idiopathic generalized epilepsy. *Epilepsia* **44**, 1070-1074.

Bernasconi N, Bernasconi A, Andermann F, Dubeau F, Feindel W & Reutens DC (1999). Entorhinal cortex in temporal lobe epilepsy: a quantitative MRI study. *Neurology* **52**, 1870-1876.

Bernasconi N, Bernasconi A, Caramanos Z, Dubeau F, Richardson J, Andermann F & Arnold DL. (2001). Entorhinal cortex atrophy in epilepsy patients exhibiting normal hippocampal volumes. *Neurology* **56,** 1335-1339

Berretta N & Jones RSG (1996a). A comparison of spontaneous synaptic EPSCs in layer V and layer II neurones in the rat entorhinal cortex *in vitro*. *J Neurophysiol* **76**, 1089-1100

Berretta N & Jones RSG (1996b). Tonic facilitation of glutamate release by presynaptic NMDA autoreceptors in layer II of the entorhinal cortex. *Neuroscience* **79**, 339-344

Biggs CS, Pearce BR, Fowler LJ & Whitton PS (1992). The effect of sodium valproate on extracellular GABA and other amino acids in the rat ventral hippocampus: an *in vivo* microdialysis study. *Brain Res* **594**, 138-142

Bonilha L, Kobayashi E, Rorden C, Cendes F & Li LM. (2003). Medial temporal lobe atrophy in patients with refractory temporal lobe epilepsy. *J Neurol Neurosurg Psychiatry* **74**, 1627-1630

Borg-Graham LJ, Monier C & Fregnac Y (1998). Visual input evokes transient and strong shunting inhibition in visual cortical neurones. *Nature* **393**, 369-373

Bradford HF (1995). Glutamate, GABA and epilepsy. *Prog Neurobiol* **47**, 477-511

Bragin A, Wilson CL, Staba RJ, Reddick M, Fried I & Engel J Jr. (2002). Interictal high-frequency oscillations (80-500 Hz) in the human epileptic brain: entorhinal cortex. *Ann Neurol* **52**, 407-415.

Bragin A, Wilson CL, Almajano J, Mody I & Engel J Jr. (2004). High-frequency oscillations after status epilepticus: epileptogenesis and seizure genesis. *Epilepsia* **45**, 1017-1023

Brickley SG, Cull-Candy SG & Farrant M (1996). Development of a tonic form of synaptic inhibition in rat cerebellar granule cells resulting from persistent activation of $GABA_A$ receptors. *J Physiol* **497**, 753-759

Brodie MJ, Shorvon SD, Canger R, Halasz P, Johannessen S, Thompson P, Wieser HG & Wolf P (1997). Commission on European affairs: Appropriate standards of epilepsy care across Europe. *Epilepsia* **38,** 1245-1250

Buchheim K, Weissinger F, Siegmund H, Holtkamp M, Schuchmann S & Meierkord H (2002). Intrinsic optical imaging reveals regionally different manifestation of spreading depression in hippocampal and entorhinal structures in vitro. *Exp Neurol* **175**, 76-86

Buckmaster PS, Alonso A, Canfield DR & Amaral DG (2004). Dendritic morphology, local circuitry, and intrinsic electrophysiology of principal neurones in the entorhinal cortex of macaque monkeys. *J Comp Neurol* **470**, 317-329

Bureau I & Mulle C (1998). Potentiation of GABAergic synaptic transmission by AMPA receptors in mouse cerebellar stellate cells: changes during development. *J Physiol* **509**, 817-831

Buzsaki G (1986). Hippocampal sharp waves: their origin and significance. *Brain Res* **398**, 242-252

Buzsaki G, Leung LW & Vanderwolf CH (1983). Cellular basis of hippocampal EEG in the behaving rat. *Brain Res* **287**, 139-171

Ramon y Cajal S (1911). Histologie du systeme nerveux de l'homme et de vertebres. Paris: A. Maloine

Calabresi P, Centonze D, Marfia GA, Pisani A & Bernardi G (1999). An *in vitro* electrophysiological study on the effects of phenytoin, lamotrigine and gabapentin on striatal neurones. *Brit J Pharmacol* **126**, 689-696

Carter AG & Regehr WG (2002). Quantal events shape cerebellar interneurone firing. *Nat Neurosci* **5**, 1309-1318

Chance FS, Abbot LF & Reyes AD (2002). Gain modulation from background synaptic input. *Neuron* **35**, 773-782

Charpak S, Gahwiler B, Do KQ & Knopfel T (1990). Potassium conductances in hippocampal neurons blocked by excitatory amino-acid transmitters. *Nature* **347**, 765-768

Chen Q & Reiner A (1996). Cellular distribution of the NMDA receptor NR2A/2B subunits in the rat striatum. *Brain Res* **743**, 346-352

Cheung H, Kamp D & Harris E (1992). An *in vitro* investigation of the action of lamotrigine on neuronal voltage-activated sodium channels. *Epilepsy Res* **13**, 107-112

Chrobak JJ & Buzsaki G (1994). Selective activation of deep layer (V-VI) retrohippocampal cortical neurons during hippocampal sharp waves in the behaving rat. *J Neurosci* **14**, 6160-6170

Chrobak JJ & Buzsaki G (1996). High-frequency oscillations in the output networks of the hippocampal-entorhinal axis of the freely behaving rat. *J Neurosci* **16**, 3056-3066

Church J, Zeman S & Lodge D (1988). The neuroprotective action of ketamine and MK-801 after transient cerebral ischemia in rats. *Anesthesiology* **69**, 702-709

Clarke VR, Ballyk BA, Hoo KH, Mandelzys A, Pellizzari A, Bath CP, Thomas J, Sharpe EF, Davies CH, Ornstein PL, Schoepp DD, Kamboj RK, Collingridge GL, Lodge D & Bleakman D (1997). A hippocampal GluR5 kainate receptor regulating inhibitory synaptic inhibition. *Nature* **359**, 599-603

Cobb SR, Buhl EH, Halasy K, Paulsen O & Somogyi P (1995). Synchronisation of neuronal activity in hippocampus by individual GABAergic interneurones. *Nature* **378**, 75-78

Collingridge GL, Kehl SJ & McLennan H (1983). Excitatory amino acids in synaptic transmission in the Schaffer collateral-commissural pathway of the rat hippocampus. *J Physiol* **334**, 33-46

Collins RC, Tearse RG & Lothman EW (1983). Functional anatomy of limbic seizures: focal discharges from medial entorhinal cortex in rat. *Brain Res* **280**, 25-40

Connors BW & Long MA (2004). Electrical synapses in the mammalian brain. *Ann Rev Neurosci* **27**, 393-418

Cossart R, Aronov D & Yuste R (2003). Attractor dynamics of network up-states in the neocortex. *Nature* **423**, 283-288

Coulter DA, Huguenard JR & Prince DA (1989a). Specific petit mal anticonvulsants reduce calcium currents in thalamic neurones. *Neurosci Lett* **98**, 74-78

Coulter DA, Huguenard JR & Prince DA (1989b). Characterization of ethosuximide reduction of low-threshold calcium current in thalamic neurones. *Ann Neurol* **25**, 582-93

Cowan RL & Wilson CJ (1994). Spontaneous firing patterns and axonal projections of single corticostriatal neurons in the rat medial agranular cortex. *J Neurophysiol* **71**, 17–32.

Cunningham MO, Dhillon A, Wood SJ & Jones RSG (2000). Reciprocal modulation of glutamate and GABA release may underlie the anticonvulsant effect of phenytoin. *Neuroscience* **95.2**, 343-351

Cunningham MO & Jones RSG (2000). The anticonvulsant, lamotrigine, decreases spontaneous glutamate release but increases spontaneous GABA release in the rat entorhinal cortex *in vitro*. *Neuropharmacology* **39**, 2139-2146

Cunningham MO & Jones RSG (2001). Dendrotoxin sensitive potassium channels modulate GABA but not glutamate release in the rat entorhinal cortex in vitro *Neuroscience* **107**, 395-404

Cunningham MO, Pervouchine DD, Racca C, Kopell NJ, Davies CH, Jones RSG, Traub RD & Whittington MA (2006). Neuronal metabolism governs cortical network response state. *Proc Nat Acad Sci USA* **103**, 5597-5601

Cunningham MO, Woodhall GL, Thompson SE, Dooley DJ & Jones RSG (2004). Dual effects of gabapentin and pregabalin on glutamate release at rat entorhinal synapses *in vitro*. *Eur J Neurosci* **20**, 1566-1576

Cunningham MO, Woodhall GL & Jones RSG (2003). Valproate modifies spontaneous excitation and inhibition at cortical synapses *in vitro*. *Neuropharmacology* **45**, 907-917

D'Arcangelo G, Tancredi V and Avoli M (2001). Intrinsic optical signals and electrographic seizures in the rat limbic system. *Neurobiol Dis* **8**, 993-1005

Davies JA & Shakesby A (1999). Blockade of GABA uptake potentiates GABA-induced depolarizations in adult mouse cortical slices. *Neurosci Lett* **266**, 201-204

DeFelipe J (1999). Chandelier cells and epilepsy. *Brain* **122**, 1807-1822

Del Castillo J & Katz B (1954). Quantal components of the end-plate potential. *J Physiol* **124**, 560-573

Destexhe A & Pare D (1999). Impact of network activity on the integrative properties of neocortical pyramidal neurones in vivo. *J Neurophysiol* **81**, 1531-1547

Destexhe A, Rudolph M, Fellous J-M & Sejnowski TJ (2001). Fluctuating synaptic conductances recreate in vivo-like activity in neocortical neurons. *Neuroscience* **107** 13-24

Destexhe A, Rudolph M & Pare D (2003). The high-conductance state of neocortical neurons *in vivo*. *Nat Rev Neurosci* **4**, 739-751

Dhillon A & Jones RSG (2000). Laminar differences in recurrent excitatory transmission in the rat entorhinal cortex *in vitro*. *Neuroscience* **99**, 413-422

Dickson CT, Mena AR & Alonso A (1997). Electroresponsiveness of medial entorhinal cortex layer III neurones *in vitro*. *Neuroscience* **91**, 937-950

Dichter MA & Brodie MJ (1996). New antiepileptic drugs. *NEJM* **334**, 1583-1590

Dooley DJ, Donovan CM, Meder WP & Whetzel SZ (2002). Preferential action of gabapentin and pregabalin at P/Q-type voltage-sensitive calcium channels: inhibition of K+-evoked [3H]-norepinephrine release from rat neocortical slices. *Synapse* **45**, 171-190

Dorval AD & White JA (2005). Channel noise is essential for perithreshold oscillations in entorhinal stellate neurones. *J Neurosci* **25.43**, 10025-10028

Du F & Schwarz R (1992). Amino-oxyacetic acid causes selective neuronal loss in layer III of the rat medial entorhinal cortex. *Neurosci Lett* **147**, 185-188.

Du F, Whetsell WO, Abu-Khalil B, Blumenkopf B, Lothman EW & Schwarz R (1993). Preferential neuronal loss in layer III of the entorhinal cortex in patients with temporal lobe epilepsy. *Epilepsy Res* **16**, 223-233.

Du F, Eid T, Lothman EW, Kohler C & Schwarz R (1995). Preferential neuronal loss in layer III of the medial entorhinal cortex in rat models of temporal lobe epilepsy. *J Neurosci* **5**, 6301-6313.

Duguid IC & Smart TG (2004). Retrograde activation of presynaptic NMDA receptors enhances GABA release at cerebellar interneuron-Purkinje cell synapses. *Nat Neurosci* **7**, 525-533

Dupont S, Crozie AC, Semah F, Hasboun D, Samson Y, Clemenceau S & Baulac M (2001). Is amygdalohippocampectomy really selective in medial temporal lobe epilepsy? A study using Positron Emission Tomography with ^{18}Flurodeoxyglucose. *Epilepsia* **42**, 731-740

Eichenbaum H, Otto T, Cohen NJ (1994). Two functional components of the hippocampal memory system. *Brain Behav Res* **17**, 449.517

Fountain NB, Bear J, Bertram EH 3rd & Lothman EW (1998). Responses of deep entorhinal cortex are epileptiform in an electrogenic rat model of chronic temporal lobe epilepsy. *J Neurophysiol* **80**, 230-240

Fellous JM, Rudolph M, Destexhe A & Sejnowski TJ (2003). Synaptic background noise controls the input/output characteristics of single cells in an *in vitro* model of *in vivo* activity. *Neuroscience* **122**, 811-829

Finch DM, Wong EE, Derian EL & Babb TL (1986). Neurophysiology of limbic system pathways in the rat: projections from the subicular complex and hippocampus to the entorhinal cortex. *Brain Res* **397**, 205-213

Finch DM, Tan AM & Isokawa-Akesson M (1988). Feedforward inhibition of the rat entorhinal cortex and subicular complex. *J Neurosci* **8**, 2213-2226

Fountain NB, Bear J, Bertram EH & Lothman EW (1998). Responses of deep entorhinal cortex are epileptiform in an electrogenic rat model of chronic temporal lobe epilepsy. *J Neurophysiol* **80**, 230-240

Fried I (1993). Anatomic temporal lobe resections for temporal lobe epilepsy. *Neurosurg Clin N Am* **4**, 233-242

Fujikawa DG (1995). Neuroprotective effect of ketamine administered after status epilepticus onset. *Epilepsia* **36**, 186-195

Funahashi M & Stewart M (1998). GABA receptor-mediated post-synaptic potentials in the retrohippocampal cortices: regional, laminar and cellular comparisons. *Brain Res* **787**, 19-33

Gallyas F, Ball SM & Molnar E (2003). Assembly and cell surface expression of KA-2 subunit-containing kainate receptors. *J Neurochem* **86**, 1414-1427

Galvan M, Grafe P & ten Bruggencate G (1982). Convulsant actions of 4-aminopyridine on the guinea pig olfactory cortex slice. *Brain Res* **241**, 75-86

Gean PW, Huang CC, Hung CR & Tsai JJ (1994). Valproic acid suppresses the synaptic response mediated by NMDA receptors in rat amygdalar slices. *Brain Res Bull* **33**, 333-336

Gee NS, Brown JP, Dissanayake VUK, Offord J, Thurlow R & Woodruff GN (1996) The novel anticonvulsant drug, Gabapentin (Neurontin), binds to the $\alpha_2\delta$ subunit of a calcium channel. *J Biol Chem* **271**, 5768–5776

Gentet LJ, Stuart GJ & Clements JD (2000). Direct measurement of specific membrane capacitance in neurons. *Biophys J* **79**, 314-320

Germroth P, Schwerdtfeger WK & Buhl EH (1989). Morphology of identified entorhinal neurones projecting to the hippocampus: a light microscopical study combining retrograde tracing and intracellular injection. *Neuroscience* **30**, 683-691

Glitsch M & Marty A (1999). Presynaptic effects of NMDA in cerebellar Purkinje cells and interneurons. *J Neurosci* **19**, 511-519

Gloveli T, Dugladze T, Schmitz D, & Heinemann U (2001). Properties of entorhinal cortex deep layer neurones projecting to the rat dentate gyrus. *Eur J Neurosci* **13**, 413-420

Gloveli T, Schmitz D, Empson RM & Heinemann U (1997). Frequency-dependent information flow from the entorhinal cortex to the hippocampus. *J Neurophysiol* **78.6**, 3444-3449

Goa KL, Ross SR & Chrisp P (1993). Lamotrigine – a review of its pharmacological properties and clinical efficacy in epilepsy. *Drugs* **46**, 152-76

Goldring S, Edwards I, Harding GW & Bernardo KL. (1992) Results of anterior temporal lobectomy that spares the amygdala in patients with complex partial seizures. *J Neurosurg* **77**, 185-193.

Goldring S, Edwards I, Harding GW & Bernardo KL. (1993) Temporal lobectomy that spares the amygdala for temporal lobe epilepsy. *Neurosurg Clin N Am* **4**, 263-272

Gomora JC, Daud AN, Weiergraber M & Perez-Reyes E (2001). Block of cloned human T-type calcium channels by succinimide antiepileptic drugs. *Mol Pharmacol* **60**, 1121-1132

Gustafsson B, Galvan M, Grafe P & Wigstrom H (1982). A transient outward current in a mammalian central neurone blocked by 4-aminopyridine. *Nature* **299**, 252-254

Haider B, Duque A, Hasentstaub AR & McCormick DA (2006). Neocortical network activity *in vivo* is generated through a dynamic balance of excitation and inhibition. *J Neurosci* **26**, 4535-4545

Hara K & Sata T (2007). Inhibitory effect of gabapentin on N-methyl-d-aspartate receptors expressed in Xenopus oocytes. *Acta Anaesthesiologica Scandinavica* **51**, 122-128

Harsch A & Robinson HP (2000). Postsynaptic variability of firing in rat cortical neurones: the roles of input synchronisation and synaptic NMDA receptor conductance. *J Neurosci* **20**, 6181-6192

Harty TP & Rogawski MA (2000). Felbamate block of recombinant *N*-methyl-D-aspartate receptors: selectivity for the NR2B subunit. *Epilepsy Res* **39**, 47-55

Hausser M & Clark BA (1997). Tonic synaptic inhibition modulates neuronal output pattern and spatiotemporal synaptic integration. *Neuron* **19**, 665-678

Heinemann U, Schmitz D, Eder C & Gloveli T (2000). Properties of entorhinal cortex projection cells to the hippocampal formation. *Ann NY Acad Sci* **911**, 112-126

Hendry SH, Jones EG, Emson PC, Lawson DE, Heizmann CW & Streit P (1989). Two classes of cortical GABA neurones defined by differential calcium binding protein immunoreactivities. *Exp Brain Res* **76**, 467-472

Hines ML & Carnevale NT (1997). The NEURON simulation environment. *Neural Comput* **9**, 1179-1209

Ho N & Destexhe A (2000). Synaptic background activity enhances the responsiveness of neocortical pyramidal neurons. *J Neurophysiol* **84**, 1488-1496

Hoffman SN & Prince DA (1995). Epileptogenesis in immature neocortical slices induced by 4-aminopyridine. *Brain Res Dev Brain Res* **85**, 64-70

Hopfield JJ (1982). Neural networks and physical systems with emergent collective computational abilities. *Proc Nat Acad Sci USA* **79**, 2554-2558

Hu RQ & Davies JA (1997). Tiagabine hydrochloride, an inhibitor of γ-aminobutyric acid (GABA) uptake, induces cortical depolarizations in vitro. *Brain Res* **753**, 260-268

Iijima T, Witter MP, Ichikawa M, Tominaga T, Kajiwara R & Matsumoto G (1996). Entorhinal-hippocampal interactions revealed by real-time imaging. *Science* **272**, 1176-1179

Ino T, Kaneko T & Mizuno N (2000). Intrinsic and commissural connections within the entorhinal cortex. An anterograde and retrograde tract-tracing study in the cat. *Neurosci Res* **36**, 45-60

Insausti R, Herrero MT & Witter MP (1997). Entorhinal cortex of the rat: cytoarchitectonic subdivisions and the origin and distribution of cortical efferents. *Hippocampus* **7**, 146-183

Jang I-S, Jeong H-J & Akaike N (2001). Contribution of Na-K-Cl cotransporter on $GABA_A$ receptor-mediated presynaptic depolarization in excitatory nerve terminals. *J Neurosci* **21**, 5962-5972

Jang I-S, Nakamura M, Ito Y & Akaike A (2006). Presynaptic $GABA_A$ receptors facilitate spontaneous glutamate release from presynaptic terminals on mechanically dissociated rat CA3 pyramidal neurons. *Neuroscience* **138**, 25-35

Jayalakshmi K, Sairam M, Sing SB, Sharma SK, Ilavazhagan G & Banerjee PK (2005). Neuroprotective effect of N-acetyl-cysteine of hypoxia-induced oxidative stress in primary hippocampal culture. *Brain Res* **1046**, 97-104

Jensen AA, Mosbacher J, Elg S, Lingenhoel K, Lohmann T & Johansen TN (2002). The anticonvulsant gabapentin (neurontin) does not act through gamma-aminobutyric acid-B receptors. *Mol Pharmacol* **61**, 1377–1384

Jones RSG (1987). Complex synaptic responses of entorhinal cortical cells to subicular stimulation *in vitro*: demonstration of an NMDA-receptor mediated component. *Neurosci Lett* **81**, 209-214

Jones RSG (1988). Epileptiform events induced in entorhinal cortical cells by GABA-antagonists in vitro are partly mediated by N-methyl-D-aspartate receptors. *Brain Res* **457**, 113-121

Jones RSG (1993). Entorhinal-hippocampal connections: a speculative view of their function. *Trends Neurosci* **16**, 58-64

Jones RSG (1994). Synaptic and intrinsic properties of neurones of origin of the perforant path in layer II of the rat entorhinal cortex *in vitro*. *Hippocampus* **4**, 335-353

Jones RSG (1995). Frequency dependent alterations in synaptic transmission in entorhinal-hippocampal pathways. *Hippocampus* **5**, 125-128

Jones RSG & Buhl EH (1993). Basket-like interneurones in layer II of the entorhinal cortex exhibit a powerful NMDA-mediated synaptic excitation. *Neurosci Lett* **149**, 35-39

Jones RSG & Heinemann U (1987). Pre- and postsynaptic K^+ and Ca^{2+} fluxes in area CA1 of the rat hippocampus *in vitro*: effects of Ni^{2+}, TEA and 4-AP. *Exp Brain Res* **68**, 205-209

Jones RSG & Heinemann U (1988). Synaptic and intrinsic responses of medial entorhinal cortical cells in normal and magnesium free medium in vitro. *J Neurophysiol* **59**, 1476-1496

Jones RSG & Heinemann U (1989). Spontaneous activity mediated by NMDA receptors in immature rat entorhinal cortex in vitro. *Neurosci Lett* **104**, 93-98

Jones RSG & Lambert JD (1990a). Synchronous discharges in the rat entorhinal cortex *in vitro*: site of initiation and the role of excitatory amino acid receptors. *Neurosci* **34**, 657-670

Jones RSG & Lambert JD (1990b).The role of excitatory amino acid receptors in the propagation of epileptiform discharges from the entorhinal cortex to the dentate gyrus *in vitro*. *Exp Brain Res* **80**, 310-322

Jones RSG & Woodhall GL (2005). Background synaptic activity in rat entorhinal cortical neurones: differential control of transmitter release by presynaptic receptors. *J Physiol* **562.1,** 107-120

Jutila L, Ylinen A, Partanen K, Alafuzoff I, Mervaala E, Partanen J, Vapalahti M, Vainio P & Pitkanen A. (2001). MR volumetry of the entorhinal, perirhinal, and temporopolar cortices in drug-refractory temporal lobe epilepsy. *Am J Neuroradiol* **22**, 1490-1501

Klink R & Alonso A (1997). Morphological characteristics of layer II projection neurons in the rat medial entorhinal cortex. *Hippocampus* **7**, 571-583

Kobayashi M, Wen X & Buckmaster PS (2003). Reduced inhibition and increased output of layer II neurons in the medial entorhinal cortex in a model of temporal lobe epilepsy. *J Neurosci* **23**, 2440-2452

Koga H, Ishibashi H, Shimada H, Jang I-S, Nakamura TY & Nabekura J (2005). Activation of presynaptic $GABA_A$ receptors increases spontaneous glutamate release onto noradrenergic neurons of the rat locus coeruleus. *Brain Res* **1046**, 24-31

Kohling R, Lucke A, Straub H, Speckmann EJ, Tuxhorn I, Wolf P, Pannek H & Oppel F (1998). Spontaneous sharp waves in human neocortical slices excised from epileptic patients. *Brain* **121**, 1073-1087

Kohling R, Qu M, Zilles K & Speckmann EJ (1999). Current-source-density profiles associated with sharp waves in human epileptic neocortical tissue. *Neuroscience* **94**, 1039-1050

Kostyuk PG, Molokanova EA, Pronchuk NF, Savchenko AN & Verkhratsky AN (1992). Different action of ethosuximide on low- and high-threshold calcium currents in rat sensory neurones. *Neuroscience* **51**, 755-758

Kovari E, Gold G, Herrmann FR, Canuto A, Hof PR, Bouras C & Giannakopoulos P (2003). Lewy body densities in the entorhinal and anterior cingulated cortex predict cognitive defects in Parkinson's disease. *Acta Neuropathol (Berl)* **106**, 83-88

Kumar SS, Jin X, Buckmaster PS & Huhguenard JR (2007). Recurrent circuits in layer II of medial entorhinal cortex in a model of temporal lobe epilepsy. *J Neurosci* **27**, 1239-1246

Kume A, Greenfield LJ, MacDonald RL & Albin RL (1996). Felbamate inhibits [3H]t-butylbicycloorthobenzoate (TBOB) binding and enhances Cl− current at the gamma-aminobutyric acid$_A$ (GABA$_A$) receptor. *J Pharm Exp Ther 277*, 1784-1792.

Kunig G, Niedermeyer B, Deckert J, Gsell W, Ransmayr G & Riederer P (1998). Inhibition of AMPA binding by the anticonvulsant valproate in clinically relevant concentrations: an autoradiographic investigation in human hippocampus. *Epilepsy Res* **31**, 153-157

Kuo CC, Lin BJ, Chang HR & Hsieh CP (2004). Use-dependent inhibition of the NMDA currents by felbamate: a gating modifier with selective binding to the desensitised channels. *Mol Pharmacol* **65**, 370-380

Kwan P & Brodie MJ (2000). Early identification of refractory epilepsy. *NEJM* **342**, 314-319

Leach MJ, Marsden CM & Miller AA (1986). Pharmacological studies of lamotrigine, a novel antiepileptic drug: 2 – neurochemical studies on the mechanism of action. *Epilepsia* **27**, 490-497

Leresche N, Parri HR, Erdemli G, Guyon A, Turner JP, Williams SR, Asprodini E & Crunelli V (1998). On the action of the anti-absence drug ethosuximide in the rat and cat thalamus. *J Neurosci* **18**, 4842-4853

Lopantsev V & Avoli M (1996). Reverberation of chloride-dependent synaptic potentials in the rat entorhinal cortex in vitro. *Neurosci Lett* **210**, 5-8

Lorente de No R (1933). Studies on the structure of the cerebral cortex I: The area entorhinalis. *J Psychol Neurol* **45**, 381-483

Löscher W (1981). Valproate induced changes in GABA metabolism at the subcellular level. *Biochem Pharmacol* **30**, 1364-1366

Löscher W (1993). *In vivo* administration of valproate reduces the nerve terminal (synaptosomal) activity of GABA aminotransferase in discrete brain areas of rats. *Neurosci Lett* **160**, 177-180

Löscher W (1999). Valproate: A reappraisal of its pharmacodynamic properties and mechanisms of action. *Prog Neurobiol* **58**, 31-59

Löscher W & Frey HH (1977). Effect of convulsant and anticonvulsant agents on level and metabolism of gamma-aminobutyric acid in mouse brain. *NS Arch Pharmacol* **296**, 263-269

Louvel J, Pumain R, Roux FX & Chodkievicz JP (1992). Recent advances in understanding epileptogenesis in animal models and in humans. *Adv Neurol* **57**, 517-523

Lu T & Trussell LO (2000). Inhibitory transmission mediated by asynchronous transmitter release. *Neuron* **26**, 683-694

Maccaferri G & Dingledine R (2002). Control of feedforward dendritic inhibition by NMDA receptor-dependent spike timing in hippocampal interneurons. *J Neurosci* **22**, 5462-5472

Maneuf YP, Gonzalez MI, Sutton KS, Chung FZ, Pinnock RD & Lee K (2003). Cellular and molecular action of the putative GABA-mimetic, gabapentin. *Cell Mol Life Sci* **60**, 742-750

Mattson RH, Cramer JA, Collins JF, Smith DB, Delgado-Escueta AV, Browne TR, Williamson PD, Treiman DM, McNamara DO & McCutchen CB (1985). Comparison of carbamazepine, phenobarbital, phenytoin and primidone in partial and secondarily generalised tonic-clonic seizures. *NEJM* **313**, 145-151

Matsuki N, Quandt FN, ten Eick RE & Yeh JZ (1984). Characterisation of the block of sodium channels by phenytoin in mouse neuroblastoma cells. *J Pharmac. Exp. Ther.* **228**, 523-530

Matsumura M, Cope T & Fetz EE (1988). Sustained excitatory synaptic input to motor cortex neurons in awake animals revealed by intracellular recording of membrane potentials. *Exp. Brain Res* **70**, 463–469

McCormick, DA & Contreras D (2001). On the cellular and network basis of epileptic seizures. *Ann Rev Physiol* **63**, 815-846

McCormick DA, Shu Y, Hasenstaub A, Sanchez-Vives M, Badoual M & Bal T. (2003). Persistent cortical activity: mechanisms of generation and effects on neuronal excitability. *Cereb Cortex* **13**, 1219-1231

MacDonald RL & Kelly KM (1994). Mechanisms of action of currently prescribed and newly developed antiepileptic drugs. *Epilepsia* **35** S41-50

McLean MJ & MacDonald RL (1983). Multiple actions of phenytoin on mouse spinal cord neurones in cell culture. *J Pharmac. Exp. Ther.* **227**, 779-789

McLean MJ & MacDonald RL (1986). Sodium valproate, but not ethosuximide, produces use- and voltage-dependent limitation of high frequency repetitive firing of action potentials of mouse central neurones in cell culture. *J Pharm Exp Ther* **237**, 1001-1011

McNamara, JO (1992). The neurobiological basis of epilepsy. *Trends Neurosci* **15**, 357- 359

Miller AA, Wheatley P, Sawyer DA, Baxter MG & Roth B (1986). Pharmacological studies on lamotrigine, a novel potential antiepileptic drug: I. Anticonvulsant profile in mice and rats. *Epilepsia* **27**, 483-489

Monyer H, Burnashev N, Laurie DJ, Sakmann B & Seeburg PH (1994). Developmental and regional expression in the rat brain and functional properties of four NMDA receptors. *Neuron* **12**, 529-540

Nagao T, Alonso A & Avioli M (1996). Epileptiform activity induced by pilocarpine in the rat hippocampal-entorhinal slice preparation. *Neurosci* **72**, 399-408

Pare D, Lang EJ & Destexhe A (1998a). Inhibitory control of somatodendritic interactions underlying action potentials in neocortical pyramidal neurons in vivo; an intracellular and computational study. *Neuroscience* **84**, 377-402

Pare D, Shink E, Gaudreau H, Destexhe A & Lang EJ (1998b). Impact of spontaneous synaptic activity on the resting properties of cat neocortical pyramidal neurons in vivo. *J Neurophysiol* **79**, 1480-1460

Pellock JM & Brodie MJ (1997). Felbamate: 1997 update. *Epilepsia* **38**, 1261-1267

Pennanen C, Kivipelto M, Tuomainen S, Hartikainen P, Hanninen T, Laakso MP, Hallikainen M, Vanhanen M, Nissinen A, Helkala EL, Vainio P, Vanninen R, Partanen K & Soininen H (2004). Hippocampus and entorhinal cortex in mild cognitive impairment and early AD. *Neurobiol Aging* **25**, 303-310

Petersen CCH, Hahn TTG, Mehta M, Grinvald A & Sakmann B (2003). Interaction of sensory responses with spontaneous depolarization in layer 2/3 barrel cortex. *Proc Natl Acad Sci USA* **100**, 13638 –13643

Prasad KM, Patel AR, Muddasani S, Sweeney J & Keshavan MS (2004). The entorhinal cortex in first-episode psychotic disorders: a structural magnetic resonance imaging study. *Am J Psychiatry* **161**, 1612-1619

Pugliese AM & Corradetti R (1996). Effects of the antiepileptic drug felbamate on long-term potentiation in the CA1 region of rat hippocampal slices. *Neurosci Lett* **215**, 21-24

Ragsdale DS, Scheuer T & Caterall WA (1991). Frequency and voltage-dependent inhibition of type IIA Na^+ channels, expressed in a mammalian cell line, by local anaesthetic, antiarrhythmic and anticonvulsant drugs. *Molec Pharmac* **40**, 726-765

Rho JM, Donevan SD & Rogawski MA (1994). Mechanism of action of the anticonvulsant felbamate: opposing effects on N-methyl-D-aspartate and gamma-aminobutyric acid A receptors. *Ann Neurol* **35**, 229–234.

Rho JM, Donevan, SD & Rogawski MA (1997). Barbiturate-like actions of the propandiol dicarbamates felbamate and meprobamate. *J Pharmacol Exp Ther* **280**, 1383–1391

Rock DM, Kelly KM & MacDonald RL (1993). Gabapentin actions on ligand- and voltage-gated responses in cultured rodent neurones. *Epilepsy Res* **16**, 89–98

Rogawski MA & Loscher W (2004). The neurobiology of antiepileptic drugs. *Nat Rev Neurosci* **5**, 553-564

Rudolph M & Destexhe A (2003). Characterization of subthreshold voltage fluctuations in neuronal membranes. *Neural Comp* **15**, 2577-2618

Rudolph M & Destexhe A (2004). Inferring network activity from synaptic noise. *J Physiol Paris* **98**, 452-466

Rudolph M, Piwkowska Z, Badoual M, Bal T & Destexhe A (2004). A method to estimate synaptic conductances from membrane potential fluctuations. *J Neurophysiol* **91**, 2884-2896

Rudolph M, Pelletier JG, Pare D & Destexhe A (2005). Characterisation of synaptic conductances and integrative properties during electrically induced EEG-activated states in neocortical neurons *in vivo J Neurophysiol* **94**, 2805-2821

Rudolph M, Pospischil M, Timofeev I & Destexhe A (2007). Inhibition determines membrane potential dynamics and controls action potential generation in awake and sleeping cat cortex. *J Neurosci* **27**, 5280-5290

Rusakov DA, Saitow R, Lehre KP & Konishi S (2005). Modulation of presynaptic Ca^{2+} entry by AMPA receptors at individual GABAergic synapses in the cerebellum. *J Neurosci* **25**, 4930-4940

Rutecki PA, Grossman RG, Armstrong D & Irish-Loewen S. (1989). Reduced inhibition and increased output of layer ii neurons in the medial entorhinal cortex in a model of temporal lobe epilepsy. *J Neurosurg* **70**, 667-675.

Salin PA & Prince DA (1996). Spontaneous $GABA_A$ receptor-mediated inhibitory currents in adult rat somatosensory cortex. *J Neurophysiol* **75**, 1573-1588

Salvati P, Maj R, Caccia MA, Cervini MG, Fornaretto E, Lamberti P, Pervello GA, Skeen HS, Wolf L, Faravelli M, Mazzanti M, Varasi M & Fariello RG (1999). Biochemical and electrophysiological studies on the mechanism of action of PNU-15 1774E, a novel antiepileptic compound. *J Pharm Exp Ther* **288**, 1151-1159

Sander JWAS (1993). Some aspects of prognosis in the epilepsies: a review. *Epilepsia* **34**, 1007-1016

Sanchez-Vives MV & McCormick DA (2000). Cellular and network mechanisms of rhythmic recurrent activity in neocortex. *Nat Neurosci* **3**, 1027-1034

Sara Y, Virmani T, Deak F, Liu X & Kavalali ET (2005). An isolated pool of vesicles recycles at rest and drives spontaneous neurotransmission. *Neuron* **45**, 563-573

Scharfman HE, Goodman JH, Du F & Schwarcz R (1998) Chronic changes in synaptic responses of entorhinal and hippocampal neurons after amino-oxyacetic acid (AOAA)-induced entorhinal cortical neuron loss. *J Neurophysiol* **80**, 3031-3046

Schwarcz R, Eid T & Du F (2000). Neurons in layer III of the entorhinal cortex: a role in epileptogenesis and epilepsy? *Ann NY Acad Sci* **911**, 328-342

Seal RP & Amara SG (1999). Excitatory amino acid transporters: a family in flux. *Ann Rev Pharmacol Toxicol* **39**, 431-56

Sekhon B, Sekhon C, Khan M, Patel SJ, Singh I & Singh AK (2003). N-acetyl-cysteine protects against injury in a rat model of focal cerebral ischemia. *Brain Res* **971**, 1-8

Shu Y, Hasenstaub A, Badoual M, Bal T & McCormick DA (2003a). Barrages of synaptic activity control the gain and sensitivity of cortical neurons. *J Neurosci* **23**, 10388-10401

Shu Y, Hasenstaub A, & McCormick DA (2003b). Inhibitory interactions between ferret thalamic reticular neurons. *J Neurophysiol* **87**, 2571-2576

Siegel AM, Weiser HG, Wichmann W & Yasargil GM (1990). Relationships between MR-imaged total amount of tissue removed, resection scores of specific mediobasal limbic subcompartments and clinical outcome following selective amygdalohippocampectomy. *Epilepsy Res* **63**, 56-65

Silva-Barrat C, Brailowsky S, Levesque G, Menini C (1988). Epileptic discharges induced by intermittent light stimulation in photosensitive baboons: a current source density study. *Epilepsy Res* **2**, 1-8

Simeone TA, Otto JF, Wilcox KS & White HS (2006). Felbamate is a subunit selective modulator of recombinant $GABA_A$ receptors expressed in *Xenopus* oocytes. *Eur J Pharmacol* **552**, 31-35

Spencer SS & Spencer DD. (1994). Entorhinal-hippocampal interactions in medial temporal lobe epilepsy syndrome. *Epilepsia* **35**, 721-727

Sperling MR, O'Connor MF, Saykin AJ & Plummer C (1996). Temporal lobectomy for refractory epilepsy. *Epilepsia* **35**, 721-727

Stacey WC & Durand DM (2000). Stochastic resonance improves signal detection in hippocampal CA1 neurons. *J Neurophysiol* **83**, 1394-1402

Stacey WC & Durand DM (2001). Synaptic noise improves detection of subthreshold signals in hippocampal CA1 neurons. *J Neurophysiol* **86**, 1104-1112

Stefani A, Spadoni F & Benardi G (1997) Differential inhibition by riluzole, lamotrigine and phenytoin of sodium and calcium currents in cortical neurones: implications for neuroprotective strategies. *Exp Neurol* **147**, 115-122

Stevens CF & Zador AM (1998). Input synchrony and the irregular firing of cortical neurons. *Nat Neurosci* **1**, 210-217

Steriade M, Nunez A & Amzica F (1993). A novel slow (<1 Hz) oscillation of neocortical neurons *in vivo*: depolarizing and hyperpolarizing components. *J Neurosci* **73,** 3252–3285.

Steriade M, Timofeev I & Grenier F (2001) Natural waking and sleep states: a view from inside neocortical neurons. *J Neurophysiol* **85**, 1969–1985

Stringer JL. (1994). Pentylenetetrazol elicits epileptiform activity in the dentate gyrus of the urethane anesthetized rat by activation of the entorhinal cortex. *Brain Res* **636**, 221-226.

Su T, Lunney E, Campbell G & Oxender DL (1995). Transport of gabapentin, a γ-amino acid drug, by system L *a*-amino acid transporters: a comparative study in astrocytes, synaptosomes and CHO cells. *J Neurochem* **64**, 2125–2131

Suarez LM, Suarez F, Del Olmo N, Ruiz M, Gonzalez-Escalada JR & Solis JM (2005). Presynaptic NMDA autoreceptors facilitate axon excitability: a new molecular target for the anticonvulsant gabapentin. *Eur J Neurosci* **21**, 197-209

Suzdak PD & Jansen JA (1995). A review of the preclinical pharmacology of tiagabine: a potent and selective anticonvulsant GABA uptake inhibitor. *Epilepsia* **36**, 612-626

Suzuki SS & Smith GK (1987). Spontaneous EEG spikes in the normal hippocampus. I. Behavioral correlates, laminar profiles and bilateral synchrony. *EEG Clin Neurophysiol* **67**, 348-359

Szinyei C, Stork O & Pape HC (2003). Contribution of NR2B subunits to synaptic transmission in amygdaloid interneurons. *J Neurosci* **23**, 2549-2556

Tahvildari B & Alonso A (2005). Morphological and electrophysiological properties of lateral entorhinal cortex layer II and III principal neurons. *J Comp Neurol* **491**, 123-40

Tamamaki N & Nojyo Y (1993). Projection of the entorhinal layer II neurons in the rat as revealed by intracellular pressure-injection of neurobiotin. *Hippocampus* **3**, 471-480

Tan YP and Llano I (1999). Modulation by K^+ channels of action potential-evoked intracellular Ca^{2+} concentration rises in rat cerebellar basket cell axons. *J Physiol* **520**, 65-78

Taverna S, Mantegazza M, Francheschetti S & Avanzini G (1998). Valproate selectively reduces the persistent fraction of Na^+ current in neocortical neurones. *Epilepsy Res* **32**, 304-308

Taylor CP, Gee NS, Su TZ, Kocsis JD, Welty DF, Brown JP, Dooley DJ, Boden P & Singh L (1998). A summary of mechanistic hypotheses of gabapentin pharmacology. *Epilepsy Res* **29**, 233-239

Timmerman W, Bouma M, De Vries JB, Davis M & Westerink BH (2000). A microdialysis study on the mechanism of action of gabapentin. *Eur J Pharmacol* **398**, 53-57

Tomaselli GF, Marban E & Yellen G (1989). Sodium channels from human brain RNA expressed in *Xenopus* oocytes: basic electrophysiological characteristics and their modification by diphenylhydantoin. *J Clin Invest* **83**, 1724-1732

Tzingounis AV & Nicoll RA (2004). Presynaptic NMDA receptors get into the act. *Nat Neurosci* **7**, 419-420

Uhlenbeck GE & Ornstein LS (1930). On the theory of Brownian motion. *Phys Rev* **36**, 823-841

Van Haeften T, Baks-te-Bulte L, Goode PH, Wouterlood FG & Witter MP (2003). Morphological and numerical analysis of synaptic interactions between neurones in deep and superficial layers of the entorhinal cortex of the rat. *Hippocampus* **13**, 943-952

Van Hooft JA, Dougherty JJ, Endeman D, Nichols RA & Wadman WJ (2002). Gabapentin inhibits presynaptic Ca^{2+} influx and synaptic transmission in rat hippocampus and neocortex. *Eur J Pharmacol* **449**, 221-228

Vignes M & Collingridge GL (1997). The synaptic activation of kainate receptors. *Nature* **388**, 179-182

Waldmeier PC, Baumann PA, Wicki P, Feldtrauer JJ, Stierlin C & Schmutz M (1995). Similar potency of carbamazepine, oxcarbamazepine and lamotrigine in inhibiting the release of glutamate and other neurotransmitters. *Neurology* **45**, 1907-1913

Waldmeier PC, Martin P, Stocklin K, Portec C & Schmutz M (1996). Effect of carbamazepine, oxcarbamazepine and lamotrigine on the increase in extracellular glutamate elicited by veratridine in rat cortex and striatum. *N S Arch Pharm* **354**, 164-172

Wall MJ & Usowicz MM (1997). Development of action potential-dependent and independent spontaneous $GABA_A$ receptor-mediated currents in granule cells of postnatal rat cerebellum. *E J Neurosci* **9**, 533-548

Wamil AW & McLean MJ (1991). Effect of anticonvulsant medications on responses to NMDA by mouse central neurones in cell culture. *Epilepsia* **32**, 42

Wang SJ, Huang CC, Hsu KS, Tsai JJ & Gean PW (1996a). Presynaptic inhibition of excitatory neurotransmission by lamotrigine in rat amygdalar neurones. *Synapse* **24,** 248-255

Wang SJ, Huang CC, Hsu KS, Tsai JJ & Gean PW (1996b). Inhibition of N-type calcium currents by lamotrigine in rat amygdalar neurones. *Neuroreport* **7**, 3037-3040

Waters J & Helmchen F (2004). Boosting of action potential backpropagation by neocortical network activity *in vivo*. *J Neurosci* **24**, 11127-11136

Waters J & Helmchen F (2006). Background activity is sparse in the neocortex. *J Neurosci* **26**, 8267-8277

Weissinger F, Buchheim K, Siegmund H, Heinemann U & Meierkord H. (2000). Optical imaging reveals characteristic seizure onsets, spread patterns, and propagation velocities in hippocampal-entorhinal cortex slices of juvenile rats. *Neurobiol Dis* **7**, 286-298

Welty DF, Scheilke GP, Vartanian MG & Taylor CP (1993). Gabapentin anticonvulsant action in rats: disequilibrium with peak drug concentrations in plasma and brain microdialysate. *Epi Res* **16**, 175-181

Wennberg R, Arruda F, Quesney LF & Olivier A. (2002). Pre-eminence of extra-hippocampal structures in the generation of mesial temporal seizures: evidence from human depth electrode recordings. *Epilepsia* **4**, 716-726

White HS, Smith MD & Wilcox KS (2007). Mechanisms of action of antiepileptic drugs. *Int Rev Neurobiol* **81**, 85-110

Wikinski SI, Acosta GB & Rubio MC (1996). Valproic acid differs in its *in vitro* effect on glutamic acid decarboxylase activity in neonatal and adult rat brain. *Gen Pharmacol* **27,** 635-638

Witter MP, Van Hoesen GW & Amaral DG (1989). Topographical organisation of the entorhinal projection to the dentate gyrus of the monkey. *J Neurosci.* **9**, 216-228

Wolf R, Tscherne U & Emrich HM (1988). Suppression of preoptic GABA release caused by push-pull-perfusion with sodium valproate. *N S Arch Pharmacol* **338**, 658-663

Wolfart J, Debay D, Le Masson G, Destexhe A & Bal T (2005). Synaptic background activity controls spike transfer from thalamus to cortex. *Nat Neurosci* **8.12**, 1760-1767

Woodhall GL, Evans DIP, Cunningham MO & Jones RSG (2001). NR2B-containing NMDA autoreceptors at synapses on entorhinal cortical neurones. *J Neurophysiol* **86**, 1644-1651

Woodhall GL, Bailey SJ, Thompson SE, Evans DIP & Jones RSG (2004). Fundamental differences in spontaneous synaptic inhibition between deep and superficial layers of the rat entorhinal cortex. *Hippocampus* **15**, 232-245

Xiao C, Zhou C, Li K & Ye J-H (2007). Presynaptic $GABA_A$ receptors facilitate GABAergic transmission to dopaminergic neurones in the ventral tegmental area of young rats. *J Physiol* **580**, 731-743

Xie X, Lancaster B, Peakman T & Garthwaite J (1995). Interaction of the antiepileptic drug lamotrigine with recombinant rat brain type IIA Na^+ channels and with native Na^+ channels in rat hippocampal neurones. *Eur J Physiol* **430**, 437-446

Yaari Y, Selzer ME & Pincus JH (1986). Phenytoin: mechanisms of its anticonvulsant action. *Ann Neurol* **20**, 171-184

Yang L & Benardo LS (2001). Laminar properties of 4-aminopyridine-induced synchronous network activities in rat neocortex. *Neuroscience* **111**, 303-313

Yang J, Woodhall GL & Jones RSG. (2006). Tonic facilitation of glutamate release by presynaptic NR2B-containing NMDA receptors is increased in the entorhinal cortex of chronically epileptic rats. *J Neurosci* **26**, 406–410

Yang J, Wetterstrand W & Jones RSG (2007). Felbamate but not phenytoin or gabapentin reduces glutamate release by blocking presynaptic NMDA receptors in the entorhinal cortex. *Epi Res* (In press)

Ylinen A, Bragin A, Nadasdy Z, Jando G, Szabo I, Sik A & Buzsaki G (1995). Sharp wave-associated high-frequency oscillation (200 Hz) in the intact hippocampus: network and intracellular mechanisms. *J Neurosci* **15**, 30-46

Zeise ML, Kasparow S & Zieglgansberger W (1991). Valproate suppresses NMDA evoked, transient depolarisations in the rat neocortex *in vitro. Brain Res* **544**, 345-348

Zola-Morgan S, Squire LR (1993). Neuroanatomy of memory. *Annu Rev Neurosci* **16**, 547-563

Zou Q, Rudolph M, Roy N, Sanches-Vives M, Contreras D & Destexhe A (2005). Reconstructing synaptic background activity from conductance measurements *in vivo*. *Neurocomputing* **65**, 673-678

Publications

Conference Abstracts:

Greenhill, S.D. and Jones, R.S.G. (2006) Global inhibitory and excitatory background conductances in rat entorhinal cortical neurone. *FENS meeting***,** Vienna, July 2006

Greenhill, S.D. and Jones, R.S.G. (2007) Effect of lamotrigine on network and cellular excitability in the rat entorhinal cortex *in vitro*. *Proc. Brit. Pharm. Soc*. http://www.pa2online.org/abstract/abstract.jsp?abid=28510

Greenhill, S.D. and Jones, R.S.G. (2007) Activity-driven transmitter release contributes more to global background inhibition than excitation in pyramidal neurones of the rat entorhinal cortex. *Proc. BNA*. **19**: Abstr. 13.05, p69

Greenhill, S.D., Chamberlain, S.E.L. and Jones, R.S.G. (2007) Effects of GABA and glutamate uptake blockers on global background synaptic activity and excitability in entorhinal cortical neurones *in vitro*. Presented at the BPS Meeting, Brighton, December 2007

Chamberlain, S.E.L., Greenhill, S.D. and Jones, R.S.G. (2007) Increased activation of presynaptic GluR5 kainate receptors may contribute to generation of slow wave oscillations in entorhinal cortical neurones *in vitro.* Presented at the BPS Meeting, Brighton, December 2007

Papers:

Greenhill, S.D. and Jones, R.S.G. (2007) Simultaneous estimation of global background synaptic inhibition and excitation from membrane potential fluctuations in layer III neurones of the rat entorhinal cortex in vitro. *Neuroscience* **147,** 884-892

Papers in Preparation:

Greenhill, S.D., Chamberlain, S.E.L. and Jones, R.S.G. Effects of GABA and glutamate uptake blockers on global background synaptic activity and excitability in entorhinal cortical neurones *in vitro.* (To be submitted to *Neuroscience*)

Greenhill, S.D. and Jones, R.S.G. Effects of anticonvulsants on background synaptic activity and cellular excitability in the rat entorhinal cortex *in vitro*. (To be submitted to the *British Journal of Pharmacology*)